# FINAL REPORT

## Unexploded Ordnance Characterization and Detection in Muddy Estuarine Environments

## SERDP Project MR-2730

JUNE 2020

Arthur C. Trembanis
Carter DuVal
**University of Delaware**

*Distribution Statement A*
*This document has been cleared for public release*

SERDP
DOD ▪ EPA ▪ DOE

This report was prepared under contract to the Department of Defense Strategic Environmental Research and Development Program (SERDP). The publication of this report does not indicate endorsement by the Department of Defense, nor should the contents be construed as reflecting the official policy or position of the Department of Defense. Reference herein to any specific commercial product, process, or service by trade name, trademark, manufacturer, or otherwise, does not necessarily constitute or imply its endorsement, recommendation, or favoring by the Department of Defense.

# REPORT DOCUMENTATION PAGE

*Form Approved*
*OMB No. 0704-0188*

The public reporting burden for this collection of information is estimated to average 1 hour per response, including the time for reviewing instructions, searching existing data sources, gathering and maintaining the data needed, and completing and reviewing the collection of information. Send comments regarding this burden estimate or any other aspect of this collection of information, including suggestions for reducing the burden, to Department of Defense, Washington Headquarters Services, Directorate for Information Operations and Reports (0704-0188), 1215 Jefferson Davis Highway, Suite 1204, Arlington, VA 22202-4302. Respondents should be aware that notwithstanding any other provision of law, no person shall be subject to any penalty for failing to comply with a collection of information if it does not display a currently valid OMB control number.
**PLEASE DO NOT RETURN YOUR FORM TO THE ABOVE ADDRESS.**

| **1. REPORT DATE** *(DD-MM-YYYY)* | **2. REPORT TYPE** | **3. DATES COVERED** *(From - To)* |
|---|---|---|
| 30/06/2020 | SERDP Final Report | 6/21/2017 - 6/20/2021 |

**4. TITLE AND SUBTITLE**

Unexploded Ordnance Characterization and Detection in Muddy Estuarine Environments

**5a. CONTRACT NUMBER**
17-C-0044

**5b. GRANT NUMBER**

**5c. PROGRAM ELEMENT NUMBER**

**6. AUTHOR(S)**
Arthur C. Trembanis
Carter DuVal

**5d. PROJECT NUMBER**
MR-2730

**5e. TASK NUMBER**

**5f. WORK UNIT NUMBER**

**7. PERFORMING ORGANIZATION NAME(S) AND ADDRESS(ES)**
University of Delaware
Newark, DE 19716

**8. PERFORMING ORGANIZATION REPORT NUMBER**
MR-2730

**9. SPONSORING/MONITORING AGENCY NAME(S) AND ADDRESS(ES)**
Strategic Environmental Research and Development Program (SERDP)
4800 Mark Center Drive, Suite 16F16
Alexandria, VA 22350-3605

**10. SPONSOR/MONITOR'S ACRONYM(S)**
SERDP

**11. SPONSOR/MONITOR'S REPORT NUMBER(S)**
MR-2730

**12. DISTRIBUTION/AVAILABILITY STATEMENT**

DISTRIBUTION STATEMENT A. Approved for public release: distribution unlimited.

**13. SUPPLEMENTARY NOTES**

**14. ABSTRACT**

There remains a recognized need for better quantitative understanding of the impact of coastal environments on munitions ad explosives of concern (MEC) mobility and burial. Recent studies have investigated the mobility and burial of MEC in sandy coastal areas, leading to a more comprehensive understanding of munitions mobility and burial in non-cohesive sediments. A significant data gap was identified regarding MEC in shallow, cohesive-sediment environments, where munitions phenomenology is less clear. The goal of this study is to address this data gap though observations of MEC mobility and burial in cohesive-sediment environment and to compare findings to observations and models for munitions in non-cohesive sediments. The primary objectives of this study were to: 1) monitor the mobility and behavior of sensor-integrated surrogate munitions in muddy environments using a high-accuracy acoustic positioning system, 2) observe surrogate munition response to hydrodynamic forcing through in situ hydrodynamics and sonar imagery, and 3) monitor morphological site changes through repetitive geophysical site surveying and benthic sediment sampling.

**15. SUBJECT TERMS**

UXO, Unexploded Ordnance Characterization, Detection, Muddy Estuarine Environments

| **16. SECURITY CLASSIFICATION OF:** | | | **17. LIMITATION OF ABSTRACT** | **18. NUMBER OF PAGES** | **19a. NAME OF RESPONSIBLE PERSON** |
|---|---|---|---|---|---|
| **a. REPORT** | **b. ABSTRACT** | **c. THIS PAGE** | | | Arthur C. Trembanis |
| UNCLASS | UNCLASS | UNCLASS | UNCLASS | 129 | **19b. TELEPHONE NUMBER** *(Include area code)* 302-831-2498 |

# Contents

**1. Abstract** ..... **1**
**2. Executive Summary** ..... **2**
2.1. Introduction ..... 2
2.2. Objectives ..... 3
2.3. Technical Approach ..... 3
2.4. Results and Discussion ..... 6
2.5. Implications for Future Research and Benefits ..... 11
**3. Objective** ..... **12**
**4. Technical Approach** ..... **13**
4.1. Background ..... 13
4.1.1. Object Burial ..... 14
4.1.2. Object Mobility ..... 15
4.2. Materials and Methods ..... 16
4.2.1. Task 1 – Tracking and Motion Sensor Technology Design ..... 16
4.2.1.1. Surrogate MEC Development ..... 16
4.2.1.2. Surrogate Fabrication and Instrumentation ..... 17
4.2.1.3. Vemco Positioning System ..... 20
4.2.1.4. Vemco Position System Testing and Configuration ..... 22
4.2.2. Interim Milestone 1: Go / No-Go Decision ..... 24
4.2.3. Task 2 – Field Implementation ..... 25
4.2.3.1. Field Study Site and Methods Overview ..... 26
4.2.3.2. Fall 2017 Field Deployment ..... 31
4.2.3.3. Spring 2018 Field Deployment ..... 35
4.2.4. Task 3 – Data Analysis, Project Review, and Reporting ..... 37
4.2.5. Interim Milestone 2: Task 4 Go / No-Go Decision ..... 37
4.2.6. Task 4: Optional Additional Field Study ..... 37
4.2.6.1. Fall 2018 Field Deployment ..... 39
4.2.6.2. Spring 2019 Field Deployment ..... 42
**5. Results and Discussion** ..... **45**
5.1. Results by Deployment ..... 45
5.1.1. Fall 2017 Deployment ..... 45
5.1.2. Spring 2018 Field Deployment ..... 48
5.1.3. Fall 2018 Field Deployment ..... 52

5.1.4. Spring 2019 Field Deployment ..... 57
5.2. Cumulative Results and Discussion ..... 59
5.2.1. Hydrodynamics ..... 59
5.2.2. Sediment Analysis ..... 62
5.2.2.1. Sediment Classification ..... 62
5.2.2.2. Sediment Transport ..... 66
5.2.3. Surrogate Scour and Burial ..... 71
5.2.4. Surrogate Mobility ..... 78
**6. Conclusions and Implications for Future Research/Implementation ..... 81**
6.1. Performance by Task ..... 81
6.1.1. Task 1 – Tracking and Motion Sensor Technology Design ..... 83
6.1.2. Task 2 – Field Implementation ..... 85
6.1.3. Task 3 – Data Analysis, Project Review and Reporting ..... 86
6.1.4. Task 4 – Optional Additional Field Study ..... 86
6.2. Munitions Mobility and Burial in Cohesive Sediments ..... 87
6.2.1. Munitions Mobility ..... 87
6.2.2. Munitions Burial ..... 87
6.3. Implications for Future Research / Implementation ..... 88
**7. Literature Cited ..... 90**
**Appendix A** ..... I
A.1. Surrogate Deployment Summary ..... I
A.2. Sediment Samples ..... VI
A.3. Magnetometer Data ..... XVIII
**Appendix B** ..... XXI
B.1. Vemco VPS Data Sheets ..... XXI

# Tables

Table 2.1: Properties of surrogates used in MR-2730. ..... 4

Table 2.2: Comparison of the 6 nor'easter events in observed by MR-2730 in 2018. All conditions reported are the maximum measured / estimated values during the storm. Peak wave direction (Dp) are contemporaneous with max wave height observations. Bolded text highlights notable measurements. ..... 6

Table 4.1: Properties of surrogates used in MR-2730. ..... 18

Table 4.2: xi-o NGIMU Specifications. ..... 19

Table 4.3: MR-2730 Vemco V9 acoustic tag specifications. ..... 22

Table 4.4: Data collection and Quantitative Performance Metrics ..... 25

Table 4.5: Summary of activities associated with Task 2 Fall 2017 deployment ..... 31

Table 4.6: Summary of activities associated with Task 2 Spring deployment. ..... 35

Table 4.7: Summary of activities associated with Task 4 Fall 2018 deployment ..... 40

Table 4.8: Summary of activities associated with Task 4 Spring 2019 deployment ..... 42

Table 5.1: Comparison of the 6 nor'easter events in observed by MR-2730 in 2018. All conditions reported are the maximum measured / estimated values during the storm. Peak wave direction (Dp) are contemporaneous with max wave height observations. Bolded text highlights notable measurements. ..... 61

Table 6.1: Performance objectives and assessment of MR-2730. ..... 82

# Figures

Figure 2.1: Surrogate MEC design plans for 60mm mortar, 81mm mortar, and 155mm artillery shell. ..... 4

Figure 2.2: Sonar mosaics of Site 1 and Site 2 and surrounding area. Note the darker backscatter at the Site 2 (A) indicating a softer, more acoustically absorbent sediment than the Site 1 (B). An idealized VPS array diagram (C) illustrates the field setup for each deployment. ..... 5

Figure 2.3: Comparative diagram of surrogate status for each of the four field deployments. Note the difference in burial depth between Site 1 and Site 2 deployments under similar conditions. ..... 7

Figure 2.4: Estimated surrogate burial by settling depth related to sediment bearing capacity using simply Hertzian contact model for rigid cylinders and elastic surfaces. Results for 155mm surrogate only are shown for each penetrometer sample with the samples taken at Sites 1 and 2 highlighted in gray. The bottom diagram illustrates the difference between model results and observations. Note that this does not account for the tilt of the 60mm (>45° pitch) mortars at Site 2, which would agree more with the estimated settling depth. ..... 8

Figure 2.5: VPS position estimates for surrogate 60A during nor'easter Toby (top) with contemporaneous IMU data from the onboard x-io NGIMU (middle). Displacement (bottom) was estimated from the acoustic tag located in the tail of the surrogate..... 9

Figure 2.6: Penetrometer measurements (inset) compared to sonar mosaic classification results. Note the 2 distinct groups reflecting higher percent sands (e.g. Site 1) and higher percent muds (e.g. Site 2). ..... 10

Figure 4.1: Variation of the Hjulström curve for sediment transport (see Hjulström, 1935). ..... 13

Figure 4.2: Surrogate MEC design plans for 60mm mortar, 81mm mortar, and 155mm artillery shell. ..... 17

Figure 4.3: Ten surrogate munitions prepared for deployment on Nov. 2, 2017. Four 4.2-inch mortar surrogates were later added to the suite. ..... 18

Figure 4.4: IMU and battery configurations in 60mm (A), 81mm (B), and 155mm (C) surrogates. ..... 20

Figure 4.5: Diagram of 4.2 inch mortar surrogate. ..... 20

Figure 4.6: Vemco Position System. HR2 Acoustic Receivers (A) are placed in a network (B) that records the difference in arrival times of small acoustic tags (C). Multiple tags can be tracked over time (D) with position accuracies down to 10cm (Images courtesy of Vemco)..... 21

Figure 4.7: Comparison of Vemco estimated positions versus RTK GPS positions taken during the 2016 UD boat basin field test of the VPS acoustic tracking network. ..... 23

Figure 4.8: RTK GPS and VPS positional offset (with model overlay) for the surrogate in the 2016 UD field test. ..... 24

Figure 4.9: A sediment classification map of the Broadkill, DE area from previously collected Roxan sonar data and sediment sampling (Wilson et al., 2010) with the MR-2730 field site location indicated. The field site is located 10.5 km northwest of the UD Marine Operations facilities and Marine Sciences Campus, which allowed for easy access and frequent site monitoring. ..... 26

Figure 4.10: VPS receiver arrangement designed with assistance from Vemco to maximize acoustic detection overlap and positional accuracy. Minimum anticipated receiver overlap is overlaid with example reference tag, surrogate MEC, and instrument frame placement. ..... 27

Figure 4.11: Instrument frame developed for MR-2730. Shown here with Teledyne RDI Sentinel ADCP, Nortek Aquadopp HR PC-ADCP, AML Plus-X CTD, and Imagenex 881 Tilt-Head rotary sonar. ..... 28

Figure 4.12: The University of Delaware a) R/V Joanne Daiber equipped with Edgetech 6205 PMES, and b) Teledyne Gavia modular autonomous underwater vehicle with Geometrics G-880 magnetometer. ..... 29

Figure 4.13: Magnetometer results from blind ordnance detection survey. The peaks are strong magnetic signals, compared to the ordnance test subjects (ESTCP Project MR-201002). ..... 30

Figure 4.14: a) Local monthly historic wind and b) predicted near-bed wave orbital velocity for Broadkill Beach field site prior to field study. ..... 31

Figure 4.15: Task 2 study area. The VPS array was located in the center of the inset sonar mosaic. ..... 32

Figure 4.16: HR2 receiver locations (A), HR2 pole mounts installation design (B), HR2 receivers and pole mounts prior to deployment (C), and reference tag pole mounts (D). ..... 33

Figure 4.17: VPS array in Fall 2017 deployment as mapped by the Gavia AUV. Waterfall snapshots show an HR2 receiver on augured pole (top), reference tag post (middle), and instrument frame (bottom) with 155mm surrogate visible (right) ..... 34

Figure 4.18: Delaware State Police SCUBA Unit operations during the Fall 2017 VPS retrieval. A hard-hat diver with surface supply with communications (A) was monitored and guided to targets by the surface team using a sector-scanning sonar (B). The diver can be seen as the bright return in the center of sonar image (C) ..... 34

Figure 4.19: Comparison of magnetometer picks and VPS estimated last known position for the missing 81mm and 60mm surrogates. ..... 36

Figure 4.20: Example Hjulström diagram (A) and historic wind record (B) illustrated remaining data gaps potentially addressed through additional deployment in Task 4. ..... 38

Figure 4.21: A sediment classification map of the Broadkill, DE area from previously collected Roxan sonar data and sediment sampling (Wilson et al., 2010) helped inform the Task 4 deployment site (Site 2). ..... 39

Figure 4.22: Sonar mosaics of Task 2 and Task 4 sites and surrounding area. Note the darker backscatter at the Task 4 site (bottom left) indicating a softer, more acoustically absorbent sediment than the Task 2 site (bottom right). ..... 40

Figure 4.23: Geotechnical site characterization was provided by Dr. Nina Stark (MR18-1233) and her team. Data was collected with a portable freefall penetrometer (a), and ground-truthed with sediment samples and gravity cores (b). ..... 44

Figure 5.1: Time-series measurements from the Fall 2017 deployment showing near-bed orbital and unidirectional current (A), pressure depth (b), and example IMU data from a 60mm mortar (C). ..... 45

Figure 5.2: Snapshots from the rotary sonar data collected in the Fall 2017 deployment. Note the smaller surrogates become less distinguishable as time progresses from Nov. 3 (left), to Nov. 15 (center), and to Nov. 29 (right). ..... 46

Figure 5.3: Surrogate munitions status during the Fall 2017 deployment as reported by DSPSU divers. ..... 47

Figure 5.4: Preliminary VPS acoustic tracking results from the Fall 2017 deployment. VPS estimated measurements of surrogate length derived from acoustic tag locations compare well to true surrogate length. Note the shift in position of the 155mm is likely due to a sharp change in sound speed. ..... 47

Figure 5.5: Daily VPS detection count for surrogate tags over the Fall 2017 deployment. ..... 48

Figure 5.6: Significant wave height and peak wave period (A), near bed wave orbital and unidirectional currents (B), and turbidity (C) recorded over the Spring 2018 deployment. Note the turbidity unit did not properly auto-scale to adjust for higher magnitudes during storm – values shown are corrected using scaler estimated from the Spring 2019 deployment. ..... 48

Figure 5.7: Sonar images of a 155mm surrogate partially buried by nor'easter Riley taken on Mar. 6, 2018 (A), and the same 155mm partially buried in a scour pit taken on Apr. 10, 2018 (B). ROV image of a partially buried 81mm surrogate taken on March 18, 2018 (C). ..... 49

Figure 5.8: Diagram illustrating the general conditions of each surrogate type at deployment and upon recovery based on the Delaware State Police SCUBA Unit observations for the Spring 2018 field study ..... 50

Figure 5.9: Roll and pitch recorded during Toby in a 60mm surrogate. Note the 10-15 degree increase in pitch, which appears during periods of rolling and for extended periods in static moments, suggesting the unit may have rolled into and out of a scour pit. ..... 50

Figure 5.10: VPS total surrogate detection count by day from the Spring 2018 deployment. Note the effects of the four nor'easters. Riley and Toby cause pronounced decreases in detection, suggesting burial, while Skyler leads to a brief increase in detections, suggesting re-exposure of buried surrogates. ..... 51

Figure 5.11: Significant wave height and peak wave period (A), near bed wave orbital and unidirectional currents (B), and turbidity (C) recorded over the Fall 2018 deployment. Note the turbidity unit did not properly auto-scale to adjust for higher magnitudes during storm – values shown are corrected using scaler estimated from the Spring 2019 deployment. ..... 52

Figure 5.12: The instrument frame migrated 316m to the SE (b) in three separate episodes concurrent with ebbing tides. ..... 53

Figure 5.13: Last estimated positions of surrogates on Oct. 1, 2018 from the VPS. The initial location of the instrument frame is shown in sonar collected on Aug. 29, 2018, although the frame itself was no longer in the field area on Oct. 1. ..... 54

Figure 5.14: The burial of the instrument frame on Oct. 27 as estimated from the downward facing Nortek Aquadopp HR profiler acoustic backscatter (a), and offset in mean water level from the AML-PlusX CTD (b). The seafloor is estimated in the Aquadopp from the bins with the highest backscatter. ..... 54

Figure 5.15: Diagram illustrating the general conditions of each surrogate type at deployment and upon recovery based on the Delaware State Police SCUBA Unit observations for the Fall 2018 field study ..... 55

Figure 5.16: VPS total surrogate detection count by day from the Fall 2018 deployment. Note the effects of the Sep. and Oct. extra-tropical cyclones, as well as a gale on Sep. 25, 2018. ..... 56

Figure 5.17: Significant wave height and peak wave period (A), near bed wave orbital and unidirectional currents (B), and turbidity (C) recorded over the Spring 2019 deployment. ..... 57

Figure 5.18: Diagram illustrating the general conditions of each surrogate type at deployment and upon recovery based on the Delaware State Police SCUBA Unit observations for the Spring 2019 field study ..... 58

Figure 5.19: VPS total surrogate detection count by day from the Spring 2019 deployment. ..... 58

Figure 5.20: A) Historical monthly average wind speeds at Lewes, DE from 2005-2019 with MR-2730 deployment coverage overlaid. The six 2018 extra-tropical cyclones are demarcated. B) Comparison of hourly averaged winds for 2005-2017 (left) and 2018 (right). The highest average wind speed for the nor'easters are overlaid indicating that nor'easter Riley, Toby, and the Oct ETC were outlier events. ..... 60

Figure 5.21: Storm return periods estimated from (A) in situ hydrodynamic observations in the Delaware Bay, and (B) U.S. Army Corps of Engineers Engineer Research and Development Center (Nadal-Caraballo et al., 2015). Figure courtesy of Stephanie M. Dohner. ..... 61

Figure 5.22: Shepard (1954) sediment ternary diagram for sediment samples from MR-2730 field sites and wider Broadkill Slough region. ..... 62

Figure 5.23: Penetrometer results for MR-2730 field sites and surrounding Broadkill Slough (top) showing quasi-static bearing capacity (QSBC) scaled to penetration depth (deeper penetration = larger symbol). The samples in and around Site 1 (Task 2) and Site 2 (Task 4) are shown below. Note the difference in QSBC and penetration depth between the two field sites. 63

Figure 5.24: Segmented mosaic for composite sonar imagery using an ESRI ArcGIS supervised classification. Sediment samples, showing percent sand, and penetrometer sample locations are overlaid. ..... 64

Figure 5.25: Segmented sonar mosaic classes compared to sand and mud fraction. The results show strong agreement between backscatter intensity and sand / mud fraction..... 65

Figure 5.26: Penetrometer measurements compared to sonar mosaic classification results. Note the 2 distinct groups reflecting higher percent sands (e.g. Site 1) and higher percent muds (e.g. Site 2). ..... 66

Figure 5.27: Critical Shields threshold estimates using the traditional Shields (1936) and Whitehouse et al., (2000) method for mixed cohesive sediments. ..... 67

Figure 5.28: Near-bed shear stress and critical shear stress for erosion for Site 1 sediments during the Spring 2018 deployment. ..... 68

Figure 5.29: Surficial sediment changes as estimated by sediment classification maps before and after Riley (left), and before and after Quinn, Skyler, and Toby (right)..... 68

Figure 5.30: Near-bed shear stress and critical shear stress for erosion for Site 2 sediments during the Fall 2018 deployment..... 69

Figure 5.31: Initial PMES sonar of the wider Site 2 field area (left) with VPS array location indicated (green) Note the evidence of sediment dredging. Over the course of the deployment, the sediment texture and backscatter intensity changes (middle). Snapshots from the AUV sonar (right) shows the creation of irregular textural features..... 70

Figure 5.32: Surficial sediment changes as estimated by sediment classification maps before and after the Fall 2018 deployment (left), and between the Fall 2018 and Spring 2019 deployments (right). ..... 71

Figure 5.33: Comparative diagram of surrogate status for each of the four field deployments. Note the difference in burial depth between Site 1 and Site 2 deployments under similar conditions. ..... 72

Figure 5.34: Scour burial predictions for surrogates for each deployment. Dashed lines indicate average burial depth by surrogate type reported by divers at time of recovery. Depth is reported

as the furthest estimated point of surrogates from the seabed surface (i.e. deepest part of the surrogate). ..... 73

Figure 5.35: Estimated surrogate burial by settling depth related to sediment bearing capacity using simply Hertzian contact model for rigid cylinders and elastic surfaces. Results for 60mm (top), 81mm (middle), and 155mm (bottom) surrogate are shown for each penetrometer sample with the samples taken at Sites 1 and 2 highlighted in gray. The bottom diagram illustrates the difference between model results and observations. Note that this does not account for the tilt of the 60mm mortars at Site 2, which would agree more with the estimated settling depth. ..... 77

Figure 5.36: VPS position estimates for surrogate 60A during nor'easter Toby (top) with contemporaneous IMU data from the onboard x-io NGIMU (middle). Displacement (bottom) was estimated from the acoustic tag located in the tail of the surrogate..... 79

Figure 5.37: Object mobility (see Rennie et al., 2017) calculated for 60mm mortar surrogates during the Spring 2018 deployment assuming various states of constant scour burial. ..... 80

Figure 6.1: Acoustic noise for at each HR2 receiver during the 2018 deployment. Storm activity did not significantly introduce noise, although consistently high noise are noted in both the central and northern receivers. The instrument frame was recovered on Mar. 18, and redeployed 20m east of the array on Mar 19. No corresponding change in noise is observed over that period. ..... 84

Figure 6.2: VPS results on Mar. 20, showing the initial position and subsequent movement of the four tagged whelk (inset) to the east and out of the grid. The whelks' positions continued to be recorded beyond the grid but were filtered out for low reliability in this image. ..... 85

# List of Acronyms

ADCP: Acoustic Doppler Current Profiler
AUV: Autonomous Underwater Vehicle
DNREC: Delaware Department of Natural Resources and Environmental Control
DOD: Department of Defense
DSPSU: Delaware State Police SCUBA Unit
ESTCP: Environmental Security Technology Certification Program
ETC: Extra-Tropical Cyclone
FUDS: Formerly-Used Defense Site
GPS: Global Position Systems
HPE: Horizontal Positional Error
IMU: Inertial Motion Unit
LBL: Long Baseline
MEC: Munitions and Explosives of Concern
MHHW: Mean Higher-High Water
MLLW: Mean Lower-Low Water
MOI: Munitions of Interest
MR: Munitions Response
MRS: Munitions Response Site
MRSON: Munitions Response Statement of Need
NOAA: National Oceanic and Atmospheric Administration
PC-ADCP: Pulse Coherent Acoustic Doppler Current Profiler
PMES: Phase-Measuring Echo Sounder
QSBC: Quasi-Static Bearing Capacity
RMSE: Root Mean Square Error
ROV: Remotely Operated Vehicle
RTK: Real-Time Kinematic
SCUBA: Self-Contained Underwater Breathing Apparatus
SERDP: Strategic Environmental Research and Development Program
UD: University of Delaware
UnMES: Underwater Munitions Expert System
USACE: United States Army Corps of Engineers
USBL: Ultra-Short Baseline
UXO: UneXploded Ordnance
VPS: Vemco Positioning System

# 1. Abstract

*Objectives:* There remains a recognized need for better quantitative understanding of the impact of coastal environments on munitions ad explosives of concern (MEC) mobility and burial. Recent studies have investigated the mobility and burial of MEC in sandy coastal areas, leading to a more comprehensive understanding of munitions mobility and burial in non-cohesive sediments. A significant data gap was identified regarding MEC in shallow, cohesive-sediment environments, where munitions phenomenology is less clear. The goal of this study is to address this data gap though observations of MEC mobility and burial in cohesive-sediment environment and to compare findings to observations and models for munitions in non-cohesive sediments. The primary objectives of this study were to: 1) monitor the mobility and behavior of sensor-integrated surrogate munitions in muddy environments using a high-accuracy acoustic positioning system, 2) observe surrogate munition response to hydrodynamic forcing through *in situ* hydrodynamics and sonar imagery, and 3) monitor morphological site changes through repetitive geophysical site surveying and benthic sediment sampling.

*Technical Approach:* A suite of custom designed and manufactured surrogate munitions were deployed at two cohesive sediment sites in the lower Delaware Bay estuary from 2017 - 2019. Surrogates were monitored for changes in mobility and burial using a Vemco (Innovasea) VPS acoustic tracking system and inertial motion units (IMU). Time-series acoustic imagery and hydrodynamic sensors were also deployed to characterize MEC response to varied hydrodynamic conditions. A series of repetitive surveys were conducted using a hull-mounted, high-resolution phase-measuring bathymetric sonar and autonomous underwater vehicle (AUV) equipped with a magnetometer. In total, 4 deployments were conducted between 2017 and 2019, spanning 226 days.

*Results:* The effects of six separate extra-tropical cyclones were recorded during the deployments, leading to wide-spread sediment transport. Burial was the predominant result across all four deployments, ranging from 50% to greater than 100% burial of surrogates depending on sediment composition and near-bed forcing. No large-scale horizontal mobility of surrogates were observed, although minor motion was recorded during peak-near bed velocities of several storm events. Models developed for munition mobility and burial in non-cohesive sediments were adapted for cohesive sediments and compared to field observations. MEC burial is linked to scour burial in mixed-cohesives with higher sand fraction and plastic deformation and bed fluidization in soft muds. Sediment bearing capacity is shown to be an important predictor for surrogate burial, and a simple model is introduced to predict burial due to bearing capacity. Shallow subsurface geotechnical properties influencing surrogate burial are linked to surficial sediment distributions via seabed classification and discussed in light of site management.

*Benefits:* The results from this study will inform key parameters for MEC behavior in storms and muddy environments for integration into the existing expert system modeling of MEC burial and mobility (e.g. Underwater Munitions Expert System, Rennie, 2017; SERDP Munitions Mobility and Modeling Workshop, Dec. 8-9, 2015). Our observations will expand our knowledge into an understudied but abundant environment with respect to munitions contamination, and aid in understanding historical and present conditions at FUDS containing cohesive sediments.

# 2. Executive Summary

## 2.1. Introduction

The detection, monitoring, and mitigation of munitions and explosives of concern (MEC) remains a topic of interest in coastal and underwater sites (MRSON-20-C1). SERDP has recognized the need for a better quantitative understanding of the influence of coastal environments on MEC detection and the fate of MEC in underwater munitions response sites (MRSON-17-01). Formerly-used defense sites (FUDS) span a wide-range of environmental settings and dynamics, which contribute uniquely to the fate of MEC. The interplay between historical and contemporary physical forces (e.g. wave and currents), sedimentology (e.g. cohesive vs. non-cohesive, composition), and MEC type are at the center of the underwater MEC question. As such, there is a critical need for better characterization of FUDS sites, focusing on, but not limited to, the interactions between sediment dynamics and MEC.

A number of SERDP studies are investigating MEC and sediment dynamics to better understand the question of monitions mobility and burial. These studies are primarily focused on MEC mobility and burial in sandy, non-cohesive, coastal settings (e.g. Calantoni SERDP MR-2320, Traykovski and Austin, 2017, Puleo MR-2503). Observations from these studies provide relevant information to probabilistic models developed to assist in the management of FUDS sites (e.g. Rennie MR-2645). The influence of MEC density on burial and mobility is a consistent finding amongst these studies. Munitions with densities greater than the sediment are more likely to bury, while those less dense are more likely to mobilize in energetic conditions (Calantoni SERDP MR-2320, Traykovski and Austin, 2017). Burial and mobility is likewise influenced by the threshold for transport of non-cohesive sediments. Identified mechanisms for burial include scour burial and burial by granular sorting or bed liquefaction under high-energy conditions (Klammler et al., 2019). For mobility, Rennie et al. (2017) found that the threshold for mobility is dependent upon the ratio of the MEC diameter to the seabed roughness. Features such as ripple bedforms and scour pits greatly reduce the potential for object mobility.

The influence of sediment properties on MEC burial and mobility becomes more challenging when considering MEC in cohesive (muddy) sediments. A significant data gap was identified for MEC at sites containing cohesive sediments, with a notable deficiency of observations of MEC mobility and burial in cohesive sediments (SERDP Munitions Mobility and Modeling Workshop, Dec. 8-9, 2015). The transition from non-cohesive to mixed-cohesive or cohesive sediments results in a departure from classic sediment transport models, with increasing thresholds for sediment erosion (Whitehouse et al., 2000). The cohesive nature of the muddy sediments reduces the potential for burial mechanisms typical of non-cohesive sediments, inhibiting scour and granular sorting mechanisms, and thus complicates the direct application of previously-developed burial and mobility predictive models to cohesive sediments. Wide variations in the rheology of cohesive sediments compounds this issue. Stiff muds may altogether inhibit burial processes beyond initial impact burial (Inman and Jenkins, 2002), and thus increase the potential for munitions mobility. Calantoni observed mobility of a surrogate sitting on a stiff cohesive layer, until the surrogate reached a sand pocket and buried (MR-2320). Conversely, burial may be accentuated in soft muds. If the buoyant weight of an MEC exceeds the bearing capacity of soft muds, the bed will undergo plastic deformation, allowing the object to effectively sink into the sediment over time (Richardson et al., 2001). Increasing wave energy

amplifies this process. Mud layer thickness increases under increasing wave height (Soltanpour et al., 2009), with a corresponding increase in water content and associated decreases in sediment bulk density and bearing capacity (Sahin et al., 2012).

While the majority of coastal FUDS sites fall within non-cohesive sediment environments, a review of available FUDS data (compiled by Calantoni MR-2320 and Puleo MR-2503) suggests as many as 139 FUDS sites lay partially or wholly in tidally-driven, mixed-cohesive or cohesive sediment environments. Likewise, a large percentage of inland FUDS sites are situated on mixed cohesive or cohesive sediment environments (see SERDP Underwater MEC Standardized Demonstration Sites [Test Beds] Workshop Report, Dec. 2018). Thus, the lack of observations and quantitative understanding of MEC mobility and burial in cohesive sediments constitutes as significant data gap for FUDS site management.

### 2.2. Objectives

The purpose of this study is to begin addressing the data gap by examining munitions mobility and burial in cohesive sediment environments. We proposed to achieve this goal through infield experimentation in a cohesive sediment setting subject to high-energy forcing. The primary objectives of this study were to: 1) monitor the mobility and behavior of sensor-integrated surrogate munitions in muddy environments using a high-accuracy acoustic positioning system, 2) observe and compare surrogate munition response to hydrodynamic forcing using *in situ* hydrodynamic data and sonar imagery, and 3) monitor morphological site changes through repetitive geophysical site surveying and benthic sediment sampling. The results from this study will inform key parameters for MEC behavior in muddy environments for integration into the existing expert system modeling of MEC burial and mobility (e.g. Underwater Munitions Expert System, Rennie, 2017; SERDP Munitions Mobility and Modeling Workshop, Dec. 8-9, 2015). These quantitative observations will expand the knowledge of an understudied but abundant environment with respect to munitions contamination, and aid in understanding historical and contemporary conditions at FUDS in cohesive sediment environments.

### 2.3. Technical Approach

To accomplish these objectives, we deployed a suite of surrogate munitions at 2 cohesive sediment sites in the lower Delaware Bay Estuary. Surrogates were monitored for changes in mobility and burial using a Vemco (Innovasea) VPS acoustic tracking system and inertial motion units (IMU). Time-series acoustic imagery and hydrodynamic sensors were also deployed to characterize MEC response to varied (e.g. storm vs. fair-weather) hydrodynamic conditions. A series of repetitive surveys were conducted using a hull-mounted, high-resolution phase-measuring bathymetric sonar and autonomous underwater vehicle (AUV) equipped with a magnetometer. In total, we conducted 4 field deployments between 2017 and 2019, spanning 226 days of *in situ* observations.

Munitions surrogates were developed to combine internal IMU measurements and acoustic tracking methods. Discussions from the SERDP Munitions Mobility and Modeling Workshops led to the selection of three munition types for this study: 60mm mortars, 81mm mortars, and 155mm artillery shells (Figure 2.1). An additional surrogate type, 4.2-inch mortars, were added later in the study. The surrogates were designed to meet best known characteristics of the

respective MEC type, including a minimum density within the estimated density distribution of measured MEC (see Table 2.1). The surrogates were designed to accommodate x-io IMU's to record fine-scale motion and additional batteries to extend deployment duration.

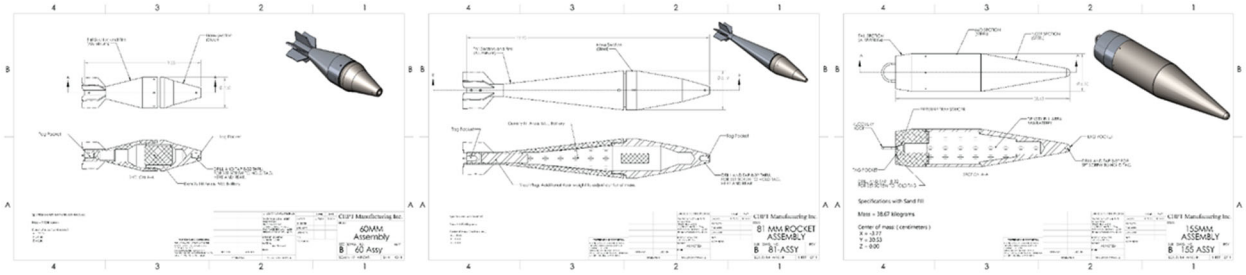


*Figure 2.1: Surrogate MEC design plans for 60mm mortar, 81mm mortar, and 155mm artillery shell.*

*Table 2.1: Properties of surrogates used in MR-2730.*

| Surrogate | Sensors | Material | Density (kg/m3) | Specific Gravity (saltwater) |
|---|---|---|---|---|
| **155mm** | IMU; Pressure Sensor | Steel/Aluminum/Lead | 3280-3590 | 3.2-3.5 |
| **4.2-inch** | IMU | Steel/Aluminum/Lead | 3170-3420 | 3.1-3.3 |
| **81mm** | IMU | Steel/Aluminum/Lead | 3640-3820 | 3.5-3.7 |
| **60mm** | IMU | Steel/Aluminum | 3970 | 3.9 |

Externally, each surrogate was designed with small cavities at either end to fit Vemco acoustic locater tags, which served as the primary surrogate tracking method during field deployments and measure any potential broad-scale mobility. The Vemco Positioning System (VPS), manufactured by Vemco (now part of Innovasea), is capable of simultaneous positioning of multiple tags within an acoustic receiver network. A field analysis of the VPS indicated that the positional estimates of the VPS were within 50 cm of RTK derived positons when moved within the array, and less than 20 cm for the initial static position of the surrogate. It was determined that the tags could not be detected when buried only a few cm below the surface of the stiff clay mud. Thus, if buried, a metal detector / magnetometer and the last known positions from the VPS were utilized to reacquire the surrogates.

Four deployments of the VPS array and surrogate munitions were conducted from 2017-2019 at two separate sites located in the lower Delaware Bay (Figure 2.2). The lower Delaware Bay is characterized by muddy or mixed sand and mud sediments (Wilson et al., 2010) and is often buffeted by high-energy events (Wright 1993; Trembanis et al., 2012). Over the course of the field study, 63 sediment samples were collected in the study area and the surrounding Broadkill Slough. An additional 23 sites were sampled using a portable freefall sediment penetrometer (collaboration with Dr. Nina Stark MR18-1233). The results show a wide distribution of mixed cohesive sediments. The area of Site 1, situated in 4.5 m MLLW depth, was predominantly poorly sorted, fine muddy sand, with 60-75% sand and 25-40% muds. The area of Site 2, situated 1 km in shore of Site 1 and in 3.5 m MLLW depth, was predominantly poorly sorted sandy mud, with 15-40% sand and 60-85% muds. Two deployments occurred at Site 1 from 2 Nov - 4 Dec 2017 and 9 Feb - 11 Apr 2018. An additional two deployments were conducted at Site 2 from 29 Aug - 19 Nov 2018 and 27 Mar - 20 May 2019.

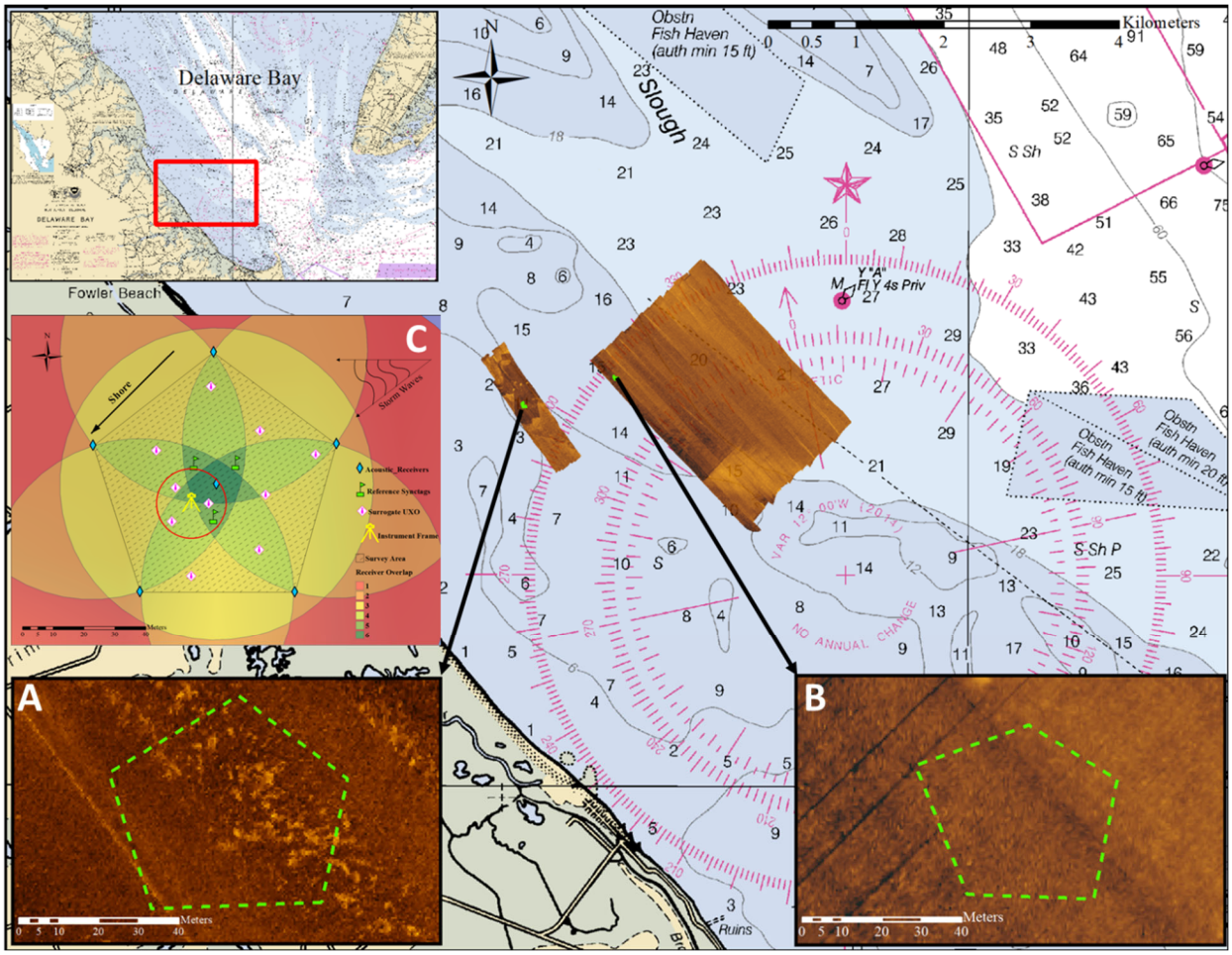



*Figure 2.2: Sonar mosaics of Site 1 and Site 2 and surrounding area. Note the darker backscatter at the Site 2 (A) indicating a softer, more acoustically absorbent sediment than the Site 1 (B). An idealized VPS array diagram (C) illustrates the field setup for each deployment.*

All deployments used a similar acoustic array configuration based on consultation with Vemco. A set of 6 Vemco HR2 receivers were set in a pentagonal grid with one receiver on each corner and one in the center to ensure overlap of the study site by multiple receivers (see Figure 2.2a). Once deployed, positions were surveyed in using an Edgetech 6205 Phase-measuring echo-sounder (PMES) equipped with Real-Time Kinematic (RTK) GPS registering centimeter horizontal accuracies. Each HR2 receiver was also equipped with an internal synchronization tag to correct for clock drift between the receivers. Additional reference "synctags" were placed within the grid at GPS marked positions to measure overall system performance during the deployment. Surrogate munitions equipped with Vemco tags were deployed within the grid. A total of 10 surrogates were deployed in 3 of the 4 experiments, with 13 surrogates deployed in the final experiment. All but one surrogate munition was recovered at the end of the study. The deployment and recovery of equipment and munitions required a combination of surface vessel operations and SCUBA or surface-supplied divers (Delaware State Police SCUBA Unit).

Hydrodynamic and morphodynamic data were monitored using an instrumented bottom frame fitted with an upward facing 600 kHz Teledyne RDI Acoustic Doppler Current Profiler (ADCP), downward facing 2 MHz Nortek Pulse-Coherent ADCP (PC-ADCP), AML Plus-X CTD with

turbidity, and 2.25 MHz Imagenex 881 fan-beam rotary sonar. Repeated geophysical site mapping was conducted using the UD Gavia AUV and Edgetech 6205 PMES. The Gavia AUV is a modular designed vehicle equipped with Marine Sonics 900/1800 kHz high-resolution side-scan sonar, a GeoAcoustics GeoSwath 500 kHz phase-measuring bathymetric sonar, 2 MP Point Grey Color Grasshopper Camera, and environmental sensors (e.g. salinity, temperature, dissolved oxygen, and turbidity. To detect buried surrogates, the Gavia was also fitted with a Geometrics G-880AUV self-oscillating split-beam cesium vapor (non-radioactive Cs133) total field magnetometer with automatic hemisphere switching coupled with an Applied Physics 539 fluxgate compass. The magnetometer system was developed and tested through a previous ESTCP project (MR-201002-DR).

Complete site acoustic backscatter, bathymetry and magnetometer map products were generated for each survey using Chesapeake Technologies, Inc. SonarWiz, and site-wide surficial sediment distribution and bathymetry were analyzed using ESRI ArcGIS 10.4. Sediment samples and short cores were processed for grain size analysis, sediment type and distribution, and shear vane analysis. Hydrodynamics were used to estimate sediment transport thresholds of the site sediments. Sediment distribution maps were generated based on geophysical survey products and ground-truthed by sediment samples collected at the site. VPS data processing was handled by Vemco, who provided precision positioning for each acoustic tag. Vemco reported positions were compared to positions calculated from magnetometer and side-scan sonar data collected by the AUV. Finally, surrogate burial and mobility were analyzed with time-series hydrodynamics and sediment properties to determine which parameters and mechanisms have the most influence on surrogate mobility in muddy environments.

### 2.4. Results and Discussion

*Table 2.2: Comparison of the 6 nor'easter events in observed by MR-2730 in 2018. All conditions reported are the maximum measured / estimated values during the storm. Peak wave direction (Dp) are contemporaneous with max wave height observations. Bolded text highlights notable measurements.*

| | Riley | Quinn | Skylar | Toby | Sept. ETC | Oct. ETC |
|---|---|---|---|---|---|---|
| Duration (hr) | **66** | 11.5 | 19 | 45 | 7 | 0 |
| dHs/dt (m/hr) | **0.15** | 0.08 | 0.05 | 0.1 | 0.02 | 0.06 |
| Hs (m) | **1.88** | 1.3 | 1.37 | 1.76 | 1.15 | 0.92 |
| Dp (º) | 329 | 340 | 60 | 55 | 60 | 49 |
| Ub (m/s) | 0.8 | 0.47 | 0.5 | **0.83** | 0.59 | 0.48 |
| Uc (m/s) | 0.35 | 0.25 | 0.23 | 0.39 | 0.41 | **0.43** |
| TWL >MHHW (m) | 0.71 | 0.59 | 0.32 | 0.59 | **1** | 0.9 |

Over the course of the 4 deployments, 6 extra-tropical cyclones (ETC) were observed (see Table 2.1). Four ETC occurred during the Spring 2018 deployment, identified as Riley, Quinn, Skyler, and Toby (or the "4'easters" of March 2018). Two additional ETC occurred during the Fall 2018 deployment (Sept. and Oct. ETC). Based on local historical wind records, all 6 storms were 99$^{th}$ percentile or higher for winds, and 5 of 6 exceeded 99.5%. While no long-term wave climate was available for the region, by leveraging local *in situ* observations (spanning 313 days over 2016-2019), we estimated a 99% threshold for significant wave height (*Hs*) at 1.05m, which 5 of the 6 storms exceeded. Of note, Riley was the longest duration above 99% wave height

threshold, highest *Hs*, and fastest rate of wave height increase (*dHs/dt*), a parameter noted to be important for mobility by Traykovski and Austin (2017). Approaching from the northeast, Toby had the greatest fetch, resulting in higher near-bed orbital velocities. Lastly, the Sept. ETC generated surge 1 m storm above mean-higher high water, which resulted in increased ebb tide currents that moved the instrument frame 316 m to the southeast of the deployment location. An analysis of storm return periods found that, while the six ETC were extreme events by wind and wave height metrics, storms of similar magnitude frequent the region on sub-decadal to decadal scales.

Surrogate burial was consistently observed over the course of the four deployments. The change from the muddy sands of Site 1 to the sandy muds of Site 2 influenced the degree of burial observed, and the dominant mechanism by which surrogate burial occurred. The overall status of the surrogates at the end of their respective deployments are shown in Figure 2.3. Two deployments occurred at each study site, of which one deployment at each site experienced low – moderate forcing and the other deployment experienced storm conditions through extra-tropical cyclones and other wave events. The comparative figure highlights the differences in burial between Site 1 and 2, despite similar forcing conditions. For instance, with no storm events, surrogates were only partially buried in Site 1, but almost completely buried in Site 2. With storm events, the surrogates at Site 1 were mostly buried or exposed in scour pits, while in Site 2, they were buried 20-30 cm deep.

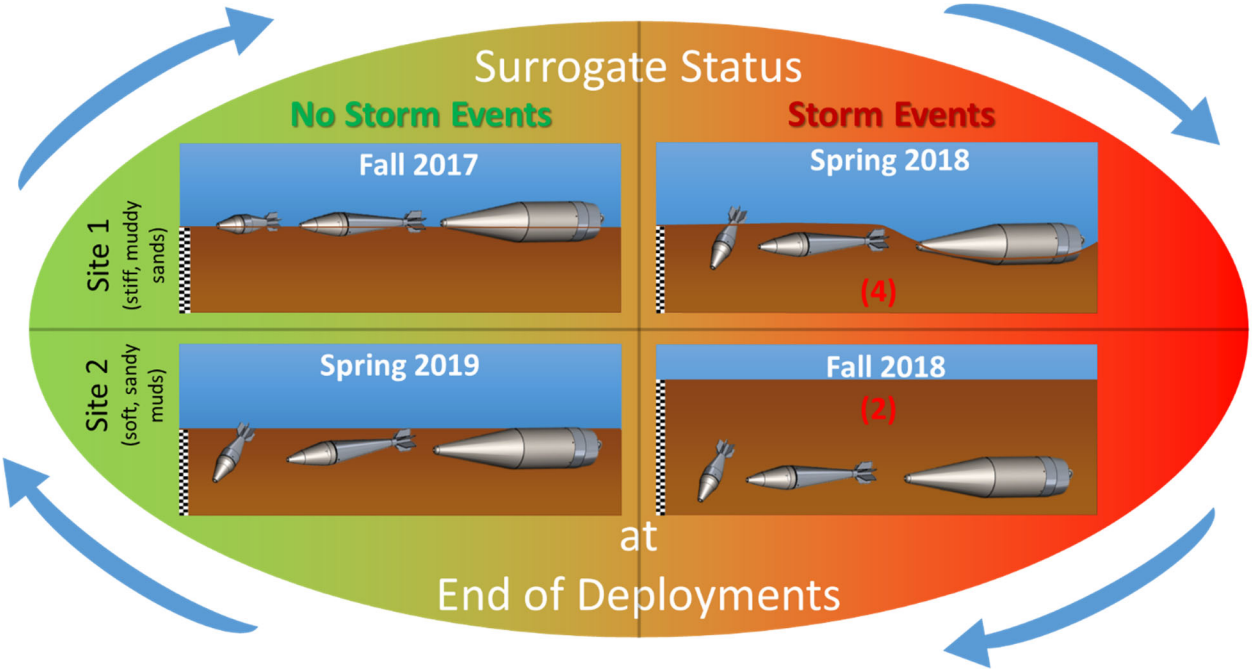



*Figure 2.3: Comparative diagram of surrogate status for each of the four field deployments. Note the difference in burial depth between Site 1 and Site 2 deployments under similar conditions.*

In absence of impact burial, the mechanisms for burial in cohesive sediments include scour burial, bearing capacity, and fluidization. Scour burial was observed by divers and in sonar imagery in the Spring 2018 deployment. Using a modified Shields parameter for mixed sediments (see Whitehouse et al., 2000), we adapted a mine scour burial model developed by Trembanis et al., (2007) for applications in cohesive sediments. Of the four deployments, good

agreement was found between the model and observations for both deployments at Site 1. For example, the model predicts 100-115% scour burial for all of the surrogates in the Spring 2018 deployment. Divers reported nearly 100% for the smaller surrogates, and while the 155mm were 50% buried, the surrogates sat recessed in large open scour pits. The departure between the scour model and the surrogate burial observed for Fall 2018 and Spring 2019 deployments, as well as a lack of observed scour pits observed in these deployments, implies other mechanisms may have contributed to surrogate burial in these deployments. We examined the potential for burial due to settling capacity, where the pressure exerted on the bed by the surrogates was estimated by using a simple Hertzian contact problem between a rigid cylinder and an elastic surface. The model was run for each surrogate and compared to the quasi-static bearing capacity (QSBC) profiles from site-wide penetrometer measurements. Maximum burial depth, estimated at the leading edge of the surrogate surface, is estimated to be the depth where QSBC >= $P_{max}$, or the depth at which the sediment bearing capacity exceed the pressure exerted by the object.

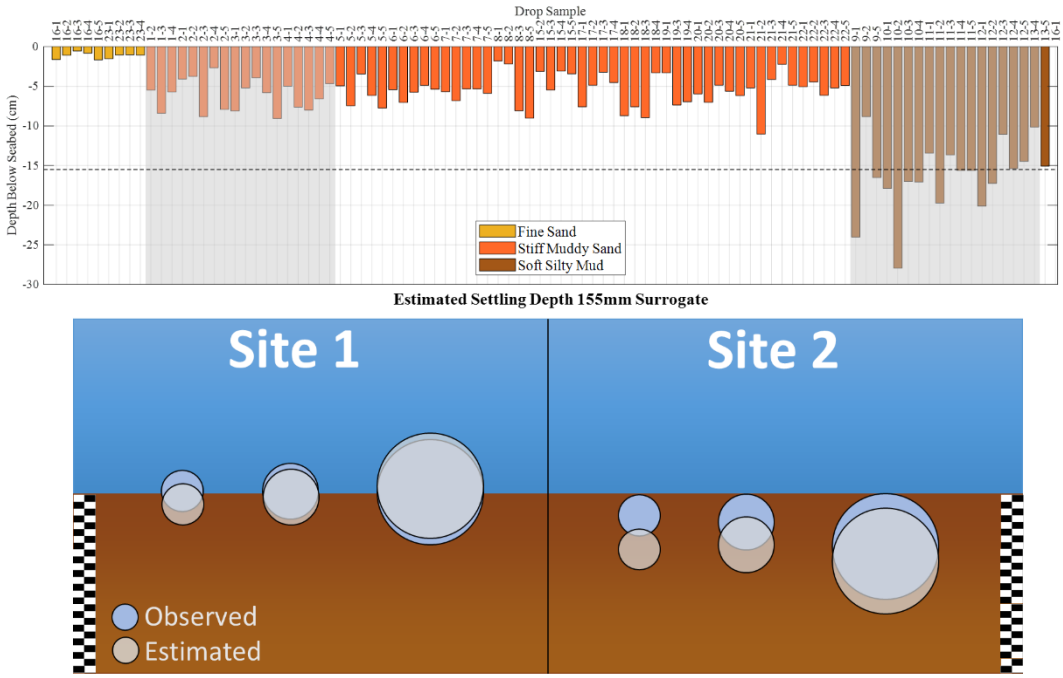



*Figure 2.4: Estimated surrogate burial by settling depth related to sediment bearing capacity using simply Hertzian contact model for rigid cylinders and elastic surfaces. Results for 155mm surrogate only are shown for each penetrometer sample with the samples taken at Sites 1 and 2 highlighted in gray. The bottom diagram illustrates the difference between model results and observations. Note that this does not account for the tilt of the 60mm (>45° pitch) mortars at Site 2, which would agree more with the estimated settling depth.*

The results for settling depth of a 155mm surrogate estimated at each penetrometer sample site are shown in Figure 2.4. The samples associated with Site 1 and 2 are highlighted. For example, the 155mm surrogates should sink to an average depth of 6.1 cm at Site 1 and 17.9 cm at Site 2, or 40% and 116% buried respectively, given no other force but the weight of the surrogate. This agrees well with observations provided by the divers. The smaller surrogates show greater deviation between estimated depth and observed depth, possibly due to the complex shape and orientation of the surrogates which are not accounted for in this basic estimate. Although this method ignores frictional forces and complex surrogate shapes, the estimated surrogate settling

depth due to the sediment bearing capacity does generally agree well with diver observations for the Fall 2017 and Spring 2019 deployments (no storms). This indicates that the weight and shape of the surrogate relative to the bearing capacity of the sediment may be a controlling factor in MEC burial in cohesive sediments, and corroborates previous observations from mine-burial studies (see Richardson et al., 2001).

During the Fall 2018 deployment, the surrogates buried significantly deeper than scour burial and bearing capacity would suggest. This enhanced burial is likely related to additional fluidization of the soft sandy muds in Site 2 during the Sept. 2018 ETC and following storm events. Increasing waves are known increase water flux into soft muds, causing a dilation of the sediments, fluidization, and associated reduction of the bulk density (Sahin et al., 2012; Soltanpour et al., 2009). The decrease in bulk density would therefore cause a corresponding drop in the bearing capacity, allowing the surrogates to settle further into the sediment. Following the storms, after wave energy decreases, the sediment would undergo settling and consolidation (Sahin et al., 2012). This process is similar to the bed fluidization and granular sorting mechanisms reported by Klammler et al., (2019).

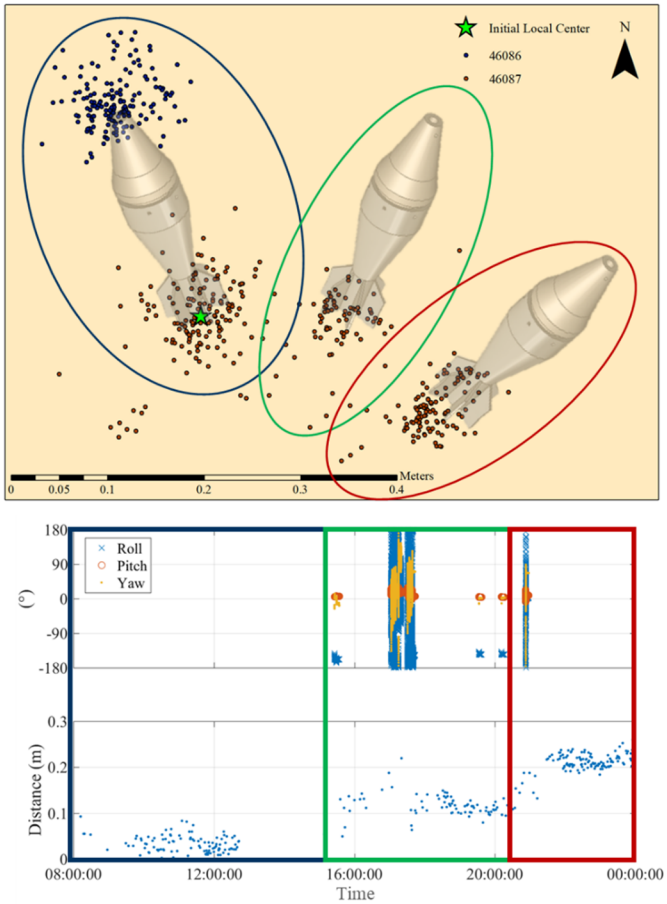



*Figure 2.5: VPS position estimates for surrogate 60A during nor'easter Toby (top) with contemporaneous IMU data from the onboard x-io NGIMU (middle). Displacement (bottom) was estimated from the acoustic tag located in the tail of the surrogate.*

Given extensive burial, no large-scale horizontal mobility was observed during MR-2730. In their studies of mobility in non-cohesive sediments, Traykovski and Austin (2017) and Calantoni (MR-2320) noted mobility in surrogates that were less dense than the surrounding sediment. The range of densities for the surrogates used in MR-2730, while slightly lighter by standards of actual munitions, were greater than that of the cohesive sediment at Sites 1 and 2. Thus, as found with munitions in non-cohesive sediments, burial mechanisms dominated with munitions denser than the sediment. It should be noted, however, that during storms, particularly nor'easter Toby, limited motion was recorded in the internal IMU of 60mm and 81mm surrogates. A detailed review of the VPS data also found that the motion of two 60mm mortars was captured during nor'easter Toby. The VPS data was compared to contemporaneous measurements from the onboard IMU for one of the surrogates (Figure 2.5). The combined series documents horizontal displace occurred in 2 episodes, moving from an initial position estimated early on March 20th. Most notable is the variation

of both yaw and rolling, suggesting that the 60mm surrogate was rolling back and forth in an arc. This corresponds to laboratory tests by Garcia (MR- 2410), who noted that mortar shaped surrogates would roll in an arc due to their shape. The final displacement of the surrogate was approximately 0.25m from initial placement.

A modified version of Rennie et al., (2017) object mobility threshold equations estimated that conditions during ETC events did momentarily exceed the theoretical threshold for motion, but scour and/or settling, as observed throughout the study, greatly reduced the potential for subsequent mobility. It should be noted that the longest duration of motion measured by the IMU were in the smallest, but densest surrogates (60mm) used in this study, while no motion was observed in the largest and least dense surrogates (155mm). It is possible that the form factor of the 60mm surrogates, with larger fin-to-body ratios, may influence the critical threshold for mobility, and that the surface area of the fins may provide more drag than the conical shape of the 155mm.

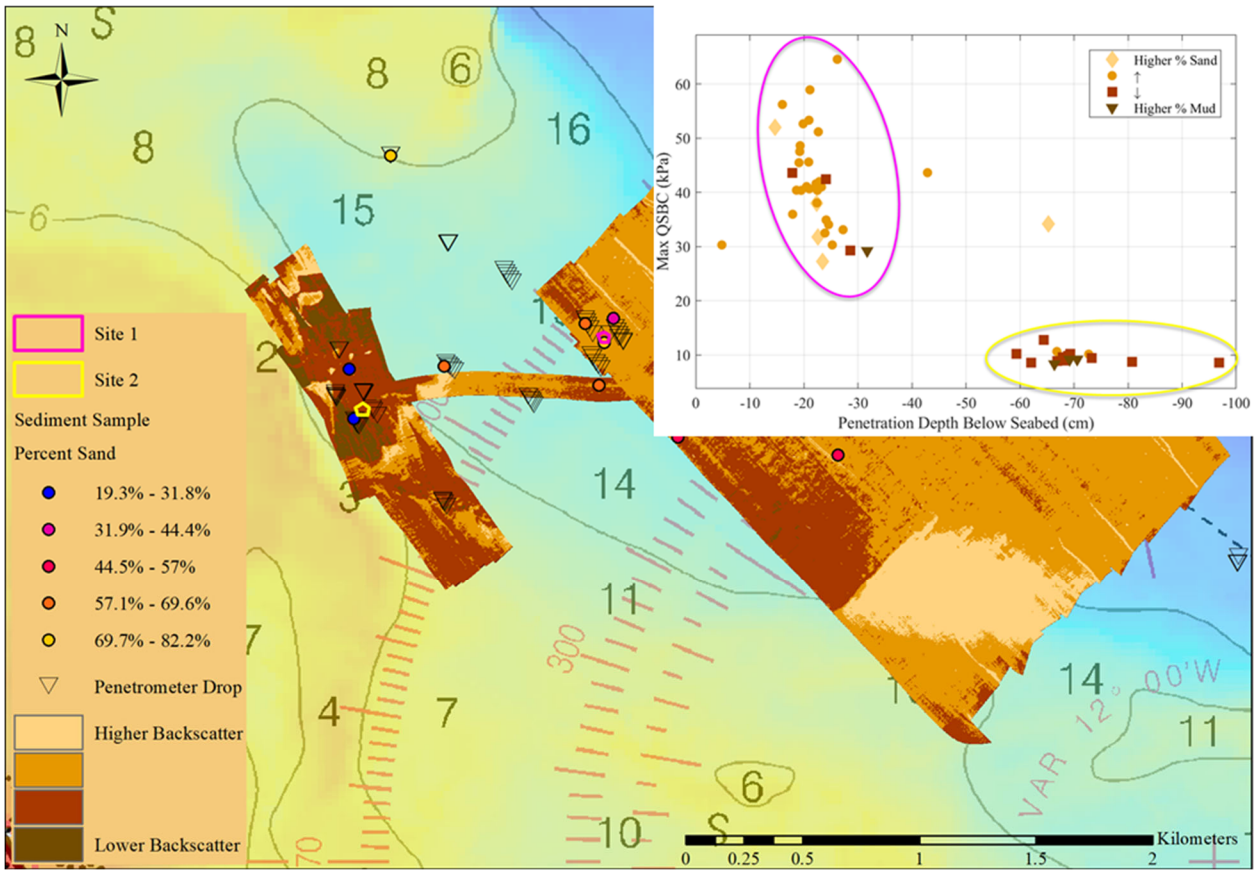



*Figure 2.6: Penetrometer measurements (inset) compared to sonar mosaic classification results. Note the 2 distinct groups reflecting higher percent sands (e.g. Site 1) and higher percent muds (e.g. Site 2).*

Sonar collected by the PMES was used to classify sediment distributions at the field sites. Sediment samples provided ground-truthing for image segmentation. The results, show in Figure 2.6, were compared to the processed sediment samples. The areas with higher backscatter (indicated as lighter classes) were assumed to contain higher percent sands. The classified raster values at each sample location were extracted and compared to the sand and mud fraction of each

sample. The results showed a strong agreement between sand / mud fraction and sonar mosaic class. While sonars have historically been used to classify surficial sediment distribution, allowing for extrapolation of sediment properties for wider coverage, Stark (MR18-1233) proposed that similar methods could be applied to predict shallow (e.g. upper 1m) sub-surface geotechnical properties. For this exercise, the sediment classes, as defined by sand/mud fraction, were extracted at overlapping penetrometer sample locations. The "classified" penetrometer results are shown in Figure 2.6 inset. Much like the penetrometer results from Sites 1 and 2, there are 2 distinct groups. Areas with higher backscatter (estimated higher sand fraction) tend to have higher QSBC and shallower penetration depth, while areas of lower backscatter (estimated higher mud fractions) show deeper penetration and lower QSBC. Similar results were found by Stark et al., (2016) in their study of Arctic nearshore marine sediments (see specifically Starke et al., 2016 Figure 12). The results are promising, and will be the subject of further analysis for SERDP project MR20-1480 report.

### 2.5. Implications for Future Research and Benefits

The data and results presented by this study lays the groundwork for future investigations of munitions mobility and burial in cohesive sediments. This study used a novel approach to track a suite of instrumented surrogate munitions deployed at two cohesive sediment sites in the lower Delaware Bay estuary. The Vemco (Innovasea) VPS acoustic tracking system provided near-continuous monitoring of surrogate lateral mobility and burial state, complemented by measurements from on-board IMU. The methods utilized in this study, in particular the Vemco VPS acoustic tracking system, can be easily implemented at any site.

Varying degrees of munition burial were observed by this study, but burial was the consistent result throughout. The fundamental conditions that varied between the deployments were the degree of near-bed forcing and the compositions of the sediment. In absence of sustentative forcing, burial occurred via settling; the bearing capacity of the surficial sediment could not support the weight of the surrogates. When exposed to higher energy, burial occurred via two mechanisms dependent upon the geotechnical properties of the sediment. In mixed-cohesive muddy sands, burial occurred through scour, with large scour pits imaged in side-scan sonar and verified by divers. In softer sandy muds, the surrogates sank through layers fluidized under increasing wave energy. Thus, this study finds that sediment bearing capacity is an important predictor for surrogate burial, and the Hertzian contact model introduced here provides a simple method to predict burial due to bearing capacity.

The ability to tie sediment geotechnical properties such as bearing capacity to sonar classification / surficial sediment distributions maps, as demonstrated in this study, has wide-ranging implications for FUDS site management. Extrapolating subsurface properties based on surficial sediment distributions will reduce the amount of geotechnical sampling required and allow for modeling of surrogate burial across a wide spatial domain. Combined with historical analysis of storm conditions, site-wide geotechnical properties and modeling will provide important threshold conditions for the informed management of munitions response sites, aiding managers in identifying when additional site investigations may be most needed.

# 3. Objective

There remains a recognized need for a better quantitative understanding of the impact of coastal environments on munitions and explosives of concern (MEC) mobility and burial (MRSON-17-01). Recent studies have investigated the mobility and detection of MEC in sandy coastal areas (Calantoni SERDP MR-2320, Traykovski and Austin, 2017, Puleo MR-2503), but a significant data gap was identified regarding MEC in shallow, cohesive-sediment environments (SERDP Munitions Mobility and Modeling Workshop, Dec. 8-9, 2015). In non-cohesive settings, MEC mobility or burial is predicated on the density of the munition relative to sediment density; burial is predicted when density of the surrogate exceeds that of the sediment, through scour burial or bed fluidization (Traykovski and Austin, 2017; Klammler et al., 2019). In mixed and cohesive sediments, munitions phenomenology is less clear and thus problematic for MEC site management: a review of catalogued Formerly Used Defenses Sites (FUDS) indicate a substantial proportion of military testing ranges (139 sites) with potential MEC are partly or completely in tidal environments with cohesive sediments (USACE 2007 FUDS). No recent observations are available with respect to MEC mobility and burial in cohesive settings.

We address this data gap though observations of MEC mobility and burial in cohesive-sediment environments. The primary objectives of this study were to:

- Monitor the mobility and behavior of sensor-integrated surrogate munitions in muddy environments using a high-accuracy acoustic positioning system.
- Observe and compare surrogate munition response to hydrodynamic forcing through instrumented bottom frame time-lapse hydrodynamic data and sonar imagery.
- Monitor morphological site changes through repetitive geophysical site surveying and benthic sediment sampling.

To accomplish these objectives, we deployed a suite of surrogate munitions at 2 cohesive sediment sites in the lower Delaware Bay Estuary. Surrogates were monitored for changes in mobility and burial using a Vemco (Innovasea) VPS acoustic tracking system and inertial motion units (IMU). Time-series acoustic imagery and hydrodynamic sensors were also deployed to characterize MEC response to varied hydrodynamic conditions. A series of repetitive surveys were conducted using a hull-mounted, high-resolution phase-measuring bathymetric sonar and an autonomous underwater vehicle (AUV) equipped with a magnetometer. In total, we conducted 4 deployments between 2017 and 2019, spanning 226 days. Six separate storm events were recorded during the deployments, leading to wide-spread sediment transport and episodes of surrogate burial. No large-scale horizontal mobility of surrogates was observed.

The results from this study will inform key parameters for MEC behavior in storms and muddy environments for integration into the existing expert system modeling of MEC burial and mobility (e.g. Underwater Munitions Expert System, Rennie, 2017; SERDP Munitions Mobility and Modeling Workshop, Dec. 8-9, 2015). Our observations will expand our knowledge into an understudied but abundant environment with respect to munitions contamination, and aid in understanding historical and present conditions at estuarine FUDS. All results from the field experiment and model parameterization will be made available for existing MEC mobility and burial models such as UnMES.

# 4. Technical Approach

## 4.1. Background

Hydrodynamic and morphological conditions typical in shallow, muddy environments pose problems for predicting MEC behavior and detection. While the behavior of small, man-made objects in non-cohesive, sandy substrates has been studied (Traykovski and Austin, 2017; Calantoni SERDP MR-2320; Puleo MR-2503) and remains under consideration (Traykovski MR-2729, Calantoni MR19-1317), the fundamental differences in sediment dynamics between cohesive and non-cohesive sediments complicate direct translation of these observations to MEC behavior in muddy environments. In non-cohesive sediments, sediment transport occurs on the granular level, and the requisite stresses to initiate transport are predictable by grain size. The stresses required to initiate cohesive sediment transport are less predictable due to particle-to-particle attraction via van der Waals forces. Characteristics such as sand-silt-clay composition, water content, compaction, and bulk density may influence the stresses needed to initiate erosion and transport (Jacobs et al., 2011; Van Prooijen and Winterwerp, 2010). Once in transport, the differences between cohesive and non-cohesive sediments remain. Non-cohesive particles travel as bedload (through individual grain rolling, sliding, or saltation) or are entrained as suspended load, while in cohesive sediments, transport may occur as suspended flocculate particles, which both aggregate and dissipate with particle interaction (Letter and Mehta, 2011), or may even travel as fluidized mobile mud beds (Inman and Jenkins, 2002). The threshold for sediment erosion and transport of non-cohesive sediments are nearly equivalent, while far less force is required to keep cohesive sediments in transport than is required for erosion. This relationship is illustrated in the classic Hjulström curve (Figure 4.1).

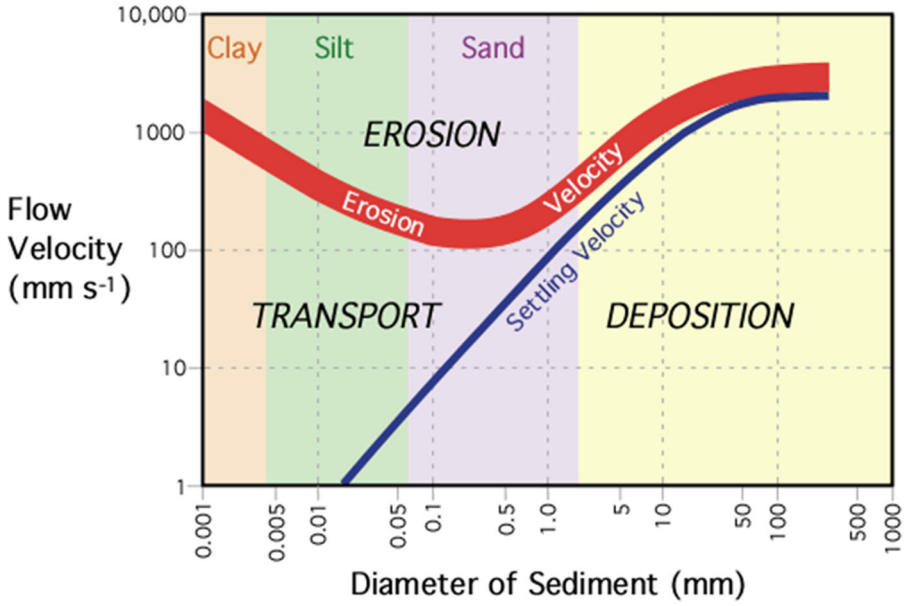



*Figure 4.1: Variation of the Hjulström curve for sediment transport (see Hjulström, 1935).*

#### 4.1.1. Object Burial

The notable differences in cohesive and non-cohesive sediment properties extend into object mobility and burial. Extensive research exists on MEC or mine-like "short cylinder" scour burial in non-cohesive sediments (Traykovski et al., 2007; Trembanis et al., 2007; Catano-Lopera and Garcia, 2006). Accelerated local flow velocity and turbulence caused by the object disrupting near bed currents results in increased local sediment transport and "scouring" of sediments away from the object; eventually the object will fall into the scour pit and continue to scour until the object presents a similar roughness to the surrounding seabed (Traykovski et al., 2007). Looking at short cylinders, Whitehouse (1998) modeled the rate of scour with empirical relationships based on a non-dimensional critical threshold for sediment motion (Shields Parameter). This relationship has been successfully adopted and tested in mine-burial and MEC applications (Rennie et al., 2017; Trembanis et al., 2007). Given the comparatively higher threshold for erosion of cohesive sediments, we would then anticipate less scour in cohesive sediments than in non-cohesive sediments at an equivalent flow velocity and duration.

When scour occurs, the potential for burial increases. In areas of strong tidal influence, such as estuaries and shallow coastal regions, fluidized muds have been shown to fill in scour pits around seabed mines, resulting in transient burial and exposure (Traykovski et al., 2007; Inman and Jenkins, 2002). Baeye et al., (2012) found transient mine burial was linked to high-concentrated mud suspension in high-turbidity areas; nearly complete mine burial was found to occur during slack tides in spring tidal cycles. The resulting high probability that mines would be missed during tracking surveys in similar environments led the authors to conclude further experiments were necessary to characterize mine burial with mud suspensions of various thickness and stability (Baeye et al., 2012).

Recent work in MEC suggests that scour is not the only mechanism for burial of MEC in non-cohesive sediments. Klammler et al., (2019) noted burial through scour and granular sorting mechanisms. Granular sorting occurs in high energy conditions where the surficial sediment is in active transport (Calantoni and Thaxton, 2008). If an object is denser than the surrounding sediments, it will sink until reaching a basement where no active sediment transport is occurring (Klammler et al., 2019). Objects can therefore bury deeper than theoretically possible with scour burial, where burial is only expected to occur such that the object presents similar roughness to the surrounding seabed (i.e. level with the far-field seabed surface). As cohesive sediments do not transport on a granular level, such a mechanism is unlikely in theory. However, under increasing wave height, mud layer thickness has been shown to increase (Soltanpour et al., 2009), with a corresponding increase in water content and decrease in sediment bulk density (Sahin et al., 2012). Much as with granular sorting, denser objects should sink through the fluidized mud until reaching a denser or stiffer mud layer.

The rheology of cohesive sediments may be predictive of object burial. As noted above, objects of sufficient density may sink through highly fluidized muds, and thus burial can be related to the sediment bearing capacity. Should the buoyant weight of the object exceed the bearing capacity of the cohesive sediment bed, the bed will undergo plastic deformation, allowing the object to effectively sink into the sediment over time (Richardson et al., 2001). This behavior has been observed with seabed mines (Inman and Jenkins, 2002). In contrast to fluid mud beds, mines in stiff muds were found to only undergo slight scour and partial burial (Inman and

Jenkins, 2002). There, impact burial was observed to be the largest contributor to mine burial, not subsequent hydrodynamics.

4.1.2. Object Mobility

While there is extensive research on scour and burial, munitions mobility is a recent topic of research. Mobility is defined here as the horizontal movement of an object, as opposed to the vertical movement of an object undergoing scour and burial. In theory, MEC-like objects may be treated much like sediment, in that sufficient hydrodynamic forcing should overcome an objects threshold for mobility, resulting in transport. However, the degree of forcing required to exceed an objects critical threshold may exceed the critical threshold for sediment transport, thereby initiating scour. Thus, scour and mobility should always be competing processes. To induce mobility, SERDP studies have experimented with varying surrogate MEC density (Traykovski and Austin, 2017; Calantoni MR-2320) to determine thresholds for mobility vs. scour/burial in non-cohesive sediments. Traykovski and Austin (2017) found that only MEC surrogates with low object to water density ratios were mobile ($\rho_{obj}/\rho_w$ < ~2), while denser MEC ($\rho_{obj}/\rho_w$ > ~2.75) were more likely to bury *in situ,* unless under extreme forcing events. Although parameterizing the relationship as MEC density to sediment grain density ($S_m = \rho_m/\rho_g$), Calantoni (MR- 2320) had similar results, finding that surrogates with $S_m$>1 would always bury after intense transport regimes in regions of stable bathymetry.

Should object mobility occur, Rennie et al., (2017) related incipient MEC motion to the object mobility parameter:

$$\Theta_U = \frac{U^2}{gD\left(\frac{\rho_{obj}}{\rho_w} - 1\right)}$$

where *U* is near-bed velocity, *g* is gravitational force and *D* is the object diameter. The critical threshold for object mobility is based on the ratio of the diameter of the MEC to the relative roughness of the seabed (k), given by the equation:

$$\Theta_{Ucrit} = a_1\left(\frac{D}{k}\right)^{b_1}$$

where $a_1$ and $b_1$ are empirically derived coefficients. Seabed roughness in the case may be granular roughness (e.g. Nikuradse Roughness), but also bedforms (e.g. ripples) or even object-induced scour. Increasing roughness increases the critical threshold for object mobility. Consequently, object mobility was found to drop drastically in sediment transport regimes where scour dominated, i.e. non-cohesive sediments (Friedrichs, MR-2224). In mixed and cohesive sediments, munitions mobility phenomenology is less clear. While burial is expected in soft sediments, and therefore no mobility, Inman and Jenkins (2002) suggest both muddy sediment layers and objects may move as a unit during intense storm events. In stiff cohesive sediments, where scour and burial are less likely, the potential for mobility increases. Calantoni observed mobility of a surrogate sitting on a stiff cohesive layer, until the surrogate reached a sand pocket and buried (MR-2320).

## 4.2. Materials and Methods

To meet the study objectives, we defined 3 primary tasks and 1 optional task. The first task included the preparation of surrogate munitions and testing of an acoustic Long-Baseline (LBL) network. The second task encompassed 2 field deployments. The third task included data analysis, data distribution, and reporting. Depending on the results of Task 1 and 2, a fourth optional task could be exercised, serving as a fallback should no energetic events be captured in the Task 2 deployments. The fourth task included 2 additional field deployments. As discussed below (section 4.2.5), the fourth task was exercised by SERDP.

### 4.2.1. Task 1 – Tracking and Motion Sensor Technology Design

Task 1 was divided into two subtasks: 1) the design and fabrication of smart surrogate munitions, and 2) the development and testing of an acoustic tracking network. Each subtask had a primary objective. The "smart" munitions were to be integrated with motion tracking sensors (IMU's) capable of measuring movement with high temporal and spatial resolution. To measure gross movements, the acoustic LBL network had to be capable of detecting multiple surrogates over a larger spatial and temporal scales. These objectives guided Task 1 efforts. Each subtask is described in detail below.

#### *4.2.1.1. Surrogate MEC Development*

The question of how to appropriately design and equip smart munitions to allow for high precision motion tracking while retaining similar characteristics to actual munitions is an ongoing discussion in SERDP/ESTCP (SERDP Munitions Mobility and Modeling Workshop June 20-21, 2017). Drawings illustrating basic munitions geometry are available from military manuals, but specific characteristics inherently relevant to munitions mobility (e.g. density, center of gravity, etc.) have not been made readily available until recently. Calantoni MR-2320 catalogued numerous practice and inert munitions and generated estimated density distributions for common MEC types. In a recent SERDP Munitions Mobility and Modeling Workshop (June 20-21, 2017), the consensus was to focus on densities within the estimated distributions of actual munitions (>2800 kg/m$^3$), since the majority of a MEC would fall within that parameter space.

In the 2015 SERDP Munitions Mobility and Modeling Workshop (Dec. 8-9, 2015), discussions focused on surrogate payload sensors for tracking motion and mobility. Inertial Motion Units (IMU) are a primary sensor for recording object motion, and are available in small form factors. A number of SERDP funded studies (Traykovski and Austin, 2017, Calantoni MR-2320, Puleo MR-2503) utilized the X-io IMU, which is capable of recording both orientation and movement up to 512 Hz. The small form factor of this unit (57x38x21mm) and relatively low cost make this unit ideal for surrogates that may potentially be lost or destroyed. It was also suggested that surrogates may be fitted with acoustic "pinger" tags in order to minimize loss. These tags emit sound at specific frequencies, allowing surface mounted or diver-held units to navigate to the tags' location through signal strength detection and directional receivers. A more advanced version of this concept utilizes Ultra-Short Baseline (USBL), which derives position estimates of surrogates. Traykovski and Austin (2017) developed USBL transponders for periodic tracking of surrogates. This method requires a larger acoustic transponder fitted to the surrogates and a direct line of site for accurate position estimates (i.e. not buried). The latter issue was solved by

attaching the USBL transponders to floats and connecting them to the surrogates via short cable. There is question over the influence of this design on surrogate munition behavior, and this method requires repetitive surveys to the field site via surface vessel or autonomous craft to log surrogate positions, which are often limited by surface conditions. Thus, major mobility or burial events, driven by strong hydrodynamic forcing, are often missed and gross movements are only recorded after the fact. Other sensors that can be fitted include SLAM sticks, which record acceleration at very high sampling rates, and are ideal for capturing mobility in high energy environments (e.g. surf zone studies; see Puleo MR-2503). On-board optical sensors and visual markers, such as bright paint or flashing LED's, were also used by Puleo (MR-2503) to determine orientation and burial, but these methods require clear visual conditions.

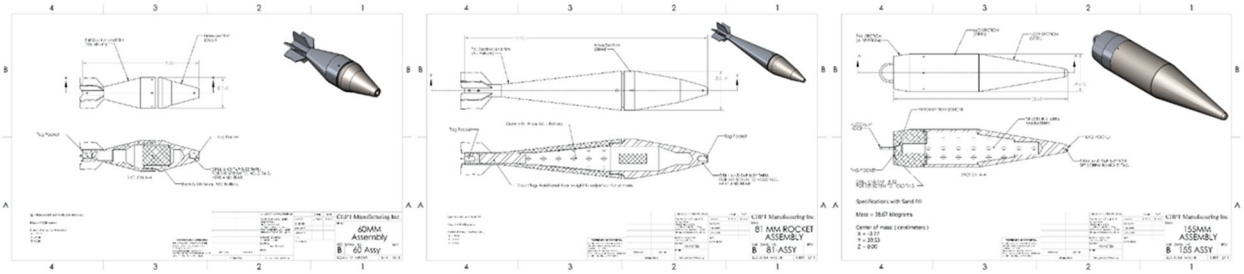



*Figure 4.2: Surrogate MEC design plans for 60mm mortar, 81mm mortar, and 155mm artillery shell.*

The discussions from the SERDP Munitions Mobility and Modeling Workshops led to the selection of three munition types for this study, each of which were identified as munitions of interest (MOI) by the USACE. These were 60 mm and 81 mm mortars and 155 mm artillery shells (Figure 4.2). The surrogates were designed to meet best known characteristics of the respective MEC type, including a minimum density within the estimated density distribution of measured MEC (from Calantoni MR-2320). The surrogates were designed with open internal cavities, allowing for customization and variation of density within the MEC density parameter space through variable fills. The open cavities would also accommodate x-io IMU's and additional batteries to extend deployment duration. The 155mm were also designed to house a water-level pressure sensor and data logger, both used also by Puleo (MR-2503). Externally, each surrogate was designed with cavities at either end to fit Vemco acoustic locater tags, which would serve as the primary surrogate tracking method during field deployments (see section 4.2.1.3). Optical sensors and visual markers were not fitted to the surrogate munitions; the depth and turbidity characteristic of the proposed field site would render these methods ineffective.

#### *4.2.1.2. Surrogate Fabrication and Instrumentation*

The surrogates were fabricated by CHPT Manufacturing, Inc., a local company that also fabricated surrogates for Puleo (MR-2503). The surrogates were constructed from steel and aluminum, the former to allow for detection by magnetometer, and the latter to lighten surrogate weight and allow for varying densities within the estimated density parameter space. Each surrogate was undercoated with anti-corrosion primers and painted with anti-biofouling paint. White paint was chosen to maximize contrast from sediments and allow for easier visual identification / discrimination by divers or remotely operated vehicles (ROV). Each surrogate was also clearly labeled "INERT" in case of unintended interaction with commercial fisherman or the wider public (Figure 4.3). For Task 1, three 60mm, four 81mm, and three 155mm

surrogates were manufactured and prepared for the study. Four 4.2-inch surrogates were also added to the study for Task 4. The physical properties for the surrogates are shown in Table 4.1.




*Figure 4.3: Ten surrogate munitions prepared for deployment on Nov. 2, 2017. Four 4.2-inch mortar surrogates were later added to the suite.*

*Table 4.1: Properties of surrogates used in MR-2730.*

| Surrogate | Sensors | Material | Density (kg/m3) | Specific Gravity (saltwater) |
|---|---|---|---|---|
| **155mm** | IMU; Pressure Sensor | Steel/Aluminum/Lead | 3280-3590 | 3.2-3.5 |
| **4.2-inch** | IMU | Steel/Aluminum/Lead | 3170-3420 | 3.1-3.3 |
| **81mm** | IMU | Steel/Aluminum/Lead | 3640-3820 | 3.5-3.7 |
| **60mm** | IMU | Steel/Aluminum | 3970 | 3.9 |

Each surrogate was fitted with an IMU sensor. Previous SERDP studies (Calantoni SERDP MR-2320, Traykovski and Austin, 2017, Puleo MR-2503) utilized the x-io IMU, a small, self-contained IMU with micro-SD card logging and Li-Ion battery. The model used by those studies was replaced by the NGIMU (Next Generation IMU), which was selected for use in this study. The xi-o NGIMU specifications are included in Table 4.2. Despite upgrades from the previous generation, including lower latency, the battery life of the 1000 mAh battery was too limited (~17 hours bench test) for the duration of the study. However, the NGIMU is also configurable for motion trigger wake up and sleep mode if no motion is detected after a preselected duration. This increases the battery life considerably at the cost of slight latency in initial motion recording. To maximize battery life, all NGIMU were configured to motion trigger wakeup, recording raw sensors at 20 Hz. After 5 minutes, if no further motion was detected, the IMU would return to a sleep mode.

To improve battery-life with the previous model, Calantoni (MR-2320) fabricated custom battery packs, fitted with multiple cellphone-style Li-ion battery packs controlled by a circuit module. After discussion with the designer of the NGIMU, it was determined that a simpler workaround might be achieved by using off-the-shelf USB battery packs, which could plug directly into the

micro-USB slot on the NGIMU board. These come in a variety of sizes and capacities, which allowed for maximizing battery life and optimizing space in the smaller surrogates. Bench top tests indicated that this method should be sufficient to extend the battery life for the planned deployment duration (8 weeks) when combined with motion triggered recording. Three battery capacities (3300 mAh, 8000 mAh, and 23000 mAh) were selected and fitted to the surrogates. For the 60mm and 81mm surrogates, the battery packs were stripped of their housing and fitted to mounts fixed in the tail cone. For the 155mm, the batteries were fixed to a longitudinal plate near the center of mass of the surrogate. The IMUs were fitted to plates and placed as close to the center longitudinal axis and vertical axis as possible (Figure 4.4c). In the 60mm (Figure 4.4a) and 81mm (Figure 4.4b) mortars, the IMUs were fitted to plates in the nose cone section, due to spatial constraints.

At the suggestion of Puleo (MR-2503), the 155mm surrogates were also fitted with TE Connectivity LM Series pressure sensors, which are capable of ±1% accuracy and wide operating temperature range. The LM series require a nominal voltage of 5V, which are the same output as USB battery packs. An additional 23000 mAh USB battery was configured to power the pressure sensor and fitted to the to 155mm longitudinal plate. A 1/2-14 NPT threaded slot was fabricated in the tail-cone of the 155mm to fit the pressure sensors, with 4 small outlet holes drilled in the cone to allow seawater exchange. The pressure sensor output, in ratiometric voltage, was logged by a Madgetech Volt101A data logger with battery, capable of recording over 2 million readings with a 10yr battery life. The pressure sensor and data logger were bench tested successfully. All configuration and testing of the surrogates was completed in Oct. 2017.

*Table 4.2: xi-o NGIMU Specifications.*

| ***Sensors*** | | | ***Communication*** | | |
|---|---|---|---|---|---|
| Gyroscope | Range: | 2000°/s | USB | Yes | |
| | Sample Rate: | 400 Hz | Serial | Yes | |
| | Resolution: | 16-bit | Wireless | Wi-Fi | |
| Accelerometer | Range: | 16 g | ***On-Board Logging*** | | |
| | Sample Rate: | 400 Hz | Memory | Micro SD Card | |
| | Resolution: | 16-bit | USB Download | Yes | |
| Magnetometer | Range: | 1300 uT | ***Power*** | | |
| | Sample Rate: | 20 Hz | External Supply | 4.5-6 V | |
| | Resolution: | 0.3 uT | Charging | USB or External Supply | |
| Pressure | Range: | 300-1100 hPa | Battery Life | 4-12 hours | |
| | Sample Rate: | 25 Hz | ***Physical*** | | |
| | Resolution: | 24-bit | Board Only | Size: | 50 × 33 × 8 mm |
| Humidity | Range: | 0-100% | | Weight: | 10 g |
| | Sample Rate: | 25 Hz | With Housing | Size: | 56 × 39 × 18 mm |
| | Resolution: | 0.01% | | Weight: | 46 g |
| ***Outputs*** | | | | | |
| **Quaternion, Rotation Matrix, Euler Angles, Linear Acceleration, Earth Acceleration** | | | | | |
| **Update Rate** | 400 Hz | Static Accuracy (Pitch/Roll) | <1° RMS | Static Accuracy (Heading) | <2° RMS |

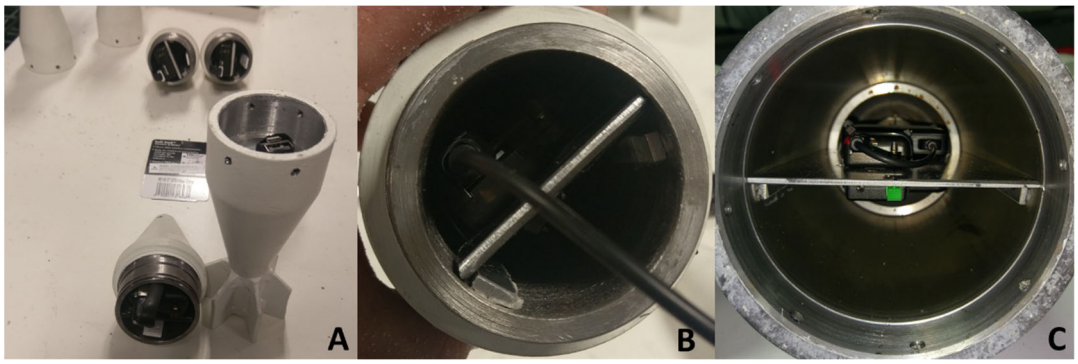


*Figure 4.4: IMU and battery configurations in 60mm (A), 81mm (B), and 155mm (C) surrogates.*

Following Task 2, battery performance was evaluated. The USB battery packs performed adequately, but were found to be susceptible to moisture and shock. For Task 4, the packs were replaced with more-efficient and smaller Li-Ion battery packs (3500, 5300, and 15600 mAh) plugged directly to the IMU boards via Molex connectors. Additionally, a fourth surrogate type, 4.2inch mortar (Figure 4.5), was introduced to the study based on recommendations from Calantoni MR-2320 (pers. comm. Joe Calantoni, U.S. Naval Research Laboratory). The 4.2-inch surrogates were also equipped with x-io NGIMU powered by 10400 mAh Li-ion battery packs. Due to delays in fabrication, the 4.2-inch surrogates were only available for the final field deployment in 2019.

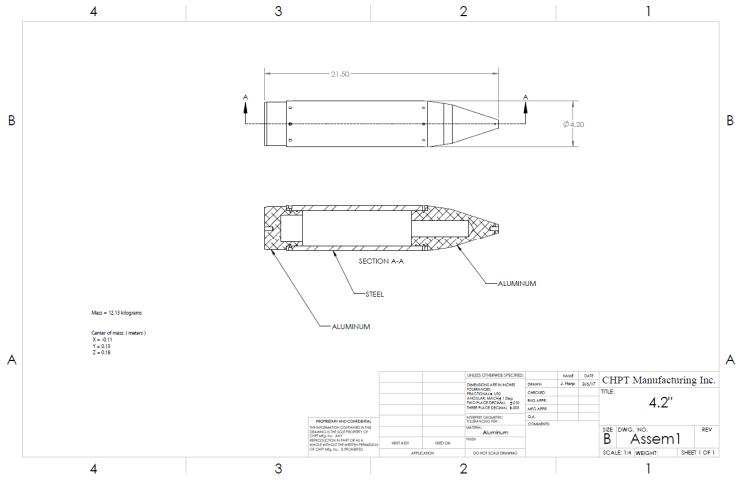


*Figure 4.5: Diagram of 4.2 inch mortar surrogate.*

#### *4.2.1.3. Vemco Positioning System*

The acoustic tracking system for this study needed to function as a Long-Baseline (LBL) system. LBL systems are industry-standard equipment for locating and tracking submerged vehicles, particularly in deep water conditions typical to the oil and deep mineral industries. A typical LBL system is composed of a grid of acoustic transponders, which use active acoustics to track underwater movement of a target receiver. Each LBL transponder is surveyed to a precisely known position, then utilizing the difference in signal arrive time from an acoustic pulse it is possible calculate the position of a tracked object. Positional accuracy of the LBL transponders

are paramount, as well as the physical conditions of the site, which may affect sound speed within the grid (e.g. thermoclines, salinoclines, etc.). Positional error can be constrained by using precise time synchronization techniques and high-resolution GPS. Typically, LBL technologies are large, expensive systems that require considerable time and effort to set up and run effectively. Deployment duration is often limited to a few days or weeks, and requires constant monitoring via wireless or satellite communications. More modest systems have been developed for smaller AUV or ROV tracking, but these systems still require larger transponders, have limited endurance (hours to days), and are designed to be constantly monitored. As such, traditional LBL systems are not ideal for a long-term munitions tracking study.

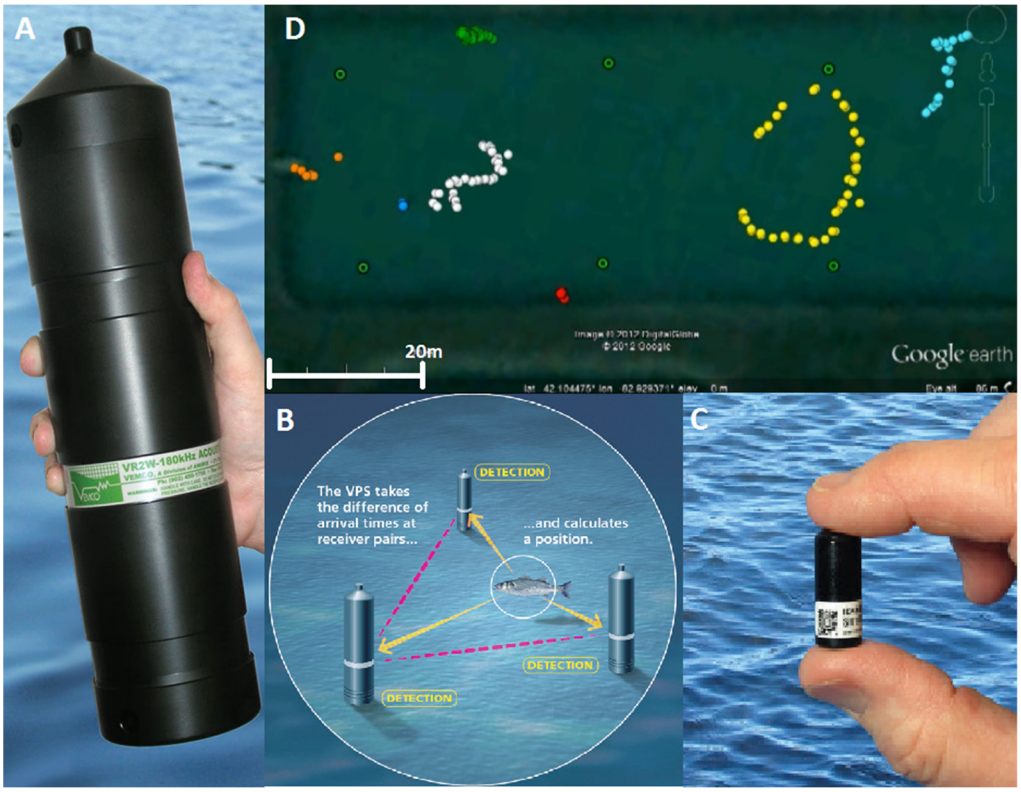



*Figure 4.6: Vemco Position System. HR2 Acoustic Receivers (A) are placed in a network (B) that records the difference in arrival times of small acoustic tags (C). Multiple tags can be tracked over time (D) with position accuracies down to 10cm (Images courtesy of Vemco).*

While traditional LBL systems were excluded from use in this study, modified acoustic positioning systems, such as those developed for fisheries studies, were identified as potential candidates. Although fishery studies typically cover large areas (>1 sq. km), recent systems have been modified for precision tracking over smaller study sites. The Vemco Positioning System (VPS), manufactured by Vemco (now part of Innovasea), was originally developed for tracking acoustically tagged biology with meter-level positional resolution. The system is capable of simultaneous positioning of multiple tags within an acoustic receiver network (Figure 4.6). The VPS is based off of previously developed and proven Vemco VR2W (69 kHz) acoustic receivers, which greatly reduces overall expense. These systems can be deployed for up to 7 months in freshwater, estuarine, coastal or even open continental shelf environments. Several recent biological tracking studies (Piraino and Szedlmayer, 2014; Roegner and Fields, 2014) used Vemco VPS with high degrees of success; one study by Piraino and Szedlmayer (2014) was

able to capture fine-scale movements of red snapper with ~1-m accuracy using the previous VR2Tx configuration. With the newer HR2 (180 kHz) receivers, the VPS is capable of positional accuracy of 10 cm. Since the acoustic tags are designed to be surgically placed within biota, the tags come in small form factors ideal for placement on the surrogate munitions. Each tag measures 9 mm x 25.5 mm in size, has extended battery life (>220 days), and can be turned on and off to extend shelf life. The tags emit two different coding schemes, which allows Vemco data analysts to filter out and exclude erroneous positions attributable to multipath propagation. Furthermore, the codes are emitted at rates that allow for multiple positions per minute. The coding specifications used in MR-2730 are shown in Table 4.3. The combination of battery life, form factor, customization, and relative low-cost to typical LBL systems led to the selection of the VPS for use in this study.

*Table 4.3: MR-2730 Vemco V9 acoustic tag specifications.*

| Usage | Tag Model | Code Type | Frequency (kHz) | Min Delay (s) | Max Delay (s) |
|---|---|---|---|---|---|
| **Surrogate** | V9-2x-180k-1 | A180 | 180 | 250 | 350 |
| | V9-2x-180k-1 | H170 | 170 | 40 | 50 |
| **Reference (Config 1)** | V9-2x-180k-3 | A180 | 180 | 70 | 130 |
| | V9-2x-180k-3 | H170 | 170 | 6 | 8 |
| **Reference (Config 2)** | V9-2x-180k-3 | A180 | 180 | 270 | 330 |
| | V9-2x-180k-3 | H170 | 170 | 25 | 35 |

VPS data processing was handled by Vemco, who provided precision positioning for each acoustic tag. Vemco has over 6 years of experience processing VPS data and has developed a robust workflow for calculating positioning from the acoustic tags. This includes data products useful to this study, such as horizontal positioning error (HPE), which allowed us to refine the results and establish positional accuracy error and confidence. Additionally, the Vemco receivers record all of the raw detection data with millisecond time resolution, which is made available in ASCII readable text files for 3rd party processing and verification.

#### *4.2.1.4. Vemco Position System Testing and Configuration*

In collaboration with Vemco, preliminary lab and field experiments of the VPS receivers were conducted prior to field deployment to test for the effects of burial, steel housing, acoustic noise, and multi-path propagation on positional accuracy and acoustic tag performance. In Sept. 2016, a VPS grid was set up and tested in the University of Delaware Marine Operations Base boat basin. The boat basin provided an ideal setting for testing the VPS array. The test area consisted of highly fluidized mud overlaying a stiff clay mud in a shallow (1.5-m depth at the array site), brackish, and an often acoustically noisy environment. The VPS array consisted of four loaner HR2 receivers set up in a square array measuring roughly 20m on a side. The HR2 receivers were mounted to stakes and fixed approximately 1m above the bed. A single reference tag was fixed to a cinder block and placed in the center of the array. To serve as the surrogate, a section of steel pipe (30.5 cm x 10.2 cm) was equipped with 2 acoustic tags, mounted on either end of the pipe. The surrogate was initially set on the surface of the bed within the grid. RTK GPS positions were taken at the VPS receivers, reference tag, and surrogate at the start of the test. The grid was left running overnight to test for multipath prorogation across a tidal cycle (ebb-

flood-ebb in a semi-diurnal tide). In the morning, the surrogate was pushed into the stiff clay mud to test for acoustic signal loss with burial. After several hours, the surrogate was excavated, and moved throughout the grid to test the VPS's ability to track a mobile object. Periodically, the surrogate was placed on bed and left for 5 minutes, during which an RTK GPS position was taken. The surrogate was moved and placed within, on the boarder, and at distances of approximately 5x, 10x and 20x water depth outside of the grid. Final RTK GPS positions were taken at the HR2 receivers, reference tag, and surrogate before removal. The data was sent to VPS for processing.

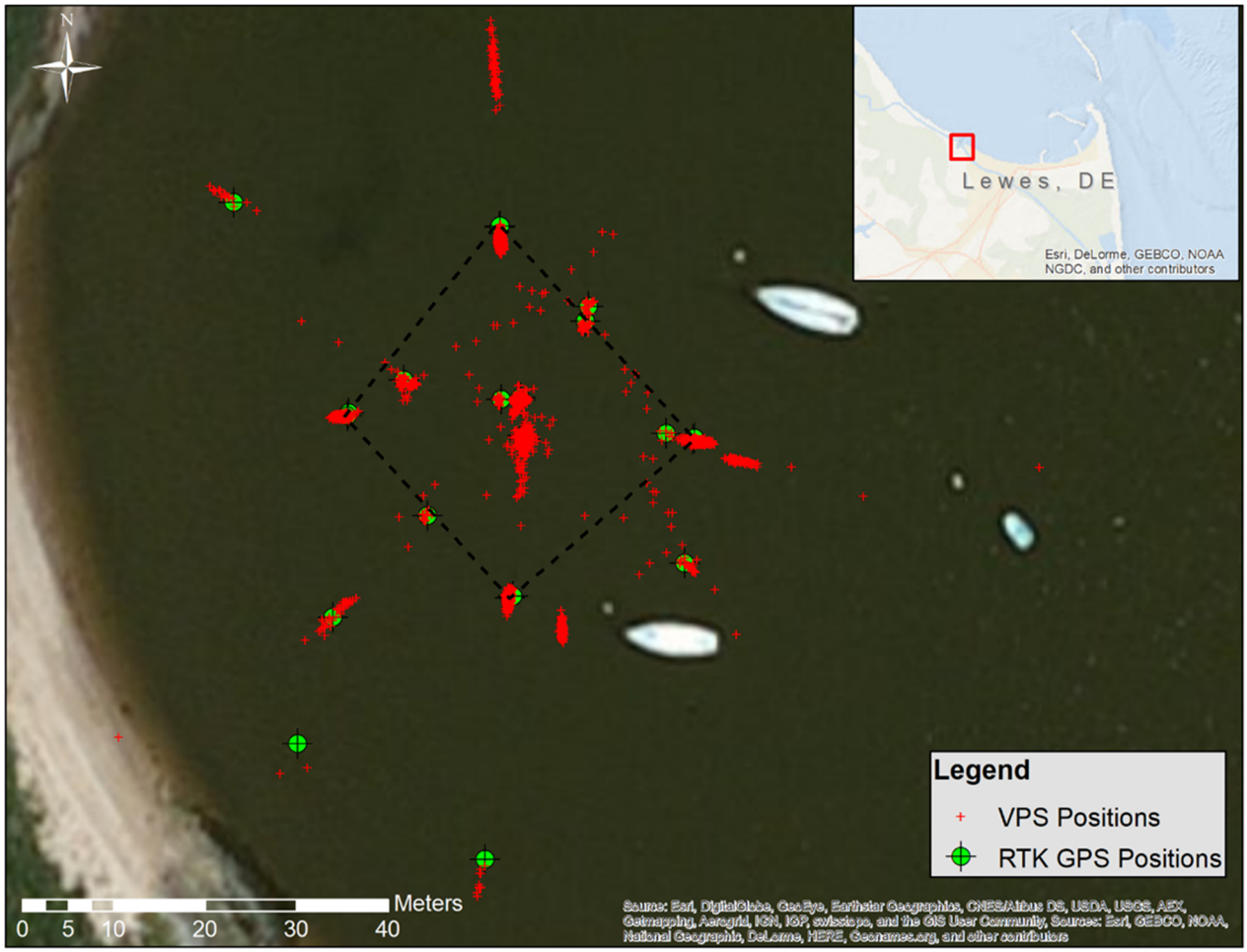



*Figure 4.7: Comparison of Vemco estimated positions versus RTK GPS positions taken during the 2016 UD boat basin field test of the VPS acoustic tracking network.*

The acoustic positioning results from Vemco were compared to the RTK GPS positions (Figure 4.7). A comparative analysis indicated that the positional estimates of the VPS were within 50 cm of the RTK positons when moved within the array, and less than 20 cm for the initial static position of the surrogate (Figure 4.8). The positional error increased as the distance outside of the array increased. However, the positional error was less than 1 m within distances of 10x water depth, and less than 3 m at distances up to 20x water depth. Vemco also estimated the distance between the two tags on the surrogate at 33 cm, which was within 2.5 cm of the actual distance (30.5 cm). In further discussion with Vemco, the field test indicated that multipath propagation was not a significant factor, and false detection could be filtered out in processing.

Acoustic noise from the surrounding environment (dock activity, recreational boats and UD research vessel activities) also did not have a significant effect on the detection rate and signal strength. It was, however, determined that the tags could not be detected when buried only a few cm below the surface of the stiff clay mud. Therefore, if buried, a metal detector / magnetometer and the last known positions from the VPS would be needed to reacquire the surrogates. Field testing was completed in Oct. 2016, and the results were used to inform the configuration for the field deployments (see section 4.2.3.1).

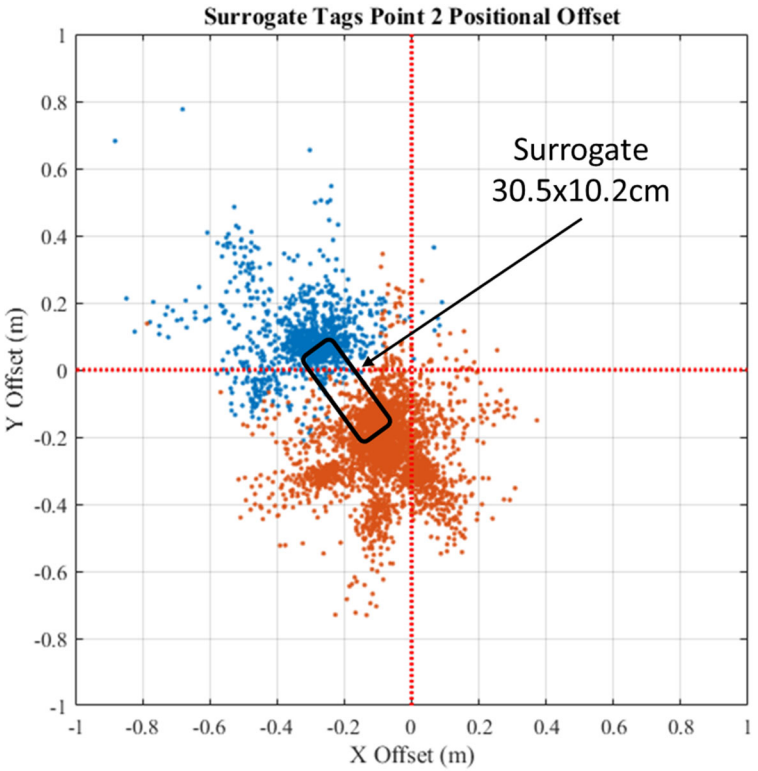



*Figure 4.8: RTK GPS and VPS positional offset (with model overlay) for the surrogate in the 2016 UD field test.*

## 4.2.2. Interim Milestone 1: Go / No-Go Decision

Prior to field implementation (Task 2), a number of quantitative performance metrics were identified to establish data collection objectives and determine final performance of this study. These metrics (Table 4.4) address the development and testing of the surrogate MEC and Vemco VPS as part of Task 1 and field data collection metrics, including site geophysical, geotechnical, and hydrodynamic characterization, as outlined in Task 2 (see section 4.2.3). Further, these metrics served to test the performance of the Vemco VPS system surrogate tracking capabilities during the two proposed field tests.

The Task 1 milestones were used to assess development and performance of the Vemco VPS system and sensor-integrated surrogates and provide SERDP and MR-2730 with quantitative results to support a go / no-go decision to continue with the project. A “Go Decision” was rendered following the successful tests of the VPS system. Task 1 was completed in October 2017, and Task 2 was initiated immediately following the Go Decision.

*Table 4.4: Data collection and Quantitative Performance Metrics*

| Performance Objective | Metric | Data Required | Success Criteria |
|---|---|---|---|
| Development of Instrumented Surrogate MEC | ➢ IMU and acoustic tag integration and data collection | ➢ IMU motion data and VEMCO VPS acoustic positioning | ➢ Collection of IMU motion data verified by acoustic positioning |
| Surrogate Tracking Positional Accuracy | ➢ Horizontal Positional Error (HPE) | ➢ Surrogate Positions calculated from VEMCO VPS Receivers | ➢ Average HPE < 1m for 50% of field deployment duration |
| Site Hydrodynamic Characterization | ➢ In-situ characterization of hydrodynamics during field deployments | ➢ Wave and current measurements from ADCP<br>➢ Near-bed velocities, turbulence, shear stress estimates from PC-ADCP | ➢ Measurements of in-situ hydrodynamics throughout field deployment period |
| Geophysical and Geotechnical Site Characterization | ➢ Complete acoustic bathymetric and backscatter coverage<br>➢ Background magnetics<br>➢ Ground control sediment classification | ➢ Bathymetric and side-scan sonar<br>➢ Magnetometry<br>➢ Surface sediment sampling<br>➢ Push core or Box core | ➢ 100% bathymetry and acoustic backscatter coverage at <1 m gridded resolution<br>➢ Complete interpolated magnetometry surface at <2 m gridded resolution<br>➢ 20 surface sediment samples<br>➢ 5 push cores |
| Instrument Verification Strip | ➢ Deployment and repetitive survey of IVS | ➢ AUV sonar and magnetics | ➢ Complete IVS characterization before and after every magnetometer survey |

### 4.2.3. Task 2 – Field Implementation

Task 2 encompassed activities related to the field experiments. This section discusses the general field site characteristics and field methodology for Task 2 deployments (Field Study Site and Methods Overview 4.2.3.1). Over the course of the Task 2 deployments, methods were adapted and optimized; improvements were made in smart surrogate design, reference tag placement, and VPS data processing. Therefore, each deployment is also described independently (Sections 4.2.3.2 and 4.2.3.3). Task 2 was initiated in mid-October 2017 and completed in early May, 2018.

*4.2.3.1. Field Study Site and Methods Overview*

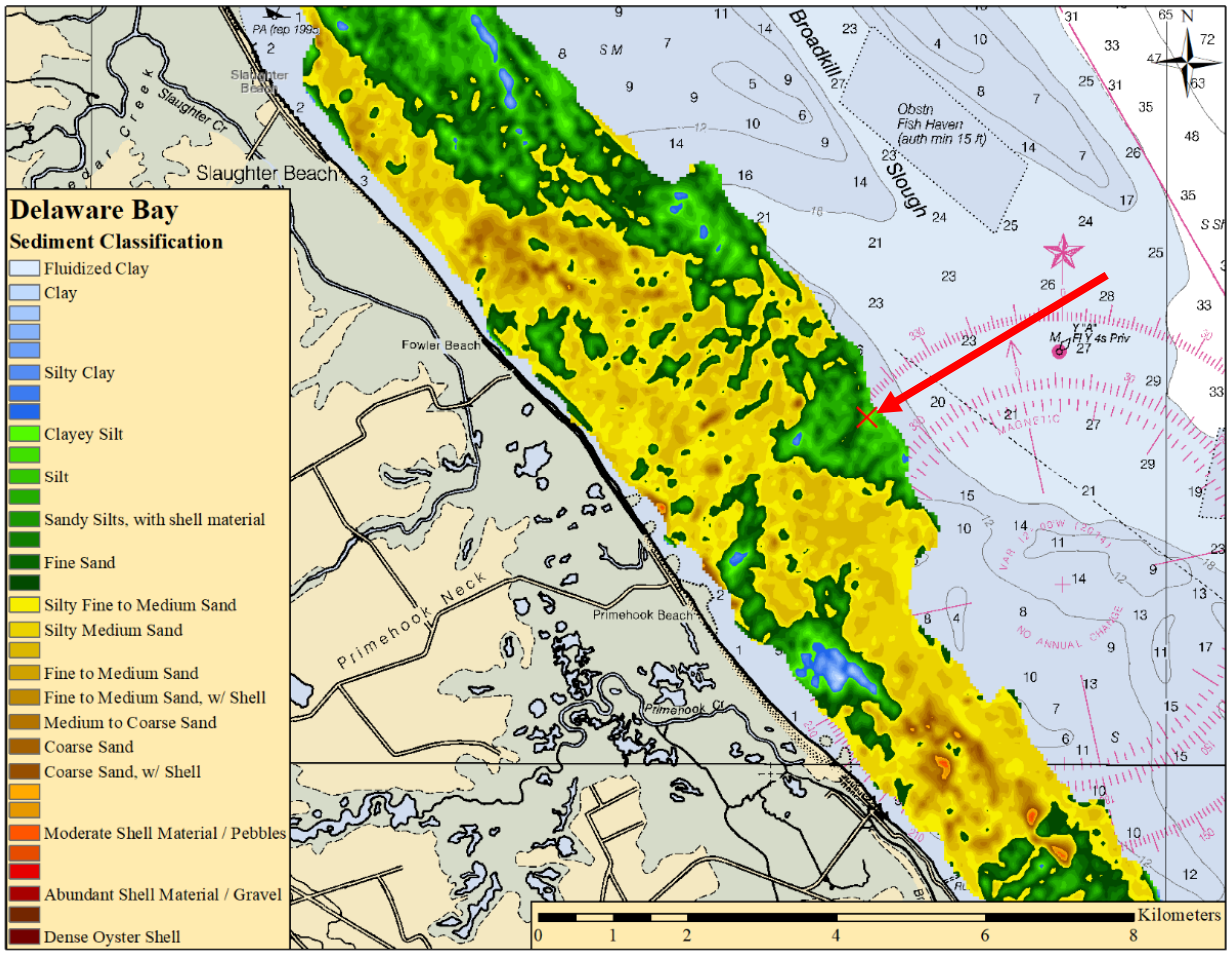



*Figure 4.9: A sediment classification map of the Broadkill, DE area from previously collected Roxan sonar data and sediment sampling (Wilson et al., 2010) with the MR-2730 field site location indicated. The field site is located 10.5 km northwest of the UD Marine Operations facilities and Marine Sciences Campus, which allowed for easy access and frequent site monitoring.*

Due to the proximity to the University of Delaware, the lower Delaware Bay estuary was selected for the field experiment. The lower Delaware Bay is characterized by muddy or mixed sand and mud sediments (Wilson et al., 2010) and is often buffeted by high-energy events (Wright 1993; Trembanis et al., 2012). A study site was selected in the area of the Broadkill Slough, approximately 10.5 km northwest of the University of Delaware Marine Operations Base (Figure 4.9). The wider Broadkill Beach and nearshore area had recently been monitored for changes in beach profile and benthic habitat (Raineault et al., 2011) and modeling beach response to storm activity (NOAA SG 2016-18 RRCE-8 TREMBANIS). This data was leveraged for wider hydrodynamic and morphological context within this study. Roxan sediment classification data collected by Wilson et al. (2010) assisted in identifying an area with cohesive sediments. The site was located in 4.5 m MLLW on a broad shallow flat. Sediment sampling confirmed the site contains cohesive stiff muddy sands (~10-40% silts and clays).

The VPS tracking network was designed with consultation from Vemco after selecting the field site. The final design utilized a grid of 6 HR2 receivers set in pentagonal grid with one HR2 receiver on each corner and one in the center. This design ensured 100% overlap of the study site by 3 or more receivers (Figure 4.10). The estimated effective range for the receivers in this environment was 50 m, thus the grid was designed to be no larger than 50m radius around the center receiver. The HR2 acoustic receivers were fitted to rigid mounts that could be firmly augured into the sediment by SCUBA divers. This allowed for accurate positioning by restricting the potential for receiver movement over the course of the deployment. For all diving-related activities, the University of Delaware team collaborated with the Delaware State Police SCUBA Unit (DSPSU). It was determined that the DSPSU would bring expertise and experience with SCUBA operations low visibility conditions, and would facilitate the deployment requirements of MR-2730, while MR-2730 provided a practical training exercise for the DSPSU. Once deployed by the divers, the VPS positions were surveyed using a surface vessel-mounted sonar equipped with Real-Time Kinematic (RTK) GPS, capable of centimeter horizontal accuracies. Each HR2 receiver was equipped with an internal synchronization tag to correct for clock drift between the receivers. Additional reference "synctags" were placed within the grid at GPS marked positions to measure overall system performance during the deployment, and to serve as fixed control points to constrain error. Once deployed, surveyed and verified to be working, surrogates were placed within the experimental grid (Figure 4.10).

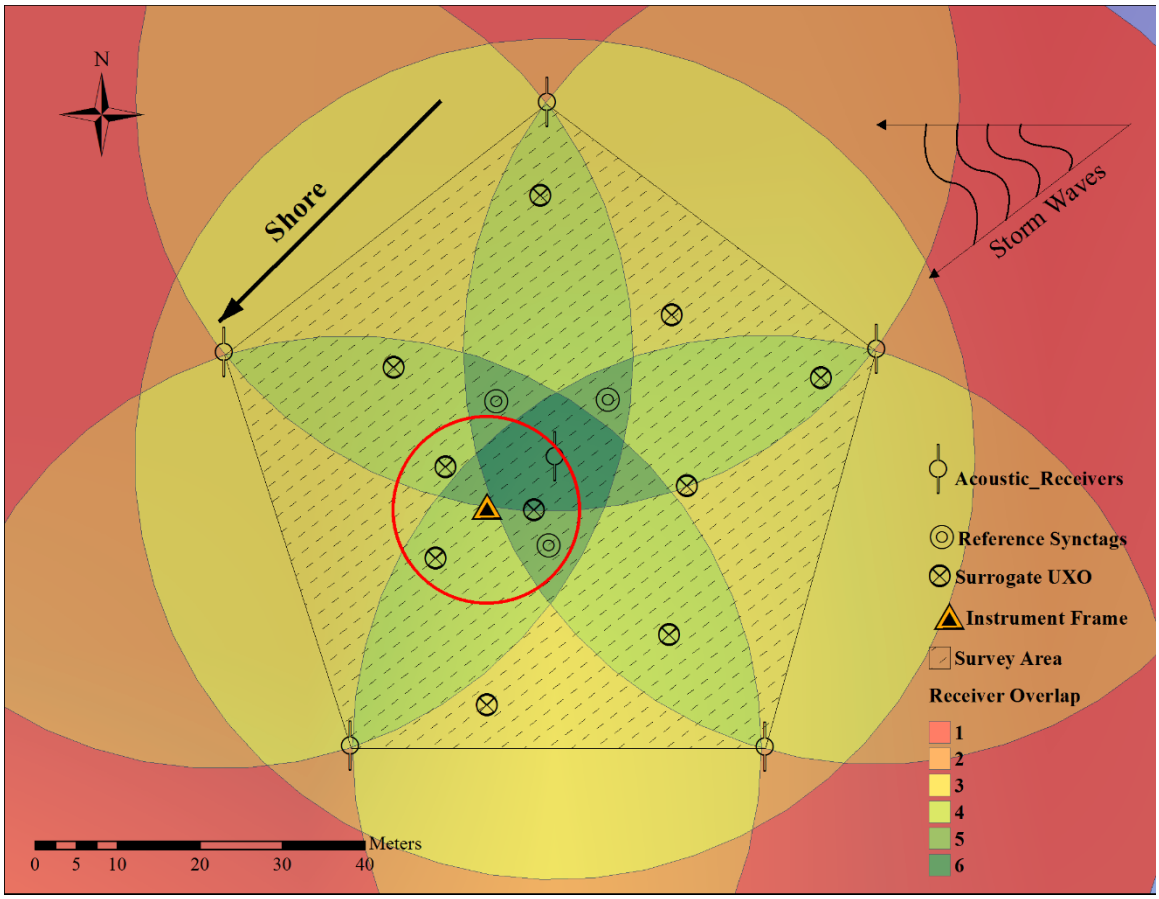



*Figure 4.10: VPS receiver arrangement designed with assistance from Vemco to maximize acoustic detection overlap and positional accuracy. Minimum anticipated receiver overlap is overlaid with example reference tag, surrogate MEC, and instrument frame placement.*

Hydrodynamic forcing was directly monitored using an instrumented bottom frame. The frame, built specifically for this study, has a 2 m x 2 m footprint and is customizable depending on instrumentation (Figure 4.11). For water column currents and wave characterization, the frame was equipped with an upward facing 600 kHz Teledyne RDI Acoustic Doppler Current Profiler (ADCP), set 1 meter above the bed. The ADCP collected wave and current data every 0.5 hr in 25 cm bins. A downward facing 2 MHz Nortek Pulse-Coherent ADCP (PC-ADCP) was mounted for high-resolution, near-bed current measurements and turbulence estimates. The PC-ADCP collected data every 0.5 hours with 3 cm bin resolution. Conductivity, temperature, depth, and turbidity were measured with an AML Plus-X, and sampled at minimum every 0.5 hr (0.25 hr in later deployments). For time-lapse acoustic imagery, the frame was equipped with a 2.25 MHz Imagenex 881 fan-beam rotary sonar. The rotary sonar is capable of effectively scanning a 360° sector around the sonar at up to 12 m ranges with sub-cm resolution. The remote sonar head is connected to a self-contained data logger and battery unit that allows for 4-6 week deployment depending on data collection frequency, with a quick turn-around time for battery replacement and data retrieval. While capable of making multiple scans per hour, to maximize endurance, the rotary sonar made a 6 m scan over a 270° sector every 0.5 hr. Similar frame configurations were used with success in previous mine-burial studies (e.g. Traykovski et al., 2007) and SERDP funded studies (e.g. Calantoni SERDP MR-2320, Traykovski and Austin, 2017).



*Figure 4.11: Instrument frame developed for MR-2730. Shown here with Teledyne RDI Sentinel ADCP, Nortek Aquadopp HR PC-ADCP, AML Plus-X CTD, and Imagenex 881 Tilt-Head rotary sonar.*

Repetitive site surveying utilized a two-method approach: wide-area surveying with surface-mounted sonar and high-resolution, near-bed surveying with an AUV. Wide-area bathymetric and side-scan sonar surveys were conducted on the University of Delaware's *R/V Joanne Daiber*. The *Daiber* was fitted with an Edgetech 6205 Phase-Measuring Echo Sounder (PMES), which collects simultaneous dual-frequency side-scan sonar at 230 and 550 kHz, and bathymetry on the 550 kHz frequency (Figure 4.12a). The PMES uses a Coda Octopus F190R+ inertial motion unit

coupled with RTK/PPK GPS to record vessel attitude (heading, pitch, roll, and heave) and horizontal position accuracy of 10 cm or less. Near-bed surveying was conducted with the University of Delaware's Teledyne Gavia AUV (Figure 4.12b). The Gavia AUV is a modular designed vehicle customizable to individual projects. Available sensor modules include a Marine Sonics 900/1800 kHz high-resolution side-scan sonar, a GeoAcoustics GeoSwath 500 kHz phase-measuring bathymetric sonar, 2 MP Point Grey Color Grasshopper Camera, and environmental sensors (e.g. salinity, temperature, dissolved oxygen, and turbidity). The Gavia AUV is navigated by a Kearfott T-24 "SEANAV" inertial navigation system (INS) coupled with an RD Instruments 1200 kilohertz (kHz) Workhorse Navigator Doppler velocity log (DVL). The DVL measures velocity of the vehicle over the seafloor and provides these measurements to the INS to constrain navigational drift error. While on the surface, a Wide Area Augmentation System (WAAS)-capable L1/L2 receiver Global Positioning System (GPS) in the AUV's sail provides position fixes to the INS before missions. When submerged, the published drift rate for the INS with an integrated DVL during submerged operation is 0.1% of distance traveled. Additional methods in survey design can further constrain AUV positional error. The Gavia has a depth rating of up to 500 meters, and can run for over 3.5 hours and cover up to 20 linear kilometers per mission.




*Figure 4.12: The University of Delaware a) R/V Joanne Daiber equipped with Edgetech 6205 PMES, and b) Teledyne Gavia modular autonomous underwater vehicle with Geometrics G-880 magnetometer.*

The Gavia AUV is also equipped with a marine magnetometer developed for the UD AUV in an Environmental Security Technology Certification Program (ESTCP) funded program (MR-201002). The AUV magnetometer module houses a Geometrics G-880AUV self-oscillating split-beam cesium vapor (non-radioactive Cs133) total field magnetometer with automatic hemisphere switching coupled with an Applied Physics 539 fluxgate compass (see MR-201002 Report). In a blind field test (Figure 4.13), the system demonstrated reliable detection of munitions as small as 60 mm mortars and larger munitions at 1.5-m altitudes and 75 mm projectiles and larger at over 2-m altitudes. More recently, the AUV magnetometer was used in

a Bureau of Ocean Energy Management study to develop methods for MEC detection in offshore wind energy areas (Carton et al., 2017). The G880-AUV magnetometer was capable of detecting MEC surrogates of 155mm shells at altitudes between 2 to 6 m. The magnetometer served as an additional surrogate tracking method, and provided a backup to the VPS when surrogates became buried and acoustic signal obscured.

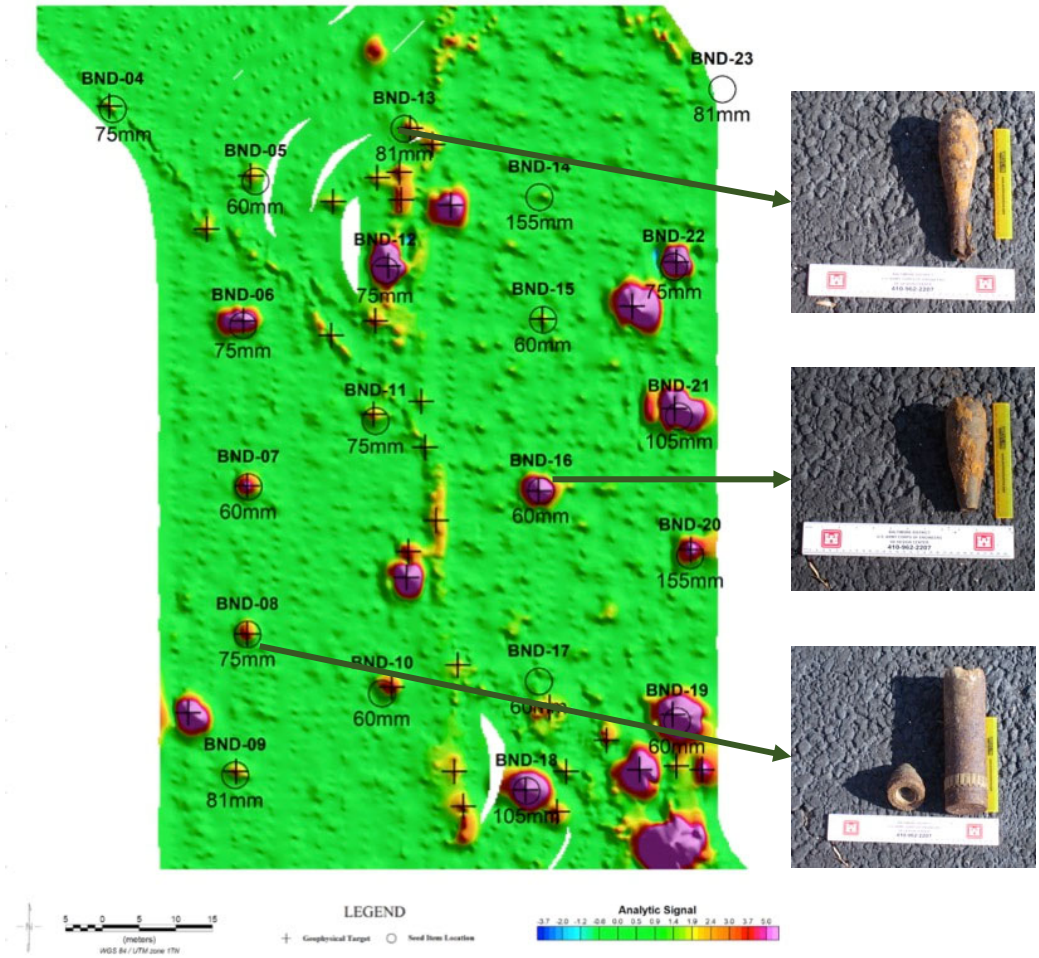



*Figure 4.13: Magnetometer results from blind ordnance detection survey. The peaks are strong magnetic signals, compared to the ordnance test subjects (ESTCP Project MR-201002).*

The final preparatory task was identifying the timeframe for the deployments. Local climate data was collected from nearby NOAA monitoring stations and used to narrow down ideal deployment windows for capturing large energy events necessary for munitions movement (Figure 4.14). Historic average wind speed records (Figure 4.14a) show increasing winds from late Aug – Nov., or what is typically hurricane season for the mid-Atlantic Region. Two hurricanes prior to the study, Irene (2011) and Sandy (2012), occurred within this window and both storms had significant impacts on the coastal zone of Delaware Bay. Average winds remain high during the late winter and early spring months, which are buffeted by episodic "nor'easter" extra-tropical cyclones (ETC). In March 2013, a large nor'easter generated waves larger than Hurricane Sandy (see DuVal et al., 2016), and in January 2016, Winter Storm Jonas generated the highest near-shore waves on record at the local NOAA observational buoy 44009 (see NOAA National Data Buoy Center). Using offshore wave records for Delaware, monthly near-

bed wave orbital velocity distributions were estimated by shoaling waves to the depths in the region of Broadkill Beach from 2013 – 2015. Similar to the wind climate, higher average near-bed orbital velocities are estimated in late summer – early fall and late winter – early spring. In summation, the highest forcing in the lower Delaware Bay ranges from Sept.-Nov., and Feb.-Apr. (Figure 4.14b). These "weather windows" were targeted for two deployments to take place in the fall of 2017 and winter/spring of 2018.

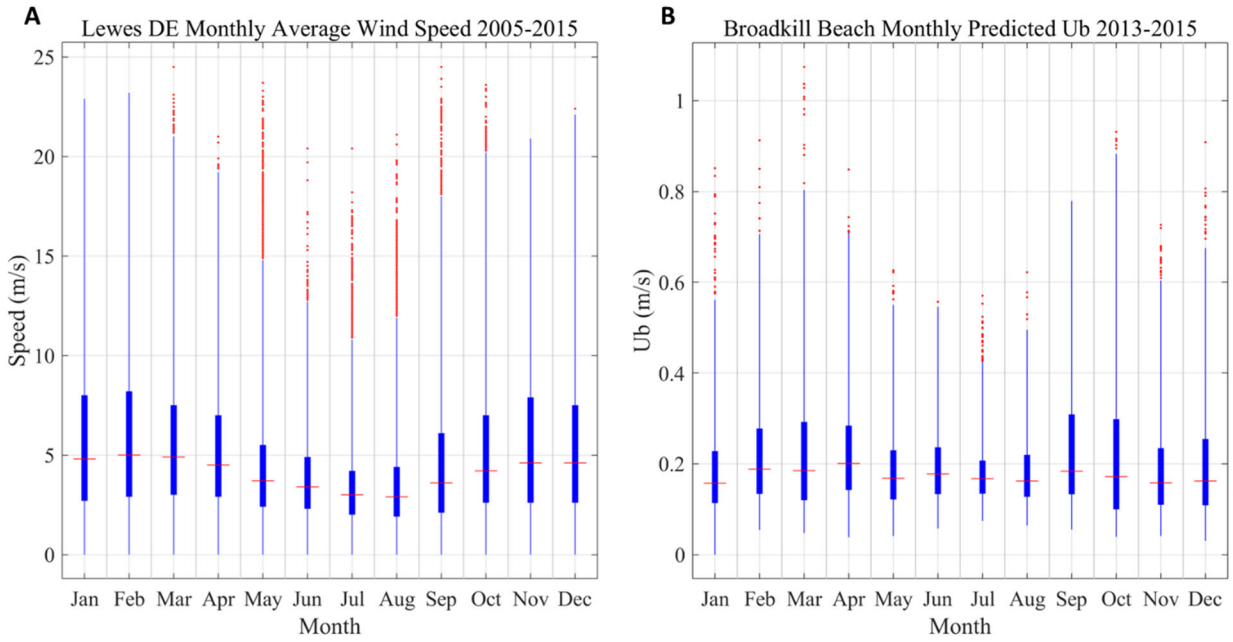



*Figure 4.14: a) Local monthly historic wind and b) predicted near-bed wave orbital velocity for Broadkill Beach field site prior to field study.*

### *4.2.3.2. Fall 2017 Field Deployment*

The first field deployment took place Nov. 2-Dec. 4 2017. Preparatory surveys and sediment samples were conducted prior to the deployment, on Oct. 18, 2017, to verify site conditions and establish baseline morphology. Repetitive site surveys and sampling continued throughout the deployment. Initial recovery began in Dec. 4, 2017, but required follow on dives to locate and recover all of the surrogates. A summary of activities is provided in Table 4.5, and discussed in more detail below.

*Table 4.5: Summary of activities associated with Task 2 Fall 2017 deployment*

| **Fall 2017 Deployment** | | | | | |
|---|---|---|---|---|---|
| *Deployment Dates* | *HR2 Receiver* | *Reference Tags* | *Surrogates* | *Instruments* | |
| 2 Nov - 4 Dec 2017 (32 Days) | 6 | 3 | 10 | ADCP, PC-ADCP, CTD, Rotary Sonar | |
| *Survey Dates* | *Side-Scan* | *Bathymetry* | *Sub-bottom* | *Magnetometry* | *Sediment Sampling* |
| 18-Oct-2017 | X | X | X | X | X |
| 2-Nov-2017 | X | X | | | X |
| 9-Nov-2017 | X | X | | X | |
| 2-Dec-2017 | X | | | X | X |

On Oct. 18, 2017, a wide-area assessment (WAA) was conducted in the Broadkill Slough using the Edgetech 6205 PMES. Through strategic sediment sampling, the study area was narrowed to an area to the SW of Slough (Figure 4.15). This area sits at 4.5m mean lower-low water depth and contains sediments qualitatively categorized as muddy sands. On Oct. 20, 2017, a more targeted sonar survey was conducted (inset Figure 4.15), including an AUV magnetometer survey to characterize any ferrous debris that could interfere with the study. No debris was detected from the surveys, and the location of the field site was finalized.

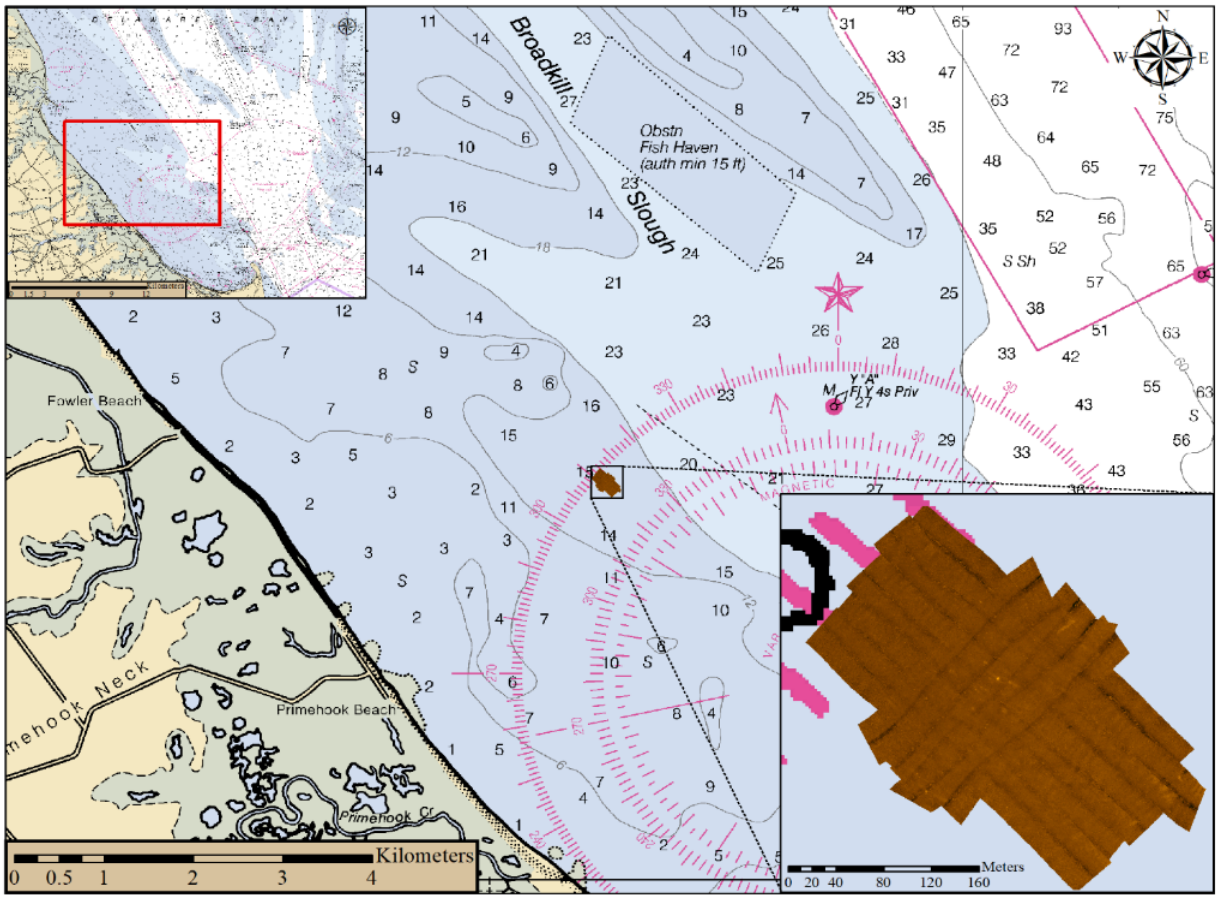



*Figure 4.15: Task 2 study area. The VPS array was located in the center of the inset sonar mosaic.*

In preparation for the VPS installation, the instrument platform was deployed at the site on Oct. 27, 2017 to begin hydrodynamic data collection. SCUBA diver operations were scheduled to follow shortly after, on Oct. 30-31, 2017, but weather conditions required the deployment be pushed back. Conditions were optimal on Nov. 2, 2017, and the VPS installation commenced. Buoys were placed by the UD team to mark the positions of the VPS pole installation (Figure 4.16a). The VPS poles were constructed with a 2-part system (Figure 4.16b and Figure 4.16c). The lower sections were augured 1 m into the seafloor by the DSPSU divers. Once secured, the upper sections, containing the HR2 receivers, were slipped over the base and locked into place. This allowed for subsequent retrieval of the upper pole and receiver, while leaving the base in

place for the second deployment. Once installed, the HR2 receivers sat approximately 2 m above the seabed.

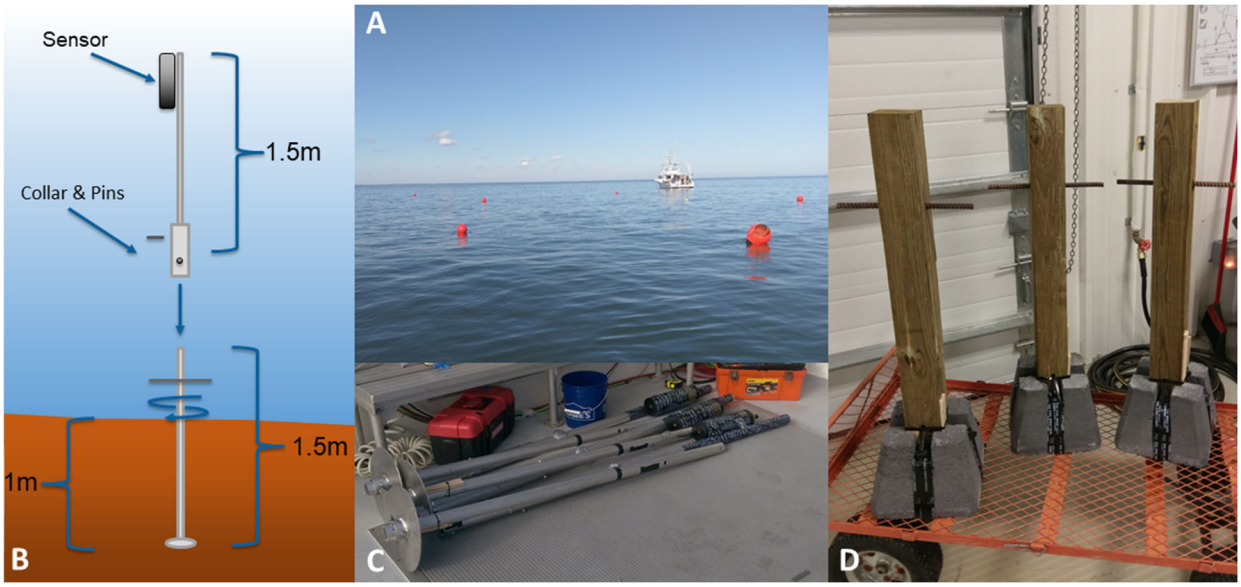



*Figure 4.16: HR2 receiver locations (A), HR2 pole mounts installation design (B), HR2 receivers and pole mounts prior to deployment (C), and reference tag pole mounts (D).*

Following the receiver installation, three reference tags, fitted to 1 m tall custom-built posts (Figure 4.16d), were lowered in place. The tags posts were designed to be easily identifiable in the PMES for georeferencing. Next, the surrogates were placed on the seafloor by the DSPSU. One surrogate of each type (60mm, 81mm and 155mm) was set within view of the rotary sonar on the instruments frame. The remaining 7 surrogates were distributed throughout the grid. Lastly, three shallow surface core samples were collected across the study area by the divers. Due to the efficiency of the DSPSU, all operations were successfully completed within 5 hours of arrival on site. Immediately following diver operations, a PMES survey was conducted to obtain precise GPS locations for each of the HR2 receivers, reference tags, and instrument platform. An AUV survey was also conducted on Nov. 9, 2017, to collect magnetics and high-resolution sonar of the deployment site (Figure 4.17).

Recovery of the VPS sensors, surrogate munitions, and instrument frame was planned for the week of Dec. 4-8, 2017, contingent upon the first opportunity with good weather conditions. On Dec. 2, 2017, an additional AUV survey was conducted prior to the recovery to assist in locating the surrogates in case mobility had occurred, although no movement was anticipated as no storm conditions were recorded over the deployment window. This was supported by the preliminary survey data analysis, which indicated that little if any mobility had occurred. Recovery operations commenced on Dec. 4, 2017 with the assistance of the DSPSU. For recovery, the DSPSU utilized a hard-hat diver with surface supply and communications (Figure 4.18a). A sector scanning sonar (Figure 4.18b) was lowered at the site and used to guide the diver to targets (Figure 4.18c). All VPS sensors and reference tags were recovered, but low-visibility at the site restricted diver operations and only 7 of 10 surrogates were located and recovered. The decision was made to leave the instrument frame on site to record conditions until the remaining 3 surrogates could be recovered. The VPS tracking data was sent to Vemco for rapid processing to

assist in locating the remaining 3 surrogates. Recovery operations resumed on Dec. 7, 2017, with the aid of the Vemco processed data. All 3 surrogates were located and recovered within 30 minutes of diver operations due to the accuracy of Vemco positioning. The instrument frame was subsequently recovered. Fall 2017 deployment operations were completed on Dec. 7, 2017.

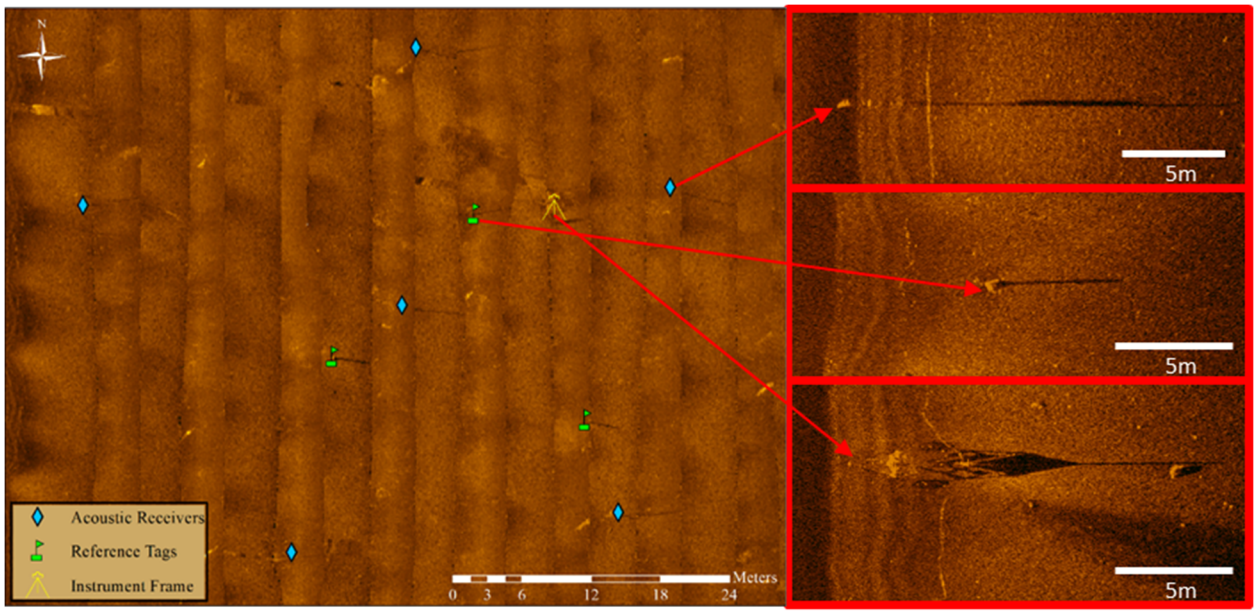



*Figure 4.17: VPS array in Fall 2017 deployment as mapped by the Gavia AUV. Waterfall snapshots show an HR2 receiver on augured pole (top), reference tag post (middle), and instrument frame (bottom) with 155mm surrogate visible (right)*

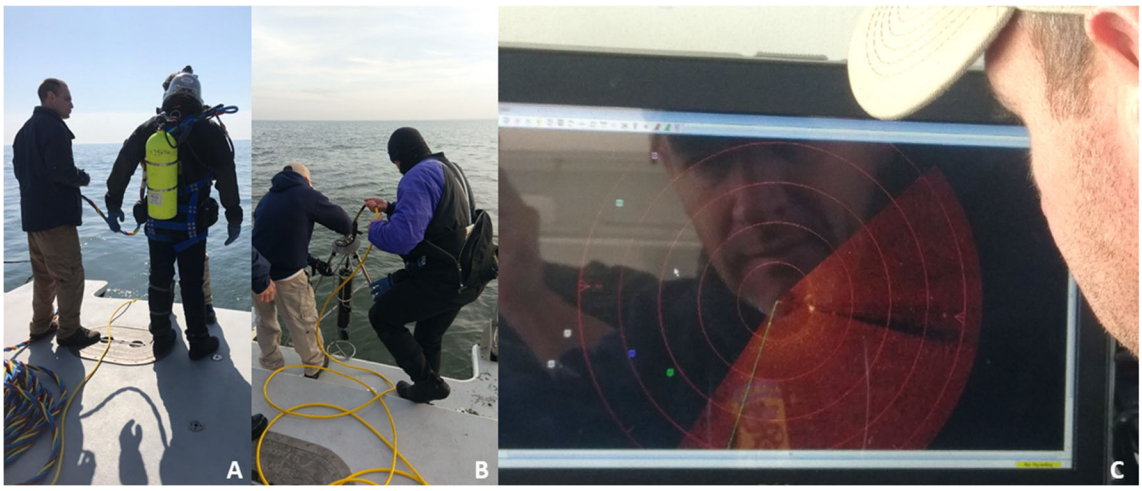



*Figure 4.18: Delaware State Police SCUBA Unit operations during the Fall 2017 VPS retrieval. A hard-hat diver with surface supply with communications (A) was monitored and guided to targets by the surface team using a sector-scanning sonar (B). The diver can be seen as the bright return in the center of sonar image (C).*

#### *4.2.3.3. Spring 2018 Field Deployment*

The Spring 2018 deployment was set for the week of Feb. 5, 2018, contingent upon weather conditions. A weather window occurred on Feb. 6, 2018, and the deployment was initiated with the assistance of the DSPSU once more. Poor visibility, strong currents and cold water hampered diving operations, and the VPS installation was halted after only 4 of 6 sensors and the oceanographic instrument frame were placed at the site. No reference tags or surrogates were put in place at that time. Operations resumed with better weather on Feb. 9, 2018, during which the 2 remaining sensors, 4 reference tag posts and 10 instrumented surrogates were placed on site. Three of the surrogates were once again placed near the instrument frame to be observed by the rotary sonar, and the remaining 7 were lowered from surface vessel in various locations around the grid. The deployment operations were completed on Feb 9, 2018.

*Table 4.6: Summary of activities associated with Task 2 Spring deployment.*

| **Spring 2018 Deployment** | | | | | |
|---|---|---|---|---|---|
| *Deployment Dates* | *HR2 Receiver* | *Reference Tags* | *Surrogates* | *Instruments* | |
| 9 Feb - 11 Apr 2018 (64 Days) | 6 | 4 | 10 | ADCP, PC-ADCP, CTD, Rotary Sonar | |
| *Survey Dates** | *Side-Scan* | *Bathymetry* | *Sub-bottom* | *Magnetometry* | *Sediment Sampling* |
| 6-Mar-2018 | X | X | | X | X |
| 10-Apr-2018 | X | | | X | X |
| 12-Apr-2018 | X | | | X | |

*ROV survey 18-Mar-2018

A site survey could not be conducted until, March 6, 2018, due to weather conditions and vessel availability (see Table 4.6). A complete survey was conducted with the surface-vessel PMES bathymetric and side-scan sonar, AUV side-scan sonar and magnetometer. Sediment samples were also collected at the study site and in the surrounding region. The survey data confirmed the locations of the VPS, reference tags, and instrument frame. The 155mm surrogates were also visible in the AUV sonar and magnetometer data, although acoustic image quality was low due to high backscatter from high turbidity following a nor'easter on March 2. On March 8 and 13, two more nor'easters passed over the study site. On March 18, an ROV was used to attach a surface line to the instrument frame, and the frame was then recovered, as the batteries for the instruments were expected to be nearly depleted. Data was downloaded from the instruments, batteries replaced, and the frame placed back at the site on March 19, 2018. The frame was not returned to the same location within the grid, as there were concerns regarding entanglement with the VPS sensors during deployment. The frame was instead placed 20m to the east of the VPS grid. Immediately after redeployment, a fourth and final nor'easter struck the study site.

Recovery operations commenced April 11, 2018, after 62 days of deployment. The site was re-surveyed on April 10, 2018, using the AUV to collect side-scan sonar and magnetometer measurements. This data was used to aid DSPSU diver operations. The DSPSU divers were able to recover all of the VPS receivers, 4 reference tags and 6 of the 10 surrogates. The divers reported significant scour and burial with the surrogates that were located. In the process of searching for the remaining 4 surrogates, numerous targets on the sonar were determined to be

whelk and horseshoe crabs. Operations were halted, as it was unlikely that the remaining surrogates would be located using the sector-scanning sonar. The data from the VPS was downloaded and sent to Vemco to assist in determining that last known locations for the remaining surrogates, believed to be partially or fully buried at the site.

While Vemco was processing the data, another AUV survey was conducted on April 12, 2018, and the instrument frame was also recovered. Without the VPS receivers or reference tag posts at the site, the AUV was able to survey nearer to the seafloor (1.5m versus 2m altitude) and there was less magnetic clutter. The survey located two distinct targets within the grid. The last estimated surrogate locations were sent from Vemco on April 13. The estimates suggested that the two 81mm mortars were located near the AUV magnetometer targets (Figure 4.19), although no magnetic targets were distinguishable in the vicinity of the two missing 60mm surrogates. Using the available magnetometer and VPS positions, operations to recover the missing surrogates resumed on April 26 using DSPSU SCUBA divers. Despite strong currents and no visibility, the two 60mm surrogates, both partially buried, were recovered by the divers. The 81mm surrogates, which were fully buried, were not recovered until May 7 via hard-hat diving operations. All four surrogates were recovered within 3 meters of the Vemco estimated positions. Field operations were completed as of May 7, 2018.

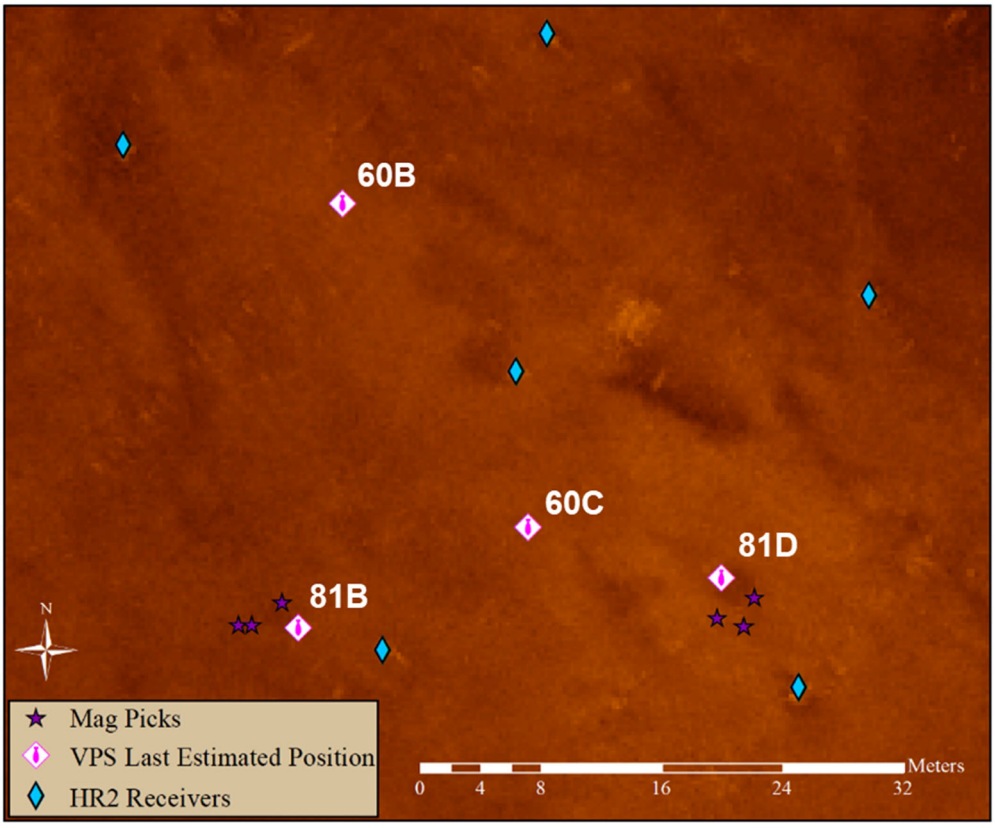



*Figure 4.19: Comparison of magnetometer picks and VPS estimated last known position for the missing 81mm and 60mm surrogates.*

### 4.2.4. Task 3 – Data Analysis, Project Review, and Reporting

Task 3 encompassed data synthesis and reporting. Complete site acoustic backscatter, bathymetry and magnetometer map products were generated for each survey using Chesapeake Technologies, Inc. SonarWiz, and site-wide surficial sediment distribution and bathymetry were analyzed using ESRI ArcGIS 10.4. Sediment samples and short-cores were processed for grain size analysis, sediment type and distribution, and shear vane analysis. Hydrodynamics were used to estimate sediment transport thresholds of site sediments. Sediment distribution maps were generated based on geophysical survey products and ground-truthed by sediment samples collected at the site. Both raw data and products were stored in Mathworks MATLAB .mat structures, geotiff image format, and tabular ASCII form, with associated metadata information. Surrogate tracking products, both raw recorded receiver times and Vemco processed positions, were summarized in tabular form. Vemco reported positions were compared to positions observed in magnetometer and side-scan sonar data collected by the AUV. Finally, surrogate burial and mobility was analyzed with time-series hydrodynamics and sediment properties to determine what parameters have the most influence on surrogate mobility and burial in muddy environments.

### 4.2.5. Interim Milestone 2: Task 4 Go / No-Go Decision

A central facet of Task 2 regards the characterization of surrogate MEC during energetic conditions. Due to the episodic nature of storm events in the Mid-Atlantic, there was no guarantee that such an event would occur during the timing of Task 2. As such, a second interim milestone was added. Should no event be captured during Task 2, an optional Task 4 could be initiated, which would enact 2 additional field efforts over the winter of 2018 – 2019. Although Task 2 was successful in capturing multiple storm events (see section 5.1) during the second deployment of the VPS system, discussions with SERDP and Rennie (MR-2227) determined that additional field data collection would be beneficial to the continued development of the Underwater Munitions Expert System, as there is a noted dearth of observations of MEC behavior in varied environments and extreme events (personal comm. Sarah Rennie, April 24, 2018). These extreme events, which may be best described as outlier events, are those in which significant scour/burial/mobility would most likely be anticipated (or potentially predicted by the UnMES). Additional field data, likely collected in conditions not represented by the field work in Task 2, would increase the observations and parameters to further develop the UnMES. Therefore, the decision was made to activate the Task 4 component for additional field deployments.

### 4.2.6. Task 4: Optional Additional Field Study

The additional field deployments for Task 4 were considered in light of the parameter space addressed by Task 2, and the remaining gaps in data required to further develop the expert system model. Figure 4.20a illustrates the sediment size parameter space in which the Task 2 field site was conducted. Task 4 deployments would target sites with higher percentage silts and clays. Sites selected with shallower or varied depth or bathymetric profile were also considered, as the Task 2 field site was a nominal 4.5 m MLLW throughout the area. An additional surrogate type, 4.2-inch mortar, was introduced to address that large gap between the 81mm and 155mm surrogates. Furthermore, it was noted that the Task 2 deployments did not include the

late spring storm season or the late summer / early fall hurricane season (Figure 4.20b). Two deployments were planned to occur within these weather windows (fall 2018 and spring 2019).

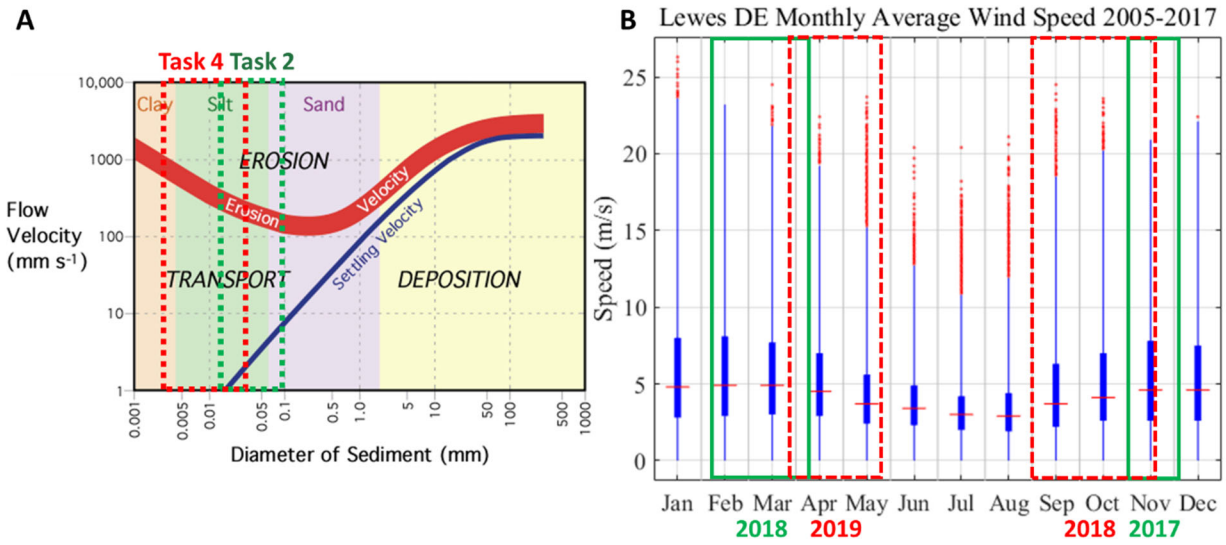



*Figure 4.20: Example Hjulström diagram (A) and historic wind record (B) illustrated remaining data gaps potentially addressed through additional deployment in Task 4.*

To identify a new site, as well as provide further characterization of the Task 2 site, additional sonar surveys and sediment sampling occurred in July 2018. Using the Roxan data, a potential site was identified approximately 1 km inshore of the Task 2 site in 3.5 m MLLW water (Figure 4.21). The area around the Task 2 site and the inshore site were surveyed with the PMES. Both surficial sediment samples and shallow cores were collected at both sites, as well as offshore of the Task 2 site and south of Broadkill Beach. Cores were collected using a HAPS sediment corer, which can collect cores up to 30 cm deep. Sheer vane measurements were conducted using a 5-cm spade for mud, requiring measurements be conducted in 5 cm sections. Four measurements were taken per 5 cm layer. Photographs were taken for each core every 5 cm. Two cores were collected at each site: one for sheer vane analysis in situ and respective sediment samples, and another retained intact for stratigraphy and further laboratory analysis. The Task 2 area showed soft, muddy sand that is highly erodible within the top 5 cm. Below 5 cm, the sediment is a stiff, compacted muddy sand that is more resistant to erosion. Both the offshore site and the south Broadkill site showed similar characteristics to the Task 2 study area. The inshore site was the only varying site, consisting of soft mud down to the limit of the corer (30 cm). Sediment analysis showed the site contains poorly sorted sandy muds (60-85% muds). The inshore site matched the target site characteristics and was confirmed as the Task 4 study site.

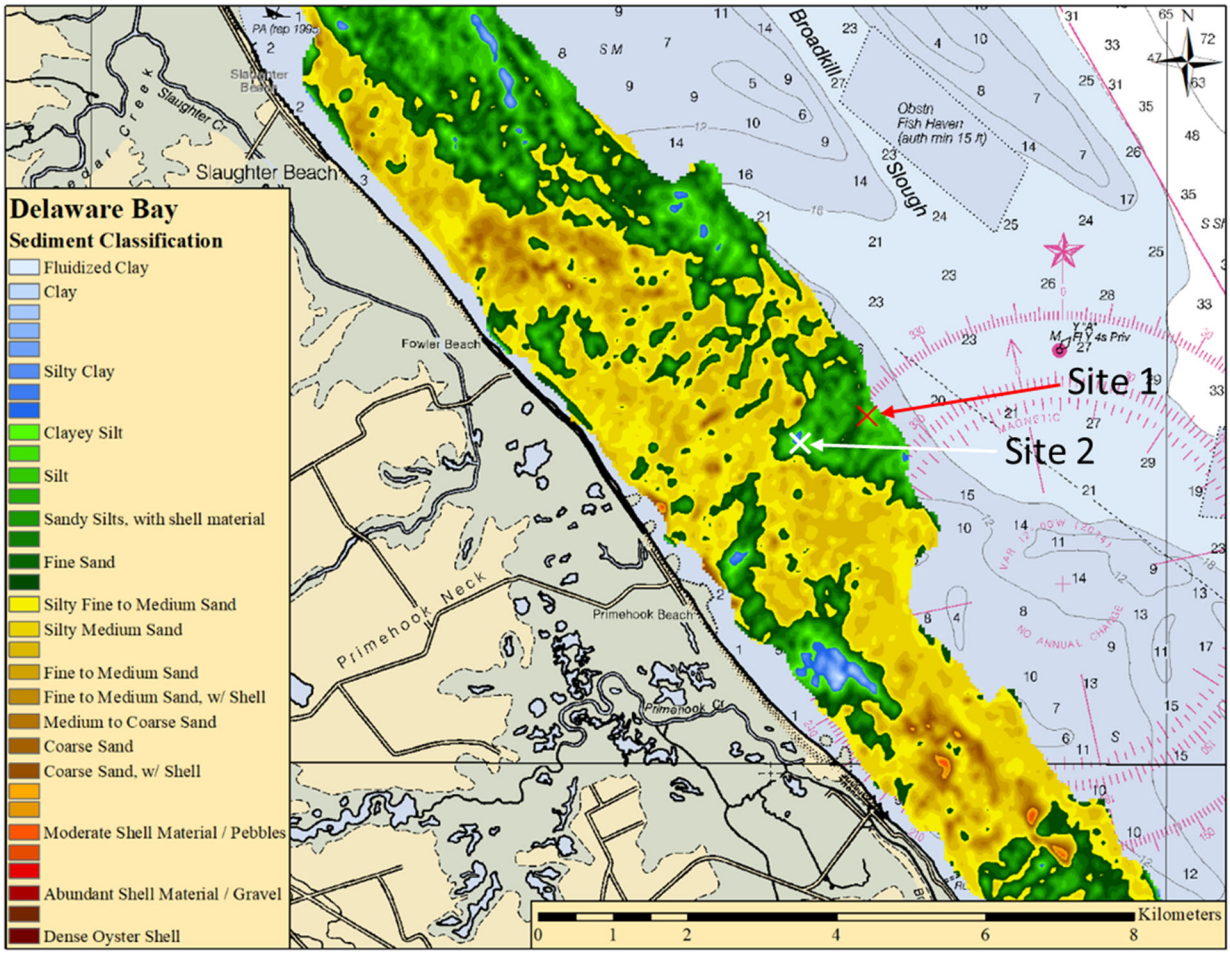



*Figure 4.21: A sediment classification map of the Broadkill, DE area from previously collected Roxan sonar data and sediment sampling (Wilson et al., 2010) helped inform the Task 4 deployment site (Site 2).*

#### *4.2.6.1. Fall 2018 Field Deployment*

The first Task 4 deployment targeted the "hurricane season" in the mid-Atlantic, which ranges from late July – late October. The deployment spanned Aug. 29 – Nov. 19, 2018 (see Table 4.7). In preparation, a full sonar survey was conducted on Aug. 27, mapping a 2 x1 km box around Task 4 site to determine a specific location for the VPS deployment (Figure 4.22). The VPS, instrument frame, and surrogates were placed at the field side on Aug. 29, 2018. Whereas previous deployments utilized divers from the Delaware State Police SCUBA Unit, this deployment experimented with surface deployable instrument moorings for the VPS receivers rather than the diver-deployed auger-moorings. These new frames would allow for rapid deployment, should the study wish to record additional data from a storm occurring outside of the standard deployment window. The VPS instrument mooring was composed of a 2 m section of pipe with a 25-cm spike, 45-lb barbell plate, and 1-m diameter wooden foot attached to the bottom. The weight and spike were designed to reduce lateral movement, while the wooden foot would reduce the likelihood of the mooring tipping over. The moorings also included a large U-Bolt for deployment from the surface, as well as recovery by ROV or diver.

*Table 4.7: Summary of activities associated with Task 4 Fall 2018 deployment.*

| Fall 2018 Deployment | | | | | |
|---|---|---|---|---|---|
| *Deployment Dates* | *HR2 Receiver* | *Reference Tags* | *Surrogates* | *Instruments* | |
| 29 Aug - 19 Nov 2018 (82 Days*) | 6 | 4 | 10 | ADCP, PC-ADCP, CTD, Rotary Sonar | |
| *Survey Dates* | *Side-Scan* | *Bathymetry* | *Sub-bottom* | *Magnetometry* | *Sediment Sampling* |
| 27-Aug-2018 | X | X | | | X |
| 30-Aug-2018 | X | | | X | |
| 16-Sep-2018 | X | | | X | |
| 23-Sep-2018 | X | | | | |
| 3-Oct-2018 | X | | | X | |
| 22-Oct-2018 | X | | | X | |
| 7-Nov-2018 | X | X | | X | X |

*VPS & Instrument Frame removed 3 Oct - 10 Oct

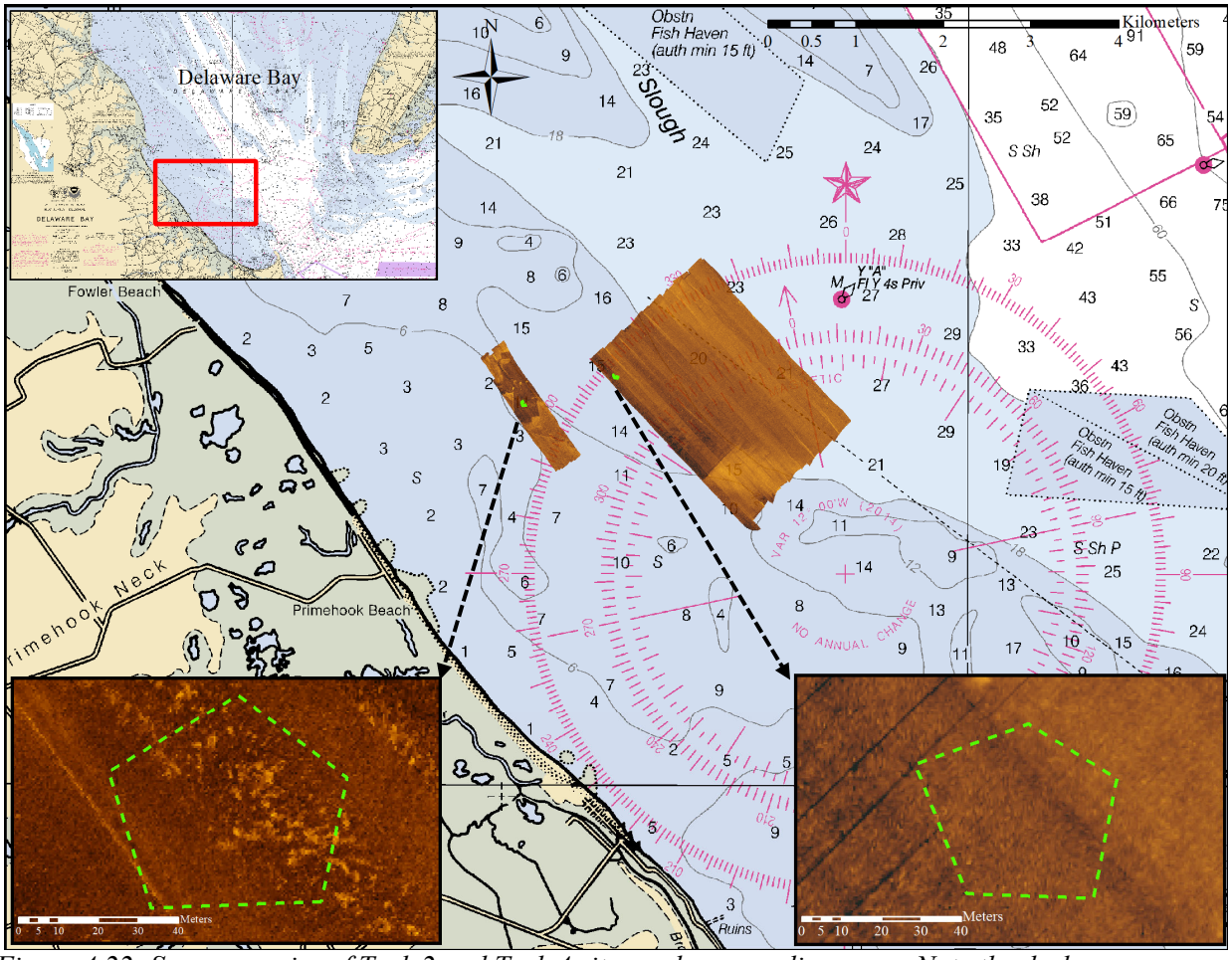



*Figure 4.22: Sonar mosaics of Task 2 and Task 4 sites and surrounding area. Note the darker backscatter at the Task 4 site (bottom left) indicating a softer, more acoustically absorbent sediment than the Task 2 site (bottom right).*

The oceanographic instrument mooring frame was first placed on site, followed by the 6 VPS moorings. Consultation with Vemco determined that the previous VPS deployments were more conservative with regards to sensor spacing than necessary. Sensors were expanded to 30 – 35m spacing for the third deployment. After VPS mooring deployment, four reference tag posts and 10 tagged munitions were distributed around the site (due to manufacturing delays, the 4.2-inch surrogates were not available for the Fall 2018 deployment). After the completion of the VPS grid, surface sonar and AUV surveying confirmed VPS and surrogate locations.

On Sept. 9-10, 2018, the field area was hit by an extra-tropical storm (ETC). An AUV survey was conducted on Sept. 17 to assess the effects of the storm on the field site. Sonar imagery showed that 4 of the 6 VPS sensors had been knocked over, and the oceanographic instrument frame was no longer on site. Due to weather conditions, sonar surveys could not be conducted until Sept 21-23 to locate the frame. On Sept. 23, the instrument frame was located. The final position of the frame was 316 m SE of the original location. Two attempts to recover the frame via ROV were unsuccessful. On Oct. 1, the instrument frame and all 6 VPS receivers were recovered by contracted commercial divers. Data was downloaded and sent to Vemco to establish whether the receivers had worked despite being knocked over, and whether the surrogates were still within the original study site. Vemco confirmed that the VPS sensors did receive data, and that the surrogates were still within the original study area. Data analysis from the instrument frame found that, despite moving 316 m, the instruments were not damaged and recorded data throughout the deployment.

With the confirmation from Vemco, the decision was made to redeploy the instrument frame and VPS in modified configurations. Deployment occurred during a weather window on Oct. 9, 2018. Four additional 25-lb plates were added to the instrument frame to increase the unit's weight, and University of Delaware divers staked the frame in place on site. From the available data, it was hypothesized that the VPS receivers were "flipped" when the storm scoured underneath the wooden feet, exposing the broad, flat surface of the feet to currents, which then caught and flipped the moorings over. In response, the wooden feet of the VPS moorings were perforated to reduce the amount of surface area for currents to apply force, and to allow for quicker "settling" of the mooring upon deployment. The 6 VPS moorings were deployed near the original positions recorded from the Aug. 29 deployment. Final recovery of the instrument frame, VPS moorings, and surrogate munitions was planned for the first week of Nov., 2018. Due to weather conditions and subsequent scheduling conflicts with the Delaware State Police SCUBA Unit (DSPSU), equipment retrieval was rescheduled for Nov. 19. To assist in recovery, surface vessel sonar and AUV magnetometer surveys were conducted on Nov. 7. The sonar surveys indicated the presence of the instrument frame at the initial deployment site, but four VPS receivers were once again knocked over. Data later retrieved from the instrument frame recorded an intense and rapidly building storm striking the site on Oct. 27-28, 2018, resulting in significant burial of the instrument frame and surrogate munitions, while once again knocking over four VPS receivers despite modifications to the receiver poles.

On Nov. 19, 2018, DSPSU divers began recovery of the instrumentation. Strong currents and zero visibility hampered retrieval. Immediately, it became apparent that significant burial had occurred, with no surrogate munitions visible in the DSPSU sector scanning sonar. Using surrogate positions estimated by Vemco after the Sept. storm, three buried surrogates were located via handheld metal detectors. The divers reported the surrogates buried anywhere from

20-30 cm below the surface. Only 1 VPS sensor was retrieved before conditions forced diver operations to be suspended. The instrument frame was also recovered before departure from the site. Diver operations resumed on Nov. 30, 2018. Targeting positions estimated from Vemco and sonar data, divers conducted circle searches with handheld metal detectors. Once again, strong current and zero visibility hampered operations. An additional 3 VPS sensors and 3 surrogates were retrieved during operations. Final operations to recover the remaining VPS sensors and surrogates was conducted on Dec. 7, 2018. The final 2 VPS sensors and 1 surrogate were recovered, leaving 3 surrogates buried on site. Due to scheduling conflicts and winter weather conditions, the decision was made to suspend diver operations until after the New Year. In all, the instrument fame, all 6 VPS receivers, and 6 out of 10 surrogates were retrieved.

#### *4.2.6.2. Spring 2019 Field Deployment*

Following the completion of the second deployment, four surrogate munitions remained on site and buried in the sediments. Seasonal conditions suspended further attempts to recover the remaining surrogates. On March 14, 2019, efforts to recover the remaining surrogates resumed with the help of the DSPSU. Despite adequate conditions and extended operations, only 1 of the 4 surrogates was recovered. Divers reported the surrogate buried 20-30cm deep in soft mud. The decision was made to cease operations to recover the remaining surrogates and turn efforts towards preparing for the fourth and final deployment. The deployment was to be conducted at the same location as the previous deployment for further site characterization, but would also allow for additional search efforts for the lost surrogates at the end of the final deployment.

*Table 4.8: Summary of activities associated with Task 4 Spring 2019 deployment*

| **Spring 2019 Deployment** | | | | | |
|---|---|---|---|---|---|
| *Deployment Dates* | *HR2 Receiver* | *Reference Tags* | *Surrogates* | *Instruments* | |
| 27 Mar - 20 May 2019 (48 Days†) | 6 | 4 | 13 | ADCP, PC-ADCP, CTD, Rotary Sonar | |
| *Survey Dates* | *Side-Scan* | *Bathymetry* | *Sub-bottom* | *Magnetometry* | *Sediment Sampling* |
| 27-Mar-2019 | X | X | | | X |
| 9-May-2019 | X | X | | | X |

†Instrument Frame removed 9 May

The final deployment was conducted over Mar 27 – May 20, 2019 (see Table 4.8). Based on the results of the previous deployment, the acoustics receiver poles were modified to reduce issues with the poles tipping over. After consultation with Vemco, the manufacturer of the acoustic receivers, the poles were reduced in height from 2 m to 1.5 m, and the bottom clump weight doubled from 45 to 90 lbs. Six HR2 acoustic receivers and the acoustic instrument frame were deployed in a grid at the field site on March 27, 2019. The site was mapped with side-scan sonar and phase-measuring bathymetry to characterize the initial conditions and verify the placement of the acoustic receivers. On March 28, 2019, the surrogate munitions were placed within the study grid, along with 4 reference tags for use with the acoustic receiver grid. To replace the missing surrogates, an additional four 4.2-inch surrogates were used in the deployment. The surrogates were new to the study and designed and implemented based on the recommendations of Calantoni MR-2320. In all, 11 surrogates were deployed within the grid. All deployment operations were conducted from the surface without the assistance of the DSPSU. Following the surrogate deployment, surficial sediment samples were collected around the study site.

On May 6-8, a second sonar survey was conducted over the site and additional sediment samples were collected. After completing the survey, the hydrodynamic instrument frame was recovered from the site due to anticipated battery depletion. On May 20, Delaware State Police SCUBA Unit successfully recovered all 6 VPS receivers at Site 2, as well as 2 surrogates from the site. Due to scheduling, efforts to retrieve the final 9 surrogates could not be resumed until July 8. Weather prevented SCUBA operations on July 8, and operations were rescheduled for July 22-23. To assist recovery operations, Vemco provided MR-2730 with last known surrogate positions from VPS sensors retrieved on May 20. Divers were rescheduled for July 22-23, 2019, but DSPSU was called to complete crime-scene investigations during this window. DSPSU diver operations were then pushed into August. Personnel and DSPSU availability resulted in delays until Aug. 19, 2019.

On August 19, 2019, diver operations resumed to recover the remaining surrogates. Divers reported only shallow burial, as compared to deeper burial observed in Fall 2018 deployment. All told, using the VPS aided positions, all spring 2019 deployed surrogates were recovered, as well as 2 of 3 surrogates left from the fall 2018 deployment, despite having been deployed for nearly a year to the day (Aug. 29, 2018 – Aug 19, 2019). Upon inspection, all surrogates were in optimal condition, although IMU battery life was exceeded with the smaller caliber surrogates. Field operations were concluded after this, with only one 60mm surrogate left unrecovered.

In concert with the final deployment, MR-2730 collaborated with Dr. Nina Stark (MR18-1233) concerning the use of a portable freefall sediment penetrometer (Figure 4.23a), per SERDP 2018 IPR recommendations. Dr. Stark and her team assisted in the geotechnical characterization of the sediments from both the Task 2 and Task 4 study sites. The sonar data and sediment samples from May 6-8, as well as sonar imagery from the 3 previous deployments, were used to inform drop penetrometer. Dr. Stark and a graduate student conducted penetrometer sampling on May 14-15 with assistance from MR-2730. Sampling occurred within, near, and in the surrounding region of MR-2730 Site 1 and 2. In all, 23 separate locations were sampled, with 4 penetrometer drops per site. Additionally, 4 static pore pressure tests were conducted (2 at each site) for a minimum of 30min per test. Surficial sediment samples were collected at each site, and 2 gravity cores (1 at each site) collected to assist the penetrometer geotechnical characterization (Figure 4.23b). MR-2730 is continuing to work with Dr. Stark to complete the analysis as part of SERDP project MR20-1480.

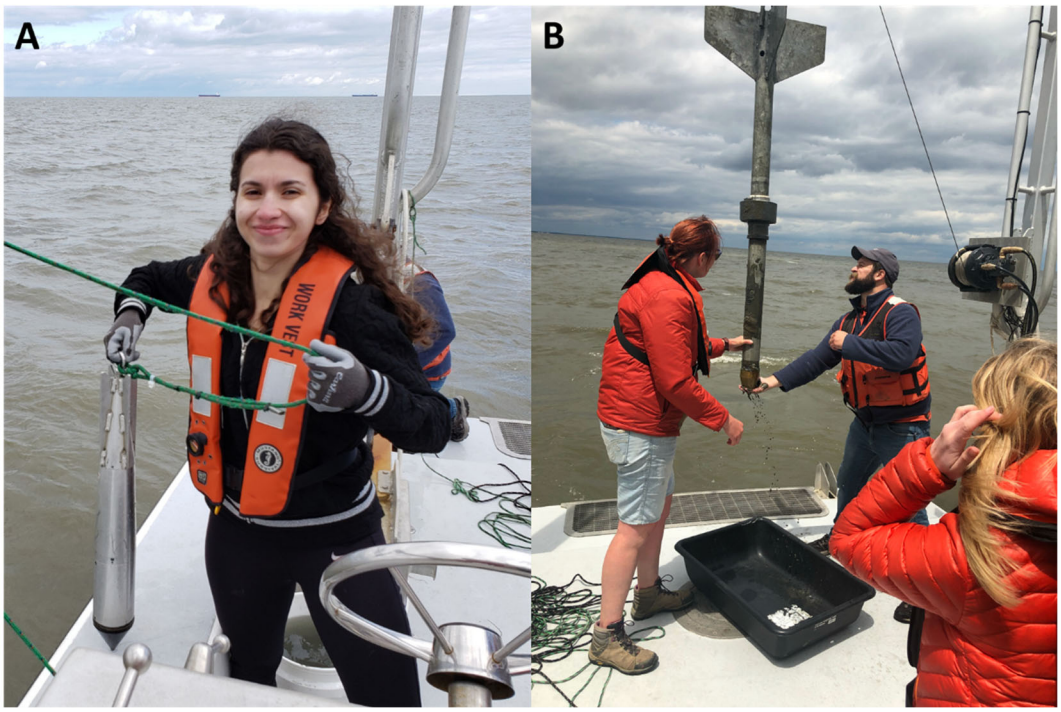



*Figure 4.23: Geotechnical site characterization was provided by Dr. Nina Stark (MR18-1233) and her team. Data was collected with a portable freefall penetrometer (a), and ground-truthed with sediment samples and gravity cores (b).*

# 5. Results and Discussion

The results and discussion of the MR-2730 field experiments are organized into 2 sections. Each deployment yielded unique results that are reviewed within the context of each individual deployment (5.2. Results by Deployment). Collectively, the entire field program (Tasks 2 and 4) presents a wider context within which to examine the deployments and discuss implications for munitions mobility and burial in cohesive settings (5.2. Cumulative Results and Discussion).

## 5.1. Results by Deployment

### 5.1.1. Fall 2017 Deployment

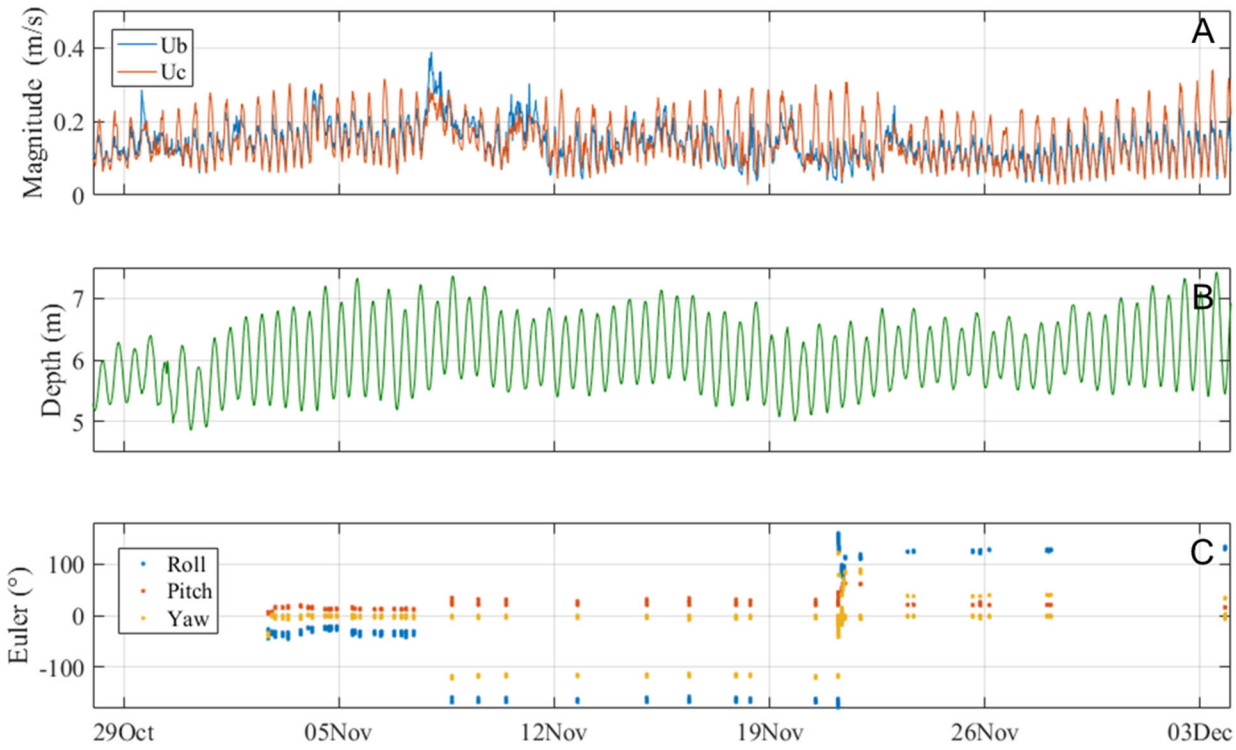



*Figure 5.1: Time-series measurements from the Fall 2017 deployment showing near-bed orbital and unidirectional current (A), pressure depth (b), and example IMU data from a 60mm mortar (C).*

Over the course of the Fall 2017 deployment, no storm activity was observed. The hydrodynamic data from the instrument frame indicated only one small wave event on Nov. 8, with the majority of the bottom currents driven by semi-diurnal tides (Figure 5.1a). Despite this, the IMU data from all three 60mm mortar and one 81mm mortar did record motion data. These IMU were set to "motion trigger wake-up," upon which only minimal motion is required to start the IMU logging. After a period of 5 minutes of no activity, the IMU would go back to "sleep" mode. There were multiple instances in the aforementioned surrogates where the IMU would wake up, but little to no motion was recorded. In the case of one 60mm mortar (Figure 5.1c), the IMU was triggered frequently after deployment, but with little indication of horizontal mobility. This pattern continued until the unit appeared to roll approximately 120 degrees, after which the IMU was triggered less frequently. This motion was captured 16 hours after the peak of the

small wave event on Nov. 8, so it is unclear whether the two are associated. It is possible the small wave event initiated scouring and a small scour pit was formed, which the surrogate later rolled into. Such behavior was noted in similar mine burial studies (e.g. Jenkins et al., 2007). One more series of close temporal measurements occurred on Nov. 21, in which slight deviation in roll, pitch, and yaw were measured. This motion occurred during slack tides (low current velocity) and with no significant wave conditions. The lack of current forcing suggests that another source, perhaps biologic in nature (the area is frequented by whelk, rays, and horseshoe crabs), resulted in the movement on Nov. 21. Data from the other surrogates do not indicate recorded movement at that time. Direct observations from the rotary sonar were limited, as the unit developed a leak around the cable connector running from the data logger to the sonar head. Despite the limited observations, images that were recorded infrequently suggest that some limited scour or setting occurred. In Figure 5.2, the smaller surrogates become notably less distinguishable as the deployment progresses, and the 155mm surrogate appears to settle into the sediments. Although difficult to discriminate in the limited rotary sonar images, the DSPSU divers did not observe any of the surrogates to have undergone complete burial (see Figure 5.3).

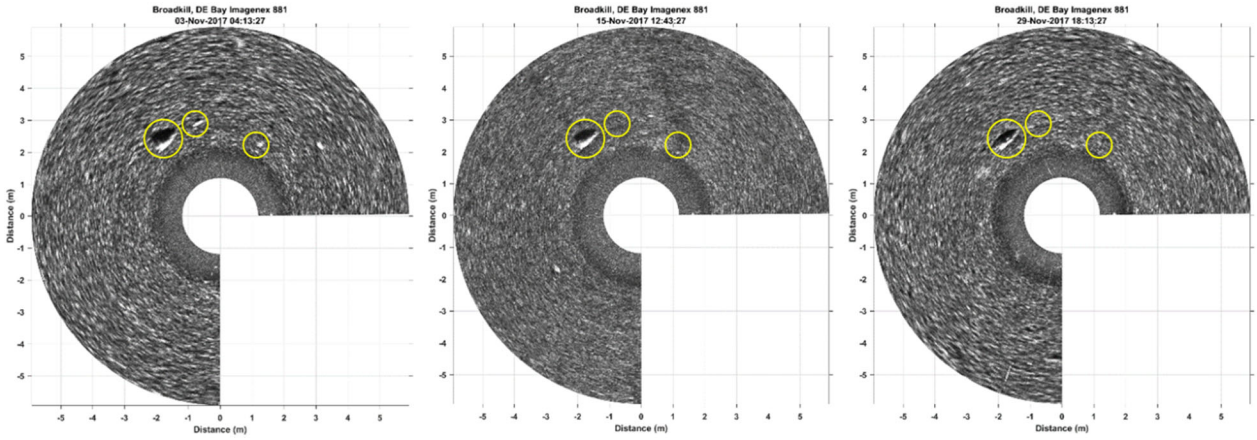



*Figure 5.2: Snapshots from the rotary sonar data collected in the Fall 2017 deployment. Note the smaller surrogates become less distinguishable as time progresses from Nov. 3 (left), to Nov. 15 (center), and to Nov. 29 (right).*

Data from the VPS array were processed by Vemco and delivered in late January. Vemco reported that the data quality was excellent overall, and only suggested the addition of one more reference tag for the Spring 2018 deployment. A filtered snapshot of the VPS results are presented in Figure 5.4. The VPS tracking data was filtered using a simple threshold filter to remove points with large Horizontal Positional Error (HPE) and Root Mean Square Error (RMSE). The more robust data points did not show significant lateral shifts, although limited scattering was noted. This was likely due to a sharp change in sound speed velocity resulting from tidal activity or fresh (rain) water input, since no corresponding motion was recorded in the IMU data. The filtered data was further analyzed to estimate the offset in tag positions between the nose and tail, which would indicate the overall length of the surrogate (Figure 5.4). Estimated length from the VPS data proved to be within 10% of the measured surrogate length. Surrogate orientation is discernable for each surrogate when both acoustic tags are clearly detected. No significant changes in orientation were recorded for any of the surrogates in the Fall 2017 deployment. With burial, the surrogate tag detection count in the VPS may serve as a proxy for burial observations; the VPS test in the boat basin (section 4.2.1.4) showed tags were

no longer detectable when buried. The VPS detection count shows little decrease in detection over the course of the deployment (Figure 5.5). Thus, no net lateral migration and little burial was distinguishable in the VPS, supporting DSPSU diver, IMU, and geophysical survey data.

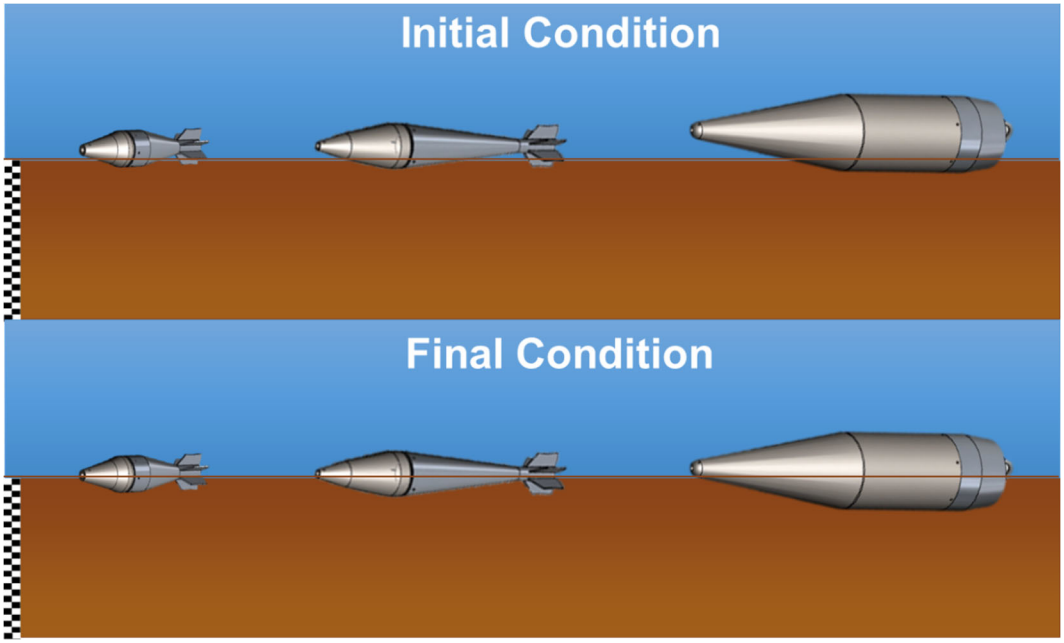



*Figure 5.3: Surrogate munitions status during the Fall 2017 deployment as reported by DSPSU divers.*

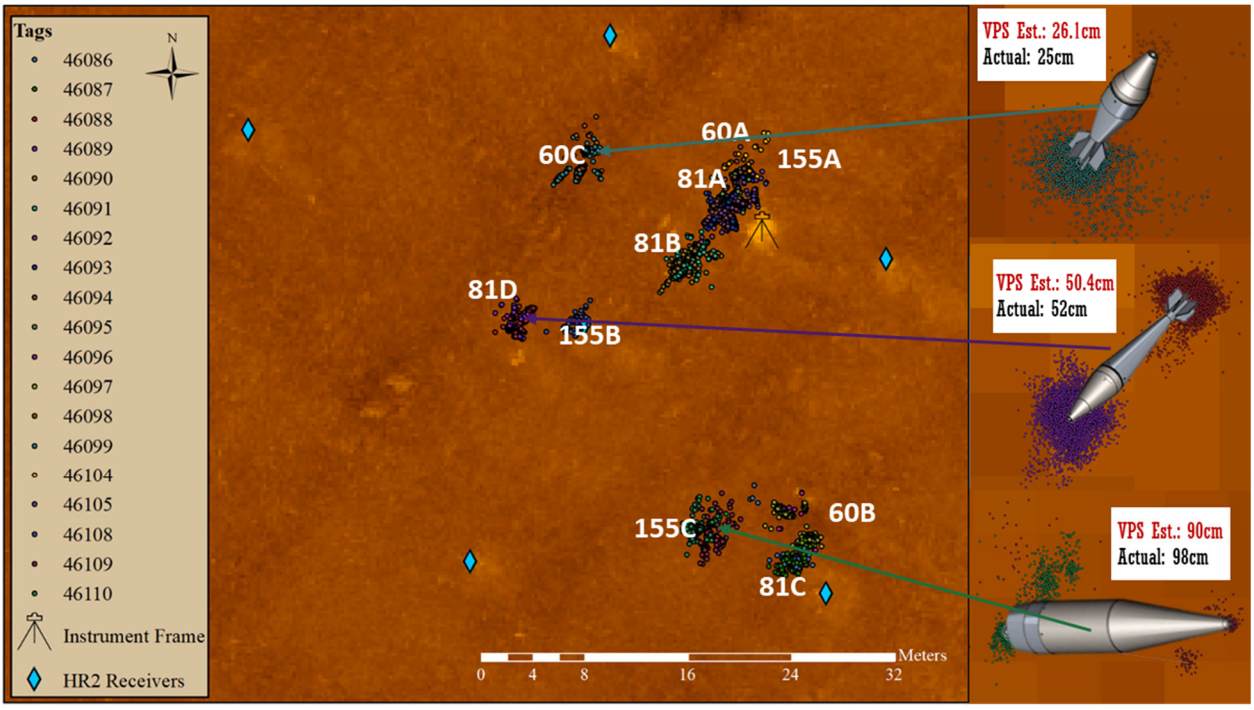



*Figure 5.4: Preliminary VPS acoustic tracking results from the Fall 2017 deployment. VPS estimated measurements of surrogate length derived from acoustic tag locations compare well to true surrogate length. Note the shift in position of the 155mm is likely due to a sharp change in sound speed.*

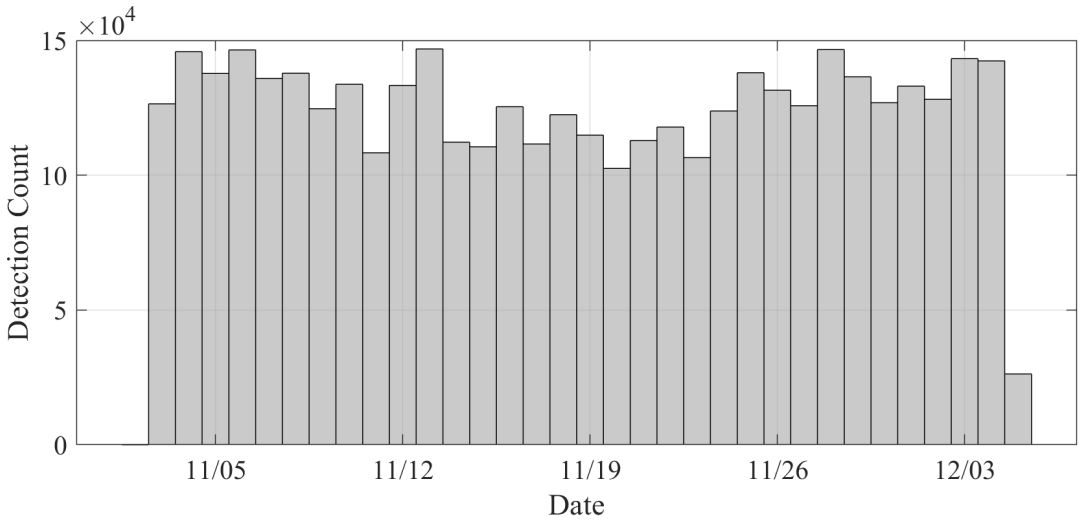



*Figure 5.5: Daily VPS detection count for surrogate tags over the Fall 2017 deployment.*

## 5.1.2. Spring 2018 Field Deployment

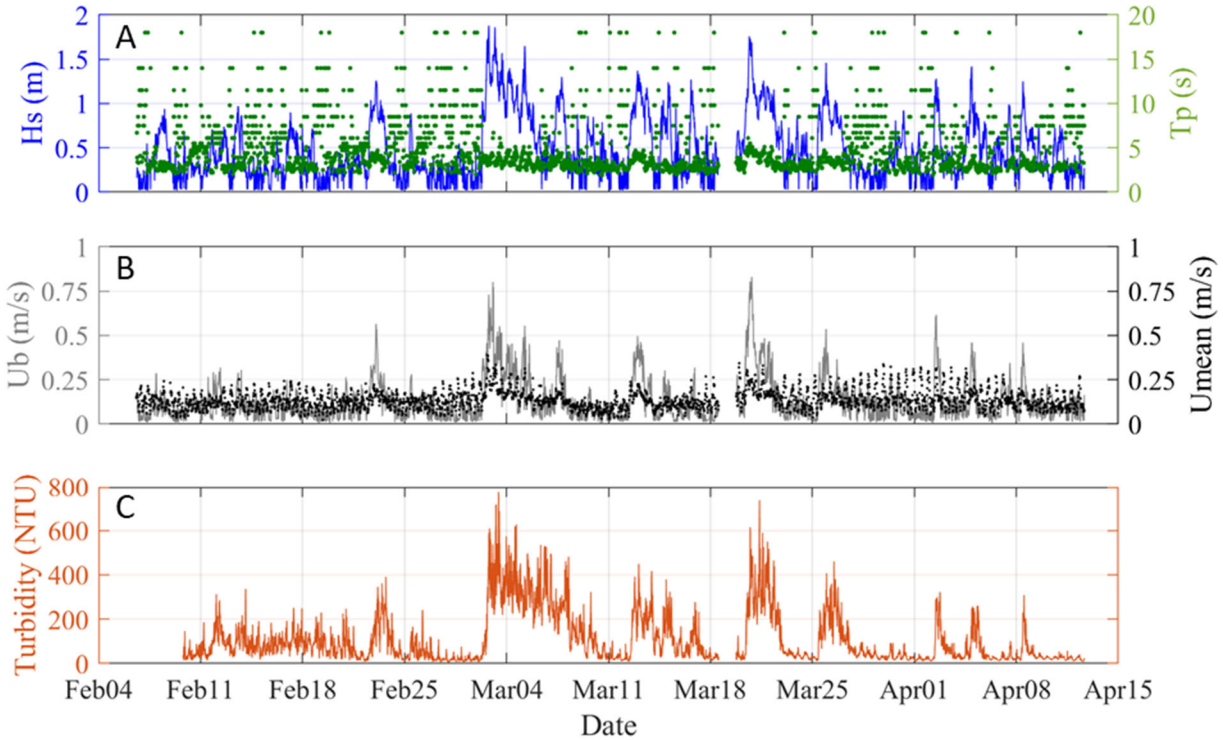



*Figure 5.6: Significant wave height and peak wave period (A), near bed wave orbital and unidirectional currents (B), and turbidity (C) recorded over the Spring 2018 deployment. Note the turbidity unit did not properly auto-scale to adjust for higher magnitudes during storm – values shown are corrected using scaler estimated from the Spring 2019 deployment.*

Whereas the Fall 2017 deployment had no storm activity, the Spring 2018 deployment captured 4 nor'easter storms and several other energetic wave-driven events. All 4 nor'easters occurred in March, bookended by "Winter Storm Riley" on Mar. 3, and "Winter Storm Toby" on Mar. 20, 2018 (Figure 5.6a). Both Riley and Toby exceeded significant wave heights (Hs) of 1.75 m and near-bed orbital velocity (estimated) above 0.8 m/s. Winds from Riley were out of the northwest, or shore-parallel, driving waves down the Delaware Bay towards the study site. From this direction, Riley was more fetch-limited, despite topping 1-m wave heights for 66 hours. Conversely, Toby generated winds out of the northeast, or shore perpendicular, and was not as fetch limited as Riley. Although exceeding wave heights of 1 m for only 45 hours, Toby generated higher wave orbital and mean currents (Figure 5.6).

The first site survey, on Mar. 6, occurred immediately after Riley and just prior to Quinn. The surrogates appeared partially buried, but with no scour pits discernable in the sonar (Figure 5.7a). The ROV survey, which showed a partially buried 81mm surrogate (Figure 5.7c), was conducted on Mar. 18, after Riley, Quinn, and Skyler, but only two days before Toby. In the AUV sonar data from April 10, the 155mm surrogates are shown sitting in large scour pits (Figure 5.7b). This corresponds with the April 11 observations from DSPSU divers, who noted that the 155mm surrogates were sitting in large scour pits and were buried 50-60%. The DSPSU divers also noted, over the course of the 3 retrieval operations (Apr. 11, Apr. 26, and May 7), that the smaller surrogates (81 and 60mm mortars) were either mostly or fully buried. DSPSU divers reported two 81mm mortars entirely buried, laying at a slight pitch angle, with the tail fins closest to the surface and under 1 inch (2.5 cm) of overburden. A third was observed with only 2 fin blades exposed (the condition of the fourth 81mm was not described). Two of the 60mm mortars were described by the divers as lying mostly buried at a nearly vertical pitch, with the tail fins exposed (the condition of the third 60mm was not described). Figure 5.8 illustrates the divers' descriptions of the surrogates.

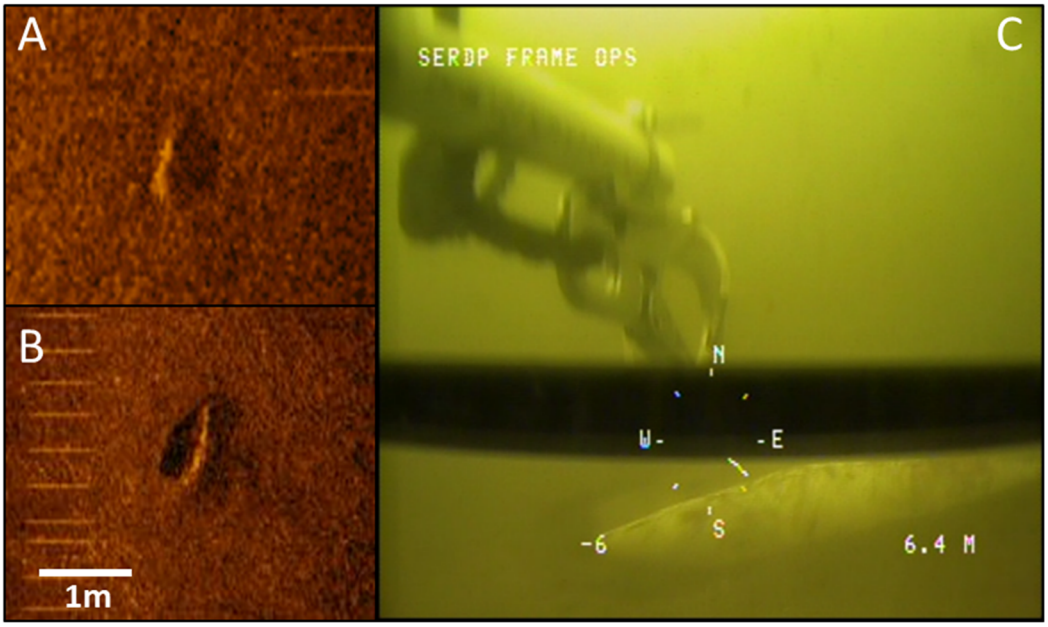



*Figure 5.7: Sonar images of a 155mm surrogate partially buried by nor'easter Riley taken on Mar. 6, 2018 (A), and the same 155mm partially buried in a scour pit taken on Apr. 10, 2018 (B). ROV image of a partially buried 81mm surrogate taken on March 18, 2018 (C).*

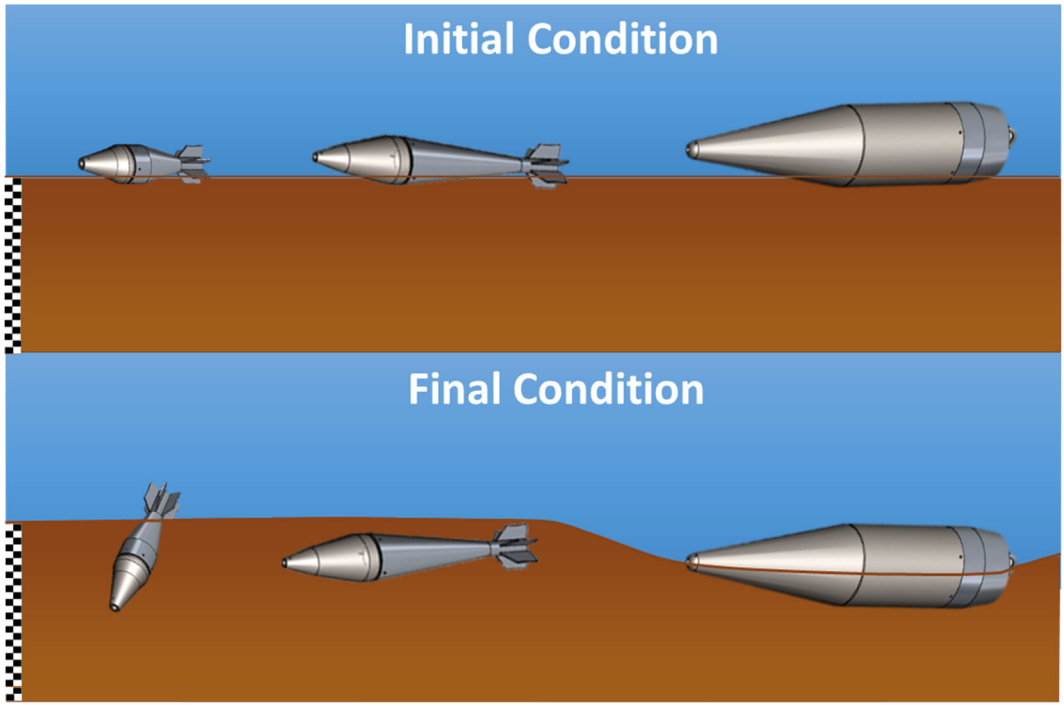



*Figure 5.8: Diagram illustrating the general conditions of each surrogate type at deployment and upon recovery based on the Delaware State Police SCUBA Unit observations for the Spring 2018 field study.*

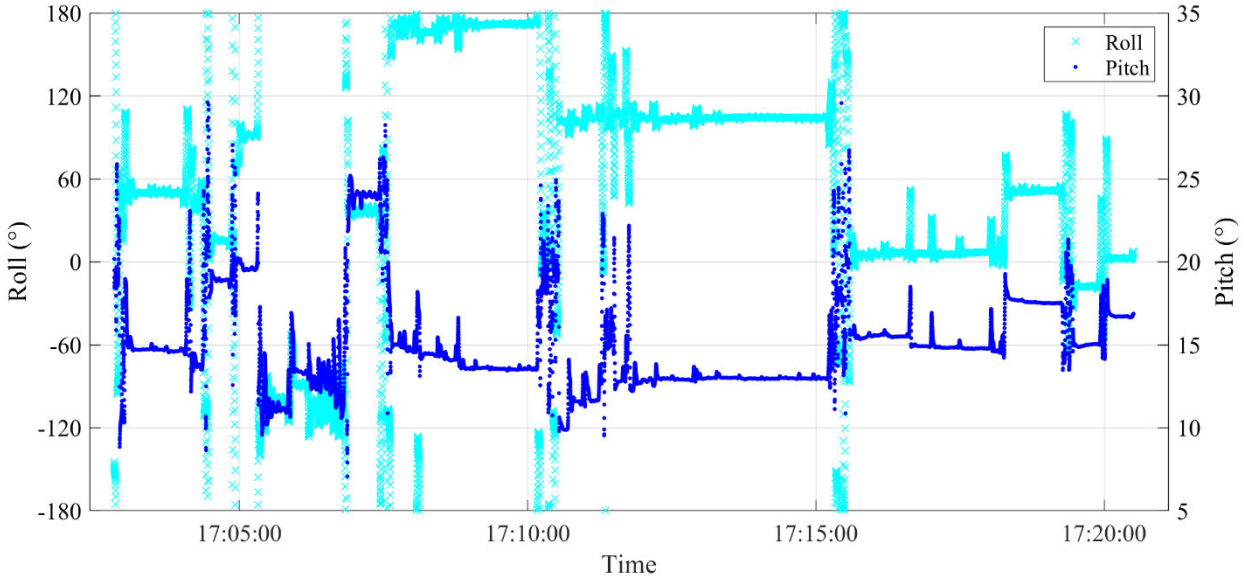



*Figure 5.9: Roll and pitch recorded during Toby in a 60mm surrogate. Note the 10-15 degree increase in pitch, which appears during periods of rolling and for extended periods in static moments, suggesting the unit may have rolled into and out of a scour pit.*

No large-scale horizontal mobility was observed in the Spring 2018 deployment despite the number and intensity of the storms. IMU data indicates some minimal movement occurred, primarily during nor'easter Toby. Episodic oscillatory rolling was recorded over the course 1500-2100 UTC March 20, 2018 in all three 60mm mortars. This time frame corresponds with the most energetic conditions recorded during nor'easter Toby ($U_b$ > 0.5m/s). Slight periodic perturbations are observed in the pitch of one 60mm mortar during its oscillatory rolling, occurring on the order of 10-15 degrees (Figure 5.9). With pitch angle reaching over 25 degrees, and at points sustained for nearly a minute at angles as much as 23 degrees, this may indicate the unit was rolling into and out of a scour pit. The unit eventually settled out with a nominal pitch of 15 degrees, but by recovery, was described by the DSPSU divers as mostly buried and having a near vertical pitch. The final near-vertical pitch not measured in the IMU, suggesting that the process was gradual and did not initiate the IMU motion-trigger wakeup.

The status of the 60mm mortars prior to Toby is unclear: no observations were made by the ROV, and the surrogates were too small to resolve in the side-scan sonar. Rotary sonar data was inconclusive (the DSPSU divers placed the surrogates too close to the rotary sonar, and the surrogates fell within the blanking distance of the unit). The mobility of the 60mm mortars during Toby suggests the 60mm mortars were mostly exposed by the time Toby reached peak forcing. A review of the VPS data sheds some light on the subject. The total detection count for surrogate tags are shown in Figure 5.10, with the date of each storm indicated by vertical dashed lines. Following Riley, the daily detection count greatly decreases (by approx. 50000 detections/day), suggesting some tags, and therefore surrogates, became buried during the storm. Quinn has little effect on the daily count, but with Skyler, the detection count temporarily increases (25.2%), before decreasing back to pre-storm counts. The same pattern is apparent with Toby (13.6% increase). This suggests that both Skyler and Toby temporarily exposed buried surrogates, which in part may explain the mobility observed in the 60mm mortars during Toby. Following Toby, surrogates were again partly buried, with general trend in decreasing daily detections suggesting an additional gradual burial over the quiescent period following Toby (22.2% decrease in detections from Toby to recovery on April 11).

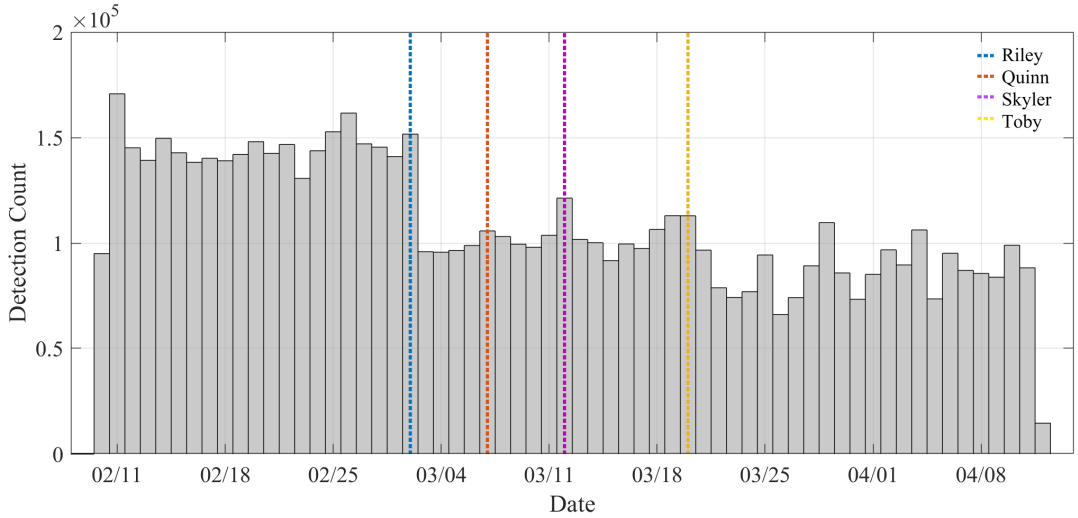



*Figure 5.10: VPS total surrogate detection count by day from the Spring 2018 deployment. Note the effects of the four nor'easters. Riley and Toby cause pronounced decreases in detection, suggesting burial, while Skyler leads to a brief increase in detections, suggesting re-exposure of buried surrogates.*

5.1.3. Fall 2018 Field Deployment

The Fall 2018 field deployment occurred at the second field site. As with the previous deployment, several wave events were observed, including two extra-tropical cyclones (ETC) (Figure 5.11). The first, on Sept. 9-10, generated wave orbital velocities in excess of 0.5 m/s. While it did not exceed the peak values of the March nor'easters, the Sept. ETC had a notable effect on the field site. Four of six VPS poles were knocked over, and the instrument frame was transported 316 m to the SE (Figure 5.12b). The storm itself brought waves out of the E-NE, suggesting that wave-generated currents were not directly responsible for the movement. The onboard attitude sensors of the ADCP indicate the frame moved over 3 separate episodes, aligning with ebbing tidal currents on Sept. 9 and 10 (Figure 5.12a). With water levels 1 m above MHHW (as measured at Lewes Tide Station 10.5 km south of the site), the increased flux of water during ebbing conditions "drug" the frame from the field area as the water rushed out of the Delaware Bay. The instrument came to rest and scoured in an area of muddy sands. The instrument frame and HR2 receivers were recovered on Oct. 1, evaluated for damage, modified, and replaced on site on Oct. 9. Both instrument frame and VPS operated normally until another rapidly building ETC struck the site on Oct. 27, 2018. A succession of high-wind events followed on 11/5, 11/9, and 11/16, the latter of which developed into Winter Storm Avery over the Northeast Unites States.

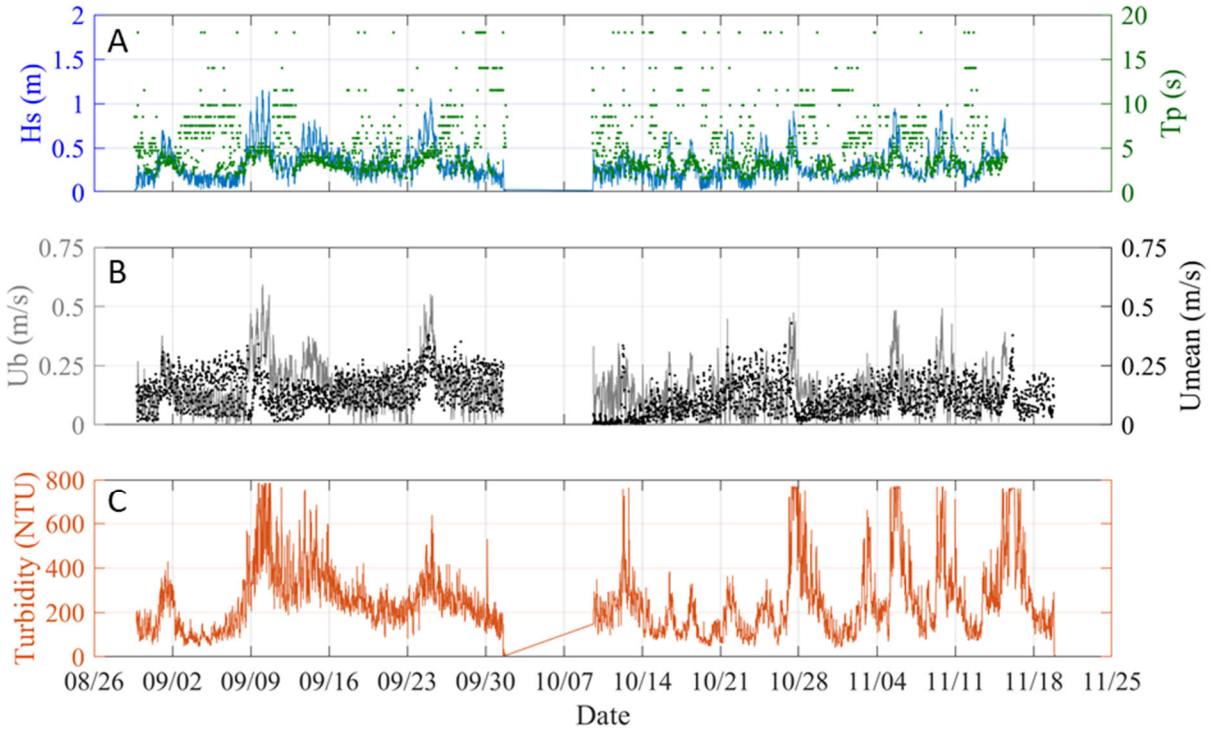



*Figure 5.11: Significant wave height and peak wave period (A), near bed wave orbital and unidirectional currents (B), and turbidity (C) recorded over the Fall 2018 deployment. Note the turbidity unit did not properly auto-scale to adjust for higher magnitudes during storm – values shown are corrected using scaler estimated from the Spring 2019 deployment.*

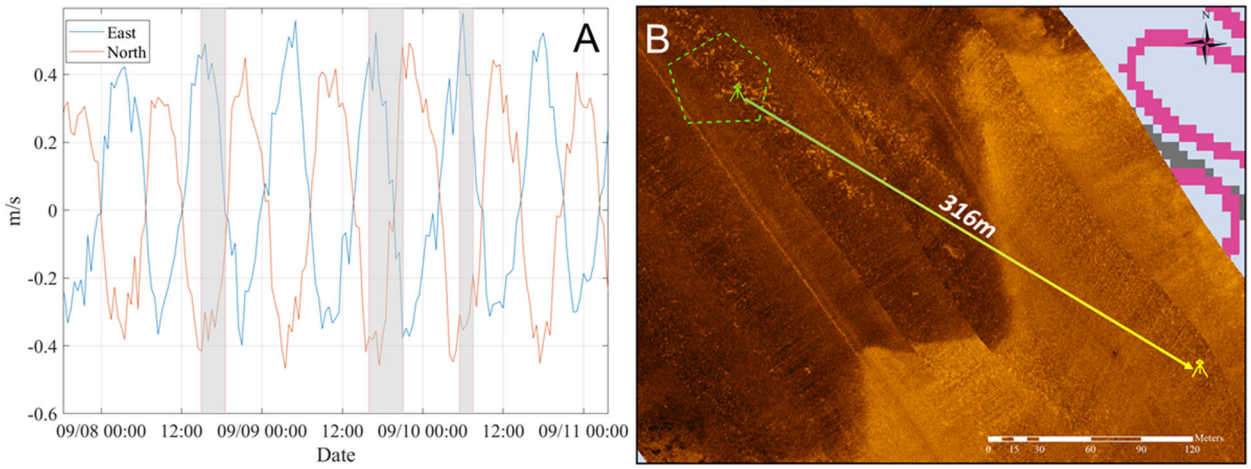



*Figure 5.12: The instrument frame migrated 316m to the SE (b) in three separate episodes concurrent with ebbing tides.*

Although four receivers were knocked over, the VPS continued to function through the deployment. Prior to redeployment on Oct. 9, the data was sent to Vemco for rapid processing to establish whether the surrogates remained in the area. Since the >200lb instrument frame had become mobile during the Sept. ETC, there remained a concern that the lighter surrogates may have mobilized as well. The data returned by Vemco estimated the last known positions of each surrogate on site (Figure 5.13). The data did not suggest the munitions had mobilized, but had instead become partially or fully buried. Several tags were still detected by the time of the VPS recovery on Oct. 1. IMU data likewise measured only limited movement of the surrogates, consistent with rocking under oscillatory currents.

Despite modifications to the VPS poles, the Oct. ETC again knocked over four HR2 receivers. The instrument frame, modified with an extra 100lbs of weight, was not transported from the field area, but instead underwent significant burial. Backscatter data from the downward-looking Aquadopp (Figure 5.14a), shows approximately 39-cm burial occurring in only 14 hours. To determine whether burial was primarily due to sediment influx or scour / settling of the instrument frame, we isolated the mean water depth as measured by the onboard CTD before and after the Oct ETC (Figure 5.14b). Based on this estimate, burial by settling accounted for 34.5 cm of the apparent 39cm burial estimated form the Aquadopp backscatter. Following the storm, the estimated distance between the sensor and bed would increase by 9-12 cm, suggesting that the offset in burial between the Aquadopp and CTD water level estimates was due to a layer of high backscatter material, possibly fluidized mud, which was either transported away or consolidated following the storm. This material would again appear during the wave events on Nov. 5$^{th}$, 9$^{th}$, and 16$^{th}$, although no further burial was estimated for the instrument frame.

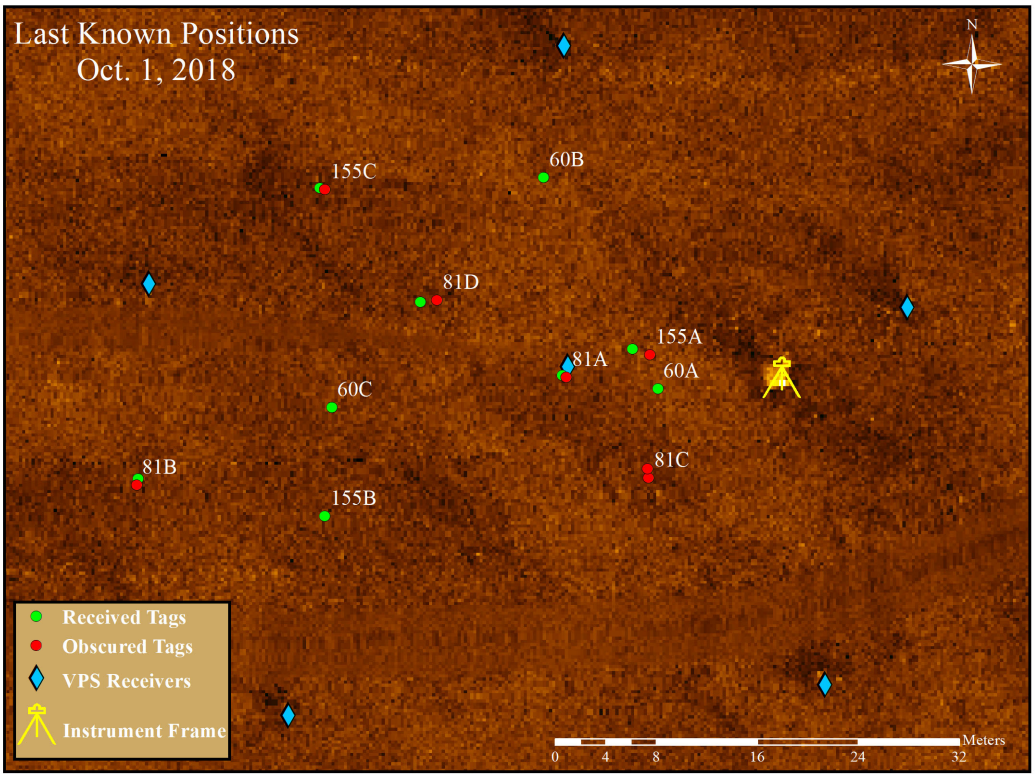



*Figure 5.13: Last estimated positions of surrogates on Oct. 1, 2018 from the VPS. The initial location of the instrument frame is shown in sonar collected on Aug. 29, 2018, although the frame itself was no longer in the field area on Oct. 1.*

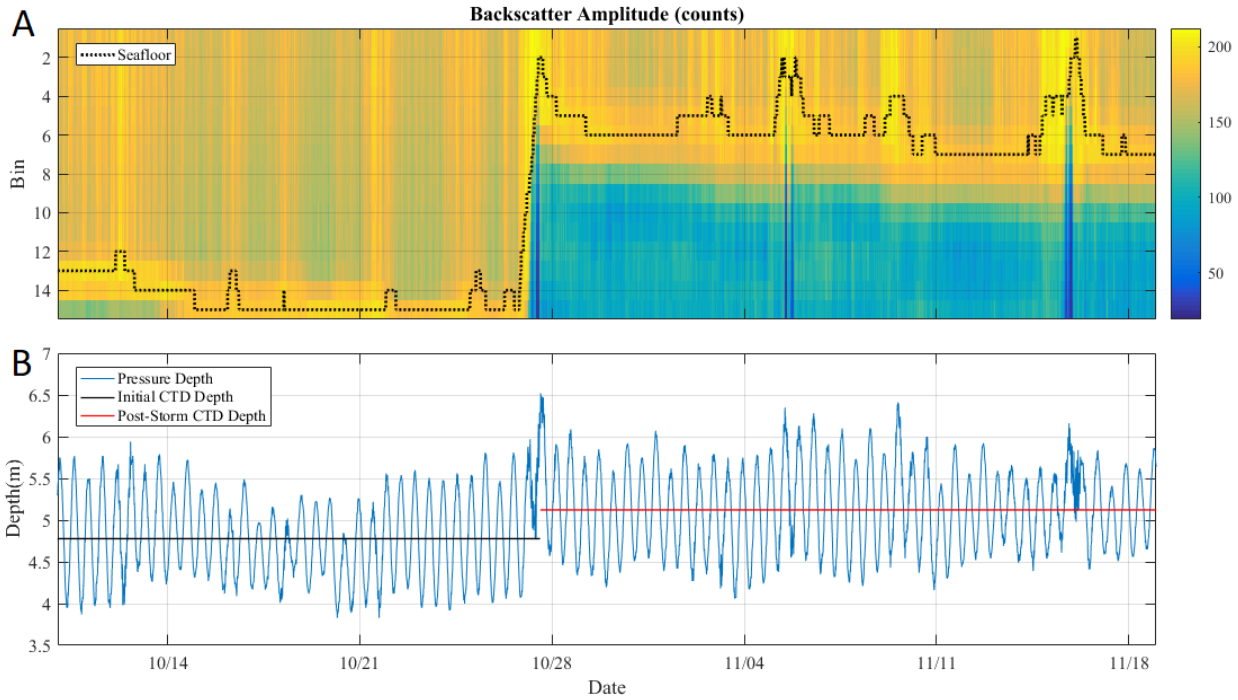



*Figure 5.14: The burial of the instrument frame on Oct. 27 as estimated from the downward facing Nortek Aquadopp HR profiler acoustic backscatter (a), and offset in mean water level from the AML-PlusX CTD (b). The seafloor is estimated in the Aquadopp from the bins with the highest backscatter.*

The recovery of the surrogates by the DSPSU diver was hampered by the burial of the surrogates. Only 7 of the 10 surrogates deployed in Aug. were recovered by the end of the calendar year. The recovered surrogates were found near the last known position estimates from the VPS on Oct. 1, 2018. Due to burial, the divers required small hand-held metal detectors to locate the surrogates. Divers reported the surrogates to be buried between 20 and 30 cm (Figure 5.15) in very soft mud (one diver reported being able to stick his arm all the way in to the mud to the shoulder). The 155mm and 81mm surrogates were laying nearly flat, while the 60mm mortars were again tilted nearly 90° nose-down.

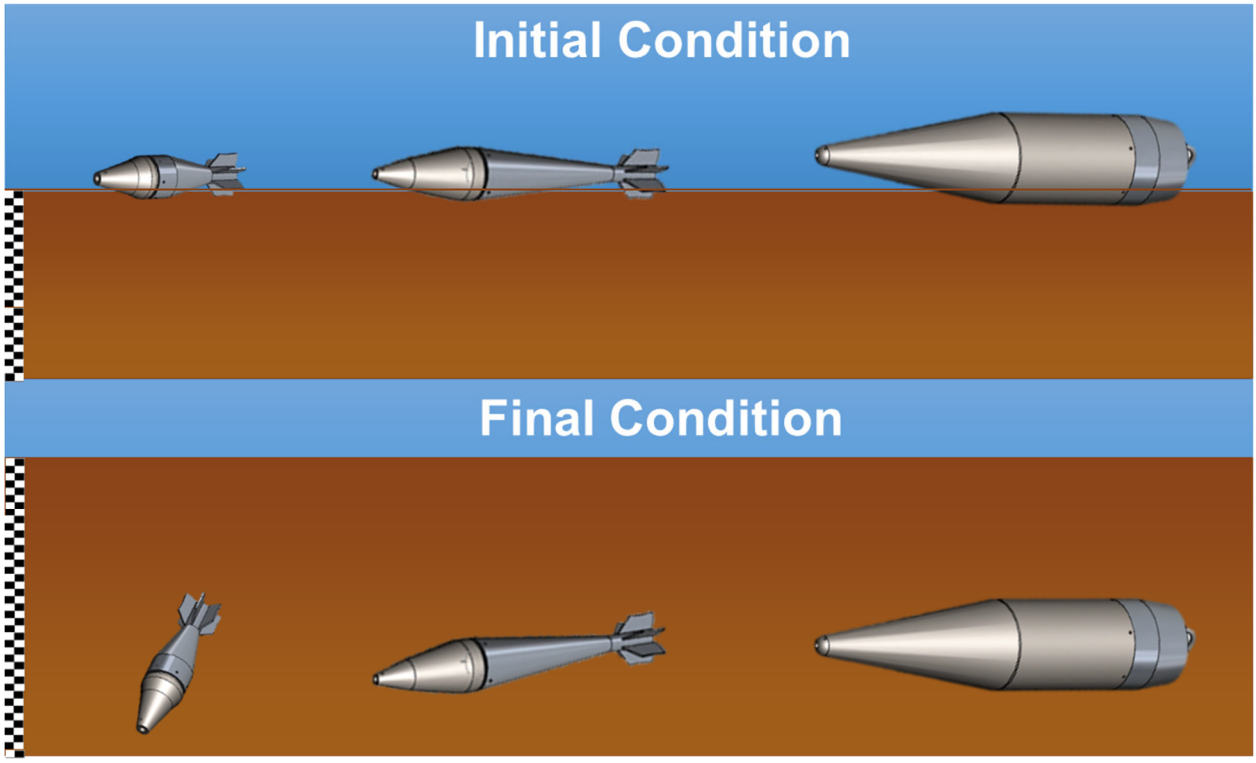



*Figure 5.15: Diagram illustrating the general conditions of each surrogate type at deployment and upon recovery based on the Delaware State Police SCUBA Unit observations for the Fall 2018 field study.*

By the Oct. 1, 2018 recovery of the VPS, several acoustic tags were still being detected, suggesting that 9 of the 10 surrogates were only partly buried. By the time the divers recovered the surrogates in late November, most surrogates were reported as totally buried with overburden. Using the VPS detection count (Figure 5.16), we can isolate when the surrogates became totally buried; however, because four HR2 receivers were knocked over, we first must establish the decrease in performance of the VPS after the receivers fell over. To do so, we isolated the detections of the VPS synctags, located in each HR2 receiver. The daily synctag detection, when all sensor are upright, should be consistent throughout a deployment. After the Sep. ETC, the total synctag detection amongst the 6 receivers dropped by 25.6%. The total surrogate tag detections, dropped by 58.2% following the Sep. ETC (and a small wave event immediately following the storm). This suggest that only some of the decrease in surrogate tag detection can be explained by HR2 performance loss. The rest is explained by partial burial of the surrogates, as indicated by the last known position estimates (Figure 5.13). When the HR2 receivers were redeployed on Oct. 9, the surrogate tag detection count decreased from the last

complete daily count on Oct. 1. This occurred despite the expected increase in performance of the upright HR2 receivers, which were placed within 10 m of their original locations. Since the instrument frame had been removed, no data were available to determine whether another event caused burial. Wind records from the local weather station show only a small event (<10m/s winds) on Oct. 5-6. The decrease in detections may be due to either settling of the surrogates in the soft mud, or burial by sediment settling out after a gale on Sept. 24-25 (Figure 5.16). Detection count remains consistent until the Oct. ETC, which caused 44.6% decrease in surrogate tag detection. Given the rapid burial of the instrument frame, this would suggest further significant burial of the surrogate munitions. However, with 4 HR2 receivers knocked over, the HR2 synctag detections dropped by 62.7%, suggesting that the drop in surrogate tag detection was primarily due to a performance decrease in the VPS. It is unclear whether additional surrogate burial occurred because of the Oct. 27 ETC. Following the ETC, the daily detection counts are low and continue decrease until the recovery of several surrogates and HR2 receivers on Nov. 19, 2018. While the divers reported total burial of all recovered surrogates, it appears that some tags were still detectable as over Nov 19. A review of the detections shows that at least one of the tags belonged to 60B, which would not be recovered until Aug 2019 (and reported as having exposed fins). It is possible then that some surrogates were not buried to the extent reported by the divers, or that the overburden, a soft fluidized mud, only partly obscured the acoustic signal.

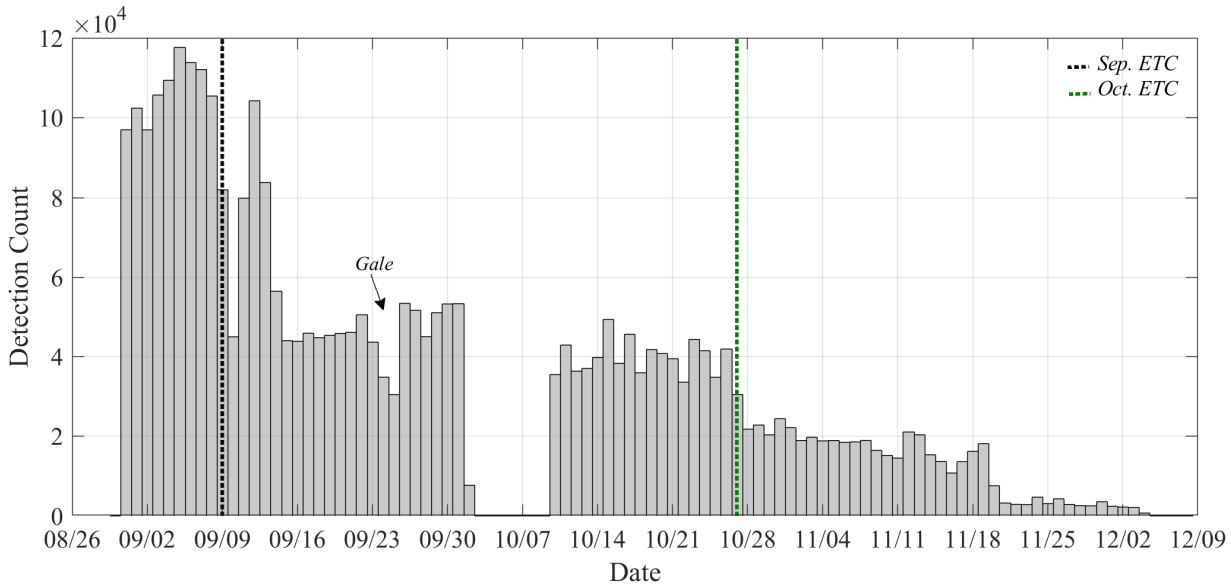



*Figure 5.16: VPS total surrogate detection count by day from the Fall 2018 deployment. Note the effects of the Sep. and Oct. extra-tropical cyclones, as well as a gale on Sep. 25, 2018.*

5.1.4. Spring 2019 Field Deployment

In March 2019, The VPS array was deployed over the same location as the Fall 2018 deployment with the objective of relocating the 3 missing surrogates from the previous deployment. An additional 11 surrogates were placed in the array. Unlike the previous spring, the 2019 deployment did not record any extra-tropical cyclones. Several wave events were recorded during the deployment, but only one, on May 5th, exceeded 1 m waves or 0.5 m/s wave orbital velocities (Figure 5.17). Comparatively, the lower relative turbidity in 2019 also suggests that less active sediment transport occurred during the deployment window.

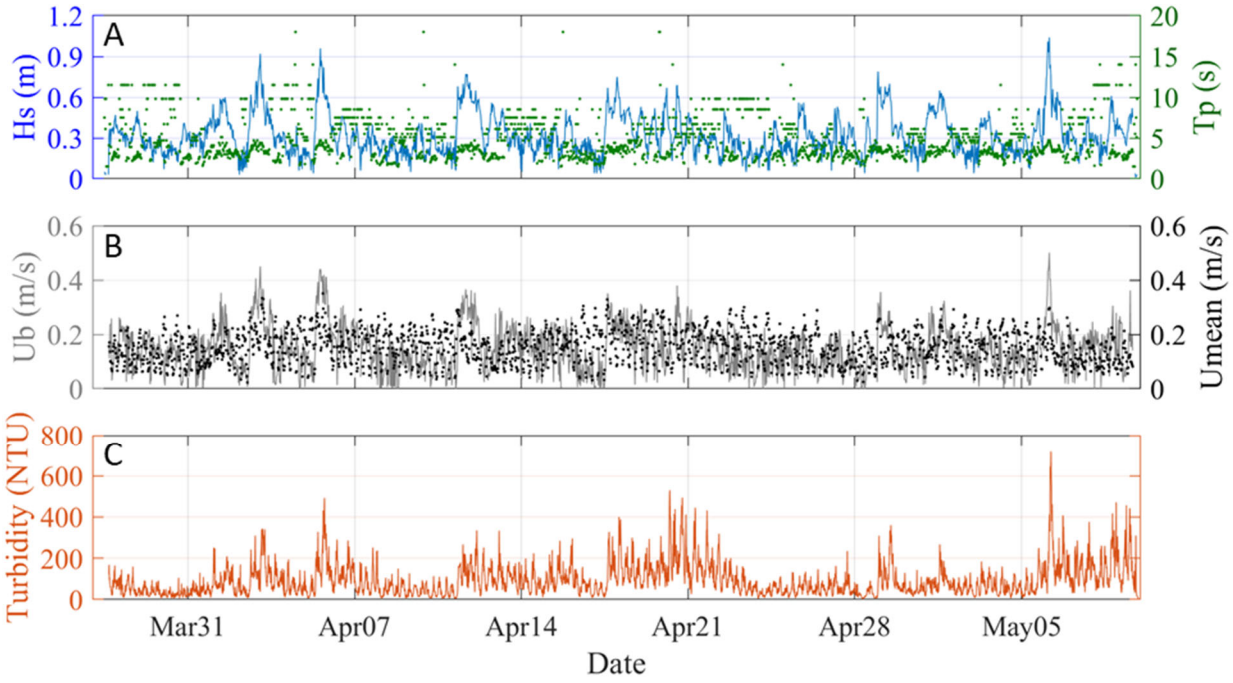



*Figure 5.17: Significant wave height and peak wave period (A), near bed wave orbital and unidirectional currents (B), and turbidity (C) recorded over the Spring 2019 deployment.*

Despite more moderate conditions, the DSPSU divers reported that all surrogates were mostly buried (Figure 5.18). The 155mm and 4.2-inch surrogates were nearly 100% buried, lying flat with just the tops of the surrogates flush with the seafloor. The 81mm were buried at a slight angle, with the fin tips flush with the seafloor. The 60mm mortars were again buried at a near 90% tilt, with the fins either partly exposed or just below the sediment surface. A review of the VPS daily detections (Figure 5.19), supports the DSPSU observations. Over the course of the deployment, the surrogate detections show a trend in decreasing detections. The May 5 event causes a discernable decrease in detections, followed by a rapid decrease in detections to 13.3% of the initial daily detections count, and only 11.3% of the maximum daily detections on May 19 (with the VPS recovered on May 20, the last complete daily count was May 19, 2019). While several surrogates remained *in situ* until Aug 19, 2019, divers reported the remaining surrogates were in similar states of burial as those recovered on May 20, 2019.

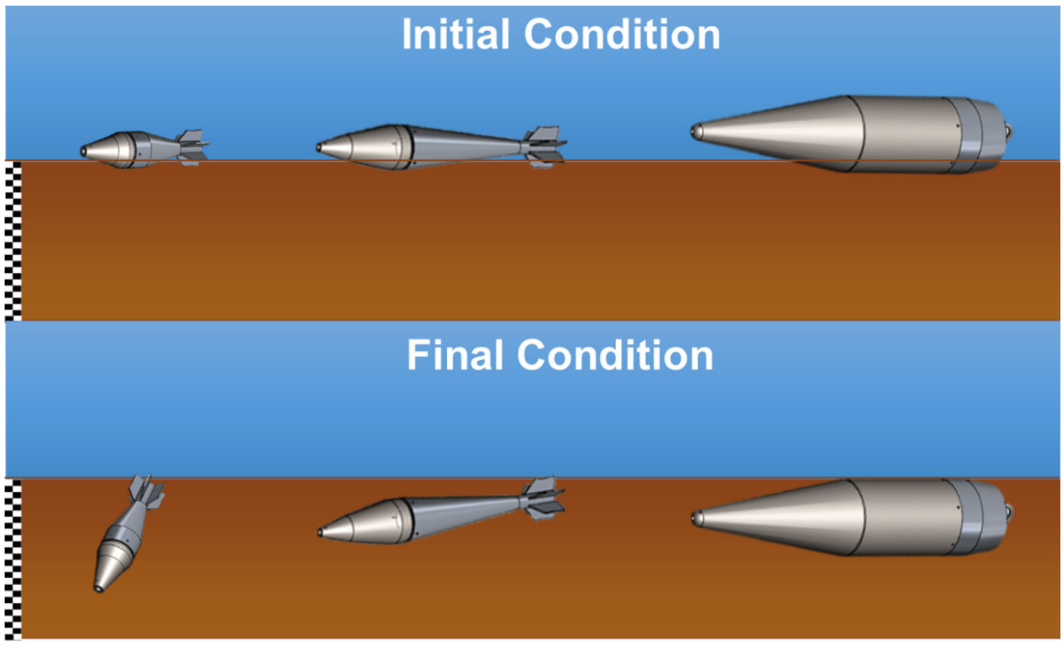



*Figure 5.18: Diagram illustrating the general conditions of each surrogate type at deployment and upon recovery based on the Delaware State Police SCUBA Unit observations for the Spring 2019 field study.*

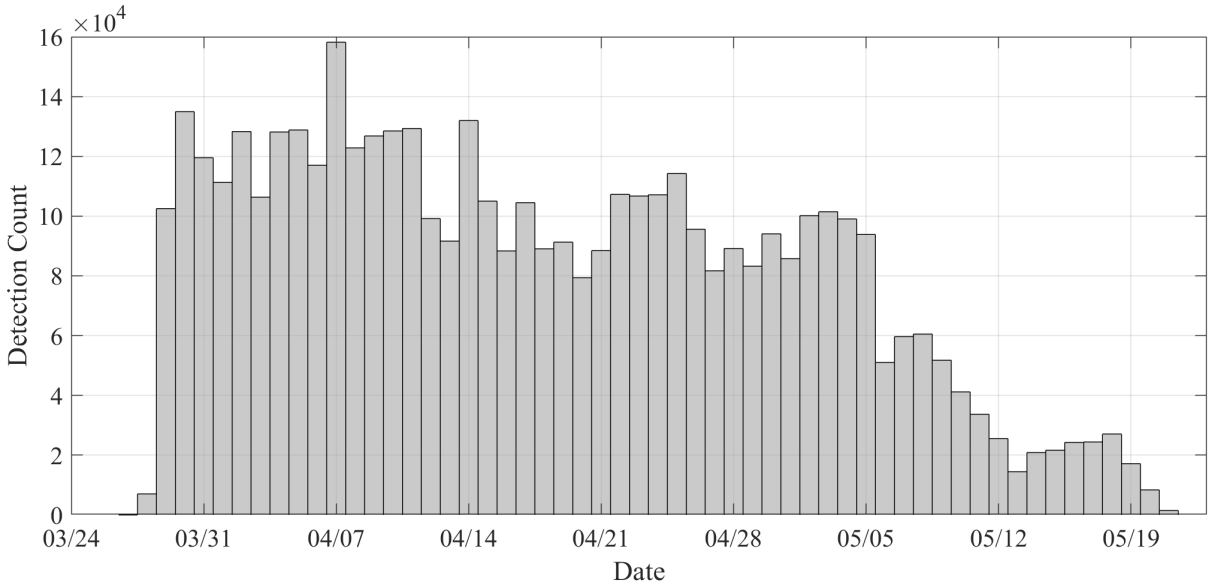



*Figure 5.19: VPS total surrogate detection count by day from the Spring 2019 deployment.*

## 5.2. Cumulative Results and Discussion

### 5.2.1. Hydrodynamics

In considering munitions mobility and burial, the context provided through analysis of historical hydrodynamic conditions is necessary for characterizing the fate of munition in underwater environments. MR-2730 documented six ETC and multiple wind-generated wave events over the course of Task 2 and 4. These events had definable physical effects on the field sites, through active sediment transport and burial of surrogate munitions. Establishing where these events fall within the context of historical data will help define whether such events are frequent or excessive for the region. Should these events be on the upper limits of intensity, then the observations in MR-2730 would provide context for munitions mobility and burial in cohesive sediments from background conditions to extreme events.

Extreme event analysis for impacts on coastal systems typically utilizes threshold value to define an extreme event. For extra-tropical cyclones, studies have typically turned to significant wave height (see Dolan and Davis, 1992), with a 99$^{th}$ percentile or higher threshold value from historical time series records. The only available long-term observations related to storm events in the lower Delaware Bay, however, are wind and water level records. For winds, the Lewes Tide Station (NOAA 8557830) recorded near-continuous hourly average winds from 2005 to present. By frequency of occurrence, the background average winds over this period are approximately 2.75 m/s. Using the 99% threshold, all storms above 14.8 m/s sustained average winds could be considered "extreme events" for the region. With average winds for all 6 ETC in 2018 exceeding 15.2 m/s, they would qualify as extreme events using this metric. All but Skyler would also exceed the 99.5% threshold (16 m/s).

We may also look at where each storm falls within historical monthly and yearly distributions. When considering historical averaged wind speed for the month of March, for example, the four nor'easter storms register as above average to outlier events compared to recorded speeds over the period of 2005-19 (Figure 5.20a). Nor'easter Riley (indicated by the blue X), recorded the second highest average wind speed of any event in March since 2005. The other 3 ETC from March 2018 were not outlier events. The Sept. 2018 ETC was also not an outlier event based on wind speeds for the month of September, although the Oct. 2018 ETC was an outlier event for the month of October. Compared to yearly distributions prior to 2018, Riley, Toby, and the Oct. 2018 ETC were all outlier events. The other 3 ETC (Quinn, Skyler, and the Sept. 2018 ETC) were neither outliers for 2018 nor compared to previous years. On the whole, 2018 did not produce the highest average winds recorded since 2005, but the year was slightly above median annual hourly winds versus historical observations (4.1 m/s vs 4 m/s).

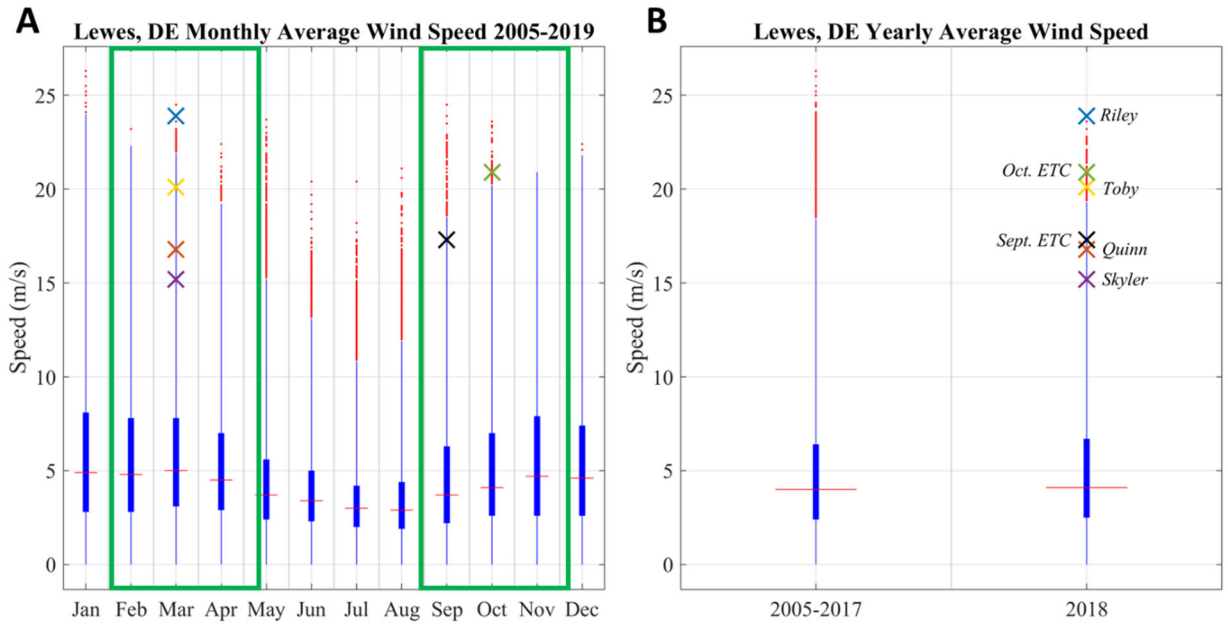



*Figure 5.20: A) Historical monthly average wind speeds at Lewes, DE from 2005-2019 with MR-2730 deployment coverage overlaid. The six 2018 extra-tropical cyclones are demarcated. B) Comparison of hourly averaged winds for 2005-2017 (left) and 2018 (right). The highest average wind speed for the nor'easters are overlaid indicating that nor'easter Riley, Toby, and the Oct ETC were outlier events.*

While no continuous hydrodynamic records exist for the Delaware Bay, instrument deployments by the MR-2730 team are available for episodic hydrodynamic measurements taken over the course of 2016-2017 in the Broadkill Beach region. With a combined 313 days of observations (including MR-2730), an analysis of significant wave height establishes background conditions at 0.24m, while the 99% and 99.5% thresholds are 1.05 m and 1.17 m respectively. Using this threshold, all four March 2018 nor'easters exceeded the 99.5% wave height threshold, and all but the Sept. 2018 ETC topped the 99% threshold. Based on these criteria, at least four of the six ETC observed by MR-2730 would be considered extreme events for the region.

Rennie (2017) and Traykovski and Austin (2017) suggest that the change in wave height over time (*dHs/dt*) and storm duration are important factors for modeling the effects of storms on munitions mobility and burial. These are shown in Table 5.1 along with other hydrodynamic observations of the six ETC of 2018. Duration is calculated by the amount of time (*hrs*) spend above the 99% *Hs* threshold. The rate of change in *Hs* is calculated for the amount of time from exceeding background conditions (*Hs* = 0.24) to the maximum wave height. Another important factor to consider is dominant wave direction, shown here as the values contemporaneous to the maximum recorded wave height. As a fetch limited system, waves approaching from the E-NE have the longest fetch. Additionally, the total water level (TWL) above mean higher-high water (MHHW) is a strong indicator for storm surge, and, as seen with the instrument frame, increased ebb tidal currents. Comparatively, Riley and Toby exceed other storms in every category except TWL. Toby, with waves out the NE, was less fetch-limited the Riley, which may indicate why the limited mobility observed in the surrogate munitions occurred during Toby. Both the Sept. and Oct. 2018 ETC were shorter in duration, but both exceeded 0.9 m TWL and 0.4 m/s mean currents. This may explain why both storms impacted the MR-2730 field site despite being less intense wave events.

*Table 5.1: Comparison of the 6 nor'easter events in observed by MR-2730 in 2018. All conditions reported are the maximum measured / estimated values during the storm. Peak wave direction (Dp) are contemporaneous with max wave height observations. Bolded text highlights notable measurements.*

| | Riley | Quinn | Skylar | Toby | Sept. ETC | Oct. ETC |
|---|---|---|---|---|---|---|
| Duration (hr) | **66** | 11.5 | 19 | 45 | 7 | 0 |
| dHs/dt (m/hr) | **0.15** | 0.08 | 0.05 | 0.1 | 0.02 | 0.06 |
| Hs (m) | **1.88** | 1.3 | 1.37 | 1.76 | 1.15 | 0.92 |
| Dp (º) | 329 | 340 | 60 | 55 | 60 | 49 |
| Ub (m/s) | 0.8 | 0.47 | 0.5 | **0.83** | 0.59 | 0.48 |
| Uc (m/s) | 0.35 | 0.25 | 0.23 | 0.39 | 0.41 | **0.43** |
| TWL >MHHW (m) | 0.71 | 0.59 | 0.32 | 0.59 | **1** | 0.9 |

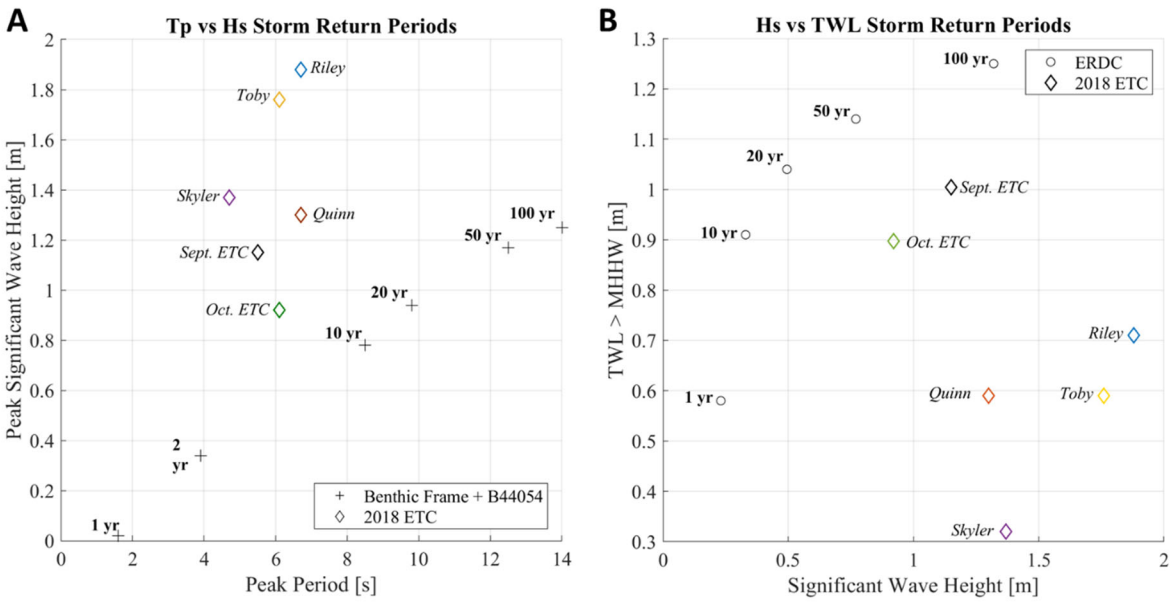



*Figure 5.21: Storm return periods estimated from (A) in situ hydrodynamic observations in the Delaware Bay, and (B) U.S. Army Corps of Engineers Engineer Research and Development Center (Nadal-Caraballo et al., 2015). Figure courtesy of Stephanie M. Dohner.*

While stochastic events, the recurrence interval of storms of the scale of those observed by MR-2730 are important to consider for managing underwater munitions response sites. How frequently a munitions response site must be surveyed is dependent upon the frequency of storms sufficient to cause pronounced sediment transport and surrogate burial or mobility. Using available hydrodynamic observations from the Delaware Bay, Dohner (2020) established storm return periods for the region of the MR-2730 field sites (Broadkill Beach) based on wave properties and TWL. Based on this analysis, the 6 ETC from 2018 were not easily defined by the storm return periods derived from *in situ* hydrodynamic observations in the Delaware Bay (Figure 5.21a) or from U.S. Army Corps of Engineers Engineer Research and Development Center models for Delaware Bay (Figure 5.21b; see Nadal-Caraballo et al., 2015). Based on wave height, the 6 ETC showed characteristics of storms with 10-yr to greater than 100-yr return periods, but with wave period, only from 2 to 10-yr return periods. With water level, only the

Sept ETC exceeded the level of a storm with a 10-yr return period. This would suggest that storms of the magnitude observed by MR-2730, while qualifying as extreme or outlier events, are relatively frequent in the Delaware Bay region. Establishing the historical context of storm events allows for a more informed site management effort.

## 5.2.2. Sediment Analysis

### *5.2.2.1. Sediment Classification*

Over the course of the MR-2730 field study, 63 sediment samples were collected in the study area and the surrounding Broadkill Slough. Of the samples 37 were fully processed. The results show a wide distribution of mixed cohesive sediments (see Figure 5.22). The area of Site 1 was predominantly poorly sorted, fine muddy sand, with 60-75% sand and 25-40% muds. The area of Site 2 was predominantly poorly sorted sandy mud, with 15-40% sand and 60-85% muds. Establishing a notable difference in sediment composition (i.e. muddier) between Sites 1 and 2 was the primary goal of Task 4. The difference in sediment composition had a significant effects on surrogate burial depth between Site 1 and 2 (see Sections 5.1.2 and 5.1.3), and as will be discussed below, has implications for the manner in which the surrogates buried.

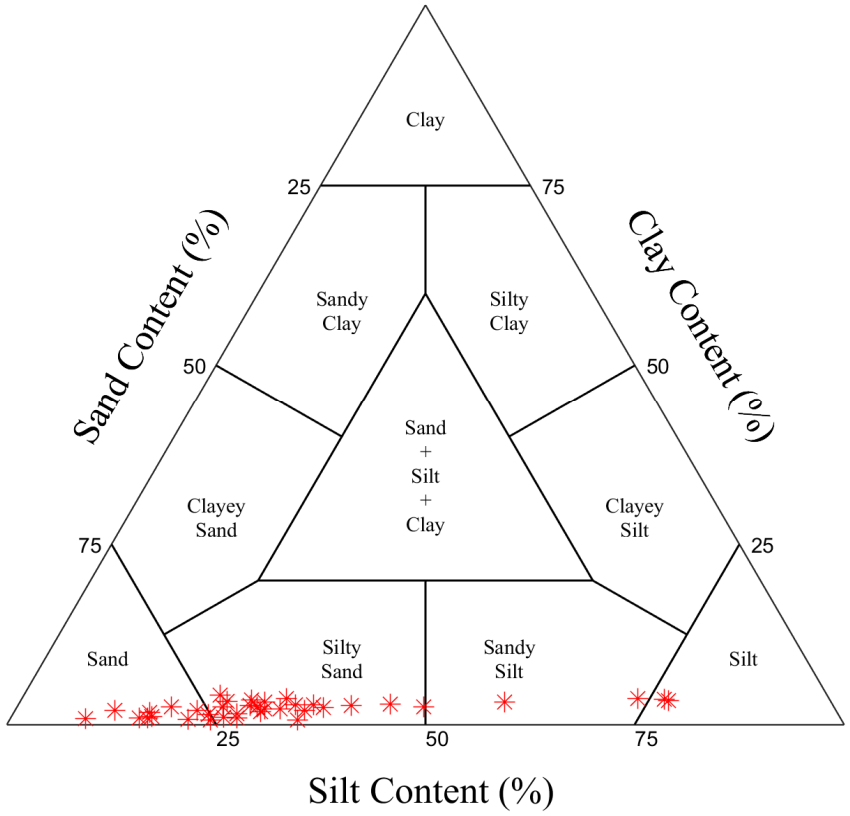



*Figure 5.22: Shepard (1954) sediment ternary diagram for sediment samples from MR-2730 field sites and wider Broadkill Slough region.*

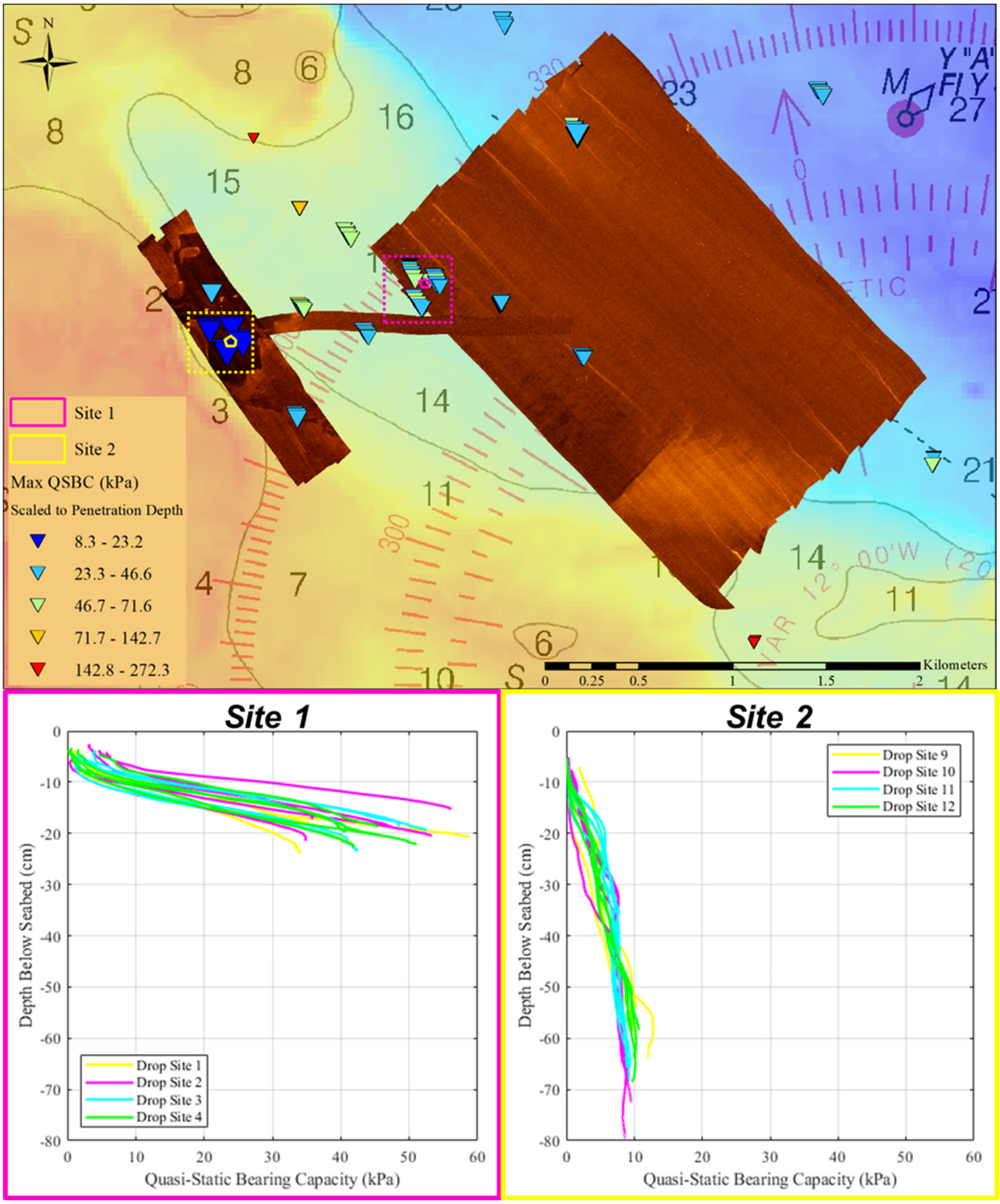



*Figure 5.23: Penetrometer results for MR-2730 field sites and surrounding Broadkill Slough (top) showing quasi-static bearing capacity (QSBC) scaled to penetration depth (deeper penetration = larger symbol). The samples in and around Site 1 (Task 2) and Site 2 (Task 4) are shown below. Note the difference in QSBC and penetration depth between the two field sites.*

To complement the sediment sampling, MR-2730 collaborated with Dr. Nina Stark (MR18-1233) concerning the use of a portable freefall sediment penetrometer (Figure 4.23a), per SERDP 2018 IPR recommendations. Twenty-three separate locations were sampled, with 4-5 penetrometer drops per site. Additionally, 4 static pore pressure tests were conducted (2 at each site) for a minimum of 30min per test. Much of this analysis will be included as part of the final report for SERDP MR20-1480. For MR-2730, the penetrometer results supported the observations of the DSPSU divers and sediment sampling (Figure 5.23). Site 1 showed considerably higher quasi-static bearing capacity (QSBC), with penetrometer measurements ranging between 30-60 kPa at only 15-25 cm depth. QSBC at Site 2 maxed out 8-12 kPa at 60-80 cm depth. Divers reported surrogates buried between 20-30 cm depth at Site 2 (>100% burial), while 100% burial or less for surrogates in Site 1. The much softer sandy mud of Site 2 promoted greater burial that Site 1, where stiffer sediment prevented >100% burial. This will be discussed in more detail in Section 5.2.3.

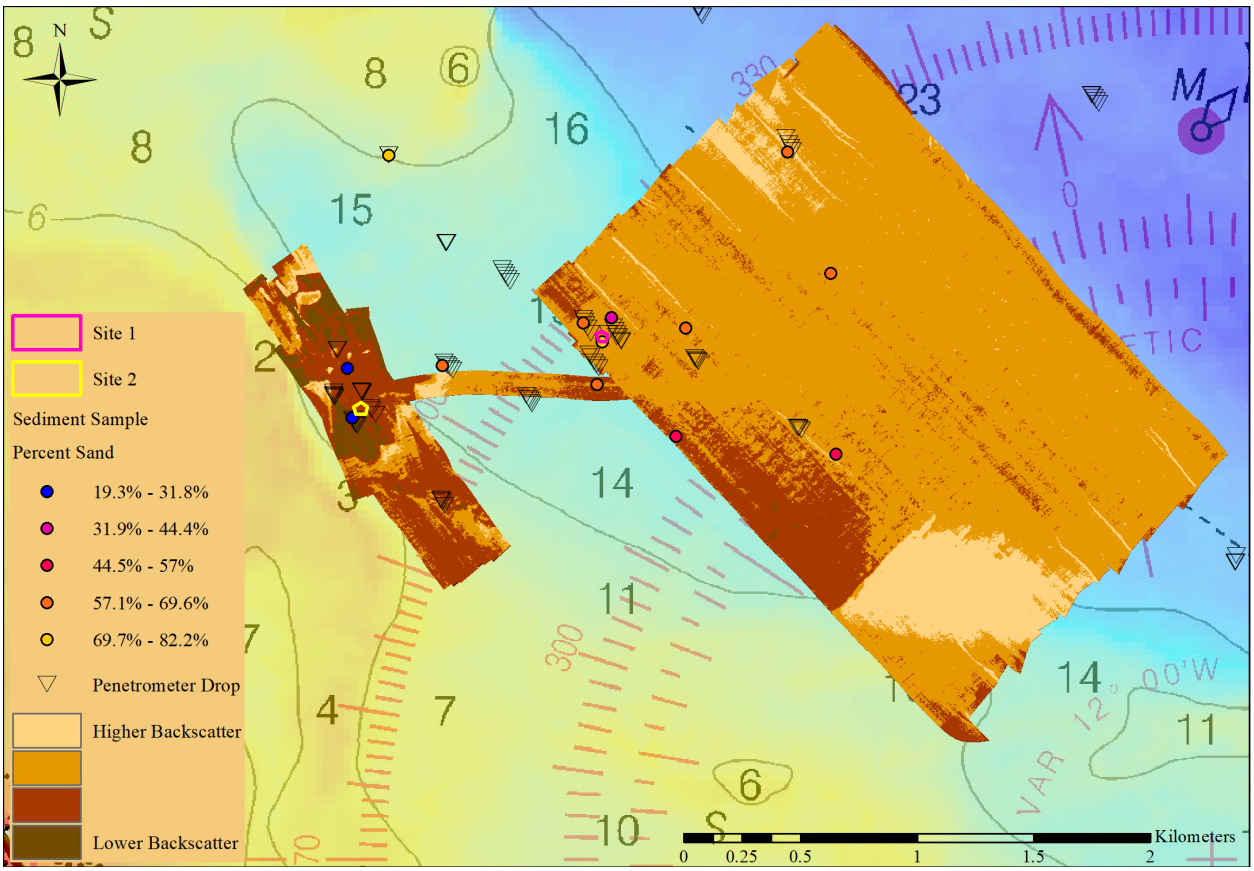



*Figure 5.24: Segmented mosaic for composite sonar imagery using an ESRI ArcGIS supervised classification. Sediment samples, showing percent sand, and penetrometer sample locations are overlaid.*

Sonar collected by the PMES was used to classify sediment distributions at the field sites. Sediment samples provided ground-truthing for image segmentation. The sonar data was mosaicked using Chesapeake Technologies Inc., SonarWiz. Identical gain settings were applied to each, and mosaics were exported with the same settings and colormap. Mosaics were classified using ESRI ArcGIS 10.4. To establish a baseline, a composite mosaic was created from all of the MR-2730 sonar surveys (see Figure 5.23 top). The composite mosaic was then classified using an unsupervised Iso Cluster classification. The Iso Cluster classification

returned 4 separate classes. These classes were then used to inform a Maximum Likelihood supervised classification. The results, show in Figure 5.24, were compared to the processed sediment samples. The areas with higher backscatter (indicated as lighter classes) were assumed to contain higher percent sands. The classified raster values at each sample location were extracted and compared to the sand and mud fraction of each sample. The results show a strong agreement between sand / mud fraction and sonar mosaic class (Figure 5.25). Using this method, the individual sonar mosaics were classified and compared for sediment changes over time (see Section 5.2.2.2).

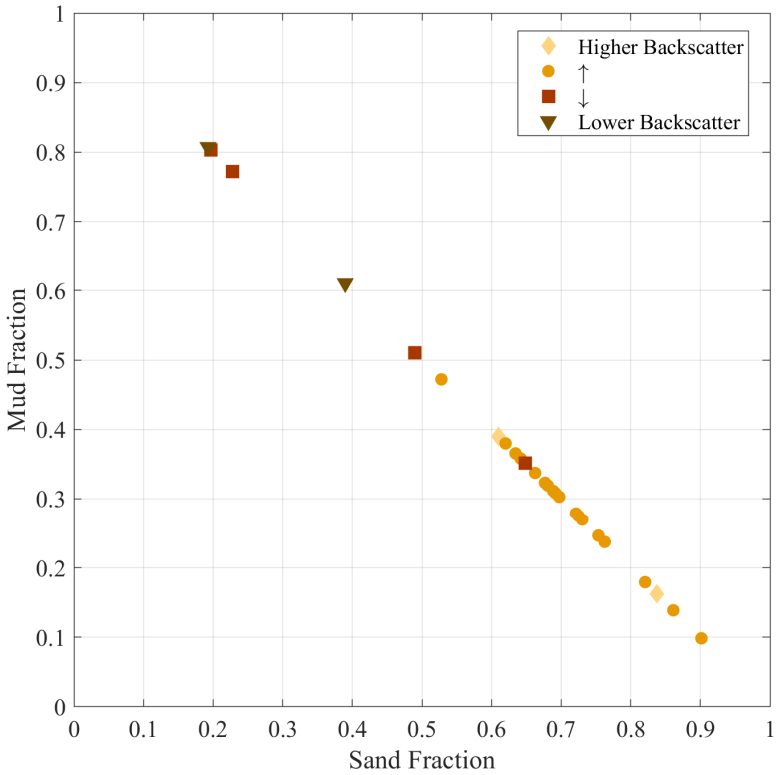



*Figure 5.25: Segmented sonar mosaic classes compared to sand and mud fraction. The results show strong agreement between backscatter intensity and sand / mud fraction.*

While sonars have historically been used to classify surficial sediment distribution, allowing for extrapolation of sediment properties for wider coverage, Dr. Stark (MR18-1233) has expressed interest in determining whether similar methods may be applied to predict sub-surface geotechnical properties. For this exercise, the sediment classes, as defined by sand/mud fraction, were extracted at overlapping penetrometer sample locations. The "classified" penetrometer results are shown in Figure 5.26. Much like the penetrometer results from Sites 1 and 2, there are 2 distinct groups. Areas with higher backscatter (estimated higher sand fraction) tend to have higher QSBC and shallower penetration depth, while areas of lower backscatter (estimated higher mud fractions) show deeper penetration and lower QSBC. Similar results were found by Stark et al., (2016) in their study of Arctic nearshore marine sediments (see specifically Starke et al., 2016 Figure 12). The results are promising, and will be the subject of further analysis for MR20-1480.

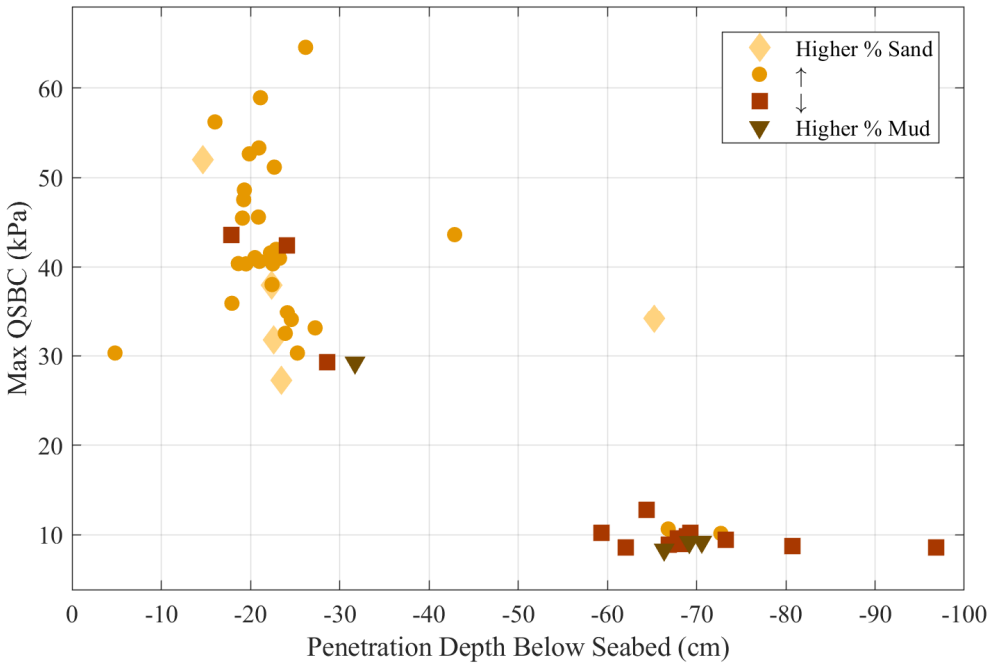



*Figure 5.26: Penetrometer measurements compared to sonar mosaic classification results. Note the 2 distinct groups reflecting higher percent sands (e.g. Site 1) and higher percent muds (e.g. Site 2).*

#### *5.2.2.2. Sediment Transport*

The mixed cohesive sediments in Site 1 and 2 complicate methods for estimating sediment transport. The relationships modeled by the traditional Shields non-dimensional parameter and critical threshold for sediment mobility break down with cohesive forces. As little as 5-15% muds can introduce cohesive effects to sediment, and above 15% muds, sediments are considered cohesive in nature (Whitehouse et al., 2000). Whitehouse et al., (2000) note that mixed sediment with 5-30% muds can increase the critical shear stresses by five times that of equivalent pure sands. All sediments sampled within the study areas and the surrounding Broadkill Slough were transitional to cohesive by this definition.

Modeling the critical shear stress for mixed cohesive sediments is an ongoing topic of research. Properties such as bulk density, consolidation, biological mixing, pore water, and even time can all influence the threshold for erosion of mixed cohesive sediments. Ideally, a threshold for erosion would be estimated from *in situ* measurements (i.e. cohesive strength meter). However, such measurements were not available in MR-2730. In lieu of these, a threshold may be indirectly estimated based on grain size and sand / mud fractionation using the Whitehouse et al. (2000) method. Although the Whitehouse et al. (2000) method does not directly include all of the properties noted above, it provides an empirically-derived threshold estimate that may be applied using the extensive sediment samples collected across the spatio-temporal domain of the MR-2730 field study. Where unavailable, *in situ* values were estimated from existing empirical field values from other studies with similar geotechnical parameters as the MR-2730 samples and utilized in threshold calculations.

A baseline critical threshold value ($\tau_{cr}$) was established using assuming 100% sand for a given d50 grain size from representative sediment samples. Whitehouse et al., (2000) found that the highest critical shear stress for erosion ($\tau_e$) occurred at 20% mud in mixed samples, and was 5x the $\tau_{cr}$ for 100% sand. As no field sample had 100% mud, a representative $\tau_e$ value ($\tau_e$=0.1 N/m$^2$) was used establish the critical shear stress for muds using Whitehouse et al., (2000). Two equations for estimating $\tau_e$ were then solved for using the values estimated above for sediment with mud fractions falling in between the 0-20% and 20-100%. In addition to $\tau_e$, an equivalent mixed cohesive Shields parameter ($\theta$) was estimated using the sampled sediment d50 and the density of the sediment. With the addition of muds, the density of the sediment at field Sites 1 and 2 would not be accurately represented by purely quartz sand density (2650 kg/m$^3$). Instead, we used the density of illite (2660-2720 kg/m$^3$), commonly found in the Delaware Bay sediments (see Velde and Church, 1999). The critical Shields for mixed sediments using the Whitehouse et al., (2000) methods are plotted against the equivalent traditional Shields critical threshold for non-cohesive sediments (quartz density 2650 kg/m$^3$) in Figure 5.27.

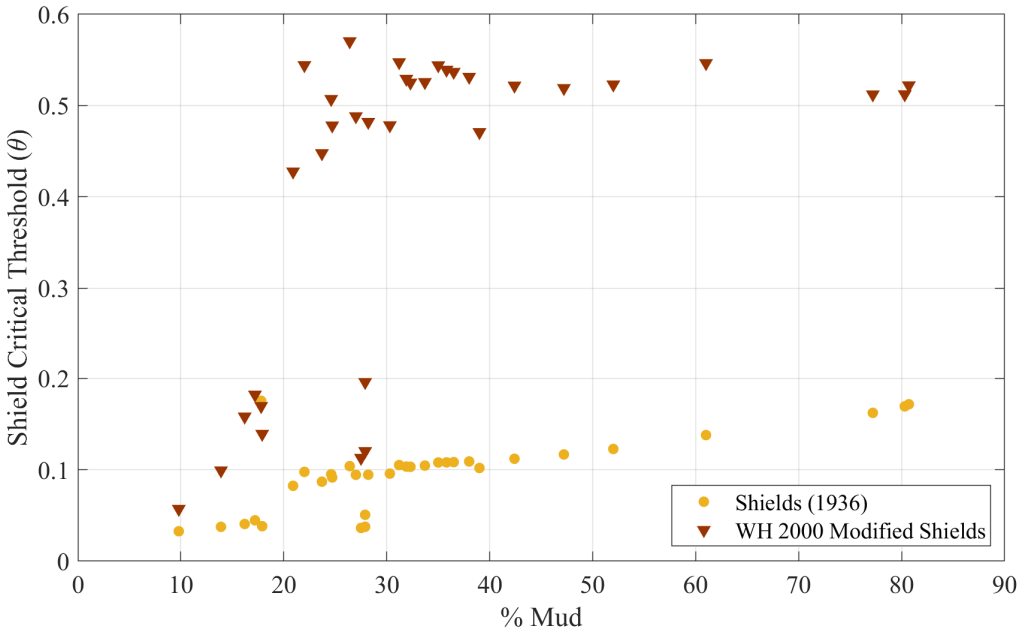



*Figure 5.27: Critical Shields threshold estimates using the traditional Shields (1936) and Whitehouse et al., (2000) method for mixed cohesive sediments.*

Using the calculated critical threshold for erosion, we can begin to characterized the effects of the six 2018 ETC on the field site. Shear stress was estimated using both wave-orbital and unidirectional current, defaulting to whatever mechanism generated the highest stress at the time of each observation. Sediment samples in the area of both Sites 1 and 2 were reviewed, and the upper and lower bounds for mud fraction established. Critical shear stress for erosion was then calculated for these bounds. In Site 1, the sediment was consistent, with mud fraction ranging from 28-36%. For Site 2, a wider range in mud fraction was observed (61-81%), due in part to temporal changes in surficial sediment composition as will be shown below.

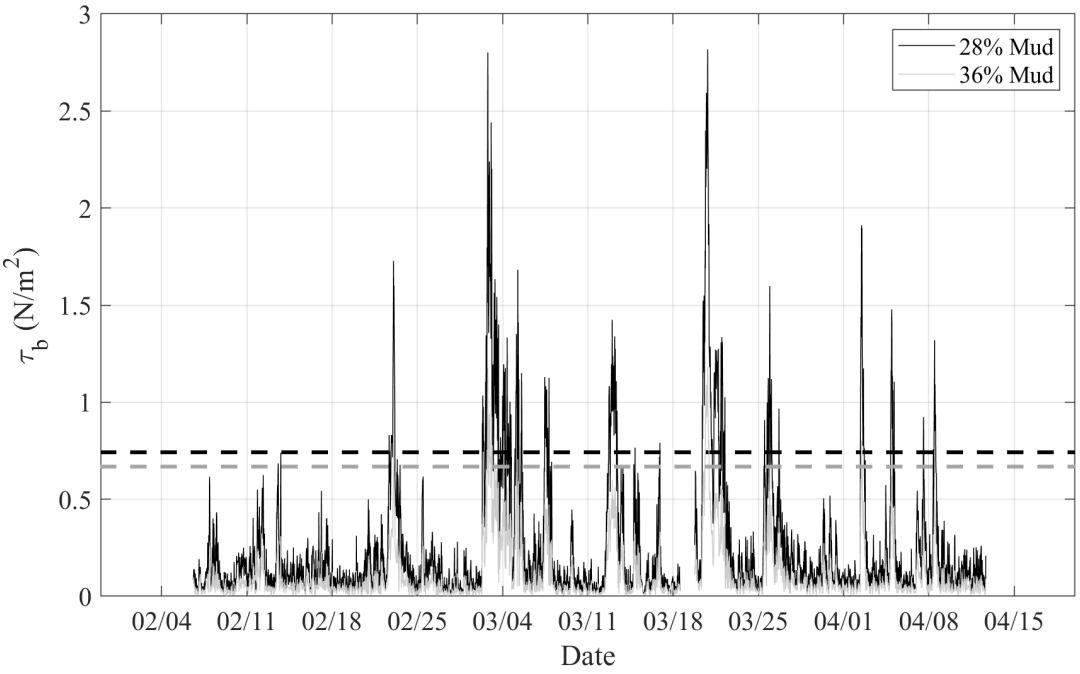



*Figure 5.28: Near-bed shear stress and critical shear stress for erosion for Site 1 sediments during the Spring 2018 deployment.*

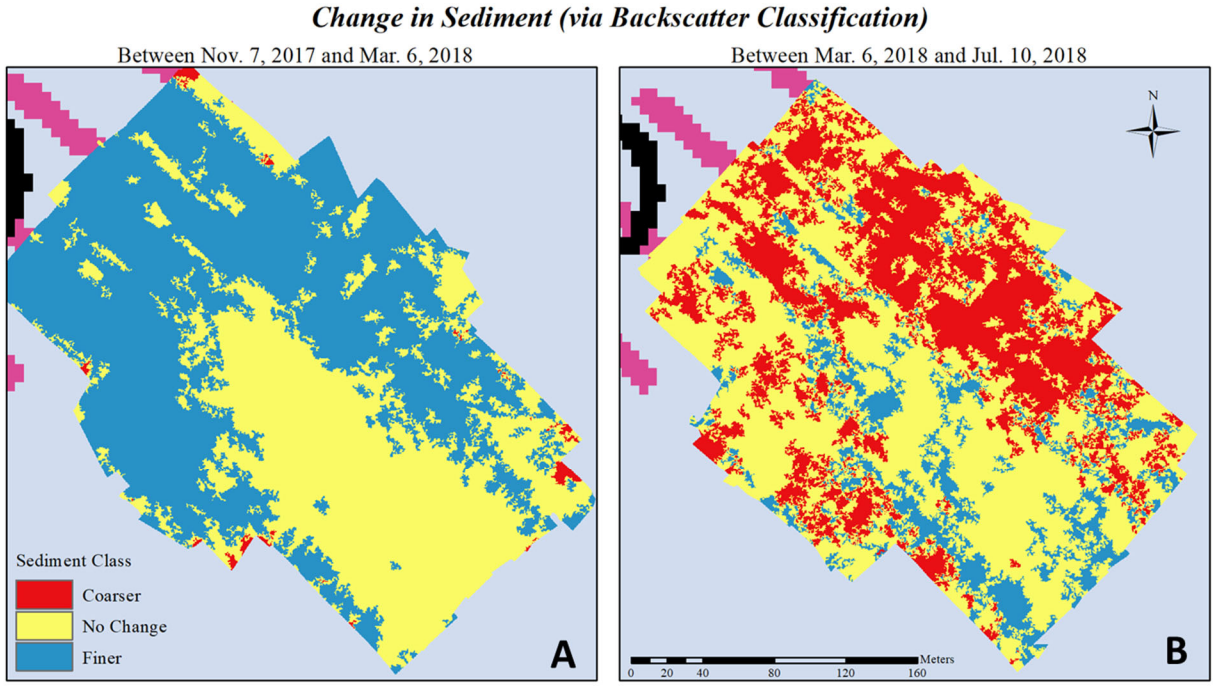



*Figure 5.29: Surficial sediment changes as estimated by sediment classification maps before and after Riley (left), and before and after Quinn, Skyler, and Toby (right).*

The Fall 2018 deployment at Site 2 did not experience the same level of near-bed forcing as Site 1. Only the Sept. ETC and the Sept. 25th gale are estimated to have exceeded the critical threshold for erosion for the 61% mud sediments (Figure 5.30). Conditions are estimated to have exceeded critical threshold for the softer muds more frequently. Regardless, sonar data collected by both the PMES and AUV show significant surficial changes over the course of the deployment. Figure 5.31 highlights 3 separate surveys conducted during the Fall 2018 deployment. Qualitatively, the backscatter intensity in the PMES appears to increase in the later portions of the deployment (Figure 5.31 middle). Snapshots from the AUV sonar (Figure 5.31 right) show the development of an irregular texture to the seabed by Oct 22, 2018. These features have a negative relief, suggesting that sediment was scoured out to create the features. By Nov. 7, these features are no longer apparent.

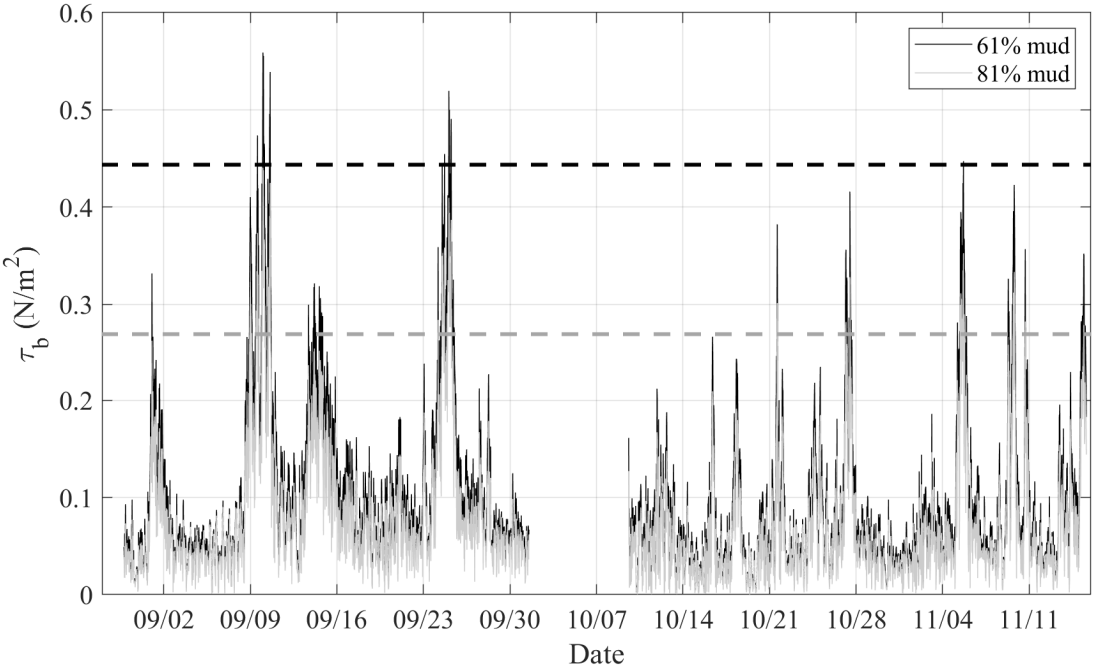



*Figure 5.30: Near-bed shear stress and critical shear stress for erosion for Site 2 sediments during the Fall 2018 deployment.*

Classified sonar mosaics qualitatively support this assessment. Between Aug. 28 and Nov. 7, 2018 the field area becomes coarser, over almost the entirety of the surveyed area (Figure 5.32a). The shear stress time-series does not suggest significant erosion would have occurred for the sediment on the site, although the irregular features observed in the AUV sonar appear to be erosional features. Contemporaneous to the coarsening, the VPS data indicates widespread surrogate burial, although burial may not be due entirely to sediment deposition. However, a review of the contextual sonar suggests that the coarsening was due to sediment influx to the site. PMES sonar of the wider area shows irregular boundaries between the sandy muds and muddy sands similar to Site 1 (see Figure 5.31). It was determined that the field site was located in a former dredging location. Sandy material at the site was dredged to repair breaches to the nearby Prime Hook Beach caused by earlier storms (U.S. Fish and Wildlife Service, 2015). This exposed the softer sandy mud deposits and created a bathymetric low. The coarsening of sediment during the Fall 2018 deployment was likely due to influx of coarse muddy sands and

fine sands of the surrounding shoal features, rather than the erosion of site sediments. By the Spring 2019 deployment, the sediments at the site have become finer (Figure 5.32b). It is unclear whether the sediment was again transported away in the interim period, or whether the material became mixed with the underlying, soft fluid muds.

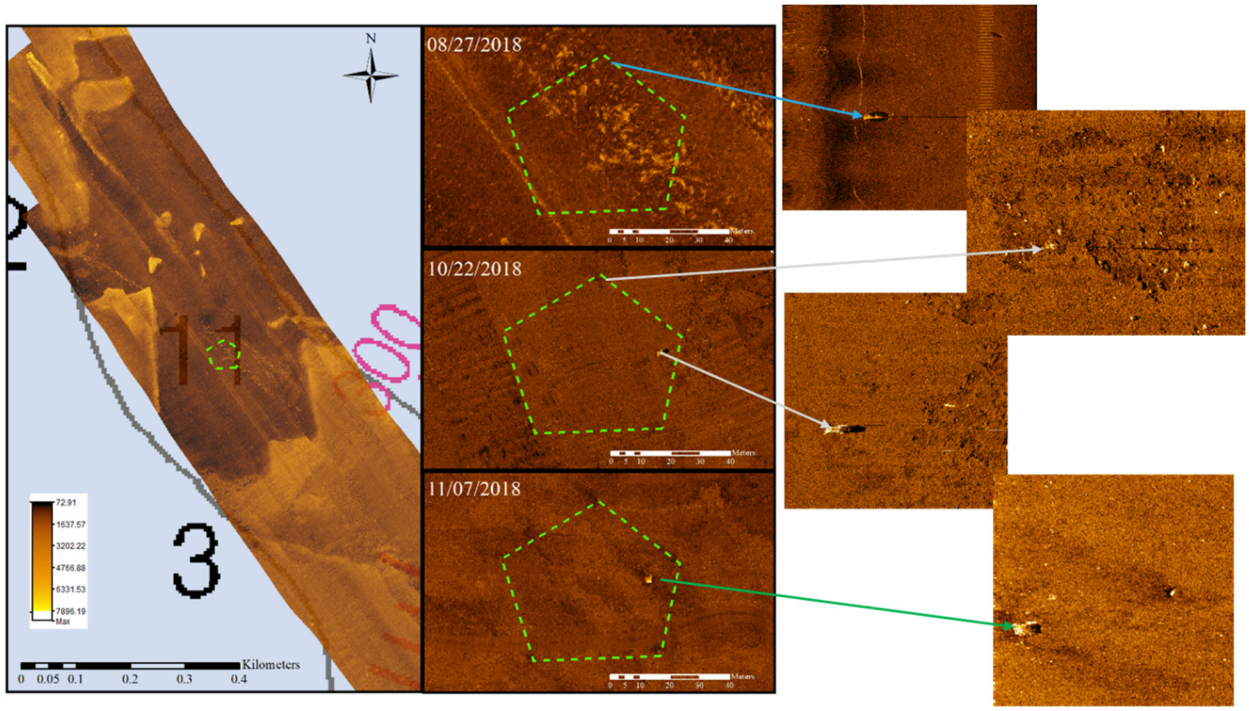



*Figure 5.31: Initial PMES sonar of the wider Site 2 field area (left) with VPS array location indicated (green) Note the evidence of sediment dredging. Over the course of the deployment, the sediment texture and backscatter intensity changes (middle). Snapshots from the AUV sonar (right) shows the creation of irregular textural features.*

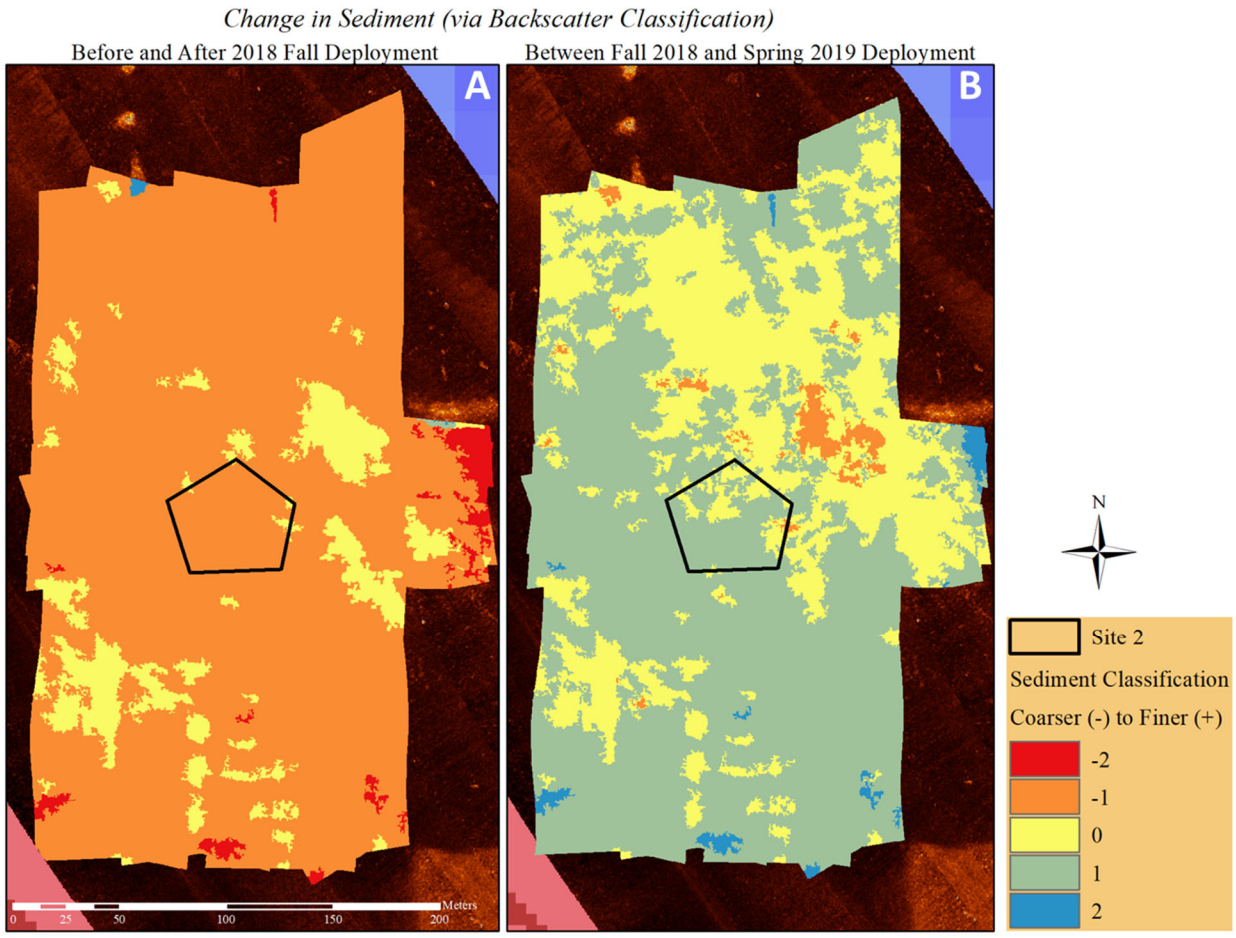



*Figure 5.32: Surficial sediment changes as estimated by sediment classification maps before and after the Fall 2018 deployment (left), and between the Fall 2018 and Spring 2019 deployments (right).*

## 5.2.3. Surrogate Scour and Burial

Over the course of the four deployments, surrogate burial was consistently observed. The change from the muddy sands of Site 1 to the sandy muds of Site 2 influenced the degree of burial observed, and potentially the mechanism by which surrogate burial occurred. The status of the surrogates at the end of their respective deployments are shown in Figure 5.33. Two deployments occurred at each study site, of which one deployment at each site experienced low – moderate forcing and the other deployment high forcing through extra-tropical cyclones and other wave events. The comparative figure highlights the differences in burial between Site 1 and 2, despite similar forcing conditions. For instance, with no storm events, surrogates were only partially buried in Site 1, but almost completely buried in Site 2. With storm events, the surrogates at Site 1 were mostly buried or exposed in scour pits, while in Site 2, they were buried 20-30 cm deep. With conditions being equivalent, surrogate burial, and the mechanisms driving burial, must be dependent upon the properties of the cohesive sediments.

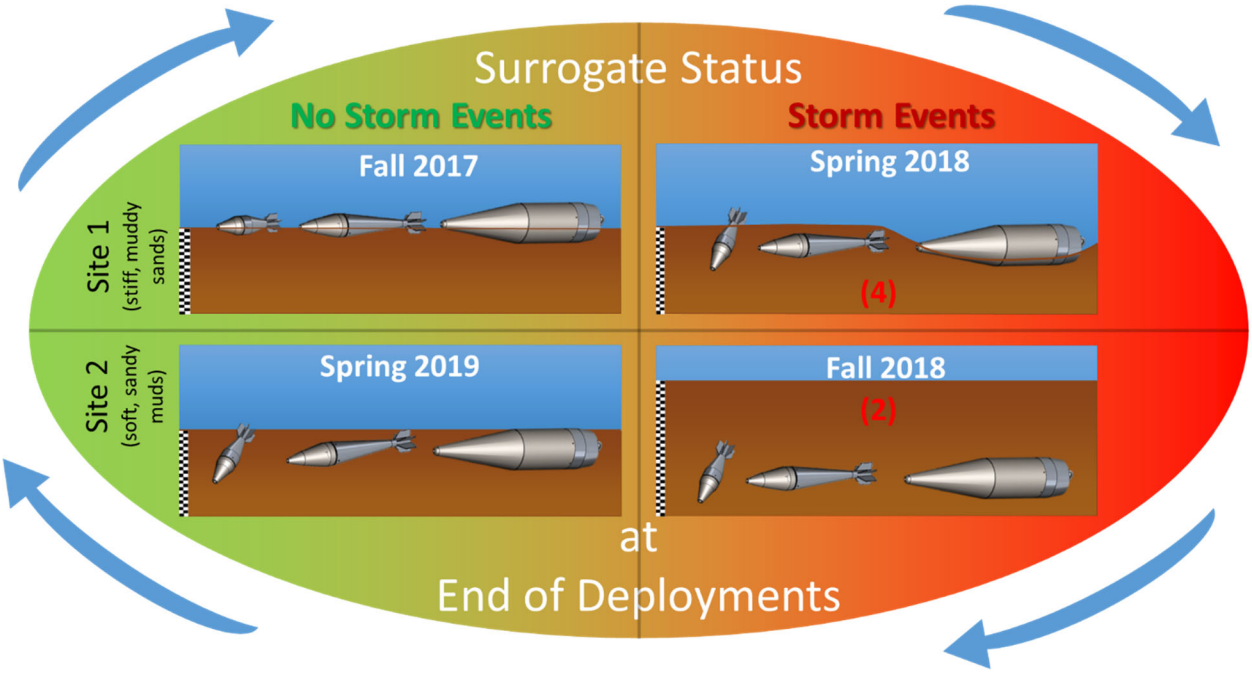



*Figure 5.33: Comparative diagram of surrogate status for each of the four field deployments. Note the difference in burial depth between Site 1 and Site 2 deployments under similar conditions.*

The mechanisms for burial in cohesive sediments generally fall within four processes: impact burial, scour burial, settling, and bed fluidization. As the surrogates in this study were set on the seafloor, impact burial can be ruled out. This leaves only scour burial, burial by settling, and burial through bed fluidization. With scour burial, extensive work was conducted with seabed mines to model scour burial in non-cohesive sediments (Traykovski et al., 2007; Trembanis et al., 2007; Whitehouse, 1998). Using the modified Shields parameter for mixed sediments (see Section 5.2.2.), we adapted the mine scour burial model developed by Trembanis et al., (2007) for applications in cohesive sediments. The model was run for each surrogate type over the four deployments (Figure 5.34). Scour burial, presented as the total depth of burial for each surrogate type, is compared to the burial depth reported by the divers. Depth is reported as the furthest estimated point of the surrogates from the seabed surface (i.e. deepest part of the surrogate).

The model showed good agreement with observations from the 2 deployments at Site 1 (Fall 2017 and Spring 2018 deployments). In the Fall 2017 deployment, the model estimated approximately 65% burial for each surrogate type as compared to the approximately 50% burial reported by the DSPSU divers. With the Spring 2018 deployment, the model predicts 100-115% scour burial for all of the surrogates. The DSPSU divers reported nearly 100% for the smaller surrogates, and while the 155mm were 50% buried by surface area, the surrogates sat recessed in large open scour pits such that the top of the surrogates were flush with the surrounding seabed. Since the model assumes cylinders burying on an even keel (zero pitch), the model could not account for the deeper burial observed for the 60mm mortars; the 60mm mortars were found buried with the tip of the nose cone down to approximately 20 cm below the surface. If the results are considered in percent burial, the 60mm mortars were reported as 90-100% buried, which better matches the scour model predictions. The observed scour pits around the 155mm surrogates further support the likelihood of scour burial as the primary burial mechanism during the Spring 2018 deployment.

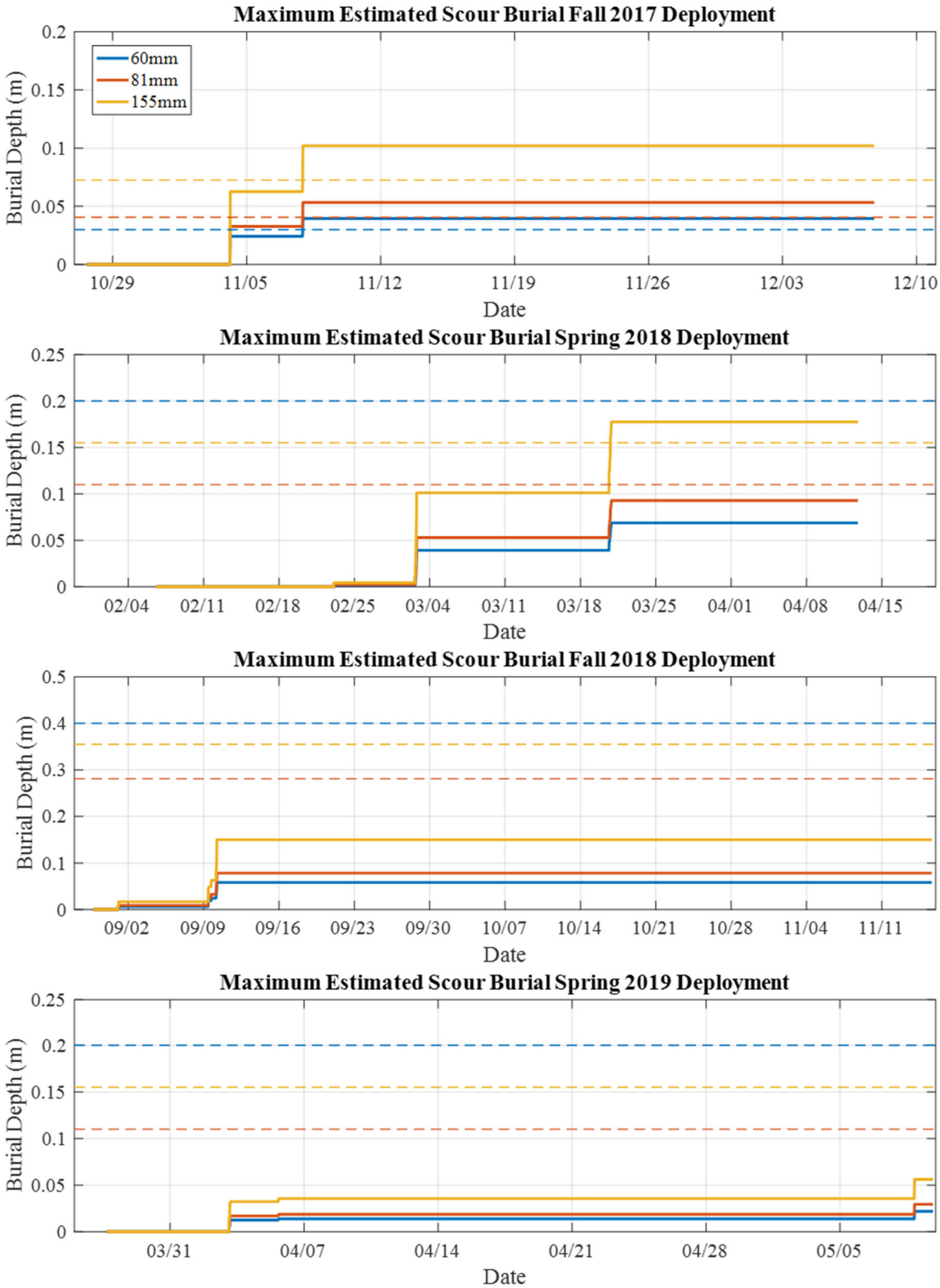



*Figure 5.34: Scour burial predictions for surrogates for each deployment. Dashed lines indicate average burial depth by surrogate type reported by divers at time of recovery. Depth is reported as the furthest estimated point of surrogates from the seabed surface (i.e. deepest part of the surrogate).*

Looking deeper into the Spring 2018 deployment, the scour process model suggests only slight scouring occurred prior to nor'easter Riley (Mar. 3-4, 2018). After Riley, the model predicts ~65% burial of all surrogates. While it is likely scour occurred, the high-resolution sonar imagery from Mar. 6th does not show large scour pits around the 155mm surrogates, as was observed in the sonar on Apr. 10. Given the extended period of increased near-bed currents following Riley, it is possible that sediment infilled scour pits prior to the Mar. 6 survey. The loss in VPS detections after Riley, as well as the increase in finer sediments in the sonar classification, would support this observation. Sediment infilling was observed in non-cohesive sediments in mine burial studies, including the episodic intrusion of cohesive sediments into pits formed around mines in non-cohesive sediments (Traykovski et al., 2007; Inman and Jenkins, 2002).

Despite the passing of Quinn (Mar. 7) and Skyler (Mar. 13), deeper scour burial was not predicted until Toby (Mar. 20). This is supported by the ROV survey on Mar. 18 (see Figure 5.7), during which an 81mm surrogate was observed to be only partially buried. The VPS detection count further supports these predictions. Following nor'easter Skyler, the VPS detection count temporarily increases (see Figure 5.10), suggesting that surrogates were partially re-exposed by Skyler, not further buried. The daily detection counts following Skyler decreases back to pre-storm numbers, indicating some degree burial (likely scour pit infill) following Skyler, but no more than observed after Riley. Tag detections again increased during Toby, with 60mm and 81mm surrogate tags recorded during the height of Toby (as well as mobility of the 60mm surrogates). After Toby that the detection rates primarily decreased, suggesting increased scour pit infill in the waning part of storm and in the following days after the storm.

Strong spring tidal currents (>0.25 m/s) were recorded following Toby, which may have contributed to the apparent sediment infill and burial of the surrogates. This would also compare to the observations noted during mine burial studies (Baeye et al. 2012, Traykovski et al., 2007), although Traykovski et al., (2007) noted mud deposition during slack tides, and partial excavation during strong tidal currents. Eventually, however, Traykovski et al. (2007) noted that the infill mud became resistant enough to limit resuspension and burial occurred. Based on the VPS detections, burial for the smaller surrogates by infill occurred rapidly at first, but then gradually over the remaining period of the deployment. With the 155mm surrogates, the observed partial burial may indicate that not enough time had passed for this process to result in total burial, and indeed the process described by Traykovski et al. (2007) for the total burial of a large cylindrical mine occurred over 28 days.

The departure between the scour model and surrogate burial observed for the Fall 2018 and Spring 2019 deployments, as well as a lack of observed scour pits, implies other mechanisms may have contributed to surrogate burial. As noted in previous mine burial studies, the bearing capacity of muds may be a primary predictor of burial depth for mine-like objects (Richardson et al., 2001). If the force exerted on the seabed by the surrogates is greater than the sediment bearing capacity, the surrogates should sink into the sediment.

To test this, we modeled the force exerted on the seabed by the surrogate munitions. The penetrometer data provided Quasi-static Bearing Capacity (QSBC) profiles for the sediment at Sites 1 and 2. QSBC estimates the load capacity of the sediment before failure under a threshold pressure. The surrogate pressure is calculated from the total weight from gravitation forcing

minus buoyant forces. If the weight of the surrogates exceeds the sediment bearing capacity, we would assume shearing or compressive failure of the sediment, resulting in the surrogates "sinking" into the seabed. Pressure along the cylinder varies as:

$$P(\varphi) = P_{max} * cos(\varphi)$$

Where φ is the contact angle of the half surface, and $P_{max}$ is calculated by:

$$P_{max} = \frac{4F}{LD} * \left[\frac{1 - \cos(\varphi_0)}{2\varphi_0 - \sin(2\varphi_0)}\right]$$

Where $F$ = force, $L$ = length of the cylinder, $D$=diameter of the cylinder, and $\varphi_0$ is the half contact angle (from the centerline to the surface). To estimate $\varphi_0$, we assume a simple Hertzian contact problem between a rigid cylinder and an elastic surface. This assumes a rectangular contact surface of deformation between the cylinder and the surface. The half-width of the rectangular contact area is calculated by:

$$\beta = sqrt\left[\frac{4F\left(\left(\frac{1-\nu_{sed}^2}{E_{sed}}\right) + \left(\frac{1-\nu_{obj}^2}{E_{ojb}}\right)\right)}{\pi L\left(\frac{1}{r_{sed}} + \frac{1}{r_{obj}}\right)}\right]$$

Where $\nu$ is Poisson's ratio for the object material (i.e. steel) and sediment, E is the elastic modulus for the object and sediment, and r is the radius of the object and sediment (in this case, we assume the surface is a cylinder of infinite radius). Without direct measurements, we used published values for Poisson's ratio and elastic modulus of sediments (Obrzud and Truty, 2012; Hamilton, 1979; Hamilton, 1971). Poisson's ratio and the elastic modulus was estimated for silty sands with medium stiffness for Site 1 and soft silts and clays for Site 2. The half-rectangular contact surface is converted to the radial surface of the object to estimate $\varphi_0$. This is then used to calculate the pressure exerted on the seabed by the object.

The model was run for each surrogate and compared to the QSBC profiles for each penetrometer sample. Maximum burial depth, estimated at the leading edge of the surrogate surface, is estimated to be the depth where QSBC >= $P_{max}$, or the depth at which the sediment bearing capacity exceed the pressure exerted by the object. The results for each penetrometer sample site are shown in Figure 5.35. The samples associated with Site 1 and 2 are highlighted. For example, the 155mm surrogates should sink to an average depth of 6.1 cm at Site 1 and 17.9 cm at Site 2, or 40% and 116% buried respectively, given no other force but the weight of the surrogate. This agrees well with observations provided by the SCUBA divers. The smaller surrogates show greater deviation between estimated depth and observed depth. This is likely due to the complex shape of the surrogates which are not accounted for in this estimate (assumes cylindrical objects). Although this method ignores frictional forces and complex surrogate shapes (and does not currently estimate the time required to reach an equilibrium settling depth), the estimated surrogate settling depth due to the sediment bearing capacity does generally agree well with diver observations for the Spring 2019 deployment at Site 2, as well as the Fall 2017 deployment at Site 1. It is notable that both deployments occurred when no storms were

observed. This indicates that the weight and shape of the surrogate and bearing capacity of the sediment may be a controlling factor in MEC burial in cohesive sediments, and supports previous observations of mine-burial studies (see Richardson et al., 2001). It should also be noted that the scour observed or predicted in the Fall 2017 and Spring 2018 deployments does not exclude the potential for burial by settling; rather, scour may have been the primary mechanism for surrogate burial at Site 1, particularly during energetic storm events. This is further illustrated by the Fall 2017 deployment, where either scour processes or settling could explain the observed burial.

During the Fall 2018 deployment, the surrogates buried significantly deeper than scour burial and bearing capacity would suggest. This enhanced burial is likely related to additional fluidization of the soft sandy muds in Site 2 during the Sept. 2018 ETC and following storm events. Increasing waves are known increase water flux into soft muds, causing a dilation of the sediments, fluidization, and associated reduction of the bulk density (Sahin et al., 2012; Soltanpour et al., 2009). The decrease in bulk density would therefore cause a corresponding drop in the bearing capacity, allowing the surrogates to settle further into the sediment. Following the storms, after wave energy decreases, the sediment would undergo settling and consolidation (Sahin et al., 2012). This process is similar to the bed fluidization and granular sorting mechanisms reported by Klammler et al., (2019).

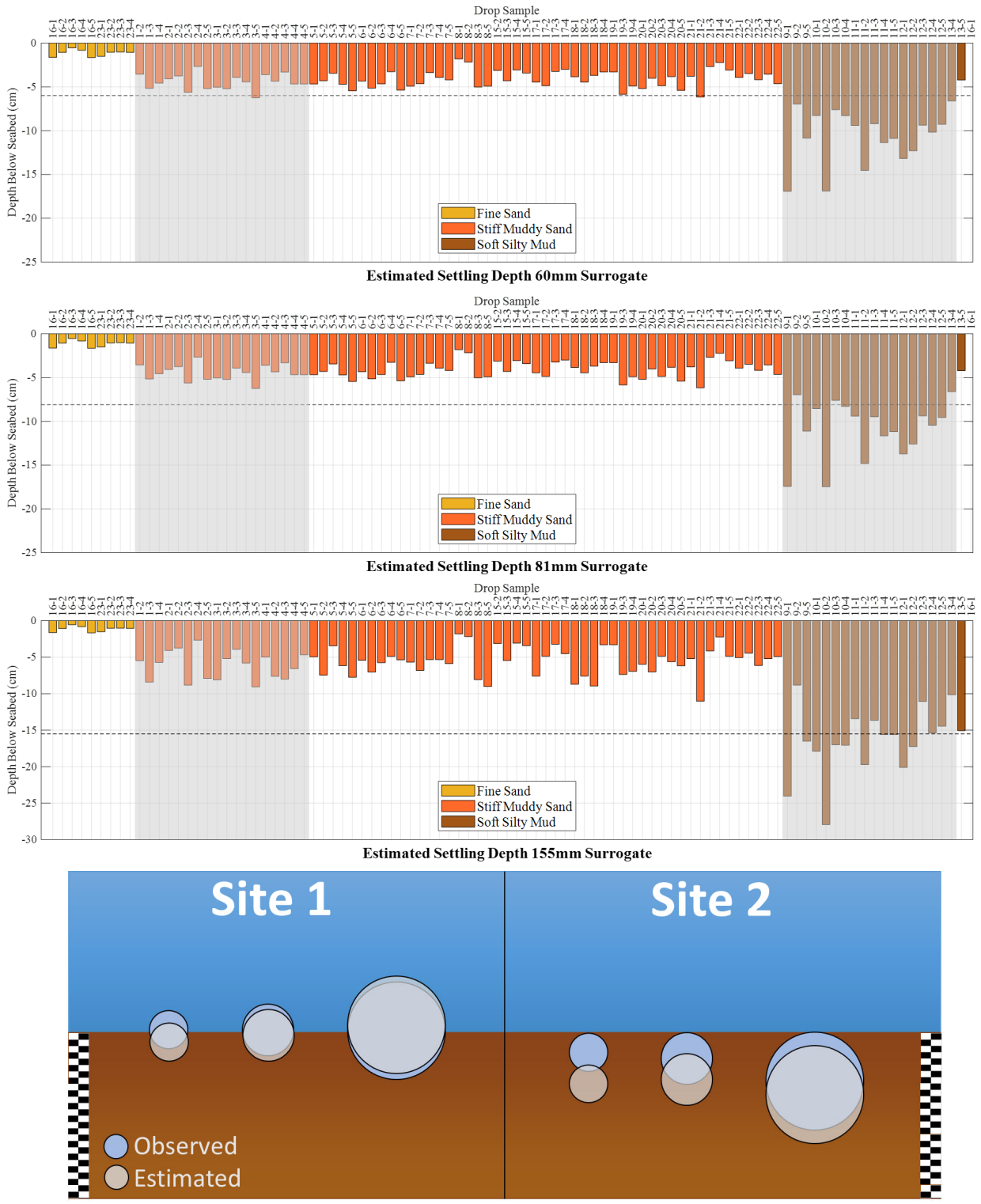



*Figure 5.35: Estimated surrogate burial by settling depth related to sediment bearing capacity using simply Hertzian contact model for rigid cylinders and elastic surfaces. Results for 60mm (top), 81mm (middle), and 155mm (bottom) surrogate are shown for each penetrometer sample with the samples taken at Sites 1 and 2 highlighted in gray. The bottom diagram illustrates the difference between model results and observations. Note that this does not account for the tilt of the 60mm mortars at Site 2, which would agree more with the estimated settling depth.*

5.2.4. Surrogate Mobility

No large-scale horizontal mobility was observed during the MR-2730 deployments. In their studies of mobility in non-cohesive sediments, Traykovski and Austin (2017) and Calantoni (MR-2320) noted mobility in surrogates that were less dense than the surrounding sediment. As noted above, the conclusion of the SERDP Munitions Mobility and Modeling Workshop (Dec. 8-9, 2015) was to use surrogates with densities within the range of the real munitions they model. Based on the densities estimated by Calantoni (MR-2320), these densities are predominantly greater than the density of quartz sediment (2650 kg/m$^3$). The range of densities for the surrogates used in MR-2730, while slightly lighter by standards of actual munitions, was also greater than that of the cohesive sediment at Sites 1 and 2. Thus, as found with munitions in non-cohesive sediments, burial mechanisms dominated with munitions denser than the sediment.

It should be noted, however, that during storms, particularly nor'easter Toby, motion was recorded in the IMU of several 60mm and 81mm surrogates. A detailed review found that the motion of two of the 60mm mortars (60A and 60C – see Appendix A Table A.2) was discernable in the VPS data during nor'easter Toby. For example, the VPS data was compared to contemporaneous measurements from the onboard IMU of surrogate 60A (Figure 5.36). The combined series documents horizontal displace occurred in 2 episodes, moving from an initial position estimated early on March 20$^{th}$. The nose acoustic tag became obscured after the initial movement between 1500-1600 UTC, when the surrogate rolled approximately 10 cm to the east. The tag may have become obscured when the unit pitched nose down (see Figure 5.9 above). Most notable is the variation of both yaw and rolling, suggesting that the 60mm surrogate was rolling back and forth in an arc. This corresponds well to laboratory tests by Garcia (MR- 2410), who noted that mortar shaped surrogates would roll in an arc due to their shape. A second displacement occurred between 2000-2100 UTC, with the surrogate rolling a further 10-15 cm to the SE. The maximum horizontal migration estimated from the VPS for 60 A is 25 cm, based on the movement of tail acoustic tag on the unit. The surrogate ceased mobility after 2100 UTC March 20. The IMU in surrogate 60C recorded motion over the same time period, with an 18-cm horizontal displacement estimated during Toby.

The critical mobility for the 60mm surrogates were estimated using the Rennie et al. (2017) method. Although the scour model predicted near total burial of the 60mm surrogates by the time of nor'easter Toby, analysis of the VPS detection count suggests Skyler and Toby temporarily exposed previously buried surrogates. To establish baseline, the critical mobility for the 60mm surrogate was calculated for 0%, 10%, 25%, and 50% scour burial (Figure 5.37). The model suggests that anything above 10% scour burial would have impeded surrogate mobility during nor'easter Toby. It should be noted, however, that this equation 1) was developed for non-cohesive sediments, and 2) assumes a cylindrical object. The shape of the 60mm mortars, as well as the mixed cohesive sediments of Site 1, would influence the threshold for motion. The exact burial status of the 60mm surrogate prior to Toby is unknown, but the ROV imagery for similarly shaped 81mm surrogates suggests they were at least 50% buried prior to Toby. Whether excavated by the increasing conditions Toby, or whether Toby exceeded the threshold for object mobility despite scour, the IMU and VPS recorded limited mobility and displacement occurred for at least one 60mm mortar. The variable pitch recorded in the IMU does suggest that a scour pit was present and the surrogate repeatedly rolled into and out the pit during Toby.

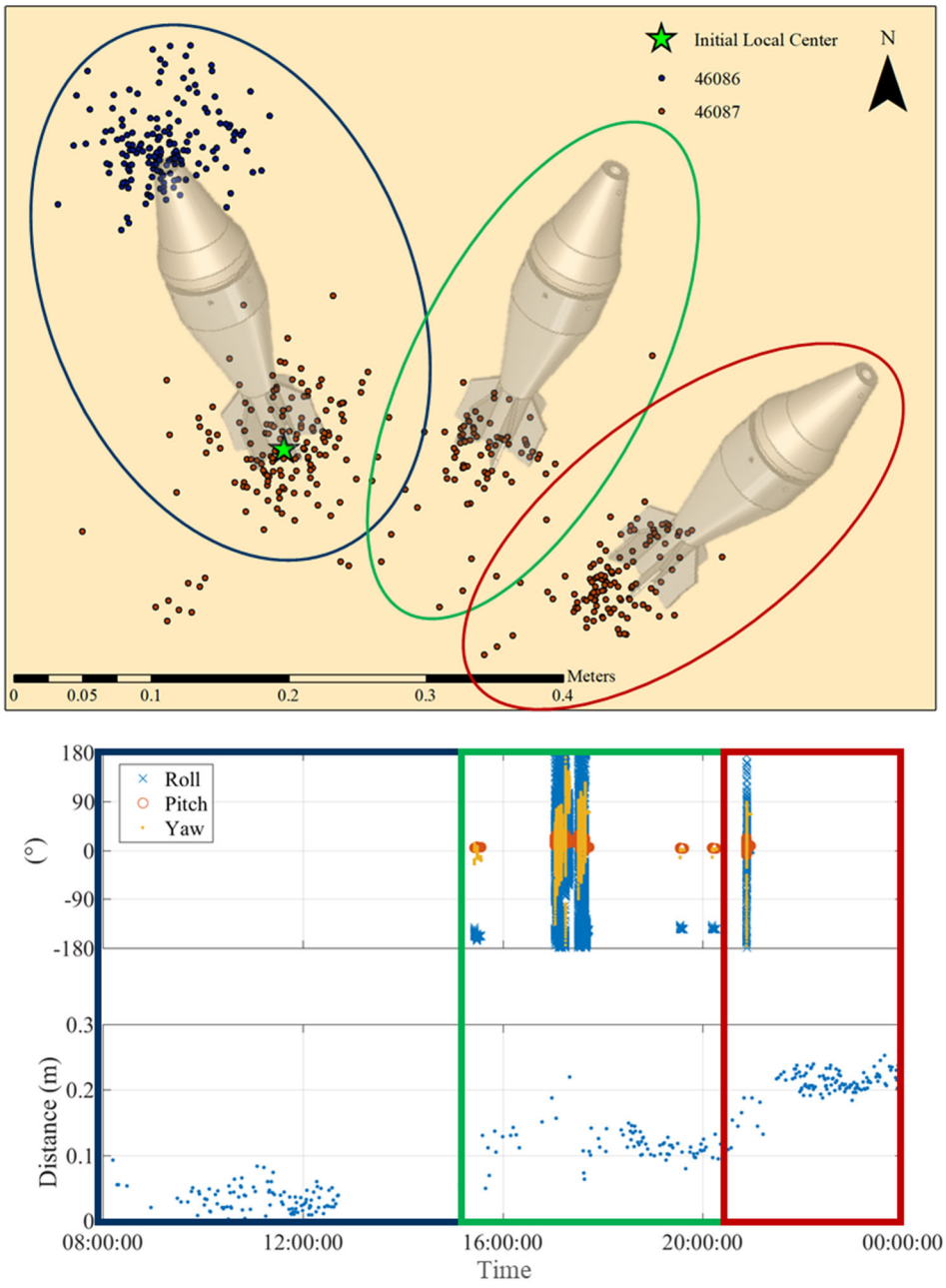



*Figure 5.36: VPS position estimates for surrogate 60A during nor'easter Toby (top) with contemporaneous IMU data from the onboard x-io NGIMU (middle). Displacement (bottom) was estimated from the acoustic tag located in the tail of the surrogate.*

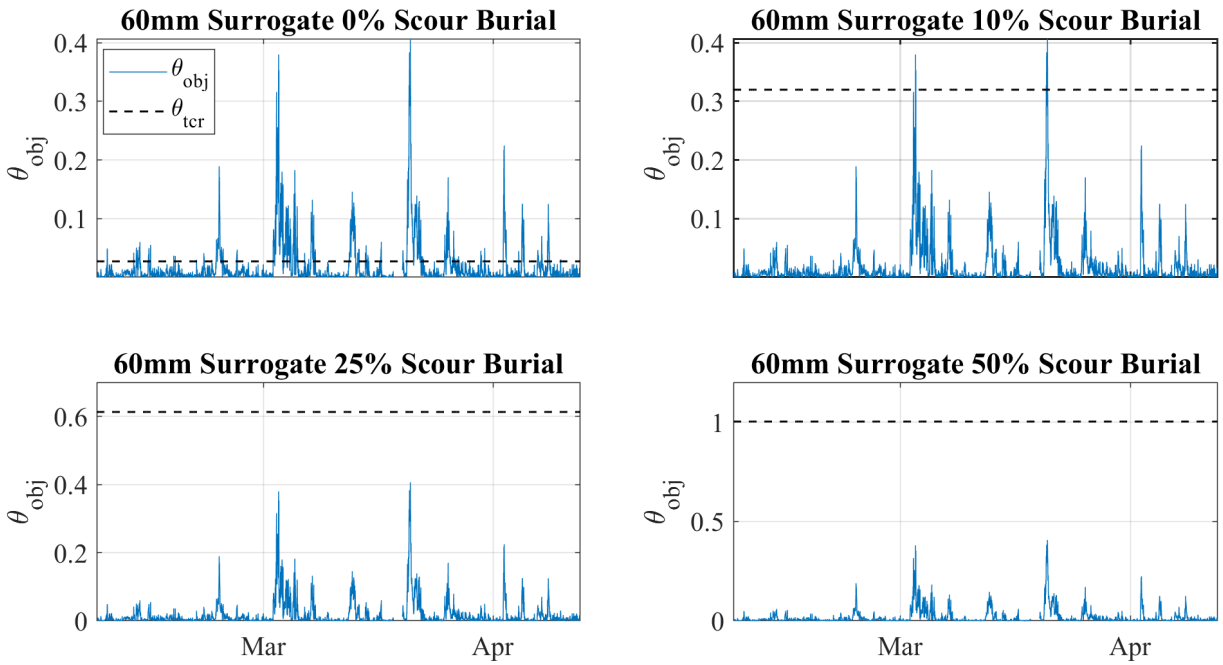



*Figure 5.37: Object mobility (see Rennie et al., 2017) calculated for 60mm mortar surrogates during the Spring 2018 deployment assuming various states of constant scour burial.*

# 6. Conclusions and Implications for Future Research/Implementation

The observations and analysis of munition mobility and burial in this study provides new insight into the behavior of MEC in cohesive sediment environments. This study used a novel approach to track a suite of custom designed and manufactured surrogate munitions deployed at two cohesive sediment sites in the lower Delaware Bay estuary. The Vemco (Innovasea) VPS acoustic tracking system provided near-continuous monitoring of surrogate mobility and burial, complemented by measurements from on-board IMU. The effects of six separate extra-tropical cyclones were recorded during four separate deployments. Burial was the predominant result across all four deployments, ranging from 50% to greater than 100% burial of surrogates depending on sediment composition and near-bed forcing. No large-scale horizontal mobility of surrogates was observed in any of our deployments, although minor motion was recorded during peak-near bed velocities of several storm events. Field observations and models developed for munition mobility and burial in non-cohesive sediments, adapted by this study for cohesive sediments, suggest munitions burial is linked to scour burial in mixed-cohesive sediment and plastic deformation and bed fluidization in soft muds. Sediment bearing capacity is an important predictor for surrogate burial, and the Hertzian contact model introduced in this study provides a simple method to predict burial due to bearing capacity.

## 6.1. Performance by Task

The primary objectives of this study were to: 1) monitor the mobility and behavior of sensor-integrated surrogate munitions in muddy environments using a high-accuracy acoustic positioning system, 2) observe surrogate munition response to hydrodynamic forcing through instrumented bottom frame time-lapse hydrodynamic data and sonar imager, and 3) monitor morphological site changes through repetitive geophysical site surveying and benthic sediment sampling. A number of performance objectives were identified for this study (Table 6.1), which guided the technical approach. The following section assesses the performance of MR-2730 in light of these objectives.

*Table 6.1: Performance objectives and assessment of MR-2730.*

| Performance Objective | Metric | Data Required | Success Criteria | Assessment |
|---|---|---|---|---|
| Development of Instrumented Surrogate MEC | ➢ IMU and acoustic tag integration and data collection | ➢ IMU motion data and VEMCO VPS acoustic positioning | ➢ Collection of IMU motion data verified by acoustic positioning | ➢ *IMU data was collected and verified in part by VPS* |
| Surrogate Tracking Positional Accuracy | ➢ Horizontal Positional Error (HPE) | ➢ Surrogate Positions calculated from VEMCO VPS Receivers | ➢ Average HPE < 1m for 50% of field deployment duration | ➢ *Median Error: 0.40m*<br>➢ *75th Error Percentile: 1.01m*<br>➢ *90th Error Percentile: 1.76m* |
| Site Hydrodynamic Characterization | ➢ In-situ character-ization of hydrodynamics during field deployments | ➢ Wave and current measurements from ADCP<br>➢ Near-bed velocities, turbulence, shear stress estimates from PC-ADCP | ➢ Measurements of in-situ hydrodynamics throughout field deployment period | ➢ *Hydrodynamics were recorded throughout 206 of 226 days of field deployment.* |
| Geophysical and Geotechnical Site Characterization | ➢ Complete acoustic bathymetric and backscatter coverage | ➢ Bathymetric and side-scan sonar | ➢ 100% bathymetry and acoustic backscatter coverage at <1 m gridded resolution | ➢ *Achieved 100% bathymetry and acoustic backscatter coverage at <1 m gridded resolution for each deployment* |
| | ➢ Background magnetics | ➢ Magnetometry | ➢ Complete interpolated magnetometry surface at <2 m gridded resolution | ➢ *Magnetometer was relegated to a secondary role per SERDP request. Mag data was inherently influenced by noise from VPS Sensors.* |
| | ➢ Ground control sediment classification | ➢ Surface sediment sampling | ➢ 20 surface sediment samples | ➢ *63 surface sediment samples collected (37 processed)* |
| | | ➢ Push core or Box core | ➢ 5 push cores | ➢ *8 push cores collected between 2 sites* |
| Instrument Verification Strip | ➢ Deployment and repetitive survey of IVS | ➢ AUV sonar and magnetics | ➢ Complete IVS characterization before and after every magnetometer survey | ➢ *IVS characterization collected during 2017 mission. Due to relegation of Magnetometer to secondary role, IVS was removed from site.* |

### 6.1.1. Task 1 – Tracking and Motion Sensor Technology Design

The surrogate munitions design and instrumentation met the minimum performance standards of the study. The motion trigger wake-up setting, customized for this project with the help of x-io, was sensitive enough to capture moments of only minimal movement, and extended the battery life of the IMU. The initial USB battery pack set-up was found to be susceptible to moisture and shock. For the Task 4 deployments, there were replaced by smaller Li-ion batteries directly connected to the IMU via Molex. This improved battery life for the surrogates and proved more robust to shock. Due to the minimal movement of the surrogates during the deployments, the IMU did not record frequent observations, and the VPS proved more useful in monitoring surrogate burial. The 155mm surrogates were also fitted with water level pressure sensors, which provided some observations of burial. However, the placement of the pressure sensors in the 155mm surrogates provide problematic. The pressure sensors were situated in milled recesses in the tail cones of the 155mm surrogates with 4 pore openings to allow water to the transducer face. This design was used by Puleo (MR-2503) with success in non-cohesive sediments. In the fine cohesive sediments of MR-2730, the pore openings clogged with sediment over time. The pore openings were milled out to reduce clogging, but proved only to be a minor improvement. Should similar surrogates be used in future studies, the pressure sensor housing would benefit from a re-design.

The VPS system proved to be a robust and simple system to program and deploy. The system was even capable of detecting surrogates after several HR2 receivers were knocked over during the Fall 2018 deployment. The V9 Vemco acoustic tags are small enough to allow for use on surrogates smaller than the 60mm surrogates used in this study, and have operational life-spans (>7 months) that would allow for much longer deployment durations. The only limiting factor for time would be the HR2 receiver battery life-span, which is still only limited to 6 months. In this case study, the lifespan of the IMU batteries, pressure sensors, and hydrodynamic sensors were the limiting factor. The VPS system can be easily customized for many different site locations, water depths, test areas, salinity, and sediment types, making it an ideal tool for further munitions mobility research or other similar research. Vemco's assistance in VPS system configuration and data processing, including pushing data through rushed analysis to successfully locate and recover the lost surrogates, contributed to the success of the field operations.

Although detection loss may be expected during the storms, the VPS results indicate neither significant noise addition nor signal loss during the storm events. A sample of HR2 receiver noise is shown from the 2018 Spring deployment (Figure 6.1). The four nor'easters caused only minimal increase in noise during this deployment. However, the HR2 receivers on the north and central poles recorded significantly higher noise throughout the deployment. The instrument frame, which was moved outside of the grid on March 18, has been ruled out. The cause of the noise remains unclear. Despite the noise, the positioning for the 2018 data was within the quantitative performance metric set in table 1 (50% of detections within a horizontal position error < 1m). To determine horizontal position error (HPE) in meters, the positions of the HR2 receivers are derived from triangulation of the sync tags within the HR2 receivers (used to sync receiver time and track HR2 movement on non-fixed mooring) over the course of the deployment. These positons were compared to the positions derived from PMES survey with RTK positioning. The median percentile error was 0.4 m, with 75$^{th}$ percentile error at 1.01 m

and 90th percentile error at 1.76 m. After filtering for high HPE and RMSE error (filtering out 44.8% of detections), the median error for the remaining 55.2% of sync tag positions was only 0.27 m, with 75th error percentile at 0.52 m and while 90th error percentile at 0.7 m.

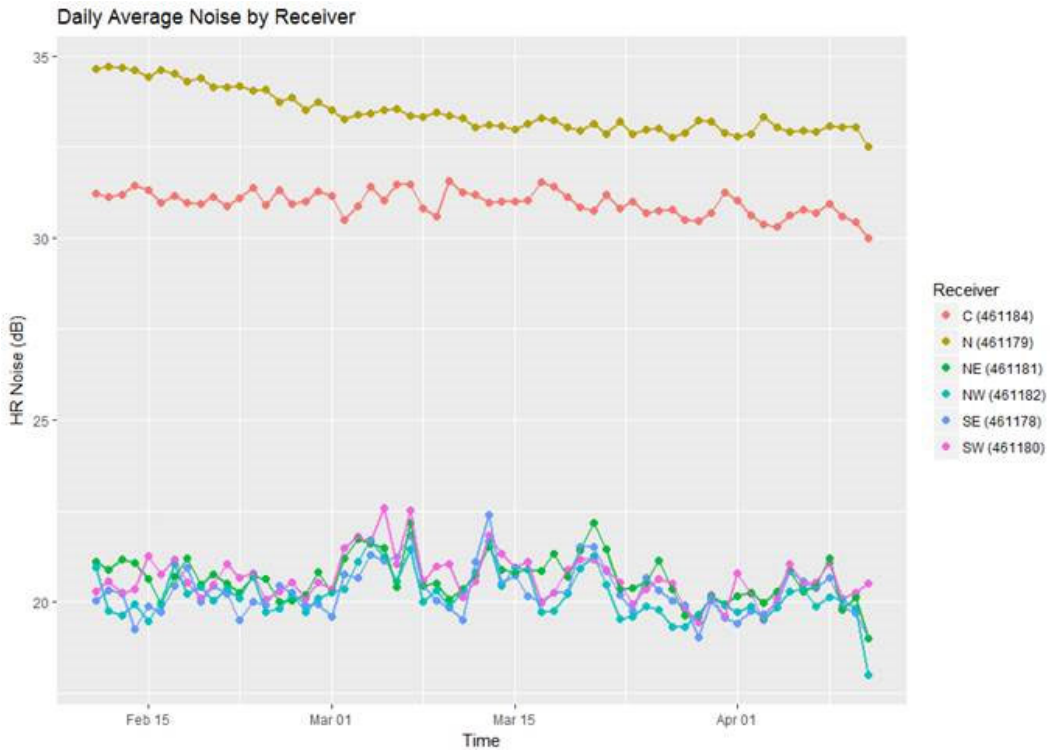



*Figure 6.1: Acoustic noise for at each HR2 receiver during the 2018 deployment. Storm activity did not significantly introduce noise, although consistently high noise are noted in both the central and northern receivers. The instrument frame was recovered on Mar. 18, and redeployed 20m east of the array on Mar 19. No corresponding change in noise is observed over that period.*

Despite limited munitions migration, the VPS was able to record the fine-scale movement of two 60mm mortar surrogates during nor'easter Toby. An additional test was also conducted during the Spring 2018 deployment. This occurred through the use of tagged whelks, four of which were deposited at the site on Mar. 11, 2018. The whelks were released to both ensure the VPS was capable of recording movement (should none have occurred with the surrogates) while simultaneously testing the systems capabilities for a study on whelks by the Delaware Department of Natural Resources and Environmental Control (DNREC). Although the whelks initially remained in place following their release, nor'easter Toby appears to have caused three of the whelks to migrate out of the site and to the east, towards deeper water. The remaining whelk also moved east but stayed within the grid, and was recovered on April 11th along with the surrogates (Figure 6.2 inset). The whelks' movement is shown in Figure 6.2, having been clearly captured by the VPS during nor'easter Toby. Overall, the performance of the VPS indicates the system is well suited for use in munitions mobility studies and under varying hydrodynamic conditions.

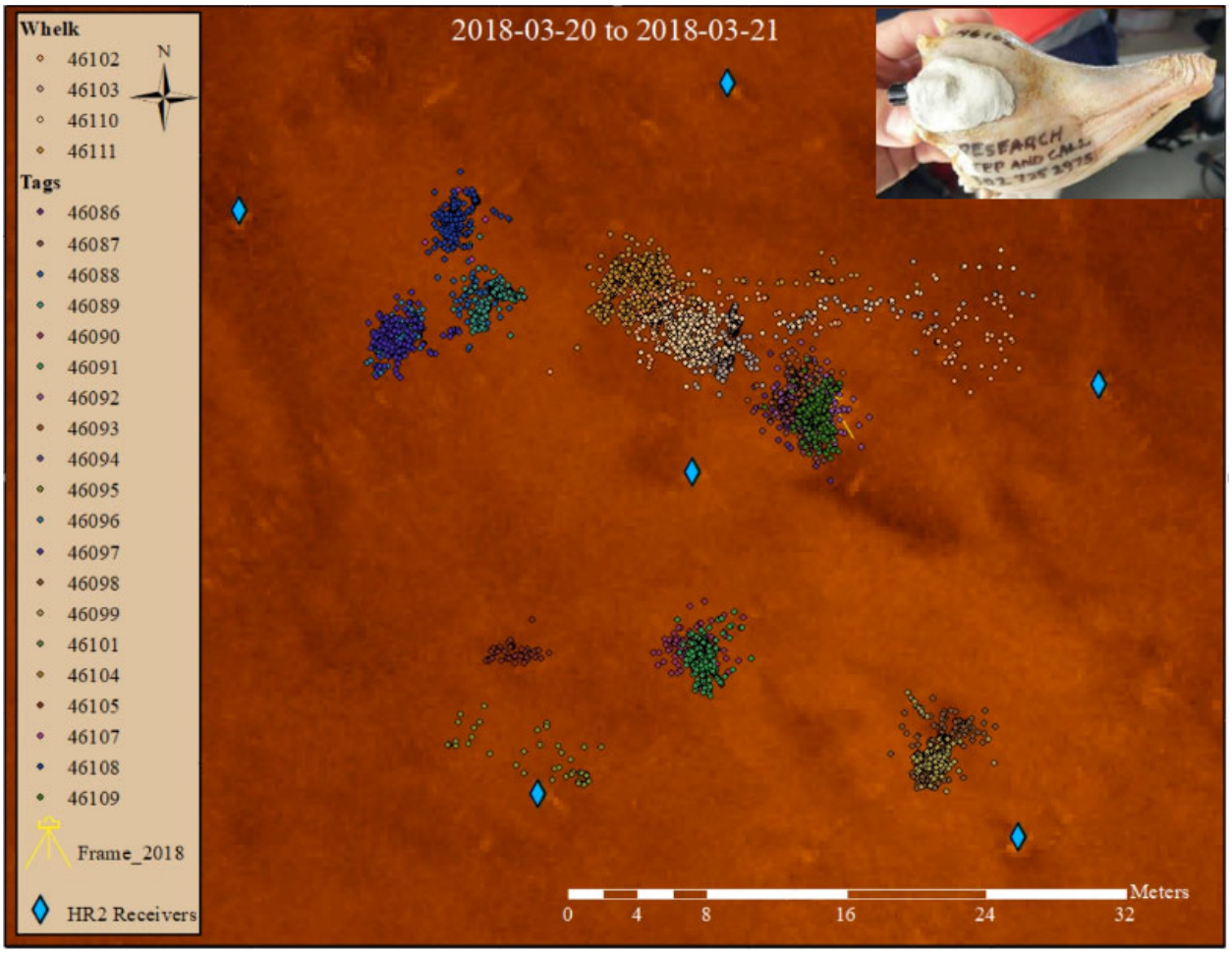



*Figure 6.2: VPS results on Mar. 20, showing the initial position and subsequent movement of the four tagged whelk (inset) to the east and out of the grid. The whelks' positions continued to be recorded beyond the grid but were filtered out for low reliability in this image.*

## 6.1.2. Task 2 – Field Implementation

The location of the field site proved ideal for deployment, recovery, and site monitoring operations. The proximity of the field site to the University of Delaware Marine Operations Base (10.5 km southeast of the site), allowed for short travel time, maximized vessel time on the field site, and reduced cost. The site's location in the lower Delaware Bay also maximized the potential for stronger observed hydrodynamic conditions; the Delaware Bay is at its widest near the location of the field site, which allows for greater fetch for wave formation. For example, the nearby areas of Fowler and Broadkill beach have undergone significant beach erosion and over wash in the past two decades due to storm activity in the area.

The assistance of the Delaware State Police SCUBA Unit for all diving related operations was invaluable to the study, and the DSPSU divers often contended with adverse conditions. Despite issues with weather, poor visibility, strong currents, and cold temperatures, the deployment and recovery operations were successfully conducted by the DSPSU. With their assistance, the VPS system was correctly installed and performed to the standards set for this study. All but one 60mm mortar surrogates were successfully deployed and recovered by the DSPSU.

Geophysical surveys were conducted as frequently as weather conditions would permit, and sensor performed up to specifications throughout field operations. Complete bathymetric and side-scan sonar coverage was achieved at least once per deployment. Complete high-resolution side-scan sonar was also collected for all but the final deployment (the AUV was damaged in shipping prior to the final deployment). At the recommendation of SERDP, the AUV magnetometer was relegated to a supporting role. The unit was unable to detect the 81mm and 60mm surrogates when the VPS and instrument frame was *in situ*, but proved useful for locating buried 81mm surrogates once the VPS and instrument frame were removed. All hydrodynamic instrumentation functioned normally during the four field deployments. The rotary sonar developed an intermittent signal loss that prevented full hourly imagery for the Fall 2017 deployment. The loss was attributed to a slow leak in the bulkhead connecter for the batter and data logger unit. The unit was repaired and functioned normally for the remaining deployments.

The extended deployments of Spring and Fall 2018 required service windows, where the instrument frame was not on site. The transport of the frame from the site in Sept. 2018 did not impact the sensors, which continued to record throughout the deployment until recovery. The recovery of the VPS and redeployment of both the VPS and instrumented frame in Oct. 2018 resulted in an 8-day window with no *in situ* measurements. The instrument frame was also removed prior to VPS recovery in the Spring 2019 deployment due to battery exhaustion. In all, hydrodynamic measurements were collected for 206 and 226 days of deployment. It is suggested that future work look to extending the battery life of the hydrodynamic sensors, through the acquisition of external battery sources, to extend the deployment window.

### 6.1.3. Task 3 – Data Analysis, Project Review and Reporting

Task 3 encompassed data synthesis and reporting. The data products produced by this study include: complete site acoustic backscatter, bathymetry and magnetometer map products (geotiff, .grid, .csv); site-wide surficial sediment classification maps (raster); sediment grain size analysis, shear vane analysis, and penetrometer geotechnical profiles (.csv, .mat); time-series hydrodynamics, conductivity-temperature-depth, and rotary sonar imagery (.mat); surrogate tracking products, both raw recorded receiver times and Vemco processed positions (.csv, .kml). The data collected and processed is organized for dissemination. Pertinent information was provided to Rennie MR-2227 for use in the UnMES model.

### 6.1.4. Task 4 – Optional Additional Field Study

The primary objective of Task 4 was to provide additional observations of munitions mobility and burial. The Task 4 study site (Site 2) expanded observations for munitions mobility and burial in a muddier, shallower site and accounted for the active late-Summer /early-Fall Hurricane season in the mid-Atlantic. The Task 4 deployments provided significant observations of surrogate burial in soft muds, leading to an innovative method for modeling munition burial in soft mud due to sediment bearing capacity.

The Task 4 deployment primarily utilized the methods applied in Task 2, but experimented with new methods for rapid VPS deployment. The auger moorings used in Task 2 for the VSP were diver deployable, but required highly-trained divers to ensure proper installment in zero-visibility conditions. The modifications to the VPS mounts in Task 4 to provide a diver-free and rapidly

deployable option was not met with immediate success. The wide wooden feet designed to reduce the potential for the frames flipping over actually exacerbated the problem. Under strong currents, sediment scoured away from the feet, causing the pole to tilt at a slight angle (~15°). Once tilted, currents caught the upturned edge of the wooden feet and flipped the pole-mounts over. Due to the robustness of the VPS system, the flipped over HR2 receivers continued to record tag detections and did not substantially affect the ability to track acoustic tags (divers were able to use the last estimated tag positions from the VPS with 4 of 6 HR2 receivers flipped over to successfully locate surrogates). The later modification of removing the wooden feet, reducing the pole height, and adding weight was successful under low-moderate conditions, but we recommend a ground-up redesign for a rapidly deployable VPS mount in the future.

Between Task 2 and Task 4, 63 MR-2730 collected 63 sediment samples, eight 30-cm push cores, 4 HAPS cores, shear vane measurements, and 2 gravity cores. The sediment samples informed sonar backscatter classification for sediment distribution maps and models for munitions mobility, scour, and burial. The addition of in situ penetrometer sampling added pertinent geotechnical properties of the sediments at the field sites, and is recommended for any similar study in the future.

## 6.2. Munitions Mobility and Burial in Cohesive Sediments

### 6.2.1. Munitions Mobility

Large-scale horizontal displacement of surrogates, as measured by Traykovski (MR-2319) and Calantoni (MR-2320), was not observed in this study in any of the deployments. Density, object diameter, and bed roughness are all primary factors controlling munitions mobility, and mobility is unlikely when the density of the munition exceeds the density of the surrounding sediment. Surrogates in this study were all denser than the sediment, and as would be expected in non-cohesive sediment, did not experience large displacement. A modified version of Rennie et al. (2017) object mobility threshold equations indicate that conditions during ETC events did momentarily exceed the theoretical threshold for motion, but any degree of scour or settling, as observed throughout the study, greatly reduced the potential for mobility The onboard IMU in the smaller surrogates did measure limited motion, primarily as oscillatory rocking and rolling, but in only two instances did the initiation of motion lead to measurable displacement (< 25 cm). It should be noted that the longest duration of motion measured by the IMU were in the smallest, but densest surrogates (60mm) used in this study, while no motion was observed in the largest and least dense surrogates (155mm). It is possible that the form factor of the 60mm surrogates, with larger fin-to-body ratios, may influence the critical threshold for mobility as the surface area of the fins may provide more drag than the conical shape of the 155mm. The influence of surrogate shape on motion was investigated in laboratory flume tests by Garcia (MR-2410) for rigid and non-cohesive sediment surfaces, but may benefit from more observations in cohesive sediments

### 6.2.2. Munitions Burial

Varying degrees of munition burial was observed by this study, but burial was the consistent result throughout. The fundamental conditions that varied between the deployments were the degree of near-bed forcing and the compositions of the sediment. In absence of sustentative

forcing, burial occurred via settling; the bearing capacity of the surficial sediment could not support the weight of the surrogates. When exposed to higher energy, burial occurred via two mechanisms dependent upon the sediment. In mixed-cohesive muddy sands, burial occurred through scour, with large scour pits imaged in side-scan sonar and verified by divers. In softer sandy muds, the surrogates sank through layers fluidized under increasing wave energy.

The complexities of sediment transport in mixed-cohesive sediments complicate munition burial modeling. As noted above, this work used an estimation for the critical threshold of erosion developed by Whitehouse et al. (2000). Deviations between the modeled and observed behavior of the surrogates can in part be attributed to errors in the threshold approximation. However, the scour models developed for non-cohesive sediments agreed reasonably well with field observations in the muddy sand sediment of Site 1 when adapted to account for mixed-cohesive sediments in this study. The Hertzian contact model implemented in this study for surrogate settling due to bearing capacity also agreed well with the burial depth of the surrogates at both Site 1 and 2 in absence of high-energy forcing. This model currently does not incorporate a temporal component or frictional effects, and would benefit from time-series observations of munitions settling. Future investigations are also required to better understand the burial depth of surrogates due to bed fluidization in cohesive sediments. Existing models for fluid mud layer thickness under waves (see Soltanpour et al., 2009) and may be adapted for application with munitions burial in soft muds.

It should also be noted that this study did not include the effects of impact burial. Previous mine-burial studies noted that impact burial was the largest contributor to mine burial in stiff muds, not subsequent burial processes (Inman and Jenkins, 2002). In soft muds, the forces exerted by impact would greatly exceed the bearing capacity of the sediment and result in burial deeper than observed in this study. It is unclear whether any subsequent processes could contribute re-exposure or further object burial. Therefore, impact burial for MEC in cohesive sediments should be a topic of future research.

### 6.3. Implications for Future Research / Implementation

The data and results presented by this study lays the groundwork for future investigations of munitions mobility and burial in cohesive sediments. The methods utilized in this study, in particular the Vemco VPS acoustic tracking system, can be easily implemented at any site. While the field work for this study was extensive and measured a variety of conditions, this work is by no means an exhaustive examination of the problem. The variety of cohesive sediments and environments in which cohesive sediment are found are much wider than captured in this study, including riverine environments where many active munitions response sites are located (USACE 2007 FUDS). Although in the Delaware Bay Estuary, this study occurred in a location impacted more by strong wind-wave events than excessive tidal or flood-stage currents often experienced in riverine settings. That mobility was not observed in the mixed cohesive or soft muddy sediments of the lower Delaware Bay does not preclude the potential for mobility on stiff, rigid muds (as observed by Calantoni MR-2730) or under strong unidirectional currents recorded in rivers during flood stages. Additional observations in more and varied cohesive sediment environments will continue to improve our understanding and modeling of munitions mobility and burial in cohesive sediment environments. Historical analysis of storm conditions, combined with *in situ* hydrodynamic and geotechnical data for the surface and shallow sub-surface,

provides important threshold conditions for the informed management of munitions response sites, aiding managers in identifying when additional site investigations may be most needed.

This study finds that sediment bearing capacity is an important predictor for surrogate burial, and the Hertzian contact model introduced here provides a simple method to predict burial due to bearing capacity. Further, the ability to tie sediment geotechnical properties such as bearing capacity to sonar classification / surficial sediment distributions maps, as demonstrated in this study, has wide-ranging implications for FUDS site management. Extrapolating subsurface properties based on surficial sediment distributions will reduce the amount of geotechnical sampling required and allow for modeling of surrogate burial across a wide spatial domain. This topic will be investigated in more detail in the MR20-1480 report.

# 7. Literature Cited


Baeye, M., Fettweis, M., Legrand, S., Dupont, Y., and V. Van Lanker, 2012. Mine burial in the seabed of high-turbidity area- findings of a first experiment. *Continental Shelf Research* 43, pp. 107-119.

Blott, S.J. and Pye, K. 2001. GRADISTAT: a grain size distribution and statistics package for the analysis of unconsolidated sediments. Earth Surf. Process. Landforms, 26: 1237-1248.doi:10.1002/esp.261

Calantoni, J., and C.S. Thaxton. 2008. Simple power law for transport ratio with bimodal distributions of coarse sediments under waves. J. of Geophys. Res., 113, C03003, doi:10.1029/2007JC004237.

Carton, G., DuVal, C., Trembanis, A., Edwards, M., Rognstad, M., Briggs, C., and S. Shjegstad. 2017. Munitions and explosives of concern survey methodology and in-field testing for wind energy areas on the Atlantic outer continental shelf. Report prepared for the Bureau of Ocean Energy Management, BOEM 2017-063, July 2017.

Cataño-Lopera, Y. A., Demir, S. T., and M. H. García, 2007. Self-burial of short cylinders under oscillatory flows and combined waves plus currents. *IEEE J. Ocean. Eng.,* 32(1), pp. 191–203.

Cataño-Lopera, Y. A., and M. H. García, 2006. Burial of Short cylinders Induced by Scour under Cominedd Waves and Currents. *J. Waterway, Port, Coast, Ocean Eng*. 132, 439-449.

Dohner, S. 2020. Estuarine Morphodynamic Response and Recovery to Extreme Events *(In Press)*. Dissertation for Ph.D. Submitted to the University of Delaware.

Edwards, M., Wilkens, R., Kelley, C., DeCarlo, E., MacDonald, K., Shjegstad, S., Van Woerkom, M., Payne, Z., Dupra, V., Rosete, M., Akiba, M., Fineran, S., Zheng, W., King, J.C., and G. Carton, 2012. Methodologies for Surveying and Assessing Deep-Water Munitions Sites. *Marine Technology Society Journal,* 46 (1), 51-62.

Heupel, M.R., Semmens, J.M., and A.J. Hobday, 2006. Automated acoustic tracking of aquatic animals: scales, design and deployment of listening station arrays. *Marine and Freshwater Research* 57(1), pp. 1-13

Inman, D. L. and S.A. Jenkins, 2002. Scour and Burial of Bottom Mines: a Primer for Fleet Use. SIO Reference, Scripps Institution of Oceanography, University of California, San Diego, La Jolla.

Jacobs, W., Le Hir, P., Van Kesteren, D., and P. Cann. 2011. Erosion threshold of sand-mud mixtures. Cont. Shelf Res. 31, S14-S25.

Jenkins, S.A., Inman, D.L., Richardson, M.D., Weaver, T.F, and J. Wasyl. 2007. Scour and Burial Mechanics of Objects in the Nearshore. *IEEE Journal of Oceanic Engineering,* 32 (1), 78-90.

Keller, B.M., Hamilton, T., and S. Hird, 2015. Low-Logistics AUV Pipelin Inspection: Acquiring High-Resolution Geophysical data in Very Shallow Water. Sea Technology 56(12), 37-41.

Klammler, H., Sheremet, A., and J. Calantoni. 2019. Seafloor Burial of Surrogate Unexploded Ordnance by Wave-Induced Sediment Instability. IEEE J. Ocean Eng. DOI: 10.1109/JOE.2019.2919356

Letter, Jr., J.V., and A.J. Mehta, 2011. A heuristic examination of cohesive sediment bed exchange in turbulent flows. *Coastal Engineering* 58, pp. 779-789.

Mayer, L., Raymond, R., Glang, G., Richardson, M.D., Traykovski, P. and A. Trembanis, 2007. High resolution mapping of mines and ripples at the Martha's Vineyard coastal observatory. *IEEE Journal of Oceanic Engineering* 32 (1), 133-149.

Obrzud, R. and Truty, A., 2012. The Hardening Soil Model—A Practical Guidebook (Lausanne: Zace Ltd).

Piraino, M.N. and Szedlmayer, S.T., 2014. Fine-scale movements and home ranges of red snapper around artificial reefs in the northern Gulf of Mexico. Transactions of the American Fisheries Society, 143(4), 988-998.

Raineault, N.A., Trembanis, A.C., and D.C. Miller, 2011. Mapping benthic habitats in Delaware Bay and the coastal Atlantic: acoustic techniques provide greater coverage and high resolution in complex, shallow-water environments. *Estuaries and Coasts,* 35(2), pp 682-699.

Rennie, S.E. 2017. Underwater munitions expert system to predict mobility and burial. Final Report Strategic Environmental Research Development Program MR-2227.

Rennie, S.E., Brandt, A., and C.T. Friedrichs. 2017. Initiation of motion and scour burial of objects underwater. Ocean Engineering, 131, 282-294.

Richarson, M., Valent, P., Briggs, K., Bradley, J., and S. Griffin. 2001. NRL Mine Burial Experiments. Proc. 2nd Austr.-Amer. Joint Conf. Technol. Mine Countermeasures, Sydney, Australia, Mar. 27–29, 2001.

Roegner, G.C. and Fields, S.A., 2015. Mouth of the Columbia River Beneficial Sediment Deposition Project: Benthic Impact Study 2014. Report for U.S. Army Corps of Engineers, Portland District. Accessed at: https://www.researchgate.net/profile/G_Roegner/publication/280022449_Mouth_of_the_Columbia_River_Beneficial_Sediment_Deposition_Project_Benthic_Impact_Study_2014/links/55a3f31008ae00cf99c8edce.pdf

Sahin, C., I. Safak, A. Sheremet, and A. J. Mehta. 2012. Observations on cohesive bed reworking by waves: Atchafalaya Shelf, Louisiana, J. Geophys. Res., 117, C09025, doi:10.1029/2011JC007821.

SERPD Final Report, 2013. SERDP/Office of Naval Research Workshop on Acoustic Detection and Classification of MEC in the Underwater Environment, Sept. 2013.

SERDP Draft Report, 2014. Program Review for Burial and Mobility Modeling of Munitions in the Underwater Environment. Draft Version 1.2, 15 Oct. 2014.

Sheremet, A., Mehta, A.J., Liu, B., and G.W. Stone, 2005. Wave-sediment interaction on a muddy inner shelf during Hurricane Claudette. *Estuarine, Coastal and Shelf Science* 63, pp. 225-233.

Soltanpour, M., Haghshenas, S.A., and A.J. Mehta, 2009. Fluidized Mud-Wave Interaction under Regular and Irregular Waves. *Journal of Coastal Research* 25 (3), pp. 616-626.

Stark, N., Radosavljevic, B., Quinn, B., and H. Lantuit. 2016. Application of portable free-fall penetrometer for geotechnical investigation of Arctic nearshore zone. Can. Geotech. J. 54: 31–49, dx.doi.org/10.1139/cgj-2016-0087

Steigerwalt, R., Trembanis, A.C., and M. Tchernychev, 2012. Autonomous Underwater Vehicle Munitions And Explosives Of Concern Detection System. May 2012. ESCTP IPR. Arlington, VA.

Traykovski, P. and T. Austin. 2017. Continuous monitoring of mobility, burial and re-exposure of underwater munitions in energetic near-shore environments. Final Report Strategic Environmental Research and Development Program (SERDP) Project MR-2319.

Traykovski, P., Richardson, M.D., Mayer, L.A., and J.D. Irish, 2007. Mine Burial Experiments at Martha's Vineyard Coastal Observatory. *IEEE Journal of Oceanic Engineering* 32(1), pp. 150-166.

Trembanis, A., C., DuVal, J., Beaudoin, V., Schmidt, D., Miller, L., Mayer. 2013. A detailed seabed signature from Hurricane Sandy revealed in bed forms and scour, *Geochem. Geophys. Geosyst*., 14(10), 4334-4340.

Trembanis, A.C., Friedrichs, C.T., Richardson, M.D., Traykovski, P., Howd, P.A., Elmore, P.A. and Wever, T. F., 2007. Predicting seabed burial of cylinders by wave-induced scour: application to the sandy inner shelf off Florida and Massachusetts. *IEEE Journal of Oceanic Engineering* 32(1), pp 167-183.

U.S. Fish and Wildlife Service. 2015. Draft Environmental Assessment Prime Hook National Wildlife Refuge for Recovery and Ecosystem Restoration. Accessed at: http://www.fws.gov/hurricane/sandy/pdf/PrimeHookEA.pdf

Van Prooijen, B. C., and J. C. Winterwerp (2010), A stochastic formulation for erosion of cohesive sediments, J. Geophys. Res., 115, C01005, doi:10.1029/2008JC005189

Velde, B., and T. Church. 1999. Rapid clay transformations in the Delaware salt marshes. Applied Geochemistry, 14, 559-568.

Whitehouse, R., 1998. Scour at marine structures: A manual for practical applications. Thomas Telford.

Whitehouse, R.J.S., Soulsby, R.L., Roberts, W. and Mitchener, H.J., 2000. Dynamics of estuarine muds.

Wilson, B.D., Madsen, J.A., Fox, D., Simpson, P., Moore, J., Bruce, D., and D.B. Carter, 2010. Delaware Bay Benthic Mapping Project: Mapping the Distribution of Bottom Sediments, Key Habitats, and Sub-bottom Imaging in Delaware Bay and River. Delaware Department of Natural Resources and Environmental Control. Access at: http://www.dnrec.delaware.gov/coastal/Documents/Benthic%20Mapping/Benthic_Mapping_Presentation.pdf

Wright, L. D., 1993. Micromorphodynamics of the inner continental shelf: a Middle Atlantic Bight case study. *Journal of Coastal Research*, Special Issue No. 15 Beach and Surf Zone: 93-124.

# Appendix A

## A.1. Surrogate Deployment Summary

The tables below summarize pertinent information for surrogates in each of the four MR-2730 deployments. The tables include: surrogate physical characteristics (weight, density, diameter), acoustic tags ID, x-io IMU ID, pressure sensor and logger ID (for 155mm surrogates only), estimated burial depth and percentage burial (relative to surrogate diameter), VPS estimated displacement (automated analysis), verified displacement (manual analysis), IMU motion detection, and relevant notes. Surrogate displacement was from the VPS data using the difference in daily mean estimated locations on the first and last full day of record for the each tag. Included is the estimated 90% error estimate based on filtered HR2 synctag location estimates compared to positions surveyed using a RTK GPS enabled phase-measuring bathymetric sonar (see Section 6.1.1). The Verified Displacement is a manual confirmation of whether the estimate displacement was consistently observed in the VPS data (i.e. observed for multiple days) and supported by IMU measurements, or was due to error or noise in estimated positions. It should be noted that the quality of detections decreased as surrogates started to bury, leading to a complete loss of detections with total surrogate burial. IMU Motion detection notes whether any motion was recorded in the IMU during the deployment window. Note that discrepancies between burial depth (maximum estimated depth of the deepest part of the object), and burial percentage may be attributable to burial of the surrogates at certain relative angles (e.g. nose down).

Other data such as side-scan and bathymetric data sets and hydrodynamic forcing time series are available from the lead investigator: art@udel.edu

*Table A.1: Surrogate summary table for Fall 2017 deployment.*

| Fall 2017 Deployment | | | | | | | | | | |
|---|---|---|---|---|---|---|---|---|---|---|
| **Surrogate ID** | **Nose Tag ID** | **Tail Tag ID** | **IMU** | **Pressure Sensor** | **Weight (kg)** | **Length (m)** | **Density (kg/m3)** | **Diameter (m)** | **Diver Est. Burial (m)** | **Est. Burial %** |
| 60_A | 46094 | 46095 | NGIMU_3 | N/A | 1.2 | 0.2425 | 3968 | 0.06 | 0.03 | 50 |
| 60_B | 46096 | 46097 | NGIMU_4 | N/A | 1.2 | 0.2425 | 3968 | 0.06 | 0.03 | 50 |
| 60_C | 46098 | 46099 | NGIMU_2 | N/A | 1.2 | 0.2425 | 3968 | 0.06 | 0.03 | 50 |
| 81_A | 46092 | 46093 | NGIMU_6 | N/A | 4 | 0.5067 | 3636 | 0.081 | 0.04 | 50 |
| 81_B | 46090 | 46091 | NGIMU_5 | N/A | 4 | 0.5067 | 3636 | 0.081 | 0.04 | 50 |
| 81_C | 46086 | 46087 | NGIMU_7 | N/A | 4 | 0.5067 | 3636 | 0.081 | 0.04 | 50 |
| 81_D | 46088 | 46089 | NGIMU_8 | N/A | 4 | 0.5067 | 3636 | 0.081 | 0.04 | 50 |
| 155_A | 46104 | 46105 | NGIMU_9 | N/A | 32.4 | 0.7272 | 3284 | 0.155 | 0.08 | 50 |
| 155_B | 46107 | 46108 | NGIMU_10 | N/A | 32.4 | 0.7272 | 3284 | 0.155 | 0.08 | 50 |
| 155_C | 46109 | 46110 | NGIMU_11 | N/A | 32.4 | 0.7272 | 3284 | 0.155 | 0.08 | 50 |
| | | | | | | | | | | |

| **Surrogate ID** | **VPS Est. Displacement (m) (0.62m 90% error)** | **Verified Displacement (m)** | **Motion Detection IMU** | **Notes** |
|---|---|---|---|---|
| 60_A | 0.72 | - | Yes | 60mm reported to be 50% buried |
| 60_B | 0.22 | - | Yes | 60mm reported to be 50% buried; IMU suggest rolled into scour pit (pitch and roll) |
| 60_C | 1.09 | - | Yes | 60mm reported to be 50% buried. Unit developed slight leak and IMU dead on retrieval. |
| 81_A | 0.75 | - | Yes | 81mm reported to be 50% buried |
| 81_B | 0.62 | - | Yes | 81mm reported to be 50% buried |
| 81_C | 1.51 | - | Yes | 81mm reported to be 50% buried |
| 81_D | 0.78 | - | Yes | 81mm reported to be 50% buried |
| 155_A | 0.50 | - | No | 155mm reported to be 50% buried |
| 155_B | 0.71 | - | No | 155mm reported to be 50% buried; only 1 tag detected (46107 damaged). |
| 155_C | 0.40 | - | No | 155mm reported to be 50% buried |

*Table A.2: Surrogate summary table for Spring 2018 deployment.*

| Spring 2018 Deployment | | | | | | | | | | |
|---|---|---|---|---|---|---|---|---|---|---|
| **Surrogate ID** | **Nose Tag ID** | **Tail Tag ID** | **IMU** | **Pressure Sensor** | **Weight (kg)** | **Length (m)** | **Density (kg/m3)** | **Diameter (m)** | **Diver Est. Burial (m)** | **Est. Burial %** |
| 60_A | 46086 | 46087 | NGIMU_3 | N/A | 1.2 | 0.2425 | 3968 | 0.06 | 0.20 | 333 |
| 60_B | 46088 | 46089 | NIGMU_4 | N/A | 1.2 | 0.2425 | 3968 | 0.06 | 0.20 | 333 |
| 60_C | 46090 | 46091 | NGIMU_5 | N/A | 1.2 | 0.2425 | 3968 | 0.06 | 0.20 | 333 |
| 81_A | 46092 | 46093 | NIGMU_6 | N/A | 4 | 0.5067 | 3636 | 0.081 | 0.11 | 131 |
| 81_B | 46094 | 46095 | NGIMU_7 | N/A | 4 | 0.5067 | 3636 | 0.081 | 0.11 | 131 |
| 81_C | 46096 | 46097 | NGIMU_8 | N/A | 4 | 0.5067 | 3636 | 0.081 | 0.11 | 131 |
| 81_D | 46098 | 46099 | NGIMU_9 | N/A | 4 | 0.5067 | 3636 | 0.081 | 0.11 | 131 |
| 155_A | 46101 | 46109 | NGIMU_10 | WLPS_1 | 32.8 | 0.727 | 3325 | 0.155 | 0.16 | 100 |
| 155_B | 46107 | 46108 | NGIMU_11 | WLPS_2 | 32.8 | 0.727 | 3325 | 0.155 | 0.16 | 100 |
| 155_C | 46104 | 46105 | NGIMU_12 | WLPS_3 | 32.8 | 0.727 | 3325 | 0.155 | 0.16 | 100 |
| | | | | | | | | | | |

| **Surrogate ID** | **VPS Est. Displacement (m) (0.7m 90% error)** | **Verified Displacement (m)** | **Motion Detection IMU** | **Notes** |
|---|---|---|---|---|
| 60_A | 0.88 | 0.25 | Yes | 60mm reported to be mostly buried, pitched near vertical, with only fins exposed. 25cm displacement observed in VPS on Mar 20, 2018 and supported by IMU |
| 60_B | 0.69 | - | Yes | 60mm reported to be mostly buried, pitched near vertical, with only fins exposed |
| 60_C | 1.04 | 0.18 | Yes | 60mm reported to be mostly buried, pitched near vertical, with only fins exposed. 18cm displacement observed in VPS on Mar 20, 2018 and supported by IMU |
| 81_A | 0.87 | - | Yes | 81mm reported to be buried, slight pitch, fins at surface or slightly exposed. <1" overburden above main body |
| 81_B | N/A | - | Yes | 81mm reported to be buried, slight pitch, fins at surface or slightly exposed; VPS position unavailable due to poor detection HPE and RMSE |
| 81_C | 1.31 | - | Yes | 81mm reported to be buried, slight pitch, fins at surface or slightly exposed. <1" overburden above main body |
| 81_D | 1.12 | - | Yes | 81mm reported to be buried, slight pitch, fins at surface or slightly exposed. <1" overburden above main body |
| 155_A | 0.90 | - | No | 155mm reported to be ~50% buried but in large scour pits flush with seafloor. Corroborated in SSS. |
| 155_B | 1.08 | - | No | 155mm reported to be ~50% buried but in large scour pits flush with seafloor. Corroborated in SSS. |
| 155_C | 0.34 | - | No | 155mm reported to be ~50% buried but in large scour pits flush with seafloor. Corroborated in SSS. |

*Table A.3: Surrogate summary table for Fall 2018 deployment.*

| Fall 2018 Deployment | | | | | | | | | | |
|---|---|---|---|---|---|---|---|---|---|---|
| **Surrogate ID** | **Nose Tag ID** | **Tail Tag ID** | **IMU** | **Pressure Sensor** | **Weight (kg)** | **Length (m)** | **Density (kg/m3)** | **Diameter (m)** | **Diver Est. Burial (m)** | **Est. Burial %** |
| 60_A | 46088 | 46089 | NGIMU_3 | N/A | 1.2 | 0.2425 | 3968 | 0.06 | 0.40 | 667 |
| 60_B | 46090 | 46091 | NGIMU_4 | N/A | 1.2 | 0.2425 | 3968 | 0.06 | NA | NA |
| 60_C | 46092 | 46093 | NGIMU_5 | N/A | 1.2 | 0.2425 | 3968 | 0.06 | NA | NA |
| 81_A | 46095 | 46096 | NGIMU_6 | N/A | 4.2 | 0.5067 | 3818 | 0.081 | 0.28 | 347 |
| 81_B | 46097 | 46098 | NGIMU_7 | N/A | 4.2 | 0.5067 | 3818 | 0.081 | NA | NA |
| 81_C | 46094 | 46099 | NGIMU_8 | N/A | 4.2 | 0.5067 | 3818 | 0.081 | 0.28 | 347 |
| 81_D | 46086 | 46087 | NGIMU_9 | N/A | 4.2 | 0.5067 | 3818 | 0.081 | 0.28 | 347 |
| 155_A | 46104 | 46105 | NGIMU_10 | WLPS_2 | 33.9 | 0.727 | 3436 | 0.155 | 0.36 | 229 |
| 155_B | 46108 | 46109 | NGIMU_11 | WLPS_3 | 33.9 | 0.727 | 3436 | 0.155 | 0.36 | 229 |
| 155_C | 46101 | 47671 | NGIMU_12 | WLPS_1 | 33.9 | 0.727 | 3436 | 0.155 | 0.36 | 229 |
| | | | | | | | | | | |

| **Surrogate ID** | **VPS Est. Displacement (m) (3.2m 90% error)** | **Verified Displacement (m)** | **Motion Detection IMU** | **Notes** |
|---|---|---|---|---|
| 60_A | 1.99 | - | Yes | 60mm reported to be buried near vertical with 8-12" (20-30cm) overburden |
| 60_B | 2.48 | - | Yes | 60mm not recovered until 8/19/20; divers reported near vertical pitch and shallow burial |
| 60_C | 1.98 | - | N/A | 60mm not recovered |
| 81_A | 1.71 | - | Yes | 81mm reported to be buried slight pitch with 8-12" (20-30cm) overburden |
| 81_B | 1.11 | - | Yes | 81mm not recovered until 8/19/19 - divers reported shallow burial, IMU measurements during April and May |
| 81_C | 0.64 | - | Yes | 81mm reported to be buried slight pitch with 8-12" (20-30cm) overburden |
| 81_D | 2.48 | - | Yes | 81mm reported to be buried slight pitch with 8-12" (20-30cm) overburden |
| 155_A | 1.59 | - | Yes | 155 reported to be buried with 8-12" (20-30cm) overburden |
| 155_B | 0.45 | - | No | 155 reported to be buried with 8-12" (20-30cm) overburden |
| 155_C | 1.00 | - | No | 155 reported to be buried with 8-12" (20-30cm) overburden |

*Table A.4: Surrogate summary table for Spring 2019 deployment.*

| Spring 2019 Deployment | | | | | | | | | | |
|---|---|---|---|---|---|---|---|---|---|---|
| **Surrogate ID** | **Nose Tag ID** | **Tail Tag ID** | **IMU** | **Pressure Sensor** | **Weight (kg)** | **Length (m)** | **Density (kg/m3)** | **Diameter (m)** | **Diver Est. Burial (m)** | **Est. Burial %** |
| 60_A | 46086 | 46087 | NGIMU_3 | N/A | 1.2 | 0.2425 | 3968 | 0.06 | 0.2 | 333 |
| 81_A | 46097 | 46094 | NGIMU_6 | N/A | 4.2 | 0.5067 | 3818 | 0.081 | 0.10 | 123 |
| 81_C | 47669 | 47671 | NGIMU_8 | N/A | 4.2 | 0.5067 | 3818 | 0.081 | 0.10 | 123 |
| 81_D | 47670 | 46108 | NGIMU_9 | N/A | 4.2 | 0.5067 | 3818 | 0.081 | 0.10 | 123 |
| 4.2_A | 46099 | 47096 | NGIMU_14 | N/A | 13.4 | 0.5461 | 3375 | 0.107 | 0.11 | 100 |
| 4.2_B | 46096 | 47094 | NGIMU_15 | N/A | 13.6 | 0.5461 | 3426 | 0.107 | 0.11 | 100 |
| 4.2_C | 46089 | 47095 | NGIMU_16 | N/A | 12.6 | 0.5461 | 3174 | 0.107 | 0.11 | 100 |
| 4.2_D | 46095 | 47668 | NGIMU_17 | N/A | 12.6 | 0.5461 | 3174 | 0.107 | 0.11 | 100 |
| 155_A | 46104 | 47666 | NGIMU_10 | WLPS_1 | 35.4 | 0.7272 | 3588 | 0.155 | 0.16 | 100 |
| 155_B | 46105 | 47667 | NGIMU_11 | WLPS_2 | 35.4 | 0.7272 | 3588 | 0.155 | 0.16 | 100 |
| 155_C | 47664 | 47665 | NGIMU_13 | WLPS_3 | 35.2 | 0.7272 | 3568 | 0.155 | 0.16 | 100 |

| **Surrogate ID** | **VPS Est. Displacement (m) (0.9m 90% error)** | **Verified Displacement (m)** | **Motion Detection IMU** | **Notes** |
|---|---|---|---|---|
| 60_A | 0.88 | - | Yes | 60mm buried at near vertical angle with fins slightly exposed |
| 81_A | 1.25 | - | Yes | 81mm buried w/ main body ~1in below surface |
| 81_C | 0.38 | - | Yes | 81mm buried w/ main body ~1in below surface |
| 81_D | 0.34 | - | Yes | 81mm buried w/ main body ~1in below surface |
| 4.2_A | 0.42 | - | Yes | 4.2in buried flush with surface |
| 4.2_B | 0.10 | - | Yes | 4.2in buried flush with surface |
| 4.2_C | 1.14 | - | Yes | 4.2in buried flush with surface |
| 4.2_D | 0.45 | - | Yes | 4.2in buried flush with surface |
| 155_A | 0.53 | - | Yes | 155mm buried flush with surface |
| 155_B | 0.59 | - | Yes | 155mm buried flush with surface. Pressure sensors failed upon deployment |
| 155_C | 0.99 | - | Yes | 155mm buried flush with surface. Pressure sensors failed upon deployment |

## A.2. Sediment Samples

Sediment samples were collected using a modified Young's sediment grab sampler. Two 100mL samples were collected from each grab. A 20 gram portion was sub-sampled and processed using a standard grain size analysis by sieve (for sand fraction) and pipette (for mud fraction) methods at ½ phi intervals. The data was collated and statistical analysis conducted using GRADISTAT version 9.1 (Blott and Pye, 2001). Please see Blott and Pye (2001) for more details of GRADISTAT and the tabulated data products provided below.

*Table A.5: Sediment sample grain size analysis and statistics.*

| SAMPLE | 20170706 Sample 1 | 20170706 Sample 2 | 20170706 Sample 3 | 20170706 Sample 4 | 20170706 Sample 5 | 20170706 Sample 6 |
|---|---|---|---|---|---|---|
| LAT | 38.86228333 | 38.87471667 | 38.88073333 | 38.89145 | 38.88205 | 38.87235 |
| LON | -75.19713333 | -75.19906667 | -75.21795 | -75.20651667 | -75.19041667 | -75.17783333 |
| SIEVING ERROR | -0.4% | 3.2% | 1.0% | 2.5% | 2.1% | 2.9% |
| SAMPLE TYPE | Unimodal, Poorly Sorted | Bimodal, Poorly Sorted | Bimodal, Poorly Sorted | Unimodal, Poorly Sorted | Bimodal, Poorly Sorted | Bimodal, Poorly Sorted |
| TEXTURAL GROUP | Muddy Sand | Muddy Sand | Muddy Sand | Muddy Sand | Muddy Sand | Muddy Sand |
| SEDIMENT NAME | Very Coarse Silty Medium Sand | Coarse Silty Very Fine Sand | Very Coarse Silty Medium Sand | Very Coarse Silty Very Fine Sand | Coarse Silty Very Fine Sand | Very Coarse Silty Very Fine Sand |
| ARITH MEAN MICRON | 370.6 | 94.37 | 255.3 | 102.9 | 116.3 | 92.96 |
| ARITH SORTING MICRON | 223.8 | 109.2 | 178.5 | 162.5 | 150.3 | 116.9 |
| ARITH SKEWNESS MICRON | 1.492 | 7.449 | 0.595 | 6.041 | 6.330 | 6.816 |
| ARITH KURTOSIS MICRON | 9.971 | 84.58 | 5.317 | 46.59 | 54.47 | 67.01 |
| GEOM MEAN MICRON | 239.9 | 57.26 | 150.2 | 57.10 | 67.69 | 56.10 |
| GEOM SORTING MICRON | 3.857 | 3.181 | 3.880 | 3.100 | 3.297 | 3.081 |
| GEOM SKEWNESS MICRON | -2.346 | -1.385 | -1.607 | -0.918 | -1.325 | -1.333 |
| GEOM KURTOSIS MICRON | 8.031 | 5.136 | 5.368 | 4.890 | 5.390 | 5.331 |
| LOG MEAN PHI | 2.059 | 4.112 | 2.661 | 4.108 | 3.798 | 4.138 |
| LOG SORTING PHI | 1.947 | 1.662 | 1.867 | 0.620 | 1.663 | 1.615 |
| LOG SKEWNESS PHI | 2.346 | 1.347 | 1.510 | 0.836 | 1.090 | 1.277 |
| LOG KURTOSIS PHI | 8.031 | 5.111 | 5.052 | 4.796 | 5.104 | 5.289 |
| FW MEAN MICRON | 318.1 | 59.59 | 188.1 | 58.07 | 69.17 | 56.99 |
| FW SORTING MICRON | 2.621 | 2.869 | 3.067 | 2.803 | 2.940 | 2.744 |
| FW SKEWNESS MICRON | -0.589 | -0.504 | -0.626 | -0.418 | -0.443 | -0.529 |
| FW KURTOSIS MICRON | 3.748 | 1.560 | 1.049 | 1.736 | 1.465 | 1.834 |
| FW MEAN PHI | 1.652 | 4.069 | 2.411 | 4.106 | 3.854 | 4.133 |
| FW SORTING PHI | 1.390 | 1.521 | 1.617 | 1.487 | 1.556 | 1.456 |
| FW SKEWNESS PHI | 0.589 | 0.504 | 0.626 | 0.418 | 0.443 | 0.529 |
| FW KURTOSIS PHI | 3.748 | 1.560 | 1.049 | 1.736 | 1.465 | 1.834 |
| FW MEAN | Medium Sand | Very Coarse Silt | Fine Sand | Very Coarse Silt | Very Fine Sand | Very Coarse Silt |
| FW SORTING | Poorly Sorted | Poorly Sorted | Poorly Sorted | Poorly Sorted | Poorly Sorted | Poorly Sorted |
| FW SKEWNESS | Very Fine Skewed | Very Fine Skewed | Very Fine Skewed | Very Fine Skewed | Very Fine Skewed | Very Fine Skewed |

| SAMPLE | 20170706 Sample 1 | 20170706 Sample 2 | 20170706 Sample 3 | 20170706 Sample 4 | 20170706 Sample 5 | 20170706 Sample 6 |
|---|---|---|---|---|---|---|
| FW KURTOSIS | Extremely Leptokurtic | Very Leptokurtic | Mesokurtic | Very Leptokurtic | Leptokurtic | Very Leptokurtic |
| MODE 1 MICRON | 427.5 | 94.00 | 427.5 | 94.00 | 94.00 | 94.00 |
| MODE 2 MICRON | | 27.00 | 94.00 | | 19.00 | 19.00 |
| MODE 3 MICRON | | | | | | |
| MODE 1 PHI | 1.247 | 3.494 | 1.247 | 3.494 | 3.494 | 3.494 |
| MODE 2 PHI | | 5.236 | 3.494 | | 5.736 | 5.736 |
| MODE 3 PHI | | | | | | |
| D10 MICRON | 35.54 | 11.18 | 23.94 | 11.22 | 17.12 | 10.98 |
| D50 MICRON | 370.5 | 79.92 | 275.4 | 75.69 | 91.87 | 77.95 |
| D90 MICRON | 578.4 | 160.7 | 471.0 | 124.4 | 194.1 | 122.9 |
| D90 Div D10 MICRON | 16.28 | 14.38 | 19.67 | 11.08 | 11.34 | 11.19 |
| D90 Sub D10 MICRON | 542.9 | 149.5 | 447.1 | 113.1 | 176.9 | 111.9 |
| D75 Div D25 MICRON | 1.666 | 2.857 | 4.723 | 2.631 | 2.857 | 2.355 |
| D75 Sub D25 MICRON | 182.5 | 72.34 | 310.9 | 64.00 | 92.38 | 59.62 |
| D10 PHI | 0.790 | 2.637 | 1.086 | 3.007 | 2.365 | 3.024 |
| D50 PHI | 1.433 | 3.645 | 1.860 | 3.724 | 3.444 | 3.681 |
| D90 PHI | 4.815 | 6.483 | 5.384 | 6.477 | 5.868 | 6.509 |
| D90 Div D10 PHI | 6.096 | 2.458 | 4.957 | 2.154 | 2.481 | 2.152 |
| D90 Sub D10 PHI | 4.025 | 3.846 | 4.298 | 3.470 | 3.503 | 3.484 |
| D75 Div D25 PHI | 1.651 | 1.478 | 2.668 | 1.426 | 1.538 | 1.378 |
| D75 Sub D25 PHI | 0.736 | 1.514 | 2.240 | 1.396 | 1.515 | 1.235 |
| PER GRAVEL | 0.0% | 0.0% | 0.0% | 0.0% | 0.0% | 0.0% |
| PER SAND | 86.1% | 68.1% | 82.8% | 65.0% | 71.8% | 68.8% |
| PER MUD | 13.9% | 31.9% | 17.2% | 35.0% | 28.2% | 31.2% |
| PER V COARSE GRAVEL | 0.0% | 0.0% | 0.0% | 0.0% | 0.0% | 0.0% |
| PER COARSE GRAVEL | 0.0% | 0.0% | 0.0% | 0.0% | 0.0% | 0.0% |
| PER MEDIUM GRAVEL | 0.0% | 0.0% | 0.0% | 0.0% | 0.0% | 0.0% |
| PER FINE GRAVEL | 0.0% | 0.0% | 0.0% | 0.0% | 0.0% | 0.0% |
| PER V FINE GRAVEL | 0.0% | 0.0% | 0.0% | 0.0% | 0.0% | 0.0% |
| PER V COARSE SAND | 1.3% | 0.4% | 0.9% | 1.0% | 1.6% | 0.4% |
| PER COARSE SAND | 12.8% | 0.7% | 4.1% | 1.8% | 1.1% | 1.4% |
| PER MEDIUM SAND | 67.9% | 1.3% | 51.2% | 2.7% | 2.2% | 1.8% |
| PER FINE SAND | 2.6% | 13.7% | 7.7% | 4.1% | 27.4% | 4.8% |
| PER V FINE SAND | 1.5% | 51.8% | 18.9% | 55.4% | 39.5% | 60.3% |
| PER V COARSE SILT | 4.6% | 9.9% | 5.5% | 13.7% | 8.9% | 10.1% |
| PER COARSE SILT | 3.0% | 10.1% | 5.1% | 9.6% | 11.1% | 8.7% |
| PER MEDIUM SILT | 0.7% | 4.0% | 2.1% | 3.6% | 2.0% | 4.6% |
| PER FINE SILT | 2.0% | 2.9% | 1.7% | 4.3% | 2.8% | 3.2% |
| PER V FINE SILT | 1.5% | 2.8% | 1.9% | 3.1% | 1.9% | 2.7% |
| PER CLAY | 2.0% | 2.2% | 0.9% | 0.6% | 1.5% | 1.8% |

| SAMPLE | 20171018 Sample 1 | 20171018 Sample 3 | 20171018 Sample 4 | 20171018 Sample 5 | 20171018 Sample 6 | 20171018 Sample 10 | 20171018 Sample 11 |
|---|---|---|---|---|---|---|---|
| LAT | 38.8733 | 38.88526667 | 38.8777 | 38.86926667 | 38.86321667 | 38.87925 | 38.88255 |
| LON | -75.19036667 | -75.20158333 | -75.19246667 | -75.18493333 | -75.19563333 | -75.2207 | -75.21415 |
| SIEVING ERROR | 1.7% | 0.8% | 0.5% | 5.4% | -1.5% | 1.0% | 2.3% |
| SAMPLE TYPE | Unimodal, Poorly Sorted | Unimodal, Poorly Sorted | Unimodal, Poorly Sorted | Bimodal, Very Poorly Sorted | Unimodal, Poorly Sorted | Trimodal, Poorly Sorted | Unimodal, Poorly Sorted |
| TEXTURAL GROUP | Muddy Sand | Muddy Sand | Muddy Sand | Muddy Sand | Sand | Muddy Sand | Muddy Sand |
| SEDIMENT NAME | Very Coarse Silty Very Fine Sand | Very Coarse Silty Very Fine Sand | Very Coarse Silty Very Fine Sand | Very Coarse Silty Very Fine Sand | Poorly Sorted Coarse Sand | Coarse Silty Very Fine Sand | Very Coarse Silty Very Fine Sand |
| ARITH MEAN MICRON | 154.1 | 121.5 | 115.1 | 102.2 | 541.1 | 133.7 | 80.53 |
| ARITH SORTING MICRON | 234.3 | 174.0 | 136.4 | 125.6 | 313.7 | 148.7 | 66.73 |
| ARITH SKEWNESS MICRON | 4.476 | 5.942 | 7.318 | 6.053 | 0.914 | 4.633 | 9.372 |
| ARITH KURTOSIS MICRON | 24.73 | 45.07 | 69.74 | 59.23 | 5.000 | 36.63 | 163.7 |
| GEOM MEAN MICRON | 77.52 | 63.41 | 78.57 | 49.10 | 374.5 | 77.61 | 53.92 |
| GEOM SORTING MICRON | 3.787 | 3.873 | 2.624 | 4.648 | 3.303 | 3.333 | 2.921 |
| GEOM SKEWNESS MICRON | -1.217 | -1.344 | -1.853 | -1.251 | -2.527 | -1.200 | -1.714 |
| GEOM KURTOSIS MICRON | 5.250 | 4.943 | 9.270 | 3.826 | 9.700 | 4.821 | 5.352 |
| LOG MEAN PHI | 3.571 | 3.790 | 3.598 | 3.818 | 1.411 | 3.671 | 4.192 |
| LOG SORTING PHI | 1.836 | 1.844 | 1.320 | 1.990 | 1.711 | 1.724 | 1.536 |
| LOG SKEWNESS PHI | 1.017 | 1.067 | 1.397 | 0.796 | 2.518 | 1.157 | 1.638 |
| LOG KURTOSIS PHI | 5.104 | 4.902 | 8.433 | 4.143 | 9.647 | 4.747 | 5.296 |
| FW MEAN MICRON | 85.71 | 74.47 | 89.71 | 68.26 | 486.8 | 80.15 | 55.73 |
| FW SORTING MICRON | 3.198 | 3.230 | 2.008 | 4.466 | 2.309 | 3.182 | 2.575 |
| FW SKEWNESS MICRON | -0.307 | -0.363 | -0.176 | -0.209 | -0.377 | -0.315 | -0.677 |
| FW KURTOSIS MICRON | 2.210 | 1.877 | 1.481 | 2.202 | 2.704 | 1.747 | 2.322 |
| FW MEAN PHI | 3.544 | 3.747 | 3.479 | 3.873 | 1.039 | 3.641 | 4.165 |
| FW SORTING PHI | 1.677 | 1.692 | 1.006 | 2.159 | 1.208 | 1.670 | 1.365 |
| FW SKEWNESS PHI | 0.307 | 0.363 | 0.176 | 0.209 | 0.377 | 0.315 | 0.677 |
| FW KURTOSIS PHI | 2.210 | 1.877 | 1.481 | 2.202 | 2.704 | 1.747 | 2.322 |
| FW MEAN | Very Fine Sand | Very Fine Sand | Very Fine Sand | Very Fine Sand | Medium Sand | Very Fine Sand | Very Coarse Silt |
| FW SORTING | Poorly Sorted | Poorly Sorted | Poorly Sorted | Very Poorly Sorted | Poorly Sorted | Poorly Sorted | Poorly Sorted |
| FW SKEWNESS | Very Fine Skewed | Very Fine Skewed | Fine Skewed | Fine Skewed | Very Fine Skewed | Very Fine Skewed | Very Fine Skewed |

| SAMPLE | 20171018 Sample 1 | 20171018 Sample 3 | 20171018 Sample 4 | 20171018 Sample 5 | 20171018 Sample 6 | 20171018 Sample 10 | 20171018 Sample 11 |
|---|---|---|---|---|---|---|---|
| FW KURTOSIS | Very Leptokurtic | Very Leptokurtic | Leptokurtic | Very Leptokurtic | Very Leptokurtic | Very Leptokurtic | Very Leptokurtic |
| MODE 1 MICRON | 152.5 | 94.00 | 94.00 | 94.00 | 605.0 | 94.00 | 94.00 |
| MODE 2 MICRON | | | | 19.00 | | 215.0 | |
| MODE 3 MICRON | | | | | | 19.00 | |
| MODE 1 PHI | 2.737 | 3.494 | 3.494 | 3.494 | 0.747 | 3.494 | 3.494 |
| MODE 2 PHI | | | | 5.736 | | 2.237 | |
| MODE 3 PHI | | | | | | 5.736 | |
| D10 MICRON | 16.32 | 12.21 | 37.00 | 9.347 | 66.23 | 15.75 | 8.698 |
| D50 MICRON | 104.3 | 92.02 | 91.12 | 90.22 | 503.8 | 96.54 | 79.33 |
| D90 MICRON | 242.9 | 218.9 | 176.4 | 246.5 | 892.7 | 249.8 | 117.3 |
| D90 Div D10 MICRON | 14.88 | 17.93 | 4.769 | 26.37 | 13.48 | 15.86 | 13.49 |
| D90 Sub D10 MICRON | 226.6 | 206.7 | 139.4 | 237.2 | 826.4 | 234.0 | 108.6 |
| D75 Div D25 MICRON | 2.454 | 2.677 | 2.118 | 3.237 | 1.802 | 2.625 | 1.822 |
| D75 Sub D25 MICRON | 93.69 | 90.81 | 70.46 | 100.3 | 300.9 | 102.7 | 45.70 |
| D10 PHI | 2.042 | 2.191 | 2.503 | 2.020 | 0.164 | 2.001 | 3.091 |
| D50 PHI | 3.261 | 3.442 | 3.456 | 3.470 | 0.989 | 3.373 | 3.656 |
| D90 PHI | 5.937 | 6.356 | 4.757 | 6.741 | 3.916 | 5.988 | 6.845 |
| D90 Div D10 PHI | 2.908 | 2.900 | 1.900 | 3.337 | 23.91 | 2.992 | 2.214 |
| D90 Sub D10 PHI | 3.896 | 4.164 | 2.254 | 4.721 | 3.753 | 3.987 | 3.754 |
| D75 Div D25 PHI | 1.487 | 1.510 | 1.373 | 1.609 | 2.505 | 1.537 | 1.262 |
| D75 Sub D25 PHI | 1.295 | 1.420 | 1.082 | 1.695 | 0.850 | 1.392 | 0.865 |
| PER GRAVEL | 0.0% | 0.0% | 0.0% | 0.0% | 0.0% | 0.0% | 0.0% |
| PER SAND | 76.3% | 73.0% | 75.4% | 69.7% | 90.2% | 75.3% | 73.6% |
| PER MUD | 23.7% | 27.0% | 24.6% | 30.3% | 9.8% | 24.7% | 26.4% |
| PER V COARSE GRAVEL | 0.0% | 0.0% | 0.0% | 0.0% | 0.0% | 0.0% | 0.0% |
| PER COARSE GRAVEL | 0.0% | 0.0% | 0.0% | 0.0% | 0.0% | 0.0% | 0.0% |
| PER MEDIUM GRAVEL | 0.0% | 0.0% | 0.0% | 0.0% | 0.0% | 0.0% | 0.0% |
| PER FINE GRAVEL | 0.0% | 0.0% | 0.0% | 0.0% | 0.0% | 0.0% | 0.0% |
| PER V FINE GRAVEL | 0.0% | 0.0% | 0.0% | 0.0% | 0.0% | 0.0% | 0.0% |
| PER V COARSE SAND | 3.4% | 3.0% | 1.3% | 5.7% | 4.6% | 0.6% | 0.3% |
| PER COARSE SAND | 2.3% | 1.1% | 0.8% | 0.9% | 46.0% | 1.7% | 0.4% |
| PER MEDIUM SAND | 3.7% | 2.2% | 1.6% | 3.3% | 36.7% | 7.6% | 0.6% |
| PER FINE SAND | 31.2% | 25.2% | 24.7% | 22.4% | 1.2% | 24.8% | 2.3% |
| PER V FINE SAND | 35.7% | 41.6% | 46.8% | 37.5% | 1.6% | 40.5% | 70.1% |
| PER V COARSE SILT | 8.2% | 8.6% | 16.0% | 10.2% | 3.2% | 6.0% | 6.3% |
| PER COARSE SILT | 5.8% | 7.3% | 3.6% | 7.3% | 2.9% | 8.8% | 6.3% |
| PER MEDIUM SILT | 2.8% | 3.0% | 1.4% | 3.8% | 1.5% | 3.8% | 4.5% |
| PER FINE SILT | 2.8% | 3.0% | 1.4% | 3.6% | 0.8% | 2.7% | 4.6% |
| PER V FINE SILT | 2.2% | 2.6% | 1.5% | 2.8% | 0.6% | 2.1% | 3.7% |
| PER CLAY | 2.0% | 2.5% | 0.6% | 2.6% | 0.8% | 1.4% | 1.0% |

| SAMPLE | 20171019 Sample 12 | 20171207 North | 20171207 Center A | 20171207 SA | 20180306 Site 1 | 20180306 Site 2 | 20180306 Site 3 |
|---|---|---|---|---|---|---|---|
| LAT | 38.87603333 | 38.875732 | 38.875513 | 38.8753 | 38.88611667 | 38.8729 | 38.87625 |
| LON | -75.21398333 | -75.213027 | -75.21305 | -75.213024 | -75.21215 | -75.22561667 | -75.21258333 |
| SIEVING ERROR | 1.4% | -6.6% | 4.6% | -1.5% | 0.6% | 2.5% | 1.5% |
| SAMPLE TYPE | Bimodal, Very Poorly Sorted | Bimodal, Very Poorly Sorted | Bimodal, Poorly Sorted | Bimodal, Very Poorly Sorted | Trimodal, Very Poorly Sorted | Unimodal, Poorly Sorted | Bimodal, Poorly Sorted |
| TEXTURAL GROUP | Muddy Sand | Muddy Sand | Muddy Sand | Muddy Sand | Muddy Sand | Sandy Mud | Muddy Sand |
| SEDIMENT NAME | Very Coarse Silty Medium Sand | Very Coarse Silty Coarse Sand | Very Coarse Silty Very Fine Sand | Coarse Silty Coarse Sand | Very Coarse Silty Medium Sand | Very Fine Sandy Very Coarse Silt | Very Coarse Silty Very Fine Sand |
| ARITH MEAN MICRON | 195.1 | 357.9 | 125.7 | 362.5 | 285.1 | 44.97 | 82.95 |
| ARITH SORTING MICRON | 187.0 | 271.0 | 201.3 | 270.9 | 299.1 | 69.63 | 106.1 |
| ARITH SKEWNESS MICRON | 2.576 | 0.085 | 4.542 | 0.054 | 1.786 | 10.21 | 8.977 |
| ARITH KURTOSIS MICRON | 17.41 | 2.384 | 27.35 | 2.405 | 7.437 | 158.1 | 109.8 |
| GEOM MEAN MICRON | 90.48 | 153.7 | 59.10 | 156.3 | 119.4 | 24.64 | 49.40 |
| GEOM SORTING MICRON | 4.958 | 6.123 | 3.841 | 6.148 | 5.312 | 3.259 | 3.261 |
| GEOM SKEWNESS MICRON | -1.092 | -1.195 | -0.905 | -1.218 | -0.955 | -0.664 | -1.403 |
| GEOM KURTOSIS MICRON | 3.333 | 3.266 | 4.362 | 3.339 | 3.231 | 3.091 | 4.883 |
| LOG MEAN PHI | 3.430 | 2.673 | 4.036 | 2.648 | 2.924 | 5.343 | 4.321 |
| LOG SORTING PHI | 2.285 | 2.589 | 1.920 | 2.594 | 2.289 | 1.705 | 1.698 |
| LOG SKEWNESS PHI | 1.078 | 1.197 | 0.834 | 1.220 | 0.875 | 0.664 | 1.355 |
| LOG KURTOSIS PHI | 3.325 | 3.273 | 4.330 | 3.350 | 3.027 | 3.091 | 4.879 |
| FW MEAN MICRON | 114.8 | 171.6 | 59.21 | 173.2 | 145.4 | 24.31 | 53.28 |
| FW SORTING MICRON | 4.290 | 5.392 | 3.553 | 5.524 | 4.799 | 3.297 | 2.866 |
| FW SKEWNESS MICRON | -0.837 | -0.725 | -0.360 | -0.761 | -0.455 | -0.352 | -0.599 |
| FW KURTOSIS MICRON | 0.978 | 0.930 | 1.950 | 0.936 | 1.003 | 1.129 | 1.524 |
| FW MEAN PHI | 3.123 | 2.543 | 4.078 | 2.530 | 2.782 | 5.362 | 4.230 |
| FW SORTING PHI | 2.101 | 2.431 | 1.829 | 2.466 | 2.263 | 1.721 | 1.519 |
| FW SKEWNESS PHI | 0.837 | 0.725 | 0.360 | 0.761 | 0.455 | 0.352 | 0.599 |
| FW KURTOSIS PHI | 0.978 | 0.930 | 1.950 | 0.936 | 1.003 | 1.129 | 1.524 |
| FW MEAN | Very Fine Sand | Fine Sand | Very Coarse Silt | Fine Sand | Fine Sand | Coarse Silt | Very Coarse Silt |
| FW SORTING | Very Poorly Sorted | Very Poorly Sorted | Poorly Sorted | Very Poorly Sorted | Very Poorly Sorted | Poorly Sorted | Poorly Sorted |
| FW SKEWNESS | Very Fine Skewed | Very Fine Skewed | Very Fine Skewed | Very Fine Skewed | Very Fine Skewed | Very Fine Skewed | Very Fine Skewed |

| SAMPLE | 20171019 Sample 12 | 20171207 North | 20171207 Center A | 20171207 SA | 20180306 Site 1 | 20180306 Site 2 | 20180306 Site 3 |
|---|---|---|---|---|---|---|---|
| FW KURTOSIS | Mesokurtic | Mesokurtic | Very Leptokurtic | Mesokurtic | Mesokurtic | Leptokurtic | Very Leptokurtic |
| MODE 1 MICRON | 302.5 | 605.0 | 94.00 | 605.0 | 427.5 | 54.00 | 94.00 |
| MODE 2 MICRON | 94.00 | 302.5 | 19.00 | 302.5 | 94.00 | | 19.00 |
| MODE 3 MICRON | | | | | 19.00 | | |
| MODE 1 PHI | 1.747 | 0.747 | 3.494 | 0.747 | 1.247 | 4.231 | 3.494 |
| MODE 2 PHI | 3.494 | 1.747 | 5.736 | 1.747 | 3.494 | | 5.736 |
| MODE 3 PHI | | | | | 5.736 | | |
| D10 MICRON | 7.273 | 7.896 | 8.703 | 9.856 | 12.25 | 3.608 | 7.912 |
| D50 MICRON | 250.6 | 369.2 | 80.14 | 395.3 | 226.8 | 31.94 | 74.57 |
| D90 MICRON | 341.3 | 666.8 | 225.9 | 667.6 | 655.2 | 89.75 | 120.5 |
| D90 Div D10 MICRON | 46.93 | 84.44 | 25.95 | 67.74 | 53.50 | 24.88 | 15.24 |
| D90 Sub D10 MICRON | 334.0 | 658.9 | 217.2 | 657.8 | 643.0 | 86.14 | 112.6 |
| D75 Div D25 MICRON | 7.733 | 11.45 | 2.929 | 11.69 | 8.542 | 4.075 | 2.883 |
| D75 Sub D25 MICRON | 264.7 | 540.5 | 74.34 | 543.3 | 393.6 | 42.53 | 65.75 |
| D10 PHI | 1.551 | 0.585 | 2.146 | 0.583 | 0.610 | 3.478 | 3.052 |
| D50 PHI | 1.996 | 1.437 | 3.641 | 1.339 | 2.140 | 4.969 | 3.745 |
| D90 PHI | 7.103 | 6.985 | 6.844 | 6.665 | 6.351 | 8.115 | 6.982 |
| D90 Div D10 PHI | 4.580 | 11.95 | 3.189 | 11.43 | 10.41 | 2.333 | 2.287 |
| D90 Sub D10 PHI | 5.552 | 6.400 | 4.698 | 6.082 | 5.741 | 4.637 | 3.929 |
| D75 Div D25 PHI | 2.718 | 5.653 | 1.493 | 5.722 | 3.655 | 1.488 | 1.461 |
| D75 Sub D25 PHI | 2.951 | 3.517 | 1.550 | 3.547 | 3.095 | 2.027 | 1.527 |
| PER GRAVEL | 0.0% | 0.0% | 0.0% | 0.0% | 0.0% | 0.0% | 0.0% |
| PER SAND | 69.1% | 72.1% | 67.7% | 72.5% | 72.1% | 19.7% | 64.2% |
| PER MUD | 30.9% | 27.9% | 32.3% | 27.5% | 27.9% | 80.3% | 35.8% |
| PER V COARSE GRAVEL | 0.0% | 0.0% | 0.0% | 0.0% | 0.0% | 0.0% | 0.0% |
| PER COARSE GRAVEL | 0.0% | 0.0% | 0.0% | 0.0% | 0.0% | 0.0% | 0.0% |
| PER MEDIUM GRAVEL | 0.0% | 0.0% | 0.0% | 0.0% | 0.0% | 0.0% | 0.0% |
| PER FINE GRAVEL | 0.0% | 0.0% | 0.0% | 0.0% | 0.0% | 0.0% | 0.0% |
| PER V FINE GRAVEL | 0.0% | 0.0% | 0.0% | 0.0% | 0.0% | 0.0% | 0.0% |
| PER V COARSE SAND | 1.0% | 0.7% | 1.6% | 0.7% | 3.9% | 0.1% | 0.5% |
| PER COARSE SAND | 2.6% | 45.7% | 3.9% | 46.5% | 15.1% | 0.4% | 0.5% |
| PER MEDIUM SAND | 46.7% | 17.4% | 4.1% | 17.7% | 29.2% | 0.4% | 1.1% |
| PER FINE SAND | 0.7% | 0.4% | 8.0% | 0.4% | 7.6% | 0.4% | 4.8% |
| PER V FINE SAND | 18.1% | 7.9% | 50.1% | 7.2% | 16.4% | 18.3% | 57.2% |
| PER V COARSE SILT | 8.8% | 9.4% | 9.9% | 7.2% | 10.0% | 31.1% | 12.6% |
| PER COARSE SILT | 8.1% | 5.3% | 8.9% | 7.3% | 6.7% | 22.8% | 9.2% |
| PER MEDIUM SILT | 3.6% | 3.2% | 4.1% | 4.4% | 3.2% | 8.1% | 4.0% |
| PER FINE SILT | 3.5% | 3.1% | 3.6% | 2.2% | 4.0% | 7.5% | 3.3% |
| PER V FINE SILT | 3.5% | 3.7% | 2.6% | 2.2% | 3.1% | 7.3% | 4.0% |
| PER CLAY | 3.4% | 3.2% | 3.1% | 4.1% | 0.9% | 3.5% | 2.7% |

| SAMPLE | 20180306 Site 4 | 20180306 Site 5 | 20180828 Site 3 S1 | 20180828 Site 3 S2 | 20190515 Site 2 sa | 20190515 Site 5 sb | 20190515 Site 10sa |
|---|---|---|---|---|---|---|---|
| LAT | 38.87728333 | 38.86155 | 38.87131 | 38.87333 | 38.876029 | 38.87796333 | 38.872354 |
| LON | -75.202 | -75.19728333 | -75.22549 | -75.227 | -75.213983 | -75.20171683 | -75.22542967 |
| SIEVING ERROR | 3.8% | 0.1% | 1.4% | 1.1% | 1.8% | 2.4% | 3.1% |
| SAMPLE TYPE | Bimodal, Poorly Sorted | Unimodal, Poorly Sorted | Bimodal, Poorly Sorted | Trimodal, Very Poorly Sorted | Trimodal, Poorly Sorted | Bimodal, Poorly Sorted | Bimodal, Poorly Sorted |
| TEXTURAL GROUP | Muddy Sand | Muddy Sand | Sandy Mud | Muddy Sand | Muddy Sand | Muddy Sand | Sandy Mud |
| SEDIMENT NAME | Very Coarse Silty Very Fine Sand | Very Coarse Silty Medium Sand | Very Fine Sandy Very Coarse Silt | Very Coarse Silty Medium Sand | Coarse Silty Very Fine Sand | Very Coarse Silty Very Fine Sand | Very Fine Sandy Very Coarse Silt |
| ARITH MEAN MICRON | 146.5 | 348.8 | 69.66 | 382.8 | 83.50 | 84.59 | 41.85 |
| ARITH SORTING MICRON | 269.9 | 226.9 | 98.34 | 405.9 | 111.8 | 118.3 | 46.63 |
| ARITH SKEWNESS MICRON | 3.821 | 0.995 | 8.222 | 1.570 | 8.214 | 8.063 | 9.249 |
| ARITH KURTOSIS MICRON | 18.05 | 7.163 | 104.5 | 4.910 | 94.22 | 87.97 | 200.1 |
| GEOM MEAN MICRON | 56.39 | 203.4 | 39.35 | 145.1 | 46.79 | 47.12 | 25.57 |
| GEOM SORTING MICRON | 4.326 | 4.361 | 3.208 | 6.832 | 3.429 | 3.457 | 2.955 |
| GEOM SKEWNESS MICRON | -0.612 | -1.836 | -0.929 | -1.314 | -1.136 | -1.222 | -0.791 |
| GEOM KURTOSIS MICRON | 3.845 | 5.488 | 4.234 | 3.975 | 3.956 | 4.460 | 3.383 |
| LOG MEAN PHI | 4.009 | 2.298 | 4.668 | 2.157 | 4.398 | 4.322 | 5.290 |
| LOG SORTING PHI | 2.053 | 2.125 | 1.682 | 2.128 | 1.771 | 1.760 | 1.563 |
| LOG SKEWNESS PHI | 0.439 | 1.836 | 0.929 | 1.253 | 1.089 | 1.026 | 0.791 |
| LOG KURTOSIS PHI | 3.741 | 5.488 | 4.234 | 4.408 | 3.947 | 4.438 | 3.383 |
| FW MEAN MICRON | 55.75 | 200.1 | 43.36 | 261.2 | 50.35 | 51.13 | 26.71 |
| FW SORTING MICRON | 3.801 | 3.815 | 3.036 | 4.361 | 3.016 | 3.007 | 2.953 |
| FW SKEWNESS MICRON | -0.326 | -0.728 | -0.279 | -0.292 | -0.590 | -0.552 | -0.272 |
| FW KURTOSIS MICRON | 1.875 | 3.457 | 1.317 | 1.321 | 1.218 | 1.353 | 1.195 |
| FW MEAN PHI | 4.165 | 2.321 | 4.528 | 1.937 | 4.312 | 4.290 | 5.226 |
| FW SORTING PHI | 1.926 | 1.932 | 1.602 | 2.125 | 1.593 | 1.588 | 1.562 |
| FW SKEWNESS PHI | 0.326 | 0.728 | 0.279 | 0.292 | 0.590 | 0.552 | 0.272 |
| FW KURTOSIS PHI | 1.875 | 3.457 | 1.317 | 1.321 | 1.218 | 1.353 | 1.195 |
| FW MEAN | Very Coarse Silt | Fine Sand | Very Coarse Silt | Medium Sand | Very Coarse Silt | Very Coarse Silt | Coarse Silt |
| FW SORTING | Poorly Sorted | Poorly Sorted | Poorly Sorted | Very Poorly Sorted | Poorly Sorted | Poorly Sorted | Poorly Sorted |
| FW SKEWNESS | Very Fine Skewed | Very Fine Skewed | Fine Skewed | Fine Skewed | Very Fine Skewed | Very Fine Skewed | Fine Skewed |

| SAMPLE | 20180306 Site 4 | 20180306 Site 5 | 20180828 Site 3 S1 | 20180828 Site 3 S2 | 20190515 Site 2 sa | 20190515 Site 5 sb | 20190515 Site 10sa |
|---|---|---|---|---|---|---|---|
| FW KURTOSIS | Very Leptokurtic | Extremely Leptokurtic | Leptokurtic | Leptokurtic | Leptokurtic | Leptokurtic | Leptokurtic |
| MODE 1 MICRON | 94.00 | 427.5 | 94.00 | 427.5 | 94.00 | 94.00 | 54.00 |
| MODE 2 MICRON | 27.00 | | 215.0 | 38.50 | 19.00 | 27.00 | 19.00 |
| MODE 3 MICRON | | | | 19.00 | 38.50 | | |
| MODE 1 PHI | 3.494 | 1.247 | 3.494 | 1.247 | 3.494 | 3.494 | 4.231 |
| MODE 2 PHI | 5.236 | | 2.237 | 4.720 | 5.736 | 5.236 | 5.736 |
| MODE 3 PHI | | | | 5.736 | 4.720 | | |
| D10 MICRON | 7.116 | 19.24 | 9.002 | 26.15 | 5.826 | 7.942 | 5.095 |
| D50 MICRON | 78.63 | 357.6 | 48.87 | 320.6 | 74.20 | 73.44 | 30.93 |
| D90 MICRON | 399.7 | 589.9 | 119.2 | 1453.0 | 121.2 | 123.2 | 88.35 |
| D90 Div D10 MICRON | 56.17 | 30.66 | 13.24 | 55.57 | 20.80 | 15.51 | 17.34 |
| D90 Sub D10 MICRON | 392.6 | 570.6 | 110.2 | 1426.9 | 115.4 | 115.3 | 83.25 |
| D75 Div D25 MICRON | 3.328 | 1.786 | 3.739 | 5.090 | 3.831 | 3.381 | 3.570 |
| D75 Sub D25 MICRON | 77.52 | 199.9 | 62.51 | 494.5 | 74.51 | 71.46 | 40.05 |
| D10 PHI | 1.323 | 0.761 | 3.069 | -0.539 | 3.045 | 3.021 | 3.501 |
| D50 PHI | 3.669 | 1.484 | 4.355 | 1.641 | 3.752 | 3.767 | 5.015 |
| D90 PHI | 7.135 | 5.700 | 6.796 | 5.257 | 7.423 | 6.976 | 7.617 |
| D90 Div D10 PHI | 5.393 | 7.485 | 2.214 | -9.752 | 2.438 | 2.309 | 2.176 |
| D90 Sub D10 PHI | 5.812 | 4.938 | 3.727 | 5.796 | 4.379 | 3.955 | 4.116 |
| D75 Div D25 PHI | 1.547 | 1.735 | 1.536 | 4.353 | 1.585 | 1.532 | 1.440 |
| D75 Sub D25 PHI | 1.734 | 0.836 | 1.903 | 2.348 | 1.938 | 1.758 | 1.836 |
| PER GRAVEL | 0.0% | 0.0% | 0.0% | 0.0% | 0.0% | 0.0% | 0.0% |
| PER SAND | 66.3% | 82.1% | 39.0% | 83.8% | 63.5% | 62.0% | 19.3% |
| PER MUD | 33.7% | 17.9% | 61.0% | 16.2% | 36.5% | 38.0% | 80.7% |
| PER V COARSE GRAVEL | 0.0% | 0.0% | 0.0% | 0.0% | 0.0% | 0.0% | 0.0% |
| PER COARSE GRAVEL | 0.0% | 0.0% | 0.0% | 0.0% | 0.0% | 0.0% | 0.0% |
| PER MEDIUM GRAVEL | 0.0% | 0.0% | 0.0% | 0.0% | 0.0% | 0.0% | 0.0% |
| PER FINE GRAVEL | 0.0% | 0.0% | 0.0% | 0.0% | 0.0% | 0.0% | 0.0% |
| PER V FINE GRAVEL | 0.0% | 0.0% | 0.0% | 0.0% | 0.0% | 0.0% | 0.0% |
| PER V COARSE SAND | 4.1% | 0.8% | 0.2% | 14.3% | 0.5% | 1.3% | 0.0% |
| PER COARSE SAND | 4.4% | 14.2% | 0.5% | 16.8% | 0.6% | 0.7% | 0.1% |
| PER MEDIUM SAND | 3.6% | 61.3% | 1.8% | 27.3% | 1.7% | 1.5% | 0.3% |
| PER FINE SAND | 4.2% | 2.4% | 5.4% | 16.1% | 4.7% | 5.4% | 0.4% |
| PER V FINE SAND | 50.0% | 3.3% | 31.1% | 9.2% | 56.0% | 53.1% | 18.4% |
| PER V COARSE SILT | 9.6% | 4.6% | 27.5% | 5.0% | 9.5% | 12.3% | 30.4% |
| PER COARSE SILT | 9.1% | 4.5% | 17.7% | 4.7% | 10.9% | 9.9% | 25.3% |
| PER MEDIUM SILT | 4.4% | 2.2% | 7.0% | 1.9% | 3.7% | 5.9% | 10.7% |
| PER FINE SILT | 5.1% | 2.9% | 1.5% | 2.0% | 5.7% | 4.0% | 6.9% |
| PER V FINE SILT | 3.4% | 2.1% | 4.1% | 1.7% | 4.8% | 3.2% | 4.1% |
| PER CLAY | 2.2% | 1.7% | 3.1% | 0.9% | 2.0% | 2.7% | 3.3% |

| SAMPLE | 20190515 Site 7 sa | 20190514 Site 13 sa | 20190514 Site 16 sa | 20190515 Site 18 sa | 20190515 Site 19 sb | 20190515 Site 20 sa |
|---|---|---|---|---|---|---|
| LAT | 38.874388 | 38.87428067 | 38.88252052 | 38.87094757 | 38.88265632 | 38.87164263 |
| LON | -75.22097133 | -75.22566067 | -75.22361227 | -75.20146883 | -75.20386603 | -75.20937352 |
| SIEVING ERROR | 3.1% | 0.7% | -0.2% | 3.6% | 2.8% | 0.8% |
| SAMPLE TYPE | Bimodal, Poorly Sorted | Trimodal, Poorly Sorted | Unimodal, Poorly Sorted | Bimodal, Poorly Sorted | Polymodal, Very Poorly Sorted | Bimodal, Poorly Sorted |
| TEXTURAL GROUP | Muddy Sand | Sandy Mud | Muddy Sand | Muddy Sand | Muddy Sand | Sandy Mud |
| SEDIMENT NAME | Very Coarse Silty Very Fine Sand | Very Fine Sandy Very Coarse Silt | Very Coarse Silty Medium Sand | Very Coarse Silty Very Fine Sand | Very Coarse Silty Very Fine Sand | Very Fine Sandy Very Coarse Silt |
| ARITH MEAN MICRON | 90.72 | 43.52 | 288.6 | 101.2 | 156.9 | 104.3 |
| ARITH SORTING MICRON | 143.9 | 45.42 | 169.8 | 182.3 | 265.9 | 192.7 |
| ARITH SKEWNESS MICRON | 6.525 | 11.03 | 0.247 | 5.170 | 3.728 | 5.173 |
| ARITH KURTOSIS MICRON | 57.02 | 299.6 | 4.648 | 34.73 | 18.02 | 34.39 |
| GEOM MEAN MICRON | 45.63 | 25.10 | 178.6 | 44.44 | 58.47 | 43.63 |
| GEOM SORTING MICRON | 3.670 | 3.317 | 3.967 | 3.886 | 4.809 | 4.035 |
| GEOM SKEWNESS MICRON | -0.946 | -0.828 | -1.909 | -0.621 | -0.636 | -0.521 |
| GEOM KURTOSIS MICRON | 4.014 | 2.779 | 5.775 | 3.645 | 3.278 | 3.434 |
| LOG MEAN PHI | 4.357 | 5.316 | 2.486 | 4.444 | 3.942 | 4.424 |
| LOG SORTING PHI | 1.846 | 1.730 | 1.988 | 1.946 | 2.199 | 1.988 |
| LOG SKEWNESS PHI | 0.756 | 0.828 | 1.909 | 0.541 | 0.511 | 0.377 |
| LOG KURTOSIS PHI | 3.981 | 2.779 | 5.775 | 3.626 | 3.208 | 3.380 |
| FW MEAN MICRON | 50.30 | 25.00 | 185.3 | 44.94 | 66.74 | 45.48 |
| FW SORTING MICRON | 3.241 | 3.450 | 3.503 | 3.736 | 4.618 | 3.842 |
| FW SKEWNESS MICRON | -0.441 | -0.407 | -0.679 | -0.380 | -0.208 | -0.272 |
| FW KURTOSIS MICRON | 1.360 | 1.058 | 2.675 | 1.411 | 1.451 | 1.308 |
| FW MEAN PHI | 4.313 | 5.322 | 2.432 | 4.476 | 3.905 | 4.459 |
| FW SORTING PHI | 1.697 | 1.787 | 1.809 | 1.902 | 2.207 | 1.942 |
| FW SKEWNESS PHI | 0.441 | 0.407 | 0.679 | 0.380 | 0.208 | 0.272 |
| FW KURTOSIS PHI | 1.360 | 1.058 | 2.675 | 1.411 | 1.451 | 1.308 |
| FW MEAN | Very Coarse Silt | Coarse Silt | Fine Sand | Very Coarse Silt | Very Fine Sand | Very Coarse Silt |
| FW SORTING | Poorly Sorted | Poorly Sorted | Poorly Sorted | Poorly Sorted | Very Poorly Sorted | Poorly Sorted |
| FW SKEWNESS | Very Fine Skewed | Very Fine Skewed | Very Fine Skewed | Very Fine Skewed | Fine Skewed | Fine Skewed |

| SAMPLE | 20190515 Site 7 sa | 20190514 Site 13 sa | 20190514 Site 16 sa | 20190515 Site 18 sa | 20190515 Site 19 sb | 20190515 Site 20 sa |
|---|---|---|---|---|---|---|
| FW KURTOSIS | Leptokurtic | Mesokurtic | Very Leptokurtic | Leptokurtic | Leptokurtic | Leptokurtic |
| MODE 1 MICRON | 94.00 | 54.00 | 302.5 | 94.00 | 94.00 | 94.00 |
| MODE 2 MICRON | 19.00 | 19.00 | | 19.00 | 38.50 | 6.000 |
| MODE 3 MICRON | | 3.000 | | | 19.00 | |
| MODE 1 PHI | 3.494 | 4.231 | 1.747 | 3.494 | 3.494 | 3.494 |
| MODE 2 PHI | 5.736 | 5.736 | | 5.736 | 4.720 | 7.466 |
| MODE 3 PHI | | 8.466 | | | 5.736 | |
| D10 MICRON | 6.703 | 3.361 | 20.49 | 5.746 | 6.232 | 6.009 |
| D50 MICRON | 70.28 | 35.19 | 293.8 | 65.69 | 81.76 | 60.28 |
| D90 MICRON | 135.5 | 93.13 | 478.3 | 132.0 | 410.0 | 188.2 |
| D90 Div D10 MICRON | 20.21 | 27.71 | 23.34 | 22.97 | 65.78 | 31.32 |
| D90 Sub D10 MICRON | 128.7 | 89.77 | 457.8 | 126.2 | 403.7 | 182.2 |
| D75 Div D25 MICRON | 3.832 | 4.524 | 2.032 | 4.274 | 4.944 | 4.696 |
| D75 Sub D25 MICRON | 74.97 | 46.78 | 201.8 | 75.46 | 124.7 | 82.50 |
| D10 PHI | 2.884 | 3.425 | 1.064 | 2.922 | 1.286 | 2.410 |
| D50 PHI | 3.831 | 4.829 | 1.767 | 3.928 | 3.612 | 4.052 |
| D90 PHI | 7.221 | 8.217 | 5.609 | 7.443 | 7.326 | 7.379 |
| D90 Div D10 PHI | 2.504 | 2.399 | 5.272 | 2.548 | 5.695 | 3.062 |
| D90 Sub D10 PHI | 4.337 | 4.792 | 4.545 | 4.521 | 6.040 | 4.969 |
| D75 Div D25 PHI | 1.587 | 1.537 | 1.768 | 1.627 | 1.861 | 1.686 |
| D75 Sub D25 PHI | 1.938 | 2.178 | 1.023 | 2.096 | 2.306 | 2.232 |
| PER GRAVEL | 0.0% | 0.0% | 0.0% | 0.0% | 0.0% | 0.0% |
| PER SAND | 57.6% | 22.8% | 82.2% | 52.8% | 61.0% | 49.0% |
| PER MUD | 42.4% | 77.2% | 17.8% | 47.2% | 39.0% | 51.0% |
| PER V COARSE GRAVEL | 0.0% | 0.0% | 0.0% | 0.0% | 0.0% | 0.0% |
| PER COARSE GRAVEL | 0.0% | 0.0% | 0.0% | 0.0% | 0.0% | 0.0% |
| PER MEDIUM GRAVEL | 0.0% | 0.0% | 0.0% | 0.0% | 0.0% | 0.0% |
| PER FINE GRAVEL | 0.0% | 0.0% | 0.0% | 0.0% | 0.0% | 0.0% |
| PER V FINE GRAVEL | 0.0% | 0.0% | 0.0% | 0.0% | 0.0% | 0.0% |
| PER V COARSE SAND | 1.5% | 0.0% | 0.1% | 1.4% | 4.2% | 2.1% |
| PER COARSE SAND | 1.4% | 0.1% | 6.3% | 2.8% | 3.6% | 2.1% |
| PER MEDIUM SAND | 2.5% | 0.1% | 57.1% | 2.8% | 6.9% | 3.8% |
| PER FINE SAND | 5.4% | 0.5% | 16.2% | 3.4% | 17.7% | 8.8% |
| PER V FINE SAND | 46.8% | 22.1% | 2.5% | 42.5% | 28.7% | 32.2% |
| PER V COARSE SILT | 14.8% | 31.4% | 5.0% | 17.0% | 14.1% | 18.3% |
| PER COARSE SILT | 11.5% | 19.1% | 4.0% | 12.3% | 8.9% | 14.5% |
| PER MEDIUM SILT | 4.8% | 7.5% | 2.2% | 5.3% | 4.7% | 5.7% |
| PER FINE SILT | 5.3% | 7.4% | 2.8% | 5.9% | 3.9% | 6.4% |
| PER V FINE SILT | 3.3% | 8.2% | 2.6% | 3.9% | 5.0% | 3.5% |
| PER CLAY | 2.6% | 3.6% | 1.1% | 2.8% | 2.4% | 2.5% |

In addition to sediment grain size analysis, 30-cm short-cores were collected at four separate locations using a HAPS corer (Figure A.1). Two cores were collected at each location. The first core was subjected to shear vane analysis immediately after collection. A standard 5 cm spade was used for the shear vane analysis. Measurements were collected in 5 cm vertical sections. Each 5 cm section was divided into four quadrants, and each quadrant measured using a calibrated shear vane. The average of the four measurements was used to estimate shear strength for each 5 cm section (Table A.6).

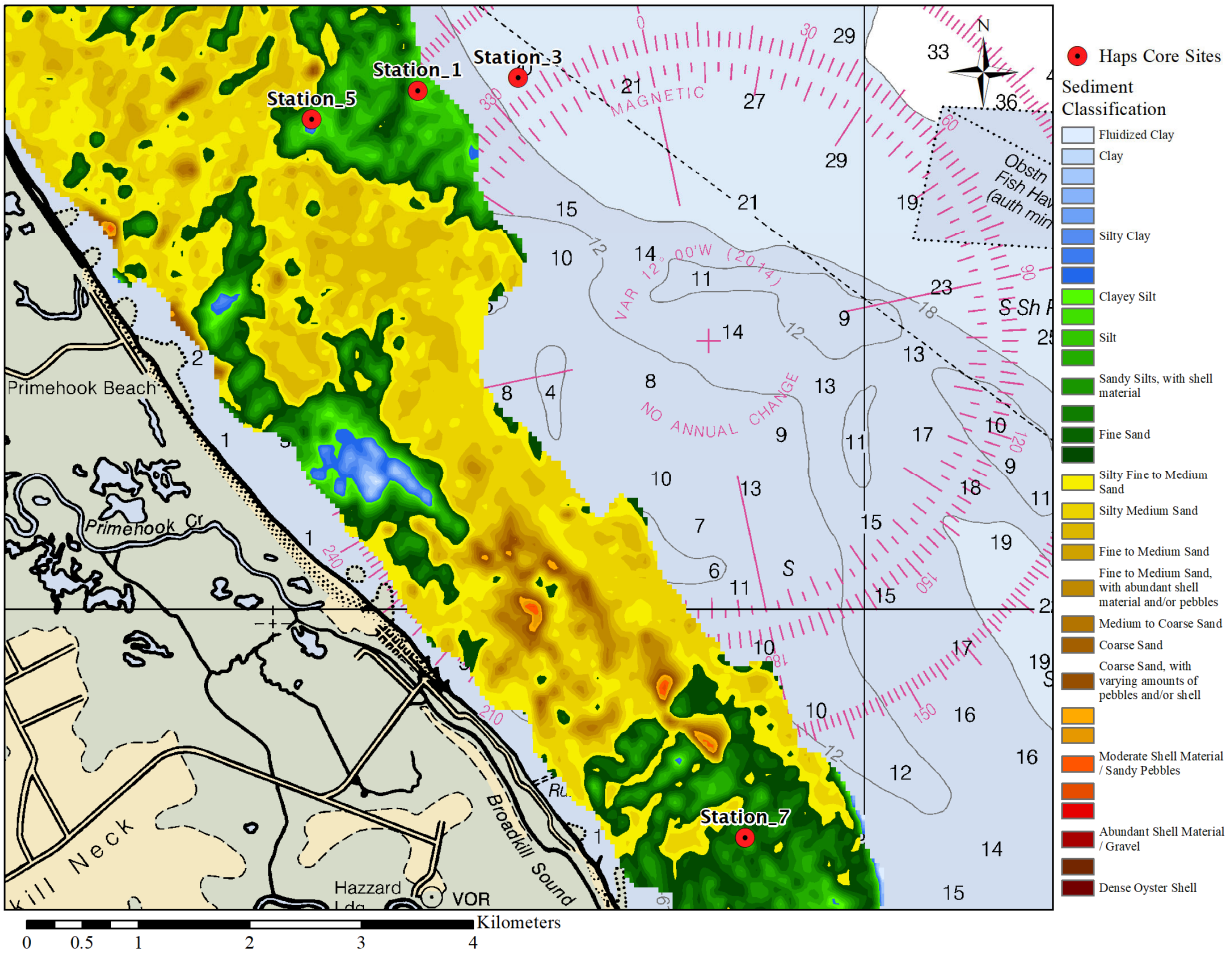



*Figure A.1: Locations for HAPS core samples collected in July 2018.*

*Table A.6: Shear-vane measurements for HAPS core samples collected in July 2018.*

| HAPS Core Shear Vane Analysis | | | | | | | |
|---|---|---|---|---|---|---|---|
| (Avg. kPA of 4 measurements per 5cm bin) | | | | | | | |
| *Core Site* | *0-5cm* | *5-10cm* | *10-15cm* | *15-20cm* | *20-25cm* | *25-30cm* | *Description* |
| *Station1* | 8.25 | 42.25 | 41.75 | NA | NA | NA | soft muddy sand overlaying stiff muddy sand |
| *Station3* | 7.75 | 40 | 31.75 | 24 | NA | NA | soft muddy sand overlaying stiff muddy sand |
| *Station5* | 3.5 | 5.75 | 2.25 | 6.25 | 10 | 6.5 | soft sandy mud |
| *Station7* | 10.25 | 17.75 | 35.5 | 34 | NA | NA | soft muddy sand overlaying stiff muddy sand |

## A.3. Magnetometer Data

Magnetic measurements were collected using a custom designed magnetometer mounted to a Teledyne Gavia AUV. The Gavia AUV is a modular designed vehicle customizable to individual projects. Available sensor modules include a Marine Sonics high-resolution, dual-frequency 900/1800 kHz, a GeoAcoustics GeoSwath 500 kHz phase-measuring bathymetric sonar, 2 MP Point Grey Color Grasshopper Camera, and environmental sensors (e.g. salinity, temperature, dissolved oxygen, and turbidity). The Gavia AUV is navigated by a Kearfott T-24 "SEANAV" inertial navigation system (INS) coupled with an RD Instruments 1200 kilohertz (kHz) Workhorse Navigator Doppler velocity log (DVL). The Gavia has a depth rating of up to 500 meters, and in standard magnetometer configuration, can run for over 3.5 hours and cover up to 20 linear kilometers, with customizable mission shape and line spacing as narrow as 1m.

The AUV magnetometer module consists of a high sensitivity Geometrics G-880AUV cesium vapor magnetometer and Applied Physics 539 fluxgate compass. Total field magnetic measurements are recorded with time-stamped data logs that include position, altitude, heading, pitch, roll, and electrical current draw. Magnetic compensation software developed as part of ESTCP Project MR-201002 by Geometrics allows for the correction of local magnetic field distortions in the magnetometer signal from permanent and induced magnetization effect from the vehicle (Steigerwalt et al., 2014).

Data was collected and processed using Geometrics MagPick 2000 and MagComp software. Compensated data was imported into ESRI ArcGIS and interpolated surfaces were generated using a spline point-to-raster interpolant. The raster surfaces were geo-rectified to account for navigational drift of the AUV by using known targets visible in the sonar (e.g. VPS HR2 receiver poles) as navigational fiducials. Examples of the magnetic data are provided below (Figures A.2. and A.3). It was determined that the magnetic noise created by the HR2 receivers, instrument frame, and synctag reference posts reduced the performance of the magnetometer. Additionally, the vehicle could not survey closer than 2-m altitude above the seabed when these sensors were in place. When the sensors were removed, the AUV could be operated nearer to the bed (1.25 m altitude), and was found capable of detecting shallow buried 81mm surrogates (Figure A.3).

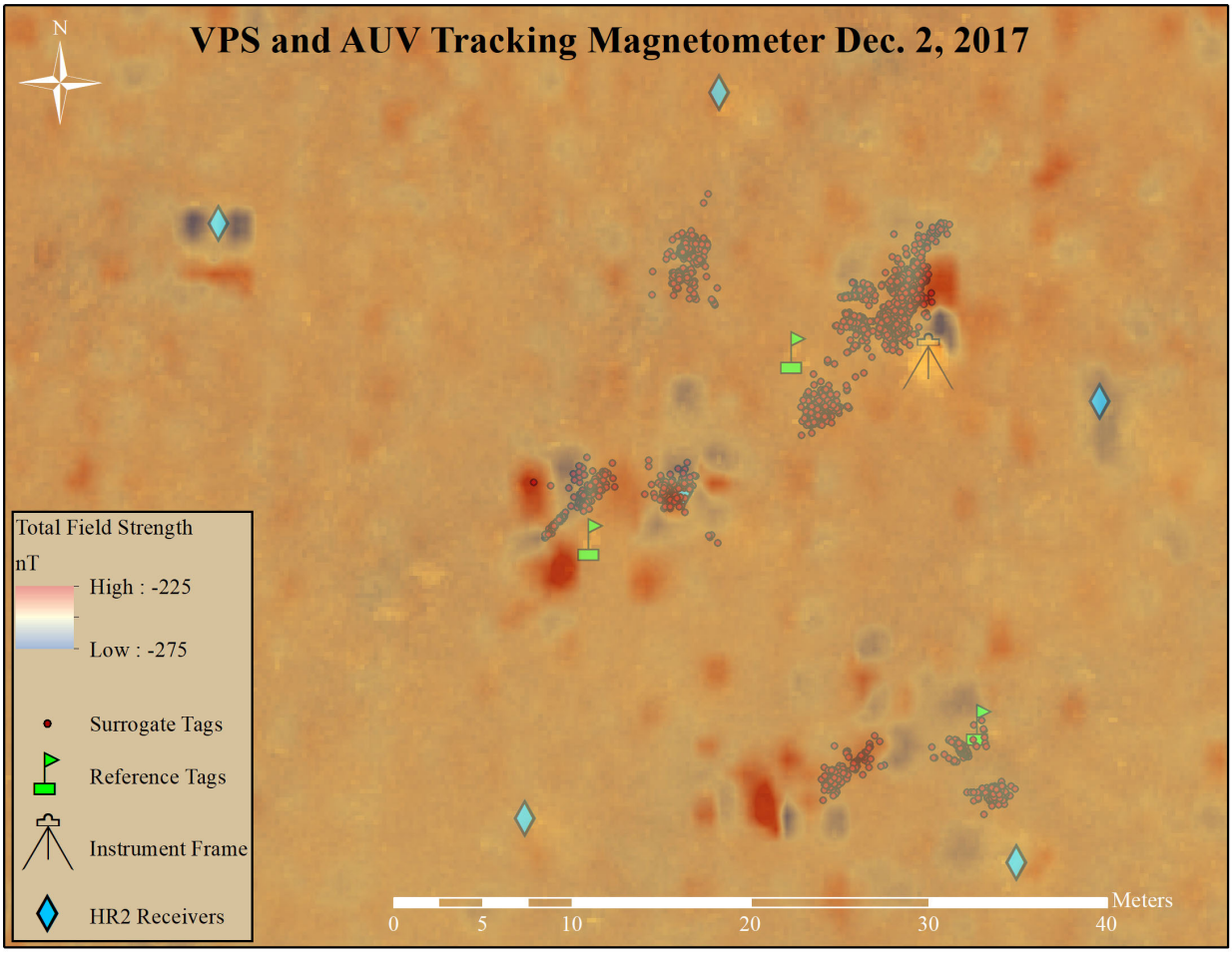



*Figure A.2: Gavia AUV magnetometer data overlaid on Vemco VPS estimated tag locations for Dec. 2, 2017. Note the noise introduced by the instrument frame, HR2 receivers, and synctag reference posts.*

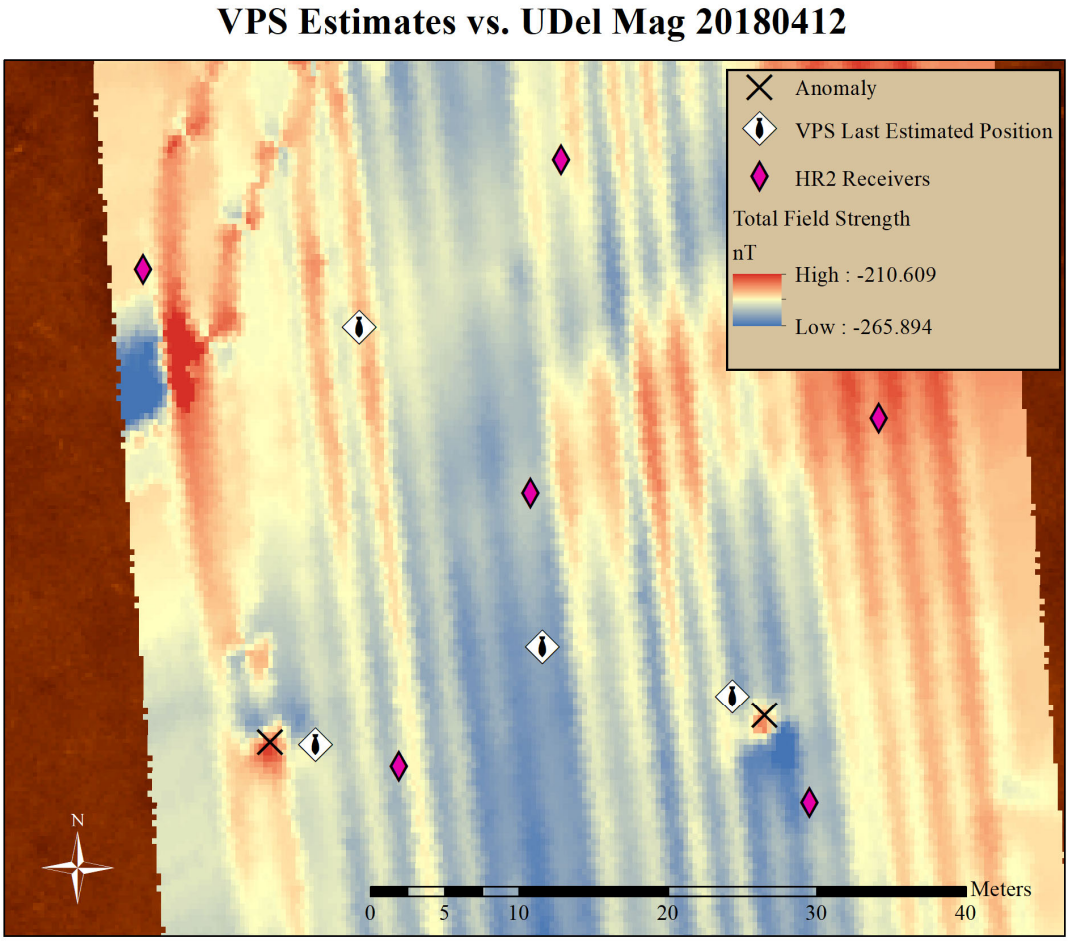



*Figure A.3: Interpolated surface of magnetic field measurements from Gavia AUV compared to last known positions for buried surrogates using VPS estimates on April 12, 2018. Note the two magnetic anomalies near surrogates in the south side of the array. These proved to be buried 81mm surrogates. The 60mm surrogates were not detectable by the magnetometer.*

# Appendix B

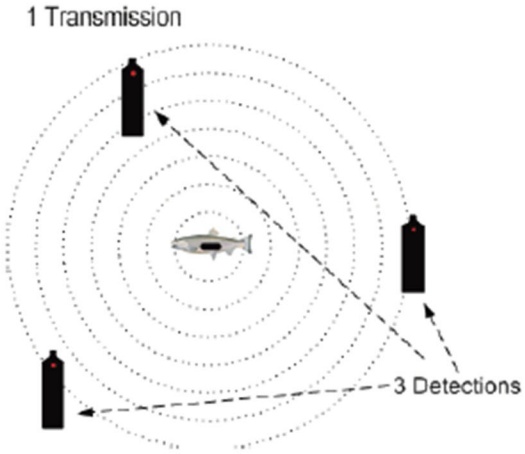
## B.1. Vemco VPS Data Sheets

vemco

# VEMCO Positioning System (VPS)

## A low cost, non-real-time underwater acoustic fine-scale positioning system





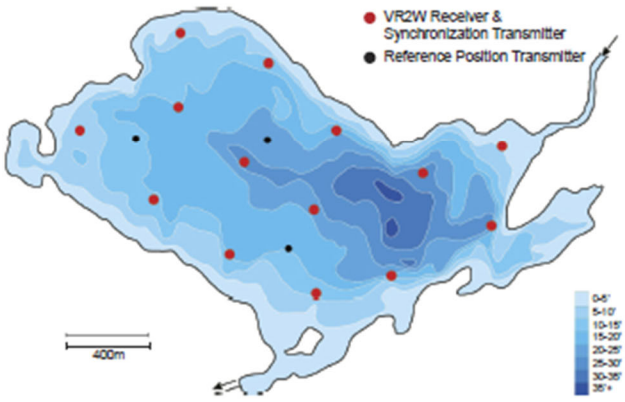

**The VEMCO Positioning System (VPS)** is a low cost, non-real-time underwater acoustic fine-scale positioning system, using the same off-the-shelf equipment used in conventional coded receiver-based studies.

The system consists of underwater acoustic transmitters and receivers that are deployed by you, and a receiver data processing service provided by VEMCO.

VEMCO will work with you to design a system layout in accordance with a set of design guidelines. You then deploy your system and collect receiver data periodically. Receiver positions can be measured using a handheld GPS unit.

On a periodic basis, you collect your receiver data, and send it to VEMCO for analysis. As a result of this analysis, VEMCO will provide interim calculated positions, and may recommend changes to the design of the system to address performance issues. At the end of the study, once all receiver data has been collected, VEMCO will provide a final report and calculated positions.

For most studies, VEMCO expects position accuracy similar to that provided by the GPS standard positioning service: 95% of positions within a 15-metre error circle. VEMCO considers this a conservative estimate, based on results from field studies conducted to date. Depending on the specifics of the study, significantly better accuracy is possible.







Tel: (902) 450-1700
Fax: (902) 450-1704

www.vemco.com

© 2013 AMIRIX Systems Inc. Information may change without notice.

## System Design Overview

Receivers are placed in a grid of triangles and squares. The objective is to ensure that every tag transmission is detected by at least 3 receivers (more is better). Ideally the area of interest is covered with enough receivers to ensure that animals are always inside of a triangle of receivers. Users will need to ensure that the receivers are placed close enough together to have greater than 100% overlap in detection range to account for worst case conditions.

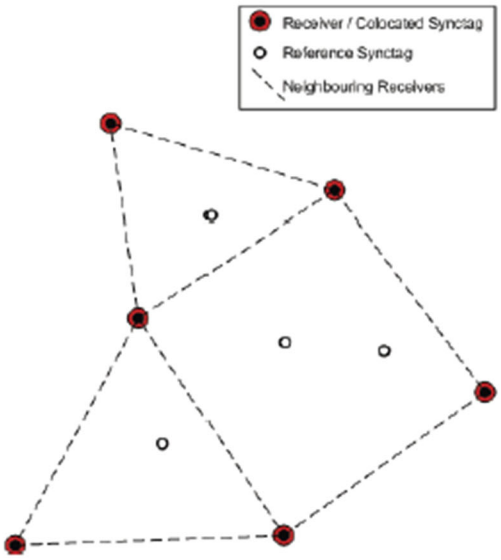
Synchronization tags, "Synctags", are moored along with each receiver to correct for clock drift between submerged receivers.

Additional reference tags are placed within the receiver grid in known measured locations to measure system performance.

Final positioning data will be provided to the user from VEMCO as shown in the Sample Output File below. **Output files can be imported to a variety of visualization tools!**

For your convenience, we also provide KMZ output files to enable you to quickly and easily visualize your position data in Google Earth.




**Principal Investigators: Jason McLellan / Matt Howell**
*Washington Department of Fish and Wildlife*
Funding provided by the Washington Department of Ecology and US Geological Survey

**Sample Output File**

| | A | B | C | D | E | F | G | H |
|---|---|---|---|---|---|---|---|---|
| 1 | TRANS | DETECTEDID | DATETIME | X | Y | D | LAT | LON |
| 2 | T01 | A69-9002-1335 | 2009-11-03 05:10 | 960.7 | 999.4 | 1.978 | 33.44486 | -118.48606 |
| 3 | T01 | A69-9002-1335 | 2009-11-03 05:32 | 916.8 | 991.1 | 1.758 | 33.44479 | -118.48653 |
| 4 | T01 | A69-9002-1335 | 2009-11-03 05:37 | 919.1 | 992.7 | 1.319 | 33.44480 | -118.48650 |
| 5 | T01 | A69-9002-1335 | 2009-11-03 05:46 | 918.2 | 993.0 | 1.319 | 33.44480 | -118.48651 |
| 6 | T01 | A69-9002-1335 | 2009-11-03 05:47 | 934.0 | 974.2 | 1.538 | 33.44463 | -118.48634 |
| 7 | T01 | A69-9002-1335 | 2009-11-03 06:05 | 915.8 | 989.1 | 1.099 | 33.44477 | -118.48654 |
| 8 | T01 | A69-9002-1335 | 2009-11-03 06:39 | 933.3 | 913.9 | 1.538 | 33.44409 | -118.48635 |
| 9 | T01 | A69-9002-1335 | 2009-11-03 06:45 | 939.4 | 944.2 | 0.879 | 33.44436 | -118.48628 |
| 10 | T01 | A69-9002-1335 | 2009-11-03 06:56 | 927.9 | 902.2 | 1.319 | 33.44399 | -118.48641 |

**For more information on VEMCO's VPS and to discuss your positioning study requirements, contact your VEMCO sales representative today!**

© 2013 AMIRIX Systems Inc. Information may change without notice.

# V9-180 kHz Coded Transmitters

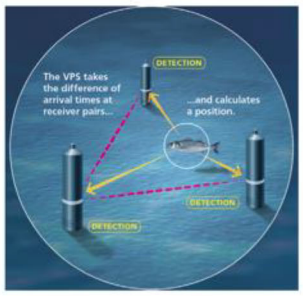
## Monitor predation, movement and positioning activity of larger animals for up to two years

Transmitters

The introduction of V9-180 kHz transmitters has expanded VEMCO's 180 kHz capability to include longer life tags that can be used on larger animals. 180 kHz tags have been used widely on a variety of fish species from salmon smolts to arctic cod to various reef species.








### Why 180 kHz Frequency?

The V9, operating at 180 kHz, is designed to work well in both fresh and salt water. Choosing this frequency enabled VEMCO to develop a small, lightweight tag that operates well in marine environments. Tags with operating frequencies greater than 200 kHz are less effective in salt water. Depending on the conditions of your location, the V9-180 kHz tag can reach 300 metres range.

### The V9-180 kHz Transmitter Allows You to:

- conduct long-term studies of predator movements for up to two years
- track a predator after it has just eaten a salmon smolt that was tagged with a V4 or V5
- monitor movements of non-native fish species to understand their impact on the ecosystem and its inhabitants

### 180 kHz Positioning Studies

If your research requires detailed movement data, the V9-180 kHz has flexible programming options that allows you to conduct long term positioning studies using our traditional VR2W-based VPS (VEMCO Positioning System).

Receivers | Transmitters | Accessories | Data Loggers

Tel: (902) 450-1700
Fax: (902) 450-1704

www.vemco.com



### Detect More Tags

The 180 kHz frequency also allows receivers to support up to three times more detections than 69 kHz in situations where a high volume of tags is present.

### Compatible with the VR2W-180kHz Receiver

The V9-180 kHz tag works with VEMCO's VR2W-180 kHz acoustic monitoring receiver and can also be detected by VEMCO's VR100 acoustic tracking receiver. A VH180 hydrophone is required for use with the VR100. The VR4-UWM, which is capable of long term deployments and communicating remotely to a surface modem, can also detect both 69 kHz and 180 kHz transmitters. V9-180 kHz tags cannot be detected by a VR2W-69 kHz receiver.

© 2015 AMIRIX Systems Inc. Information may change without notice.

## Physical Specifications

| Battery Option | V9-2H |
|---|---|
| Frequency (kHz) | 180 |
| Length (mm) | 25.5 |
| Diameter | 9 |
| Weight in air (g) | 3.7 |
| Weight in water (g) | 2.1 |
| Power Output (dB re 1uPa @1m) | 143 |

*Stated tag length, weight and output power are nominal. Small manufacturing variations can be expected.*

## Expected Battery Life

The life span of the V9-180 kHz tag depends on the delay between transmissions. The table below shows the estimated battery life for the most common delay settings. Tag life will be reduced if tags are shelved for a significant period of time (months). Contact VEMCO for information. 180 kHz tags should be activated within 30 days of delivery.

| Estimated Battery Life (Days) | |
|---|---|
| Nominal Delay (secs) | V9-2H |
| 20 | 440* (490)** |
| 40 | 700* (760)** |
| 60 | 730* (790)** |

*Notes: The transmission rate varies randomly ±50% about the nominal delay value. For example, a 40 second nominal delay indicates that the tag transmits randomly every 20 to 60 seconds. Other settings are available.*

*The projected battery life is an estimate and users will experience a decrease in battery life if their tags are operating in extreme warm or extreme cold temperatures.*

## Range Testing, VPS Sync, and Reference and Sentinel Tags



The V9-180 kHz tag can be purchased with a convenient and permanent cap that allows for easy attachment to receiver lines. In addition, the long life and transmission flexibility of the V9-180 kHz tag makes it ideal for use as a syncronization tag to synchronize receiver clocks and as a reference tag to calibrate positioning accuracy within a 180 kHz VPS study. The V9-180 kHz tag also has the same acoustic power output as a V5 making it an excellent choice for 180 kHz range testing. To order a V9-180 kHz tag with an attachment cap, specify model V9-2x-180k-3.

## VEMCO Tag Activator (VTA)



The VTA is a handheld device that enables users to quickly and easily activate 180 kHz transmitters. The manual on how to use the VTA can be found on the VEMCO website Downloads page. Note that the VTA model required by V9-180 kHz tags is VTA-180k-V9.

## Programmable ON/OFF

VEMCO transmitters are available with programming options that allow users to take greater advantage of fish behaviour over the life of their tags. In order to control the characteristics of their tags, users have the option of using between one to four programming steps to define the tags transmission: Status (ON/OFF), time interval, acoustic power level (H) and nominal delay.

This is an example of how V9-180 kHz tag programming options can be utilized to provide a staged release tag behaviour.

| Interval | Status | Time Days | Power (H) | Nominal Delay (sec) |
|---|---|---|---|---|
| Step 1 | ON | 1 | H | 30 |
| Step 2 | OFF | 9 | | |
| Step 3 | ON | 45 | H | 30 |
| Step 4 | ON | 680 | H | 60 |

Step 1: The tag is programmed to start in HIGH power mode with a nominal delay setting of 30 seconds for a period of 1 day. This allows a researcher to activate a tag and have it transmit for 1 day during the surgical implantation phase of the study.

Step 2: The tag is programmed to turn OFF for a period of 9 days. In order to conserve battery life while the animals recover from surgery, the tags are switched to the OFF status since the location of the animals is known.

Step 3: The tag is programmed to turn ON in HIGH power mode with a nominal delay setting of 30 seconds for a period of 45 days. This allows a researcher to release and track the animals during a 45 day migration period through a given study area.

Step 4: The tag is programmed to stay ON in HIGH power mode with a nominal delay setting of 60 seconds for a period of 680 days. This allows a researcher the ability to track the animals for 680 days during what might be a more residency type setting.

* *Estimated minimum battery life - 95% of tags will reach this life based on a 95% confidence level*
** *Typical life - Estimated that 50% of tags will reach this life based on a 95% confidence level*

© 2015 AMIRIX Systems Inc. Information may change without notice.